A STUDY OF SOME MAGNETOHYDRODYNAMICS PROBLEMS WITH OR WITHOUT HALL CURRENTS

A THESIS

SUBMITTED TO
THE DEPARTMENT OF APPLIED MATHEMATICS
WITH OCEANOLOGY AND COMPUTER PROGRAMMING
OF

VIDYASAGAR UNIVERSITY

IN ACCORDANCE WITH THE REQUIREMENTS FOR THE DEGREE OF

DOCTOR OF PHILOSOPHY

IN SCIENCE

Sankar Kumar Guchhait

December, 2016

Dedicated to my Parents

C E R T I F I C A T E

This is to certify that the thesis entitled *"A study of some magnetohydrodynamics problems with or without Hall currents"*, which is being submitted by *Mr. Sankar Kumar Guchhait* to the Vidyasagar University, Midnapore, West Bengal, INDIA, for the award of the degree of *Doctor of Philosophy*, is a record of bonafide research work carried out by him in the Department of Applied Mathematics with Oceanology and Computer Programming under my supervision and guidance. He has worked as a research scholar in this University for four years and in my opinion the thesis has reached the standard fulfilling the requirements of the regulations related to the degree. The results embodied in this thesis have not been submitted to any other University or Institute for the award of any degree or diploma or other similar title.

Professor Rabindra Nath Jana
Department of Applied Mathematics
with Oceanology and Computer Programming,
Vidyasagar University, Midnapore-721 102, W.B., INDIA

Acknowledgements

The completion of this doctoral thesis may not be possible without the support of several people. I would like to express my sincere gratitude to all of them. First of all, I am extremely grateful to my research guide, Professor Rabindra Nath Jana, for his valuable guidance, patience and consistent encouragement. It is a great pleasure and proud privilege to express my deep sense of gratitude and everlasting indebtedness to my research supervisor, Prof. R.N. Jana. His wisdom, knowledge and commitment to the highest standards have inspired and motivated me.

I would like to express my deep respect to Prof. Manoranjan Maiti and Prof. Tapan Kumar Pal, the former Professors of Department of Applied Mathematics with Oceanology and Computer Programming, for their inspiration and encouragement throughout my research work.

I also acknowledge my deep respect to all present teachers Prof. M. Pal, Dr.S.K. Mondal, Dr.S. Roy, Dr.D.K. Maiti, Dr.B. Sarkar, Mr.G. Ghorai and Mr.R. Giri, Department of Applied Mathematics with Oceanology and Computer Programming, for their encouragements and extraordinary support during the progress of the work. I would like to express my intense honour to Dr.Sanatan Das and Dr.Swapan Kumar Ghosh for their valuable suggestions and motivation throughout my research work. Also, I express my intense honour to my all teachers from born to now for their continuous and endless support. I wish to offer my heartily continuous endless thanks to Dr. Sovan Lal Maji for his knowledgeable, expert guidance and advices in completing this work. I convey my sincere thanks to Dr.N. Ghara, Dr.M. Jana, Dr.B.C. Sarkar for their instruction, support and ideas during my doctoral research over these past years. Their assistance has made the process a thoughtful and rewarding journey.

I would be very admiss if I do not thank my wife Mrs. Sharmistha Bhanja (Guchhait) for supporting me with her infinite understanding and continuous encouragement throughout my research work. I feel special love and affection for my little son Subhranil (Nil) who enlighten me with his innocence and childish zeal.

Finally, I wish to record that the very inspiration and co-operation of my colleagues for providing support and environment in the completion of the work. Still, I would like to thanks them again for encouraging me in all of my pursuits and inspiring me to follow my dreams.

Sankar Kumar Guchhait
Vidyasagar University

Contents

Part I

General Introduction

Chapter 1

Introduction

The fluid dynamics is the study of fluid motion. It is a branch of fluid mechanics that gives knowledge on the fluid flow. The term fluid dynamics is a science that deals with the behavior of fluids in motion and the interaction of fluids with solids or other fluids at the boundaries. It has several subdisciplines itself, including aerodynamics and hydrodynamics. Before the twentieth century, hydrodynamics was synonymous with fluid dynamics. This is still reflected in names of some fluid dynamics topics, like magnetohydrodynamics and hydrodynamic stability both of which can also be applied to gases.

The magnetohydrodynamics(MHD) is the study of the interaction between magnetic fields and moving conducting fluids. The word MHD covers the phenomena, where, in an electrically conducting fluid, the velocity field and the magnetic field are coupled. The field of MHD was initiated by Hannes Alfvén for which he received the Nobel Prize in physics in 1970. An induced electric current is generated due to the flow of an electrically conducting fluid in the presence of a magnetic field which modifies the electromagnetic field. The flow field in turn is modified by the force due to the electromagnetic field called Lorentz force. This force tends to modify the initial motion of the conductor.

The fluid dynamics has a wide range of applications, including calculating forces and moments on aircraft, determining the mass flow rate of petroleum through pipelines, predicting weather patterns, understanding nebulae in interstellar space and reportedly modeling fission weapon detonation. Some of its principles are even used in traffic engineering, where traffic is treated as a continuous fluid. Applications of magnetohydrodynamics are very broad ranging from astrophysics to plasma physics. The study of MHD has received its first importance in connection with astrophysical problems since

over 99% of baryonic matter content of the Universe is made up of plasma, including stars, the interplanetary medium (space between the planets), the interstellar medium (space between the stars) *etc.* The solar wind is also governed by MHD. There are two serious technological applications of MHD, that may both become very important in the future. First, strong magnetic fields may be used to confine rings or columns of hot plasma that will be held in place long enough for thermonuclear fusion to occur and for net power to be generated. In the second application, which is directed toward a similar goal, liquid metals are driven through a magnetic field in order to generate electricity. However, the major use of MHD is in plasma physics. It has found wide applications in problems of geophysics, power-generation, thermonuclear fusion, aeronautic, space-research, liquid-metal cooling of nuclear reactors and many other engineering fields. In aeronautical engineering MHD finds its application in MHD generators, MHD pumps, ion propulsion, MHD boundary layer control of reentry vehicles *etc.* Application in the biomedical engineering includes cardiac MRI, ECG *etc.* The principle of MHD is also used in stabilizing a flow against the transition from laminar to turbulent flow.

Hartmann[1] initiated the study of the subject in the name Hg-dynamics in his efforts to pump mercury by exploitation of hydrodynamical pressure and electromagnetic fields[2-8]. The systematic study under the present name began with discovery of transverse waves by Alfvén[9] while he was engaged in the theoretical investigations of sunspots. The study of magnetohydrodynamics in astrophysical and geophysical problem have been made by many authors, viz. Cowling[10], Bullard[11] and many others. On reducing aerodynamic heat transfer rate by MHD techniques has been analyzed by Meyer[12].

1.1 Basic equations

1.1.1 The governing equations for the flow of an electrically conducting incompressible fluid

The fundamental equations of MHD describe the motion of an electrically conducting fluid in the presence of a magnetic field. This fluid is usually either a liquid metal or a plasma. These fundamental equations of MHD are the modified electrodynamics equations together with the modified hydrodynamic equations. The electrodynamic Maxwell's equations remain unchanged whereas the Ohm's law which relates the electric current to the electric field has to be modified to include the induced current. The momentum equation has to be modified to include the Lorentz force and the modified energy equation has to include the Joule dissipation. In MHD, the displacement current

is neglected in the case of motion of fluid whose velocity is very small compared to the velocity of light. Also, for fluids which are almost neutral, the charge density is negligible. The convection current can also be neglected in comparison to the conduction current.

The equation of continuity is developed by applying the law of conservation of mass to a small volume element within a flowing fluid. For an incompressible fluid the density of fluid is constant, the equation of continuity is then written in the form

$$\nabla \cdot \vec{q} = 0, \tag{1.1}$$

where $\vec{q}$ is the fluid velocity vector.

The general momentum equation is also called the equation of motion or the modified Navier-Stoke's equation. The modified momentum equation including magnetic field is

$$\rho \left[\frac{\partial \vec{q}}{\partial t} + (\vec{q} \cdot \nabla)\vec{q} + 2(\vec{\Omega} \times \vec{q}) \right] = -\nabla p + \mu \nabla^2 \vec{q} + (\vec{j} \times \vec{B}) + \rho\, \hat{g}, \tag{1.2}$$

where $\vec{\Omega}$ is the angular velocity, ρ the fluid density, p the modified fluid pressure including centrifugal force, μ the coefficient of viscosity, $\vec{j}$ the current density vector, $\vec{B}$ the magnetic induction vector and $\hat{g}$ the acceleration due to gravity. The term $(\vec{q} \cdot \nabla)\vec{q}$ represents convective acceleration*, $2(\vec{\Omega} \times \vec{q})$ the Coriolis acceleration, ∇p the fluid pressure gradient including centrifugal force and $\mu \nabla^2 \vec{q}$ the viscous force.

Under the usual Boussinesq approximation, the equation of state is

$$\rho = \rho_0 \Big[1 - \beta (T - T_0) \Big], \tag{1.3}$$

where β is the coefficient of thermal expansion, T the fluid temperature, T_0 the reference temperature and ρ_0 the fluid density at temperature T_0.

The Maxwells equations are:

$$\nabla \times \vec{B} = \mu_e \vec{j} \quad \text{(Amperes law)}, \tag{1.4}$$

$$\nabla \times \vec{E} = -\frac{\partial \vec{B}}{\partial t} \quad \text{(Faradays law)}, \tag{1.5}$$

$$\nabla \cdot \vec{B} = 0 \quad \text{(Gausss law for magnetic field)}, \tag{1.6}$$

$$\nabla \cdot \vec{D} = \rho_e \quad \text{(Gausss law for electric field)}, \tag{1.7}$$

where μ_e is the the magnetic permeability, $\vec{E}$ the electric field vector, $\vec{D}$ the displacement vector and ρ_e the electric charge density.

*The convective acceleration is an acceleration caused by a change in velocity over position.

The Ohm's law is

$$\vec{j} = \sigma \left(\vec{E} + \mu_e \vec{q} \times \vec{B} \right), \tag{1.8}$$

where $\vec{E}$ the electric field vector and σ the electrical conductivity of the fluid.

The electric and magnetic flux densities $\vec{D}$, $\vec{B}$ are related to the field intensities $\vec{E}$, $\vec{H}$ via the so-called constitutive relations, whose precise form depends on the material in which the fields exist.

The constitutive field equations are

$$\vec{B} = \mu_e \vec{H} \text{ and } \vec{D} = \epsilon \vec{E}, \tag{1.9}$$

where ϵ is the dielectric constant.

The magnetic induction equation is

$$\frac{\partial \vec{B}}{\partial t} = \nabla \times (\vec{q} \times \vec{B}) + \nu_m \nabla^2 \vec{B}, \tag{1.10}$$

where $\nu_m = \frac{1}{\sigma \mu_e}$ is the magnetic diffusivity (or resistivity).

The generalized Ohm's law, on taking Hall current into account and neglecting ion-slip and thermo-electric effect, is (see Cowling[10])

$$\vec{j} + \frac{\omega_e \tau_e}{B_0} \left(\vec{j} \times \vec{B} \right) = \sigma \left(\vec{E} + \mu_e \vec{q} \times \vec{B} \right), \tag{1.11}$$

where ω_e is the cyclotron frequency and τ_e the collision time of electron.

The energy equation including viscous and Joule dissipations is

$$\rho c_p \left[\frac{\partial T}{\partial t} + (\vec{q} \cdot \nabla) T \right] = k \, \nabla^2 T + \mu \, \Phi + \frac{\vec{j}^2}{\sigma}, \tag{1.12}$$

where k is the thermal conductivity, c_p the specific heat at constant pressure and Φ the viscous dissipation function. The last term on the right-hand-side is due to Joule dissipation.

1.1.2 MHD boundary conditions

The flow field and the electromagnetic field are to be determined by solving the fundamental equations stated in the previous section under appropriate boundary conditions for the flow field and electromagnetic field. The boundary conditions to be satisfied are the usual hydrodynamic boundary conditions imposed on the velocity field, the continuity of the temperature distribution and the electromagnetic boundary conditions. The electromagnetic properties change abruptly at a solid boundary. Across such a surface of discontinuity, the electromagnetic variables must satisfy the following conditions.

(i) The normal component of the magnetic induction $\vec{B}$ is continuous, i.e.

$$(\vec{B}_2 - \vec{B}_1).\widehat{n} = 0, \tag{1.13}$$

where $\widehat{n}$ is the unit vector normal to the surface of discontinuity and the subscripts 1 and 2 refer to the medium on either side of the surface.

(ii) The magnetic field $\vec{H}$ satisfies the condition

$$\widehat{n} \times (\vec{H}_2 - \vec{H}_1) = \vec{J}_s, \tag{1.14}$$

where $\vec{J}_s$ is the surface current density. When the electrical conductivity of the solid is finite ($\sigma \neq \infty$) then $\vec{J}_s = \vec{0}$. But when $\sigma = \infty$ then $\vec{J}_s$ will be different from zero.

(iii) The tangential component of the electric field is continuous, i.e.

$$\widehat{n} \times (\vec{E}_2 - \vec{E}_1) = \vec{0}. \tag{1.15}$$

(iv) The dielectric displacement $\vec{D} = \epsilon\vec{E}$ must satisfy the condition

$$(\vec{D}_2 - \vec{D}_1).\widehat{n} = \rho_{es}, \tag{1.16}$$

where ρ_{es} is the surface free charge density.

1.1.3 Hall currents

In an ionized gas where the density is low and/or the magnetic field is very strong, the conductivity normal to the magnetic field is reduced due to the free spiraling of electrons and ions about the magnetic lines of force before suffering collisions and a current is induced in a direction normal to both the electric and magnetic fields. The resulting current is known as Hall currents. The effects of Hall current is likely to be important in many astrophysical situations as well as the flows of plasma through MHD power generator. A fully ionized gas can be considered as a mixture of two different ionized gases, one consisting of positively charged ions and the other negatively charged electrons. The mass of the electrons being very much less than that of ions, the velocity $\vec{q}$ of the ion gas can be taken as the velocity of the whole mixture. The current density of the ionized gas can be given as

$$\vec{J} = -e\, n_e \vec{V}, \tag{1.17}$$

where $\vec{V}$ is the velocity of the electron gas relative to the ion gas, $-e$ the charge of an electron and n_e the number of electrons per unit volume. The collision of an ion with an electron can be smoothed into a continuous force, for each collision with electron and ion, the electron loses a quantity of momentum equal to the mean momentum $m_e\vec{V}$ relative to the ion-gas where m_e is the mass of an electron. If τ_e be the mean interval between two successive collisions of an electron with ions, the total momentum lost by the electrons due to collisions with ions is $n_e m_e \vec{V}/\tau_e$ per unit volume and time. It is the loss of momentum of electrons due to a drag force $-n_e m_e \vec{V}/\tau_e$ per unit volume. The various forces acting on the electron gas are

(i) The drag force due to collisions.

(ii) The gradient $(-\nabla p_e)$ of the electron pressure p_e.

(iii) The electromagnetic force $-e\, n_e \left(\vec{E} + \mu_e \vec{q} \times \vec{H} + \mu_e \vec{V} \times \vec{H}\right)$.

(iv) The force due to gravity $n_e m_e\, g$.

The gravitational force is negligible because the electron has negligible mass and the other three forces can be considered to be in equilibrium.

Thus, by neglecting ion-slip and thermo-electric effects, we have

$$0 = -\nabla p_e - e\, n_e \left(\vec{E} + \mu_e \vec{q} \times \vec{H} + \mu_e \vec{V} \times \vec{H}\right) - \frac{n_e m_e \vec{V}}{\tau_e}. \tag{1.18}$$

On the use of equation (1.18), equation (1.17) becomes

$$\frac{m_e}{e\,\tau_e}\vec{J} = \nabla p_e + e\, n_e \left(\vec{E} + \mu_e \vec{q} \times \vec{H}\right) - \mu_e \vec{J} \times \vec{H}. \tag{1.19}$$

This equation is known as generalized Ohm's law.

Equation (1.19) can be written as

$$\vec{J} = \sigma \left(\vec{E} + \mu_e \vec{q} \times \vec{H} - \frac{\mu_e}{e\, n_e}\vec{J} \times \vec{H} + \frac{1}{e\, n_e}\nabla p_e\right), \tag{1.20}$$

where $\sigma = e^2 n_e \tau_e / m_e$ is the conductivity of the ionized gas.

For partially ionized gas, the electron pressure gradient ∇p_e is negligible and the equation (1.20) can be written as

$$\vec{J} = \sigma \left(\vec{E} + \mu_e\, \vec{q} \times \vec{H} - \frac{\mu_e}{e\, n_e}\vec{J} \times \vec{H}\right), \tag{1.21}$$

where the term $\frac{\sigma \mu_e}{e\, n_e}(\vec{J} \times \vec{H})$ is due to Hall currents.

1.1.4 Heat transfer

The term heat transfer encompasses all phenomena occurring in the transport of quantity of heat from one point of space to another. Heat transfer means the exchange in internal energy between individual elements or regions of the medium considered. It always occurs from the higher temperature region to the lower temperature region. Heat is not a storable quantity and is defined as energy in transit due to a temperature difference. The heat transfer has wide application in high speed aircraft, both in nature and industry, formation of rain and snow, heating and cooling on the Earth's surface, spreading of forest fires, re-entry vehicles and cooling of rotating turbine blades etc. Heat transfer from a heated moving or non-moving surface to a quiescent (a fluid at rest) ambient medium occurs in many manufacturing processes such as hot rolling, wire drawing and crystal growing. The heat treatment of materials traveling between a feed roll and a wind-up roll. Heat transfer mechanisms can be grouped into three broad categories.

(a) Conduction:

Regions with greater molecular kinetic energy will pass their thermal energy to regions with less molecular energy through direct molecular collisions, a process known as conduction. In metals, a significant portion of the transported thermal energy is also carried by conduction-band electrons. Conduction is because of molecular transport of heat in bodies (or between bodies) in the thermodynamical system considered. There is no actual displacement of particles from one place to another.

(b) Convection:

Convection is concerned with the fluid medium and/or the fluid in the medium. The motion of a non-isothermal fluid is called convection. The transport of heat is mainly because of the movement of fluid from one region to the other region in the medium. When heat conducts into a static fluid it leads to a local volumetric expansion. As a result of gravity-induced pressure gradients, the expanded fluid parcel becomes buoyant and displaces, thereby transporting heat by fluid motion (i.e. convection) in addition to conduction. Such heat-induced fluid motion in initially static fluids is known as free convection or natural convection. Heat transfer by thermal convection may be subdivided into two groups (i) Forced convection (ii) Free convection.

(i) Forced convection: A convection process which takes place due to motion created by an external agency such as pressure gradient or an agitator(pump,

blower, wind, vehicle motion, etc.), is known as forced convection. In incompressible fluids with constant physical properties, such flows are characterized by the fact that the velocity field is not affected by the temperature distribution but the reverse is not true. In such flows, the heat transferred at the surface of the solid body is swept away by the fluid motion without in any way affecting the local density of the fluid. In forced convection, the velocity field is independent of the temperature distribution for an incompressible fluid.

(ii) Free convection: A convective process caused by the action of body forces on the fluid which arises as a result of density gradients due to change in temperature is called free convection or natural convection. Such variation of density gives rise to buoyancy force which causes relative motion. Hence in free convective flow, the velocity field and the temperature distribution are coupled. The free convective flows have been studied most extensively because they are found frequently in nature as well as in engineering applications.

(c) Radiation:

The conversion of the internal energy of a substance into radiation energy is referred to as radiative heat transfer. It propagates by means of electromagnetic waves depending on the temperature and on the optical properties of the emitter. All materials radiate thermal energy in amounts determined by their temperature, where the energy is carried by photons of light in the infrared and visible portions of the electromagnetic spectrum. When temperatures are uniform, the radiative flux between objects is in equilibrium and no net thermal energy is exchanged. The balance is upset when temperatures are not uniform and thermal energy is transported from surfaces of higher to surfaces of lower temperature. Two limiting cases of radiative heat transfer processes are generally considered in the literature (i) optically thick limit and (ii) optically thin limit. The optical dimension of a system is defined as the ratio of the characteristic physical dimension to the penetration length of radiation. For an optically thick medium, the penetration length is small and is equivalent to the radiation mean free path. Here the radiation can be considered as a diffusive process. For an optically thin medium just the reverse is true so that the medium does not absorb its own emitted radiation.

1.2 Earlier works relevant to the present investigations

A brief review of the earlier investigations of the problems which bearing on the contents of the thesis.

1.2.1 Magnetohydrodynamic flow past a horizontal flat plate

The hydromagnetic flow past a porous flat plate with Hall effects has been studied by Gupta[13]. Pop[14] has investigated the Hall effects on MHD flow for an impulsively started flat plate using power series method. The Hall effects on hydromagnetic flow past a oscillating flat plate with or without rotation has been studied by Bhadram[15]. Mazumder et al.[16] have analyzed the fluid flow and heat transfer on hydromagnetic Ekman layer with Hall effects on a porous flat plate. The Hall effects on hydromagnetic flow for an impulsively started porous flat plate have been discussed by Jana and Datta[17]. The Hall effects on hydromagnetic flow past an infinite porous flat plate have been studied by Jana et al.[18]. Hossain and Rasid[19] have investigated the Hall effects on hydromagnetic free convective flow past a porous flat plate with mass transfer. Sattar and Maleque[20] have examined the unsteady MHD natural convection flow along an accelerated porous flat plate with Hall currents and mass transfer in a rotating porous medium. A numerical investigation on classical Blasius problem past a flat plate has been presented by Cortell[21]. The MHD natural convective boundary layer flow past a flat plate of finite dimensions have been studied by Ghosh and Pop[22]. Damseh et al.[23] have obtained the solution for a forced convectional flow with magnetic field and thermal radiation.

The boundary layer equations play central roles in many aspects of fluid mechanics since they describe the motion of a viscous fluid close to the surface. Martin and Boyd[24] have considered the momentum and heat transfer in a laminar boundary layer flow past a flat plate under the slip boundary condition. The effects of radiation in a boundary layer flow with heat transfer past a flat plate under the slip condition have been investigated by Batallar[25] and Cortell[26]. Maji et al.[27] have studied the Hall effects on hydromagnetic flow on an oscillatory porous plate. Recently, Aziz[28] has discussed the boundary layer slip flow past a flat plate under the constant heat flux condition at the surface. Bhattacharyya et al.[29] have investigated the MHD boundary layer slip flow and heat transfer past a flat plate. Gupta et al.[30] have discussed the Hall effects on magnetohydrodynamic shear flow past an infinite porous flat plate subjected to uniform suction/blowing. The computational modelling for unsteady MHD flow and heat transfer past a flat plate with Navier slip and Newtonian heating has been investigated by Makinde[31]. The MHD natural convective boundary layer flow past a flat plate have been studied by Jana et al.[32]. The magneto-nanofluid flow past an impulsively started porous flat plate in a rotating system have been considered by Das et al.[33]. The effects of mass diffusion on natural convective flow past a flat plate have been studied by Muthukumaraswamy et al.[34] and Makinde et al.[35]. Panda et al.[36]

have analyzed the mass diffusion and natural convective flow past a flat plate.

1.2.2 Flow past a vertical plate

Singh[37] has discussed the Hall effects on MHD Stoke's flow past an infinite vertical porous plate. The effects of free convection for an oscillating flow past an infinite vertical porous plate with constant suction has been studied by Soundalgekar[38]. The MHD mixed convective flow past a vertical plate embedded in a porous medium have been analyzed by Aldos et al.[39]. The hydromagnetic free convective flow past a vertical plate with variable viscosity and thermal conductivity has been discussed by Jana[40]. Sacheti et al.[41] have obtained an exact solution for unsteady MHD free convective flow with constant heat flux. Anwar[42] has studied the unsteady MHD free convective flow past a vertical porous plate. Hossain and Takhar[43] have discussed the effects of radiation on mixed convective flow past a vertical plate with uniform surface temperature. The radiation effects on MHD free convective flow on radiating gas past a semi-infinite vertical plate have been presented by Takhar et al.[44]. A comprehensive account on the boundary layer flow past a vertical plate embedded in a porous medium have been examined by Kim and Vafai[45] and Liao and Pop[46].

Sattar et al.[47] have studied the unsteady free convective flow past a vertical porous plate embedded in a porous medium. Revankar[48] has discussed the effects of free convection past an impulsively started or oscillating infinite vertical plate. Chamkha et al.[49] have examined the MHD free convective flow past a vertical plate through a porous medium in the presence of foreign mass. Raptis and Perdikis[50] have studied the free convective flow of water near 4^0C past a vertical moving plate. The effects of magnetic field on the Ekman layer flow for an oscillating plate have been investigated by Israel-Cookey and Sigalo [51]. Sahoo et al.[52] have analyzed the hydromagnetic natural convective flow past a vertical plate. The numerical solution of transient free convective MHD flow of an incompressible viscous fluid past a semi infinite inclined vertical plate with variable surface heat and mass flux have been discussed by Ganesan and Palani[53]. Ferdows et al.[54] have investigated numerically the combined effects of thermal radiation and convection in a boundary layer flow past a vertical plate with variable suction. Magyari et al.[55] have discussed the analytical solution for unsteady free convection past a vertical plate in a porous medium. The effects of transverse magnetic field on unsteady free convective flow past a vertical plate embedded in a porous medium has been discussed by Chamkha[56]. Alam and Rahman[57] have studied the MHD free convective flow and mass transfer past a vertical porous plate in a porous medium. Makinde[58] has examined the transient free convective flow past a vertical

plate. Alam et al.[59] have analyzed the local similarity solutions for unsteady MHD free convection and mass transfer flow past an impulsively started vertical porous plate with Dofour and Sorret effects. Samad and Rahman[60] have analyzed the effects of thermal radiation interaction with unsteady MHD flow past a vertical porous plate immersed in a porous medium. In this analysis, they considered a Darcy-Forchhemier model and thereafter solve numerically the corresponding momentum and energy equations. Cao and Baker[61] have studied the mixed convective flow and heat transfer past a vertical plate on taking velocity slip and temperature jump boundary conditions. Perdikis and Rapti[62] have investigated the unsteady MHD flow past a vertical porous plate in the presence of radiation. Das et al.[63] have studied the radiation effects on unsteady free convective flow past a vertical plate with Newtonian heating. Shateyi et al.[64] have investigated the MHD flow past a vertical plate with radiative heat transfer. Chaudhary and Jain[65] have studied the combined effects of heat and mass transfer on MHD free convective flow past an oscillating plate embedded in a porous medium. Zueco[66] has discussed the network simulation method for unsteady MHD free convective flow past a vertical porous plate with radiation and viscous dissipation.

Aydin and Kaya[67] have investigated the radiation effect on MHD mixed convection flow about a permeable vertical plate. The radiation effect on MHD mixed convection flow about a permeable vertical plate have been discussed by Aydin and Kaya[68]. Chaudhary and Jha[69] have analysed the heat and mass transfer in visco-elastic fluid past an impulsively started infinite vertical plate on taking Hall currents into account. Makinde[70] has studied the MHD boundary-layer flow and mass transfer past a vertical plate in a porous medium with constant heat flux. The MHD flow past a semi-infinite vertical plate with mass transfer have been investigated by Palani and Srikanth[71]. Makinde and Aziz[72] have studied the MHD mixed convective flow past a vertical plate embedded in a porous medium with convective boundary condition. The MHD flow past an impulsively started vertical plate with variable temperature and mass diffusion have been studied by Rajput and Kumar[73]. Rao et al.[74] have analyzed the unsteady MHD convective flow past a vertical porous plate with slip-flow regime. The effects of radiation and heat transfer on flow past an exponentially accelerated vertical plate with constant heat flux have been examined by Mandal et al.[75]. The Hall effects on MHD free convective boundary layer flow past a vertical plate have been studied by Das et al.[76]. Seth et al.[77, 81] have investigated the MHD flow past a vertical plate in various geometrical aspect. Makinde[82] has studied the heat and mass transfer on MHD mixed convection stagnation point flow past a vertical plate embedded in a porous medium with radiation and internal heat generation. The MHD nanofluid flow past a

permeable vertical plate with convective heating have been investigated by Mutuku-Njane and Makinde[83]. Khan et al.[84] have studied the MHD boundary layer flow of nanofluid containing gyrotactic microorganisms past a vertical plate with Navier-slip. The hydromagnetic Blasius flow on power law nanofluid past a convectively heated vertical plate have been discussed by Khan et al.[85]. Das et al.[86] have analyzed the magneto-convective boundary layer slip flow of nanofluid past a convectively heated vertical plate.

1.2.3 MHD Couette flow

The MHD flow between two parallel plates, one in uniform motion and other one held at rest is known as MHD Couette flow. The Couette flow is a classical fluid mechanics problem that has applications in magnetohydrodynamic (MHD) power generators and pumps, accelerators, electrostatic precipitation, polymer technology, petroleum industry, purification of crude oil and also in many material processing applications such as extrusion, metal forming, wire and glass fiber drawing, continuous casting etc. The hydrodynamic rotating flow of a viscous incompressible electrically conducting fluid has gained considerable attention because of its numerous applications in physics and engineering such as in designing thermosyphon tube, cooling turbine blades etc.

Gubanov and Lunkin[87] and Katagiri[88] have discussed the Couette flow on magnetohydrodynamic in different models. The heat transfer characteristics on the MHD Couette flow has been analyzed by Gupta[89]. Jana and Datta[90], Mazumder[91], Ganapathy[92] and Das et al.[93] have investigated the Couette flow of a viscous incompressible fluid in a rotating system in the absence of magnetic field whereas Mondal et al.[94], Mondal and Mandal[95], Seth and Ahmad[96], Hayat et al.[97, 99], Kumar et al.[100], Seth et al.[101] have studied the MHD Couette flow of a viscous incompressible electrically conducting fluid in the presence of uniform transverse magnetic field. Seth et al.[102] have studied the MHD Couette flow in a rotating system. Jana et al.[103] have examined the MHD Couette flow and heat transfer in a rotating system. The hydromagnetic Couette flow in a rotating system in the presence of inclined magnetic field have been analyzed by Jana and Dogra[104]. Guria et al.[105] and Das et al.[106] have investigated the unsteady Couette flow in a rotating system. The unsteady MHD Couette flow in a rotating system have been studied by Seth et al.[107]. Singh[108] has considered an oscillatory hydromagnetic Couette flow in a rotating system. Guria et al.[109] have investigated an oscillatory Couette flow in the presence of an inclined magnetic field. An oscillatory MHD Couette flow in a rotating system have been discussed by Patra et al.[110]. The mathematical modelling of an oscillatory MHD Couette flow

in a rotating system in the presence of oblique magnetic field have been investigated by Beg et al.[111].

On the other hand, the Hall effects on MHD Couette flow of an ionized gas have been examined by Chekmerev[112] and Soundalgekar et al.[113]. The Hall and ion-slip effects on MHD Couette flow with heat transfer has been studied by Soundalgekar[114]. The Hall effects for unsteady MHD Couette flow have been discussed by Jana and Datta[115]. Soundalgekar et al.[116] have studied the combined effects of Hall current and ion-slip on MHD Coutte flow with heat transfer. The Hall effects on MHD Couette flow in a rotating system have been investigated by Jana and Datta[117]. Ghara et al.[118] have investigated the effects of Hall current and ion-slip on unsteady MHD Couette flow. The Hall effects on unsteady Couette flow under boundary layer approximations have been considered by Jana and Kanch[119]. Mandal et al.[120] and Mandal and Mandal[121] have studied the combined effects of Hall current and Coriolis force on MHD Couette flow in a rotating system. Ghosh and Pop[122] have discussed the Hall effects on MHD plasma Couette flow in a rotating system. The Hall effects on MHD Couette flow in a rotating system have been studied by Das et al.[123]. The Hall effects on unsteady Couette flow in a rotating system have been studied by Maji et al.[124]. Ghosh and Pop[125] have presented the Hall effects on unsteady hydromagnetic flow in a rotating system with oscillating pressure gradient. Seth et al.[126] have discussed the Hall effects on oscillatory hydromagnetic Couette flow in a rotating system. The Hall effects on MHD flow between two parallel plates in a rotating system with heat transfer characteristics have been studied by Ghosh et al.[127]. Sarkar et al.[128] have studied the combined effects of Hall current and rotation on steady hydromagnetic Couette flow. Das et al.[129] have discussed the Hall effects on oscillatory Couette flow under boundary layer approximations. The Oscillatory hydromagnetic Couette flow in a rotating system with induced magnetic field have been analyzed by Seth et al.[130]. Ghosh and Pop[131] have examined the combined effects of Hall current and Coriolis force on MHD Couette flow in a rotating system with arbitrary magnetic field. Seth and Singh[132] have investigated the Hall effects on unsteady MHD Couette flow in a rotating system in the presence of inclined magnetic field. The unsteady MHD reactive Couette flow with heat transfer and variable properties have been presented by Makinde and Franks[133].

1.2.4 Flow through a vertical channel

The Hall effect in the viscous flow of ionized gas between parallel plates under transverse magnetic field has been investigated by Sato[134]. The Hall effects on steady flow of an

ionized gas between two parallel plates have been investigated by Yamanishi[135] and Sherman and Sutton[136]. Laminar natural convection flow and heat transfer of fluid with and without heat source in channel with wall temperature has been studied by Ostrach[137]. Ostrach[138] has also examined the unstable convection in vertical channels with heating from below, including effects of heat source and frictional heating. On combined free and forced convection in channels has been analyzed by Tao[139]. Taluber and Welch[140] have discussed the effects of free and forced convective flows with viscous dissipation through a vertical channel. The natural convective flow between two vertical plates with symmetric wall heating has been described by Bodoia[141]. The analytical study on free and forced convective flow between two vertical plates under transverse magnetic field have been discussed by Regirer[142], Mori[143], Yu[144].

Sparrow et al.[145] have analyzed the hydrodynamic free convective flow through a vertical channel. Kettleborough[146] has examined the transient laminar two dimensional motion generated by a temperature gradient perpendicular to the direction of the body force of a fluid between two heated vertical plates. Hamadah and Wirtz[147] and Cheng et al.[148] have analyzed the laminar fully developed mixed convection through a vertical channel. The effects of radiation on combined free and forced convective flow of an electrically conducting fluid between two vertical walls have been studied by Gupta and Gupta[149] and Datta and Jana[150]. Ingham et al.[151] have investigated numerically the fully developed mixed convective flow through a vertical channel. Poots[152] has considered the flow of an electrically conducting fluid between two heated vertical plates including Joule heating, viscous dissipation and internal heat sources in the energy equation. The effects of applied electric field through a vertical channel has been studied by Umavathi[153]. The magnetohydrodynamic fully developed mixed convective flow of a viscous incompressible electrically conducting fluid through a vertical channel with asymmetric heating of the wall have been investigated by Ghosh and Nandi[154] and Ghosh et al.[155].

Pop et al.[156] have analyzed the effects of Hall current on free and force convective flows through a rotating vertical channel in the presence of inclined magnetic field. Barletta[157] has investigated the combined free and forced convective flow through a vertical channel with viscous dissipation. The combined free and forced convective magnetohydrodynamic flow through a vertical channel on taking viscous and Ohmic dissipation have been analyzed by Umavathi and Malashetty[158]. Mazumder et al.[159] have discussed the Hall effects on combined free and forced convective hydromagnetic flow through a vertical channel. The Hall effects on hydromagnetic convective flow through a vertical channel with conducting walls have been investigated by Datta and

Jana[160]. Sivaprasad et al.[161] have studied the Hall effects on unsteady MHD free and forced convective flow through a porous rotating channel. The Hall effects on hydromagnetic convective flow through a rotating channel under the general wall conditions have been studied by Guria and Jana[162].

The MHD convective flow through a rotating channel with Hall effects have been discussed by Seth and Ansari[163]. The effects of radiation on three dimensional vertical channel flow subjected to a periodic suction have been analyzed by Guria et al.[164]. Das et al.[165] have examined the MHD free convection between two vertical walls. An oscillatory mixed convective flow of a visco-elastic electrically conducting fluid through an infinite vertical channel in a porous medium has been analyzed by Singh[166]. Mandal et al.[167] have discussed the effects of radiation on transient natural convective flow between two vertical walls. An exact solution of MHD mixed convection periodic flow through a rotating vertical channel with heat radiation has been investigated by Singh[168]. Singh and Pathak[169] have examined the effects of Hall current on an oscillatory convective flow in a rotating vertical porous channel with thermal radiation and slip conditions. Sarkar et al.[170] have studied the Hall effects on MHD flow in a rotating channel in the presence of an inclined magnetic field. The MHD free and forced convective flow in a rotating channel have been analyzed by Sarkar et al.[171]. The Hall effects on unsteady free convection in a heated vertical channel in the presence of heat generation have been studied by Das and Jana[172]. Recently, Das et al.[173] have analyzed the mixed convective magnetohydrodynamic flow through a vertical channel filled with nanofluids. The transient natural convection in a vertical channel filled with nanofluids in the presence of thermal radiation have been studied by Das et al.[174]. Adesanya et al.[175] have studied the hydromagnetic natural convective flow between two vertical parallel plates with periodic boundary conditions.

Present Investigations

In this thesis, we studied some problems on magnetohydrodynamics with or without Hall currents. Some problems are studied in rotating environment. In addition to that, we applied a uniform transverse magnetic field on several flow in such a way that there exists Hall currents acting on hydromagnetic flow. The thesis consists of ten Chapters, the **Chapter 1** presents the introductory part. In this Chapter, basic equations on certain relevant topics governing the flow of an electrically conducting incompressible fluid are discussed briefly. Moreover, earlier works related to the present investigations have been discussed precisely. A study of some magnetohydrodynamics problems on fluid dynamics with or without Hall currents have been presented in next *eight Chapters*.

Chapters 2-9 are developed by mathematical formulation based on the geometry of the problems and carried on graphical presentations. Furthermore, conclusion about the present investigation and suggestions for the future works have given in **Chapter 10**.

The thesis is devoted to study the following problems:

(i) Unteady MHD flow and heat transfer past a porous flat Plate in a rotating system. **(ii)** Radiation effects on unsteady MHD free convective Couette flow of heat generation/absorbing fluid. **(iii)** Hall effects on unsteady hydromagnetic flow past an accelerated porous plate in a rotating system. **(iv)** Effects of Hall current and radiation on unsteady MHD flow past a heated moving vertical plate. **(v)** Combined effects of Hall current and rotation on unsteady MHD Couette flow in a porous channel. **(vi)** Combined effects of Hall current and radiation on MHD free convective flow in a vertical channel with an oscillatory wall temperature. **(vii)** Hall effects on hydromagnetic free convection in a heated vertical channel in the presence of an inclined magnetic field and thermal radiation and **(viii)** Hall effects on an unsteady magneto-convection and radiative heat transfer past a vertical porous plate.

The unsteady MHD flow and heat transfer of an incompressible viscous fluid bounded by an infinite porous flat plate have been studied in **Chapter 2**. The effects of pertinent parameters on the velocity field and temperature distribution are studied. It is found that with an increase in either magnetic parameter or suction parameter the primary velocity and the magnitude of secondary velocity of the fluid decrease at a particular point in flow filed. This is due to the fact that variation of the magnetic parameter leads to the variation of the Lorentz force due to magnetic field and the Lorentz force produces more resistance to transport phenomena. It is found that the primary velocity decreases while the magnitude of secondary velocity increases near the plate and decreases away from the plate with an increase in rotation parameter. The mean wall temperature as well as the rate of heat transfer are also obtained. It is found that with an increase in magnetic parameter the mean wall temperature increases at a particular point in flow filed. The effects of transverse magnetic field on a viscous incompressible electrically conducting fluid is to suppress the velocity field which in turn causes the enhancement of the temperature field. It is also found that both the amplitudes of shear stresses due to primary and the secondary flow decrease with an increase in either magnetic parameter or frequency parameter.

In **Chapter 3** ,the radiation effects on transient MHD convective Couette flow confined between two infinite vertical walls have been studied. The dimensionless governing partial differential equations are solved by the usual Laplace transform technique. It is

found that the velocity decreases with an increase in magnetic parameter. An increase in either radiation parameter or Prandtl number leads to fall in the fluid temperature. Further, it is seen that the absolute value of the shear stress at the moving plate increases for the impulsive as well as accelerated motion with an increase in either magnetic parameter or radiation parameter while it decreases with an increase in either heat generation parameter or Prandtl number. It is observed that the rate of heat transfer increases with an increase in Prandtl number. It is also observed that the vertical flow rate decreases with an increase in radiation parameter.

The effects of Hall current and rotation on unsteady hydromagnetic flow of a viscous incompressible electrically conducting fluid past an accelerated porous plate in a rotating system have been carried out in **Chapter 4**. The dimensionless governing partial differential equations are solved by the usual Laplace transform technique. The effects of different parameters on the velocity and shear stresses are studied in details. It is seen that Hall currents tends to accelerate the primary and the secondary fluid velocity. The rotation has a tendency to retard the primary fluid velocity and start to accelerate the secondary fluid velocity. The primary and secondary fluid velocities are getting accelerated with the progress of time. It is also found that both the primary velocity and the magnitude of the secondary velocity decrease with an increase in magnetic parameter. The rotation tends to enhance both the shear stresses at the plate. On the other hand, the absolute value of the shear stress due to the primary flow decreases whereas the absolute value of the shear stress due to the secondary flow increases with an increase in Hall parameter. The effects of Hall current in a rotating environment will be useful in dealing with the real engineering problems.

The effects of Hall current and radiation on MHD flow of a viscous incompressible electrically conducting fluid past a moving vertical plate with variable plate temperature in the presence of a uniform transverse magnetic field have been investigated in **Chapter 5**. The dimensionless governing partial differential equations are solved by the usual Laplace transform technique. It is found that the Hall parameter accelerates the primary velocity as well as the magnitude of the secondary velocity. The temperature reduces with an increase in radiation parameter. This result qualitatively agrees with expectations, since the effect of radiation is to decrease the rate of energy transport to the fluid, thereby decreasing the temperature of the fluid. Further, the absolute value of the shear stress due to the primary flow at the moving plate decreases whereas the absolute value of the shear stress due to the secondary flow at the moving plate increases with an increase in Hall parameter. The rate of heat transfer at the plate increases with an increase in either Prandtl number or radiation parameter.

In **Chapter 6**, the combined effects of Hall current and rotation on MHD Couette flow of a viscous incompressible electrically conducting fluid between two infinitely long horizontal parallel porous plates channel in a rotating system in the presence of a uniform transverse magnetic field have been studied. The dimensionless governing partial differential equations are solved by the usual Laplace transform technique. The effects of pertinent parameters are analyzed graphically on the velocity and shear stress. It is found that the primary velocity and the magnitude of the secondary velocity decrease with an increase in Hall parameter. It is also found that the solution for small time converges more rapidly than the general solution. The asymptotic behavior of the solution is analyzed for small as well as large values of magnetic parameter, rotation parameter and Reynolds number. It is observed that a thin boundary layer is formed near the stationary plate and the thickness of the layer increases with an increase in either Hall parameter or Reynolds number while it decreases with an increase in magnetic parameter as expected since the magnetic field has a retarding influence on the flow. It is interesting to note that for large values of magnetic parameter, the boundary layer thickness is independent of the rotation parameter. The shear stresses at the stationary plate due to the primary and secondary velocities are obtained. It is found that both the shear stress due to the primary flow and magnitude of the shear stress due to secondary flow decrease with an increase in magnetic parameter when the Hall parameter is fixed while the shear stress due to primary flow first decreases, reaches a minimum and then increases and the magnitude of shear stress due to the secondary flow increases with an increase in Hall parameter when the magnetic parameter is fixed.

The combined effects of Hall current and radiation on the unsteady MHD free convective flow in a vertical channel with an oscillatory wall temperature have been studied in **Chapter 7**. The dimensionless governing partial differential equations are solved by the usual Laplace transform technique. It is observed that the primary velocity and the magnitude of the secondary velocity decrease with an increase in either radiation parameter or frequency parameter or Prandtl number for both the impulsive as well as accelerated motions of one of the channel walls. The fluid temperature increases with an increase in Prandtl number whereas it decreases with an increase in either radiation parameter or frequency parameter. Further, the shear stress due to the primary flow and the absolute value of the shear stress due to the secondary flow at the wall $\eta = 0$ decrease with an increase in either radiation parameter or Prandtl number for both the impulsive as well as accelerated motions of one of the channel walls. It is also seen that both the rate of heat transfers at the channel walls increase with an increase in radiation parameter while they decrease with an increase in frequency

parameter.

The aim concerning in **Chapter 8**, is to study the transient MHD free convective flow in a heated vertical parallel plates channel in the presence of an inclined magnetic field on taking Hall currents into the account. The effects of pertinent parameters on the velocity field, the temperature distribution, shear stresses and the rate of heat transfer have been discussed. It is found that both the primary velocity and the secondary velocity decrease with an increase in magnetic parameter. The fall of temperature will be shown with an increase in Prandtl number. Prandtl number is the ratio of the viscosity to the thermal diffusivity. An increase in thermal diffusivity leads to a decrease in Prandtl number. Therefore, thermal diffusion has a tendency to reduce the fluid temperature. The absolute values of the shear stress due to the primary flow as well as the shear stress due to the secondary flow reduce with an increase in either radiation parameter or magnetic parameter. It is also found that the rate of heat transfer at the plate increases with an increase in radiation parameter.

In **Chapter 9**, the effects of Hall current on MHD free convective flow of a viscous incompressible electrically conducting optically thick radiating fluid past a vertical porous plate in the presence of an applied transverse magnetic field and thermal radiation have been studied. The governing equations have been solved numerically using the fourth-order Runge-Kutta-Fehlberg method together with the shooting technique implemented on MatLab. The numerical results for the velocity field, temperature distribution, shear stress and the rate of heat transfer at the plate are presented graphically for pertinent parameters. It is found that the velocity components accelerate with an increase in the strength of magnetic field and buoyancy force. Further, the fluid temperature enhances for increasing values of temperature difference parameter. Suction/injection has a profound effect on the boundary layer thickness in which the suction reduces the thermal boundary layer thickness whereas injection thickens it. It is found that the shear stress increases for increasing values of magnetic parameter while it reduces with an increase in Hall parameter. The shear stresses enhance for increasing values of either magnetic parameter or Hall parameter while they reduce with an increase in Grashof number. Increasing strength of the magnetic field accelerates the primary velocity in the presence of free stream velocity. It is also found that the rate of heat transfer at the plate reduces for increasing values of heat generation parameter while it enhances with an increase in either suction parameter or Prandtl number.

Finally, **Chapter 10** covers with the conclusion and suggestion for the future work. In this last Chapter to conclude this dissertation, we would first like to remind the geometry of problems performed during this research work and in particular, the flow

characteristics which have lead to novel ideas or particularly interesting results. Then we will sketch the ideas that have arisen and that we consider important in the frame of a future continuation of this work.

Bibliography

[1] Hartmann J, Kgl. Danske Vidensk. Selsk. Mat. Fys. Medd.: **15(6)**(1937).

[2] Bershader D and Landshoff R, "Magnetohydrodynamics" in handbook of Fluid Dynamics, Streeter V.L.(ed.), McGraw-Hill Book Company, Inc., New York: (1961).

[3] Cole GH, Some aspects of Magnetohydrodynamics, Advances in phys.: **5**(1956), pp.452.

[4] Ferraro VCA and Plumpton C, An introduction to Magneto-Fluid Mech., Oxford University press: (1961).

[5] Lundquist S, Studies in Magneto-Hydrodynamics. Arkiv f Fysik: **5**(1952), pp.297.

[6] Spitzer L, Physics of fully ionized gases, 2nd Ed., Wiley Inter-sci., New York: (1962).

[7] Harris LP, Hydromagnetic channel flow, Mass. Inst. Tech. press and Wiley, New York: (1960).

[8] Ehlers FE, Linearized Magnetogasdynamic channel flow with axial symmetry, ARS J.: **31(3)**(1961), pp.334.

[9] Alfvén H, Nature: **150**(1942), pp.405.

[10] Cowling TG, Magnetohydrodynamics, Intersci. publisher, Inc, New York: (1957).

[11] Bullard EC, Mon. Nat. Roy. Astro. Soc., Geophys. Suppl.: **5**(1948), pp.245.

[12] Meyer RC, J. Aerospace Sci.: **25**(1958), pp.561.

[13] Gupta AS, Acta Mechanica: **22(3-4)**, pp.281.

[14] Pop I, J. Math. Phys. Sci.: **28**(1971), pp.375.

[15] Bhadram CVV, Acta Mechanica: **24**(1976), pp.319.

[16] Mazumder BS, Gupta AS and Datta N, Int. J. Heat Mass Trans.: **19**(1976), pp.523.

[17] Jana RN and Datta N, Acta Mechanica: **28**(1977), pp.211.

[18] Jana RN, Gupta AS and Datta N, J. Phys. Soc. Jpn.: **43**(1977), pp.1767.

[19] Hossain MA and Rasid RIMI, J. Phys. Soc. Jpn: **56**(1987), pp.97.

[20] Sattar MA and Maleque MA, J. Energy, Heat and Mass Trans.: **22**(2000), pp.67.

[21] Cortell R, Appl. Math. Comput.: **170**(2005), pp.706

[22] Ghosh SK and Pop I, J. Heat and Mass Trans.: **42(7)**(2006), pp.587.

[23] Damseh RA, Duwairi HM and Al-Odat M, Turk. J. Engg. Env. Sci.: **30**(2006), pp.83

[24] Martin MJ and Boyd ID, J. Thermophys. Heat Trans.: **20**(2006), pp.710

[25] Bataller RC, Appl. Math. Comput.: **198**(2008), pp.333

[26] Cortell R, Chin. Phys. Lett.: **25**(2008), pp.1340

[27] Maji SL, Kanch AK, Guria M and Jana RN, Appl. Math. Mech.: **30(4)**(2009), pp.503.

[28] Aziz A, Commun. Nonlinear Sci. Numer. Simulat.: **15**(2010), pp.573

[29] Bhattacharyya K, Mukhopadhyay S and Layek GC, Chin. Phys. Lett.: **28(2)**(2011), pp.247.

[30] Gupta AS, Guria M and Jana RN, Int. J. Non-Linear Mech.: **46(8)**(2011), pp.1057.

[31] Makinde OD, Brazilian J. Chemical Engg.: **29(1)**(2012), pp.159.

[32] Jana M, Das S, Maji SL, Jana RN and Ghosh SK, J. Porous Media: **15(6)**(2012), pp.585.

[33] Das S, Mandal HK, Jana RN and Makinde OD, J. Nanofluids: **4(2)**(2015), pp.167.

[34] Muthukumaraswamy R, Ganesan P and Souldalgekar VM, J. Energy, Heat and Mass Trans.: **23**(2001), pp.63.

[35] Makinde OD, Mango JM and Theuri DM, A.M.S.E., Modelling, Measurement and Control: **72(3-4)**(2003), pp.39.

[36] Panda JP, Dash GC and Dash SS, AMSE Modelling B: **72(3)**(2003), pp.47.

[37] Singh AK, Astro. Space Sci.: **93**(1983), pp.1767.

[38] Soundalgekar VM, Proc. R. Soc., A: **333**(1973), pp.25.

[39] Aldos TK, Al-Nimar MA, Jarrah MA and Al-Shaer B, Numerical Heat Trans. A: **28**(1995), pp.635.

[40] Jana RN, J. Appl. Physics, Jpn.: **13**(1974), pp.1443.

[41] Sacheti NC, Chandran P and Singh AK, Int. Commun. Heat Mass Trans.: **21**(1994), pp.131.

[42] Anwar K, J. of Appl. Math. and Mecha.: **78**(1998), pp.255.

[43] Hossain MA and Takhar HS, Heat Mass Trans.: **31(4)**(1996), pp.243.

[44] Takhar HS, Gorla RSR and Soundalgekar VM, Int. J. Numerical Methods heat Fluid Flow: **6**(1996), pp.77.

[45] Kim SJ and Vafai K, Int. J. Heat and Mass Trans.: **32**(1989), pp.665.

[46] Liao SJ and Pop I, Int. J. Heat and Mass Trans.: **47**(2004), pp.75.

[47] Sattar MA, Rahman MM and Alam MM, J. Energy Res.: **22(1)**(2000), pp.17.

[48] Revankar ST, Mech. Res. Comm.: **27**(2000), pp.241.

[49] Chamkha AJ and Abdul-Rahim Khaled A, Int. J. Numerical methods for heat and Fluid Flow: **10(5)**(2000), pp.455.

[50] Raptis A and Perdikis C, Forschung in Ingenieurwesen: **67(5)**(2002), pp.206.

[51] Israel-Cookey C and Sigalo FB, AMSE Modelling B: **72(3)**(2003), pp.25.

[52] Sahoo PK, Datta N and Biswal S, Indian J. pure Appl. Math.: **34(1)**(2003), pp.145.

[53] Ganesan P and Palani G, Int. J. Heat Mass Trans.: **47**(2004), pp.4449.

[54] Ferdows M, Sattar MA and Siddiki MNA, Thammasat Int. J. Sci. Tech.: **9(3)**(2004), pp.19.

[55] Magyari E, Pop I and Keller B, J. Engg. Math.: **48**(2004), pp.93.

[56] Chamkha AJ, Int. J. Engg. Sci.: **42**(2004), pp.217.

[57] Alam MS and Rahman MM, J. Nav. Arc. Mar. Engg.: **2(1)**(2005), pp.55.

[58] Makinde OD, Int. Comm. Heat Mass Trans.: **32**(2005), pp.1411.

[59] Alam MS, Rahman MM and Maleque MA, Thammasat Int. J. Sci. Tech.: **10(3)**(2005), pp.1.

[60] Samad MA and Rahman MM, J. Naval Architecture and Marine Engg.: **3**(2006), pp.7.

[61] Cao K and Baker J, Int. J. Heat Mass Trans.: **52**(2009), pp.3829

[62] Perdikis C and Rapti E, Int. J. Appl. Mech. Engg.: **11(2)**(2006), pp.383.

[63] Das S, Mandal C and Jana RN, Int. J. Comp. Appl.: **41(13)**(2012), pp.36.

[64] Shateyi S, Sibanda P and Motsa SS, J. Heat Trans.: **129(12)**(2007), pp.1708.

[65] Chaudhary RC and Jain A, Rom. J. Phys.: **52(57)**(2007), pp.505.

[66] Zueco J, Appl. Mathematical Modelling: **31(9)**(2007), pp.2019.

[67] Aydin O and Kaya A, Heat Mass Trans.: **45(2)**(2008), pp.239.

[68] Aydin O and Kaya A, Appl. Math. Model.: **33(11)**(2009), pp.4086.

[69] Chaudhary RC and Jah AK, Latin American Appl. Res.: **38**(2008), pp.17.

[70] Makinde OD, Int. J. Numerical Methods for Heat and Fluid Flow: **19(3/4)**(2009), pp.546.

[71] Palani G and Srikanth U, Nonlinear Analysis: Modelling and control: **14(3)**(2009), pp.345.

[72] Makinde OD and Aziz A, Int. J. of Thermal Sci.: **49(9)**(2010), pp.1813.

[73] Rajput US and Kumar S, Appl. Mathematical Sci.: **5(3)**(2011), pp.149.

[74] Rao AMM, RamanaMurthy CV and RamanaReddy GV, Int. J. Math. Archive: **2(3)**(2011), pp.399.

[75] Mandal C, Maji SL, Das S and Jana RN, Adv. in Theoretical and Appl. Math.: **6(5)**(2011), pp.579.

[76] Das S, Sarkar BC and Jana RN, Meccanica: **48(6)**(2013), pp.1387.

[77] Seth GS, Mahato GK and Sarkar S, Int. J. Appl. Mech. and Engg.: **18(4)**(2013), pp.1201.

[78] Seth GS, Sharma R and Hussain SM, Emirates J. Engg. Res.: **19(2)**(2014), pp.19.

[79] Seth GS, Tripathi R and Sharma R, Int. J. Heat and Tech.: **33(3)**(2015), pp.139.

[80] Seth GS, Sarkar S and Nandkeolyar R, J. Appl. Fluid Mech.: **8(3)**(2015), pp.623.

[81] Seth GS, Sarkar S and Sharma R, Int. J. Appl. Mech. and Engg.: **21(1)**(2016), pp.187.

[82] Makinde OD, Meccanica: **47(5)**(2012), pp.1173.

[83] Mutuku-Njane WN and Makinde OD, J. Computational and Theoretical Nanosci.: **11(3)**(2014), pp.667.

[84] Khan WA, Makinde OD and Khan ZH, Int. J. Heat and Mass Trans.: **74**(2014), pp.285.

[85] Khan WA, Culham R and Makinde OD, The Canadian J. Chemical Engg.: **93(10)**(2015), pp.1830.

[86] Das S, Jana RN and Makinde OD, J. Nanofluids: **4(4)**(2015), pp.494.

[87] Gubanov AJ and Lunkin PT, Soviet Phys. Tech. Phys.: **5**(1960), pp.984.

[88] Katagiri M, J. Phys. Soc. Jpn.: **17**(1962), pp.393.

[89] Gupta AS, The Mathematics Student: **XL**(1972), pp.103.

[90] Jana RN and Datta N, Acta Mech.: **26**(1977), pp.301.

[91] Mazumder BS, Trans. ASME J. Appl. Mech.: **58**(1991), pp.1104.

[92] Ganapathy R, ASME J. Appl. Mech.: **61**(1994), pp.208.

[93] Das BK, Guria M and Jana RN, Meccanica: **43** (2008), pp.517.

[94] Mondal G, Mandal KK and Choudhury G, J. Phys. Soc. Jpn: **51**(1982), pp.2010.

[95] Mondal G and Mandal KK, J. Phys. Soc. Jpn: **52(2)**(1983), pp.470.

[96] Seth GS and Ahmad N, J. ISTAM: **30**(1985), p.177.

[97] Hayat T, Nadeem S and Asghar S, Int. J. Engg. Sci.: **42** (2004a), pp.123.

[98] Hayat T, Nadeem S, Siddiqui AM and Asghar S, Appl. Math. Lett.: **17(5)**(2004b), pp.609.

[99] Hayat T, Wang Y and Hutter K, Int. J. Nonlinear Mech.: **39(6)**(2004c), pp.1027.

[100] Kumar A, Seth GS and Talib A, Acta Ciencia Indica: **XXXIII M**(2007), pp.937.

[101] Seth GS, Nandkeolyar R and Ansari MS, Int. J. Acad. Res.: **1(2)**(2009), pp.6.

[102] Seth GS, Hussian SM and Singh JK, J. Appl. Math. and Bioinformatics: **1(1)**(2011), pp.31.

[103] Jana RN, Datta N and Mazumder BS, J. Phys. Soc. Jpn.: **42**(1977), pp.1034.

[104] Jana RN and Dogra G, Mathematical Forum: **11**(1997), pp.26.

[105] Guria M, Jana RN and Ghosh SK, Int. J. Non-Linear Mech.: **41(6/7)**(2006), pp.838.

[106] Das BK, Guria M and Jana RN, Meccanica: **43**(2008), pp.517.

[107] Seth GS, Ansari MS and Nandkeolyar R, Int. J. Appl. Math. Mech.: **6(7)**(2010), pp.24.

[108] Singh KD, J. of Appl. Math. and Mech.: **80**(2000), pp.429.

[109] Guria M, Das S, Jana RN and Ghosh SK, Meccanica: **44**(2009), pp.555.

[110] Patra RR, Maji SL, Das S and Jana RN, Int. J. Fluid Mech. Res.: **37 (3)**(2010), pp.251.

[111] Beg OA, Ghosh SK and Narahari M, Chem. Engg. Comm.: **198(2)**(2011), pp.235.

[112] Chekmerev IB, PMM: **25**,(1961), pp.701.

[113] Soundalgekar VM, Desai GA and Gupta AS, Bulletin de la classe des sci., 5e, Series-Tome LX.: (1974).

[114] Soundalgekar VM, IEEE Trans. Plasma Sci.: **7**(1979), pp.178.

[115] Jana RN and Datta N, Int. J. Engg. Sci.: **15**(1977), pp.35.

[116] Soundalgekar VM, Vighnesam NV and Takhar HS, IEEE, Transactions on Plasma Sci.: **7**(1978), pp.178.

[117] Jana RN and Datta N, Czech. J. Physics: **30**(1980), pp.659.

[118] Ghara N, Maji SL, Das S, Jana RN and Ghosh SK, Open J. Fluid Dynamics: **2**(2012), pp.1.

[119] Jana RN and Kanch AK, J. Physical Sci.: **7**(2001), pp.74.

[120] Mandal G, Mandal KK and Choudhury G, J. Phys. Soc. Jpn.: **51**(1982), pp.2010.

[121] Mandal G and Mandal KK, J. Phys. Soc. Jpn.: **52 (2)**(1983), pp.470.

[122] Ghosh SK and Pop I, Int. J. Appl. Mech. Engg.: **9(2)**(2004), pp.293.

[123] Das S, Sarkar BC and Jana RN, Int. J. Comp. Appl.: **35(13)**(2011), pp.22.

[124] Maji SL, Das S and Jana RN, J. Mech.: **29(03)**(2013), pp.443.

[125] Ghosh SK and Pop I, Int. J. Appl. Mech. and Engg.: **8(1)**(2003), pp.43.

[126] Seth GS, Nadkeslyar R and Ansari MS, Int. J. Acad. Res.: **1**(2009), pp.6.

[127] Ghosh SK, Beg OA and Narahari M, Meccanica: **44**(2009), pp.741.

[128] Sarkar BC, Das S and Jana RN, J. Appl. Sci., Engg. and Tech.: **5(6)**(2013), pp.1864.

[129] Das S, Ghara N and Jana RN, J. Natural Sci. and Sustainable Tech.: **7(3)**(2013), pp.291.

[130] Seth GS, Mahato GK and Sarkar S, J. Magnetohydrodynamics, Plasma and Space Res.: **18(1)**(2013), pp.75.

[131] Ghosh SK and Pop I, Int. J. Appl. Mech. Engg.: **11(4)**(2006), pp.845.

[132] Seth GS and Singh JK, J. Magnetohydrodynamics, Plasma and Space Res.: **18(1)**(2013), pp.51.

[133] Makinde OD and Franks O, Open Engg.: **4(1)**(2014), pp.54.

[134] Sato H, J. Phys. Soc. Jpn: **16**(1961), pp.1427.

[135] Yamanishi T, Annual Meeting Phys. Soc., Jpn: **5**(1962), pp.29.

[136] Sherman A and Sutton GW, Engg. Magnetohydrodynamics, McGraw-Hill, Inc. New York: (1965), pp.363.

[137] Ostrach S, NACA TN: (1952), pp.2863.

[138] Ostrach S, NACA TN: (1958), pp.3458.

[139] Tao LN, J. Heat trans.: **82**(1960), pp.233.

[140] Luber TS and Welch AU, Proceedings of Third Int. Heat Trans. Conferrence, Chicago, Illinois: (1966), pp.126.

[141] Bodoia JR and Osterle JF, J. Heat Trans.: **84**(1962), pp.40.

[142] Regirer RA, Soviet Phys. JETP: **37**(1960), pp.149.

[143] Mori Y, Int. Dev. Heat Trans.: **Part 5**(1961), pp.1031.

[144] Yu CP, AIAA JI: **3**(1965), pp.1184.

[145] Sparrow EM, Chrysler GM and Azevedo LF, ASME J. Heat Trans.: **106**(1984), pp.325.

[146] Kettleborough CF, Int. J. Heat Mass Trans.: **15**(1972), pp.883.

[147] Hamadah TT and Wirtz RA, ASME J. Heat Trans.: **113**(1991), pp.507.

[148] Cheng CH, Kou HS and Hung WH, J. Thermophysics and Heat Trans.: **4**(1990), pp.375.

[149] Gupta PS and Gupta AS, Int. J. Heat Mass Trans.: **17**(1974), pp.1437.

[150] Datta N and Jana RN, Int. J. Heat Mass Trans.: **19**(1976), pp.1015.

[151] Ingham DB, Keen DJ and Huggs PJ, ASME J. Heat Trans.: **110**(1998), pp.910.

[152] Poots G, Int. J. Heat Mass Trans.: **3**(1961), pp.1.

[153] Umavathi JC, Int. J. Non-linear Mech.: **31**(1996), pp.371.

[154] Ghosh SK and Nandi DK, J. Technical Physics: **41(2)**(2000), pp.173.

[155] Ghosh SK, Pop I and Nandi DK, Int. J. Appl. Mech. and Engg.: **7(4)**(2002), pp.1211.

[156] Pop I, Ghosh SK and Nandi DK, Magnetohydrodynamics: **37(4)**(2001), pp.348.

[157] Barletta A, Int. J. Heat Mass Trans.: **41**(1998), pp.3501.

[158] Umavathi JC and Malashetty MS, Int. J. Non-linear Mech.: **40**(2005), pp.91.

[159] Mazumder BS, Gupta AS and Datta N, Int. J. Engg. Sci.: **14(3)**(1976), pp.285.

[160] Datta N and Jana RN, Int. J. Engg. Sci.: **15**(1977), pp.561.

[161] Sivaprasad R, Prasad Rao DRV and Krishna DV, Ind. J. Pure Appl. Math.: **19(7)**(1988), pp.688.

[162] Guria M and Jana RN, Magnetohydrodynamics: **43(3)**(2007), pp.287.

[163] Seth GS and Ansari MS, Int. J. Theory and Application Mechanism: **4**(2009), pp.205.

[164] Guria M, Ghara N and Jana RN, Int. J. Appl. Mech. Engg.: **15(4)**(2010), pp.1065.

[165] Das S, Ghara N and Jana RN, Int. J. Math. Archive: **2(11)**(2011), pp.2429.

[166] Singh KD, Int. J. Pysical and Math. Sci.: **3**(2012), pp.194.

[167] Mandal C, Das S and Jana RN, Int. J. Appl. Infor. Sys.: **2(2)**(2012), pp.49.

[168] Singh KD, Int. J. Appl. Mech. Engg.: **18(3)**(2013), pp.849.

[169] Singh KD and Pathak R, Int. J. Appl. Math. and Mech.: **9**(2013), pp.60.

[170] Sarkar BC, Das S and Jana RN, J. Appl. Sci. and Engg. (Taiwan): **17(3)**(2014), pp.243.

[171] Sarkar BC, Das S and Jana RN, Int. J. Comp. Appl.: **74(18)**(2013), pp.9.

[172] Das S and Jana RN, Appl. Math. and Phy.: **1(3)**(2013), pp.45.

[173] Das S, Jana RN and Makinde OD, Int. J. Engg. Sci. and Tech.: **18(2)**(2015), pp.244.

[174] Das S, Jana RN and Makinde OD, Alexandria Engg. J.: **55**(2016), pp.253.

[175] Adesanya SO, Oluwadare EO, Falade JA and Makinde OD, J. Magnetism and Magnetic Materials: **396**(2015), pp.295.

Part II

Magnetohydrodynamics Problems

Chapter 2

Unsteady MHD flow and heat transfer past a porous flat plate in a rotating system*

2.1 Introduction

An investigation on MHD flow and heat transfer of an incompressible viscous fluid over a porous plate find many important applications in modern metallurgical, metal-working processes and manufacturing processes. The heat treatment of materials travelling between a feed roll and a wind-up roll or on conveyor belts, the lamination, hot rolling, wire drawing, crystal growing, purification of molten metals from non-metallic inclusions and melt-spinning processes in the extraction of polymers possess the characteristics of moving plates/surfaces. MHD also finds applications in ion propulsion, controlled fusion research, plasma jets and chemical synthesis, etc.

The hydromagnetic viscous incompressible fluid flow due to harmonic oscillations of a plane has been analysed by Kakutani[1] and exact solution are obtained for the cases of perfectly conducting and non-conducting planes (see Kakutani[2]). Hide and Roberts[3] have studied the hydromagnetic flow due to an oscillating plane. The unsteady hydromagnetic flow in a rotating fluid have been investigated by Soundalgekar and Pop[4]. Debnath[5] have made an analysis on unsteady magnetohydrodynamic boundary layers in a rotating flow. The hydromagnetic Ekman layer near an accelerated plate have been described by Datta and Mazumdar[6]. The flow of an incompressible

* *Published in* **Int. J. of Computer Application (IJCA)**, *ISSN: 0975-8887, 33(2)(2011), pp.17-26.*

viscous fluid near a porous oscillating infinite plate subject to suction or blowing have been studied by Bühler and Zierep[7]. Turbatu et al.[8] have investigated the flow of an incompressible viscous fluid on an infinite porous plate with increasing or decreasing velocity amplitude of oscillation. Attia[9] have analyzed the transient Hartmann flow with heat transfer considering the ion slip. The flow in Ekman layer on an oscillating porous plate have been investigated by Gupta et al.[10]. Gupta et al.[11] have also studied the effects of suction or blowing on the velocity and temperature distribution in the flow past a porous flat plate of a power-law fluid. The hydromagnetic flow in the Ekman layer on an oscillating porous plate have been discussed by Guria and Jana[12]. Mohyuddin et al.[13] have investigated the unsteady magneto-fluid-dynamics fluid and heat flow with suction. The MHD flow and heat transfer driving by a power-law shear over a semi-infinite flat plate has described by Akl[14].

In this chapter, we study the unsteady MHD flow and heat transfer of an incompressible electrically conducting viscous fluid past an infinite heated porous flat plate. The plate is oscillating in its own plane with the velocity $u_0\, e^{\beta^* t} \cos \omega t$, ω being the frequency of the oscillations. A uniform magnetic field of strength B_0 is imposed perpendicular to the plate. It is assumed that the magnetic Reynolds is small enough to neglect induced magnetic field. Effects of governing parameters on the velocity components, temperature distribution, shear stresses and rate of heat transfer at the plate are presented graphically and tabulated.

2.2 Mathematical formulation and its solution

Consider the unsteady flow of viscous incompressible electrically conducting fluid past an infinite heated porous flat plate with uniform suction or blowing at the plate. The plate oscillates in its own plane with the velocity $u_0\, e^{\beta^* t} \cos \omega t$ in a given direction, where ω is the frequency of the plate oscillations, β^* the accelerating index and u_0 a constant. The amplitude of oscillations decreases for acceleration ($\beta^* > 0$) and increases for deceleration ($\beta^* < 0$). We choose a Cartesian Coordinate system with x-axis along the plate, y-axis perpendicular to the plate and z-axis normal to the xy-plane. Both the plate and the fluid are in a state of rigid body rotation with uniform angular velocity Ω about the y-axis. An external uniform magnetic field of strength B_0 is imposed perpendicular to the plate [see **Figure 2.1**] and the plate is taken electrically non-conducting. The plate is kept at the constant temperature T_w. Since the plate is infinitely long along the x and z-directions, the velocity field and temperature distribution are functions of y and t only. The equation of continuity $\nabla \cdot \vec{q} = 0$ gives $\frac{\partial v}{\partial y} = 0$

which on integration yields $v = -v_0$(constant), where $\vec{q} \equiv (u, v, w)$. The constant v_0 denotes the normal velocity at the plate, is positive for suction and negative for blowing/injection. We shall assume that the magnetic Reynolds number for the flow is small so that the induced magnetic field can be neglected. This assumption is justified since the magnetic Reynolds number is generally very small for partially ionized gases. The solenoidal relation $\nabla \cdot \vec{B} = 0$ for the magnetic field gives $B_y = B_0 =$ constant everywhere in the fluid, where $\vec{B} \equiv (0, B_y, 0)$.

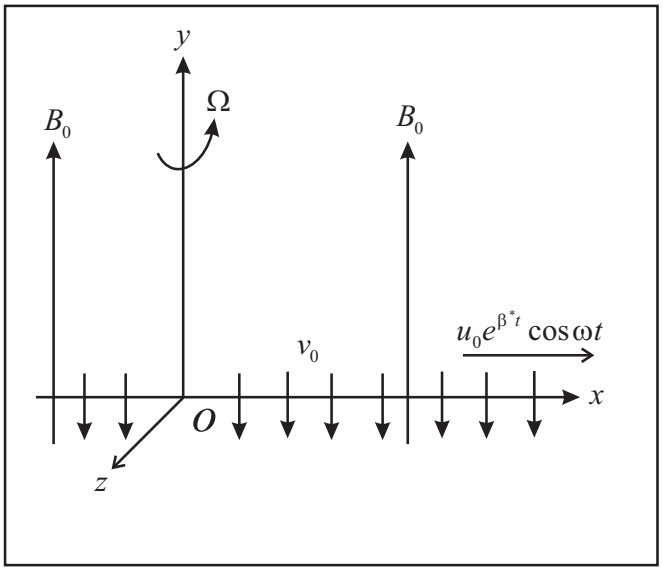

Figure 2.1: Geometry of the problem

The momentum equations along x, y and z- directions are given by

$$\frac{\partial u}{\partial t} - v_0 \frac{\partial u}{\partial y} - 2\Omega w = \nu \frac{\partial^2 u}{\partial y^2} - \frac{\sigma B_0^2}{\rho} u, \tag{2.1}$$

$$0 = -\frac{1}{\rho}\frac{\partial p}{\partial y}, \tag{2.2}$$

$$\frac{\partial w}{\partial t} - v_0 \frac{\partial w}{\partial y} + 2\Omega u = \nu \frac{\partial^2 w}{\partial y^2} - \frac{\sigma B_0^2}{\rho} w, \tag{2.3}$$

where μ_e, ρ, ν and p are respectively the magnetic permeability, the density, the kinematic viscosity and the pressure of the fluid including centrifugal force.

The boundary conditions of the problem are

$$u_1 = u_0\, e^{\beta^* t} \cos \omega\, t,\ w = 0 \text{ at } y = 0 \ \text{ and } \ u \to 0,\ w \to 0 \ \text{ as } \ y \to \infty, \tag{2.4}$$

Introducing the non-dimensional variables

$$\eta = \frac{u_0}{\nu}\, y,\ u_1 = \frac{u}{u_0},\ w_1 = \frac{w}{u_0},\ \tau = \frac{u_0^2}{\nu}\, t,\ n = \frac{\nu\,\omega}{u_0^2} \tag{2.5}$$

equations (2.1) and (2.3) become

$$\frac{\partial u_1}{\partial \tau} - S\frac{\partial u_1}{\partial \eta} - 2K^2 w_1 = \frac{\partial^2 u_1}{\partial \eta^2} - M^2\, u_1, \tag{2.6}$$

$$\frac{\partial w_1}{\partial \tau} - S\frac{\partial w_1}{\partial \eta} + 2K^2 u_1 = \frac{\partial^2 w_1}{\partial \eta^2} - M^2 w_1, \tag{2.7}$$

where $K^2 = \frac{2\omega\,\nu}{u_0^2}$ is the rotation parameter, $S = \frac{v_0}{u_0}$ the suction parameter and $M^2 = \frac{\sigma B_0^2 \nu}{\rho\, u_0^2}$ the magnetic parameter.
On the use of equation (2.5), the boundary conditions (2.4) become

$$u_1 = e^{\beta\,\tau}\cos n\tau,\ w_1 = 0 \text{ at } \eta = 0 \text{ and } u_1 \to 0,\ w_1 \to 0 \text{ as } \eta \to \infty, \tag{2.8}$$

where $\beta = \frac{\beta^* \nu}{u_0^2}$ is the dimensionless accelerated parameter.
Combining equations (2.6) and (2.7), we get

$$\frac{\partial f}{\partial \tau} - S\frac{\partial f}{\partial \eta} + 2iK^2\, f = \frac{\partial^2 f}{\partial \eta^2} - M^2 f, \tag{2.9}$$

where

$$f(\eta,\tau) = u_1(\eta,\tau) + i w_1(\eta,\tau),\ i = \sqrt{-1}. \tag{2.10}$$

The boundary conditions (2.8) now become

$$f(0) = \frac{1}{2}\left[e^{(\beta + i\,n)\tau} + e^{(\beta - i\,n)\tau}\right] \text{ and } f(\infty) = 0. \tag{2.11}$$

To solve equation (2.9) subject to the boundary conditions (2.11), we assume the solution in the following form

$$f(\eta,\tau) = f_1(\eta)e^{(\beta + i\,n)\tau} + f_2(\eta)e^{(\beta - i\,n)\tau}, \tag{2.12}$$

where f_1 and f_2 are the unknown functions of η.

Substituting equation (2.12) in the equation (2.9) we find $f_1(\eta)$ and $f_2(\eta)$ that satisfy the following equations

$$f_1''(\eta) + S f_1'(\eta) - \left[\beta + in + M^2 + 2iK^2\right] f_1(\eta) = 0, \tag{2.13}$$

$$f_2''(\eta) + S f_2'(\eta) - \left[\beta - in + M^2 + 2iK^2\right] f_2(\eta) = 0, \tag{2.14}$$

where prime denotes differentiation with respect to η.

The corresponding boundary conditions for $f_1(\eta)$ and $f_2(\eta)$ are

$$f_1(0) = \frac{1}{2},\ f_2(0) = \frac{1}{2}, \quad f_1(\infty) = 0,\ f_2(\infty) = 0. \tag{2.15}$$

The solution of equations (2.13) and (2.14) subject to the boundary conditions (2.15) are

$$f_1(\eta) = \frac{1}{2}\, e^{-(\frac{S}{2}+\alpha_1+i\,\beta_1)\eta}, \quad f_2(\eta) = \frac{1}{2}\, e^{-(\frac{S}{2}+\alpha_2 \pm i\,\beta_2)\eta}, \tag{2.16}$$

where

$$\alpha_1,\, \beta_1 = \frac{1}{\sqrt{2}}\left[\left\{\left(\frac{S^2}{4}+M^2+\beta\right)^2 + \left(2K^2+n\right)^2\right\}^{\frac{1}{2}} \pm \left(\frac{S^2}{4}+M^2+\beta\right)\right]^{\frac{1}{2}}$$

$$\alpha_2,\, \beta_2 = \frac{1}{\sqrt{2}}\left[\left\{\left(\frac{S^2}{4}+M^2+\beta\right)^2 + \left(2K^2-n\right)^2\right\}^{\frac{1}{2}} \pm \left(\frac{S^2}{4}+M^2+\beta\right)\right]^{\frac{1}{2}}, \tag{2.17}$$

and the upper sign in equation (2.16) for $n < 2K^2$ and lower sign for $n > 2K^2$.

Hence, using the equation (2.16), equation (2.12) yields

$$f(\eta,\tau) = \begin{cases} \frac{1}{2}e^{\beta\,\tau}\left[e^{-(\frac{S}{2}+\alpha_1+i\,\beta_1)\eta+in\tau} + e^{-(\frac{S}{2}+\alpha_2 \pm i\,\beta_2)\eta-in\tau}\right] & \text{for } n \neq 2K^2 \\ \\ \frac{1}{2}\left[e^{-(\frac{S}{2}+\alpha_1+i\,\beta_1)\eta+in\tau} + e^{-(\frac{S}{2}+\alpha_2^*)\eta-in\tau}\right] & \text{for } n = 2K^2 \end{cases} \tag{2.18}$$

where $\alpha_2^* = \left(\frac{S^2}{4}+M^2+\beta\right)^{\frac{1}{2}}$ and α_1, β_1, α_2 and β_2 are given by equation (2.17).

On separating into a real and imaginary parts, we have

$$u_1(\eta,\tau) \;=\; \begin{cases} \frac{1}{2}e^{\beta\,\tau}\Big[e^{-(\frac{S}{2}+\alpha_1)\eta}\cos(n\tau-\beta_1\eta) \\ \quad +e^{-(\frac{S}{2}+\alpha_2)\eta}\cos(n\tau \pm \beta_2\eta)\Big] & \text{for } n \neq 2K^2 \\ \\ \frac{1}{2}e^{\beta\,\tau}\Big[e^{-(\frac{S}{2}+\alpha_1)\eta}\cos(n\tau-\beta_1\eta) \\ \quad +e^{-(\frac{S}{2}+\alpha_2^*)\eta}\cos n\tau\Big] & \text{for } n = 2K^2 \end{cases} \tag{2.19}$$

$$w_1(\eta,\tau) = \begin{cases} \frac{1}{2}e^{\beta\tau}\left[e^{-(\frac{S}{2}+\alpha_1)\eta}\sin(n\tau-\beta_1\eta)\right. \\ \left.-e^{-(\frac{S}{2}+\alpha_2)\eta}\sin(n\tau\pm\beta_2\eta)\right] & \text{for } n\neq 2K^2 \\ \\ \frac{1}{2}e^{\beta\tau}\left[e^{-(\frac{S}{2}+\alpha_1)\eta}\sin(n\tau-\beta_1\eta)\right. \\ \left.-e^{-(\frac{S}{2}+\alpha_2^*)\eta}\sin n\tau\right] & \text{for } n=2K^2 \end{cases} \tag{2.20}$$

The above solutions are valid for both suction and blowing/injection at the plate. If $K^2 = 0$, then $w_1 = 0$ and the equation (2.19) is identical with the equations (12) of Mohyuddin et al.[13]

2.3 Results and discussion

In order to understand the effects of different physical parameters, such as magnetic parameter M^2, rotation parameter K^2, suction parameter S, frequency parameter n, accelerated parameter β, phase angle $n\tau$ and time τ, the computations are carried out for temperature and velocity of the fluid. The computed results are presented graphically.

2.3.1 Effects of parameters on the velocity profiles

It is seen from equations (2.19) and (2.20) that the velocity profile consists of two parts, one parts oscillates with amplitude $\frac{1}{2}e^{-(\frac{S}{2}+\alpha_1)\eta}$ and the other one with $\frac{1}{2}e^{-(\frac{S}{2}+\alpha_2)\eta}$, where α_1 and α_2 are given by equation (2.17). It is seen from equation (2.17) that the wave length $\frac{2\pi}{\beta_2}$ is always greater than that of $\frac{2\pi}{\beta_1}$ because β_1 is always greater than β_2. The solution represents a flow in which the oscillations decay exponentially with the distance from the plate. The layer corresponding to the former part at a distance η from the plate oscillates with phase lag of $\beta_1\eta$ while the layer corresponding to the latter part oscillates with phase advance of $\beta_2\eta$ when $n < 2K^2$ and a phase lag when $n > 2K^2$. It is interesting to note that the normal solution exists for $S = 0$ and $n = 2K^2$. This is due to the fact that $\beta_2 > 0$ when $S = 0$ and $n = 2K^2$. This result shows that the shear oscillations are also confined near the plate when $S = 0$ and $n = 2K^2$.

The effects of pertinent parameters on the primary as well as the secondary velocity are presented graphically against η in **Figures 2.2-2.9**. **Figure 2.2** shows that both the primary velocity u_1 and the magnitude of secondary velocity w_1 decreases with an increase in M^2. It clearly indicates that the transverse magnetic field opposes the transport phenomena. This is due to the fact that variation of the magnetic parameter leads to the variation of the Lorentz force due to magnetic field and the Lorentz

force produces more resistance to transport phenomena. It is observed from **Figure 2.3** that the primary velocity u_1 decreases while the magnitude of secondary velocity w_1 increases near the plate and it decreases away from the plate with an increase in K^2.

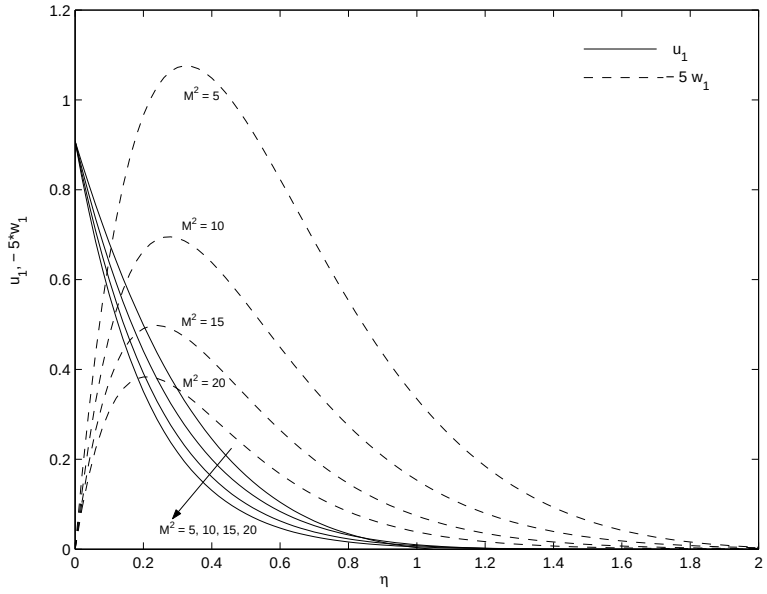

Figure 2.2: Variations of u_1 and w_1 for M^2 when $K^2 = 4$, $S = 0.5$, $n = 2$, $\beta = 0.5$, $\tau = 0.5$ and $n\tau = \frac{\pi}{4}$

Figures 2.4-2.6 show that both the primary velocity u_1 and the magnitude of secondary velocity w_1 increase with an increase in either accelerated parameter β or frequency parameter n or time τ. It is seen from **Figures 2.7-2.8** that both the primary velocity u_1 and the magnitude of secondary velocity w_1 decrease with an increase in either suction parameter S or phase angle $n\tau$. This means that the suction at the plate or the phase angle have a retarding influence on the flow field.

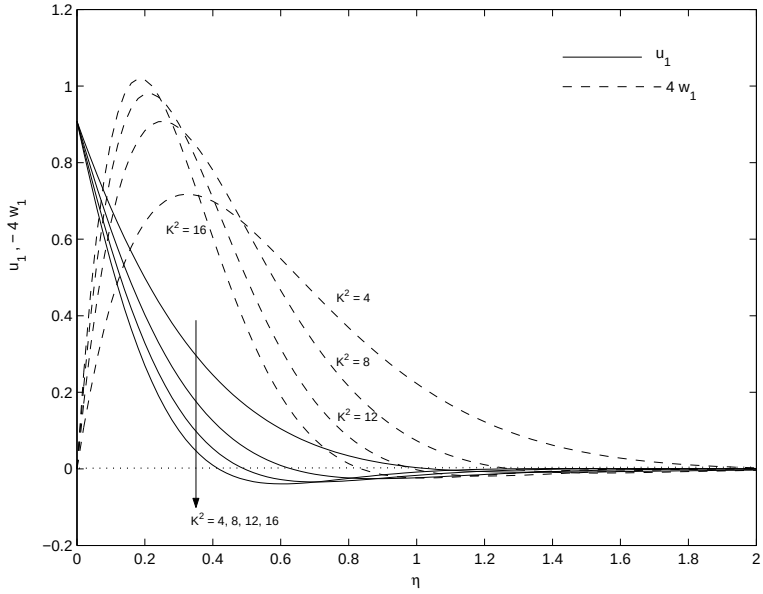

Figure 2.3: Variations of u_1 and w_1 for K^2 when $M^2 = 5$, $S = 0.5$, $n = 2$, $\beta = 0.5$, $\tau = 0.5$ and $n\tau = \frac{\pi}{4}$.

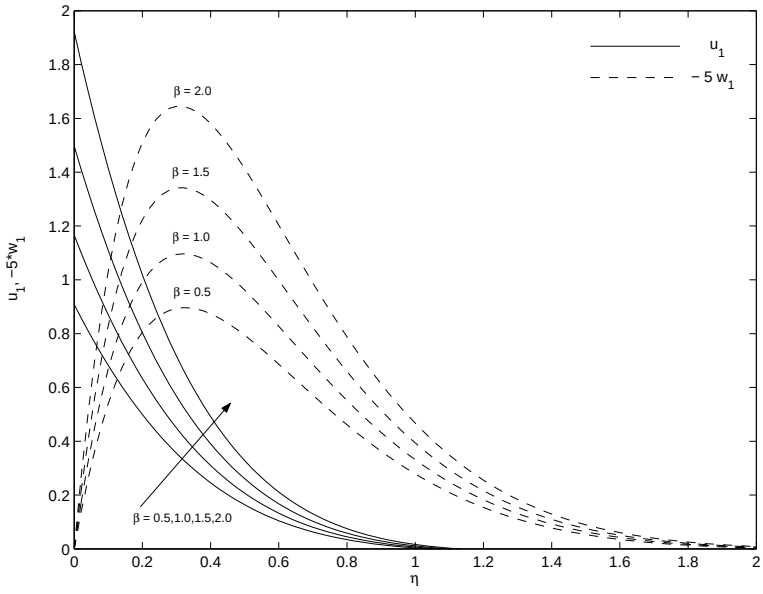

Figure 2.4: Variations of u_1 and w_1 for β when $K^2 = 4$, $S = 0.5$, $n = 2$, $M^2 = 5$, $\tau = 0.5$ and $n\tau = \frac{\pi}{4}$.

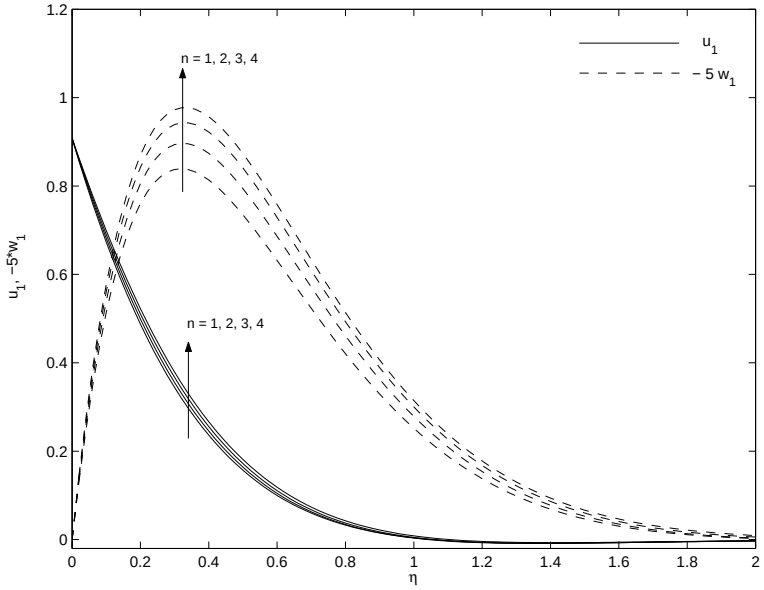

Figure 2.5: Variations of u_1 and w_1 for n when $K^2 = 4$, $S = 0.5$, $M^2 = 5$, $\beta = 0.5$, $\tau = 0.5$ and $n\tau = \frac{\pi}{4}$.

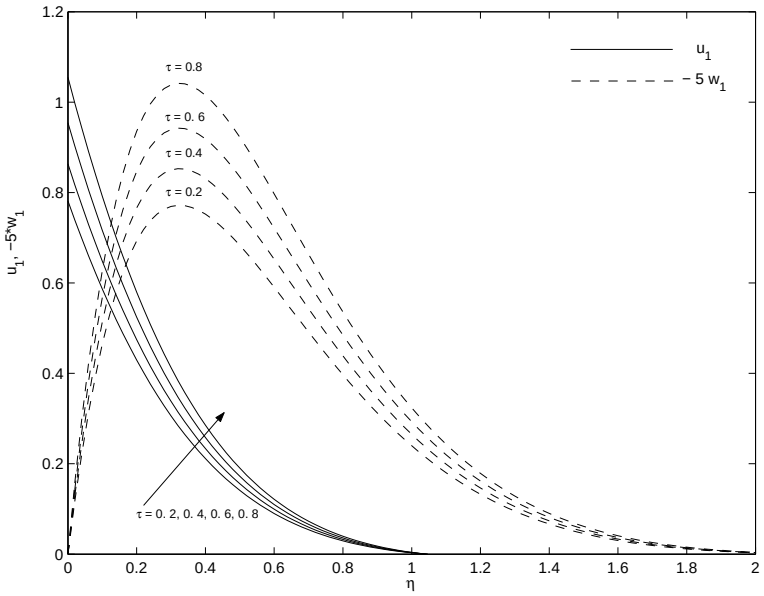

Figure 2.6: Variations of u_1 and w_1 for τ when $K^2 = 4$, $S = 0.5$, $n = 2$, $\beta = 0.5$, $M^2 = 5$ and $n\tau = \frac{\pi}{4}$.

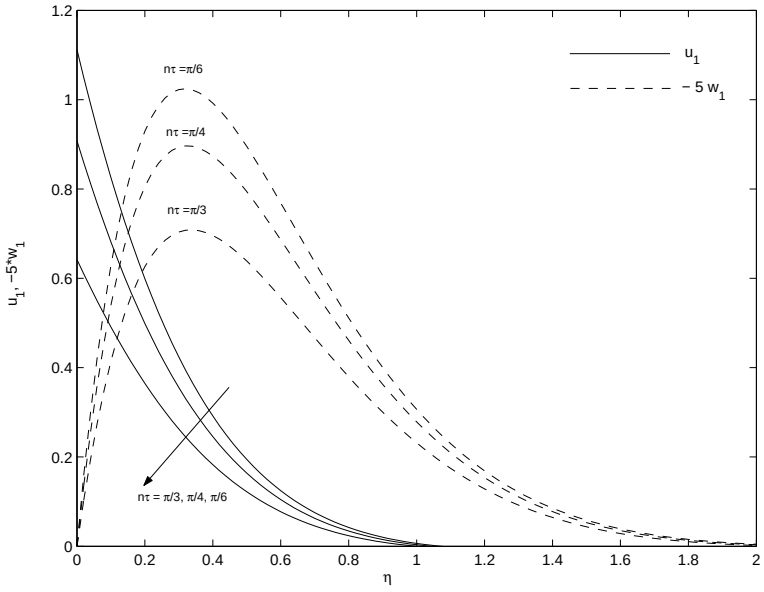

Figure 2.7: Variations of u_1 and w_1 for $n\tau$ when $K^2 = 4$, $S = 0.5$, $n = 2$, $\beta = 0.5$, $M^2 = 5$ and $\tau = 0.5$.

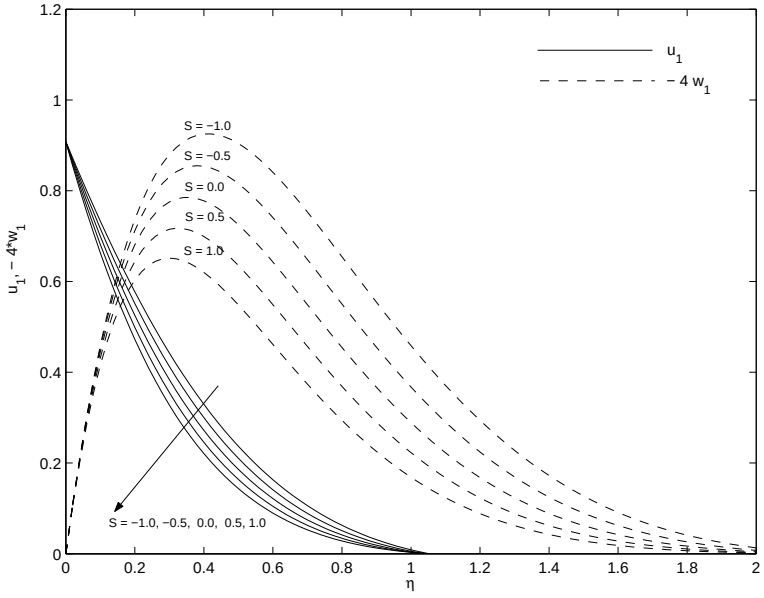

Figure 2.8: Variations of u_1 and w_1 for S when $K^2 = 4$, $M^2 = 5$, $n = 2$, $\beta = 0.5$, $\tau = 0.5$ and $n\tau = \frac{\pi}{4}$.

2.3.2 Effects of parameters on the shear stresses at the plate

For engineering purposes, one is usually interested to determine the values of the shear stresses (or skin functions). The increased shear stresses is generally a disadvantage in the technical applications.

The non-dimensional shear stress at the plate $\eta = 0$ due to the primary flow is

$$\tau_{x_0} = \left(\frac{\partial u_1}{\partial \eta}\right)_{\eta=0} = -\frac{1}{2} R_1 \cos(n\tau + \theta_1), \tag{2.21}$$

where

$$\begin{aligned} R_1^2 &= (S + \alpha_1 + \alpha_2)^2 + (\beta_1 \mp \beta_2)^2, \\ \tan\theta_1 &= \frac{(\beta_1 \mp \beta_2)}{(S + \alpha_1 + \alpha_2)}, \end{aligned} \tag{2.22}$$

Equation (2.22) shows that $0 < \tan\theta_1 < 1$. Hence from equations (2.21) and (2.17) we conclude that the shear stress due to the primary flow has a phase lead for $\theta_1 < \frac{\pi}{4}$ over the oscillations of the plate.

The non-dimensional shear stress at the plate $\eta = 0$ due to the secondary flow is

$$\tau_{y_0} = \left(\frac{\partial w_1}{\partial \eta}\right)_{\eta=0} = -\frac{1}{2} R_2 \cos(n\tau - \theta_1), \tag{2.23}$$

where

$$\begin{aligned} R_2^2 &= (\beta_1 \pm \beta_2)^2 + (\alpha_1 - \alpha_2)^2, \\ \tan\theta_2 &= \frac{(\alpha_1 - \alpha_2)}{(\beta_1 \pm \beta_2)} \end{aligned} \tag{2.24}$$

It can be seen from (2.24) that $0 < \tan\theta_2 < 1$. Hence it follows from (2.23) and (2.17) that the shear stress due to the secondary flow has a phase lag for $\theta_2 < \frac{\pi}{4}$ over the oscillations of the plate. The variations of amplitudes of shear stresses R_1, R_2 and the

tangent of the phase angles of shear stresses $\tan\theta_1$ and $\tan\theta_2$ due to primary and the secondary flows respectively against K^2 for different values of M^2, β and n with $S = 1$ and $n\tau = \frac{\pi}{4}$ are shown in **Figures 2.9-2.14**. It is observed from **Figures 2.9 and 2.10** that both the stresses R_1 and R_2 decrease with an increase in either magnetic parameter M^2 or frequency parameter n.

Figure 2.11 reveals that the amplitude R_1 increases while the amplitude R_2 decreases with an increase in accelerated parameter β. It is seen from **Figures 2.12 and 2.13** that both the tangent of the phase angles $\tan\theta_1$ and $\tan\theta_2$ decrease with an increase in either magnetic parameter M^2 or accelerated parameter β. **Figure 2.14** shows that both the tangent of the phase angles $\tan\theta_1$ and $\tan\theta_2$ increase with an increase in frequency parameter n.

The kink in the curves of the **Figures 2.12-2.14** indicates the tangent of the phase angles of the shear stresses in the critical case $n = 2K^2$.

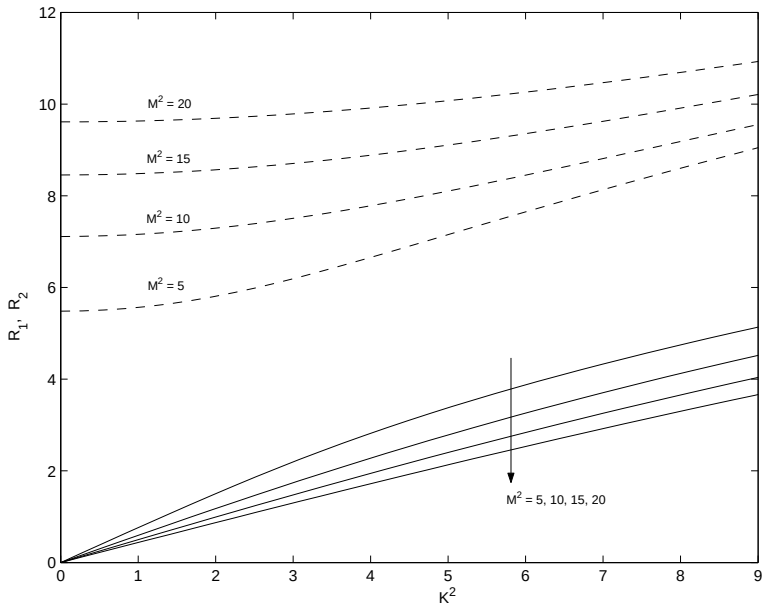

Figure 2.9: Variations of R_1 and R_2 for M^2 when $S = 0.5$, $\beta = 0.5$, $n = 4$ and $n\tau = \frac{\pi}{4}$.

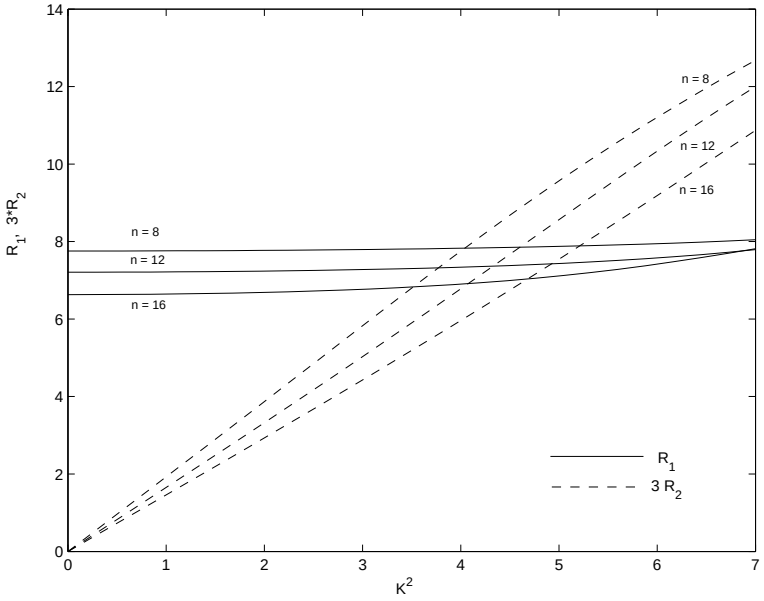

Figure 2.10: Variations of R_1 and R_2 for n when $M^2 = 5$, $\beta = 0.5$, $S = 0.5$ and $n\tau = \frac{\pi}{4}$.

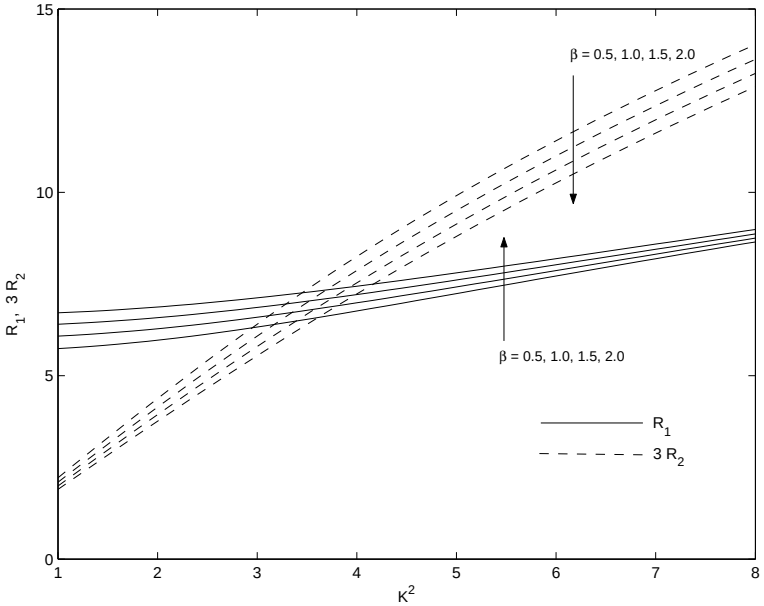

Figure 2.11: Variations of R_1 and R_2 for β when $M^2 = 5$, $n = 4$, $S = 0.5$ and $n\tau = \frac{\pi}{4}$.

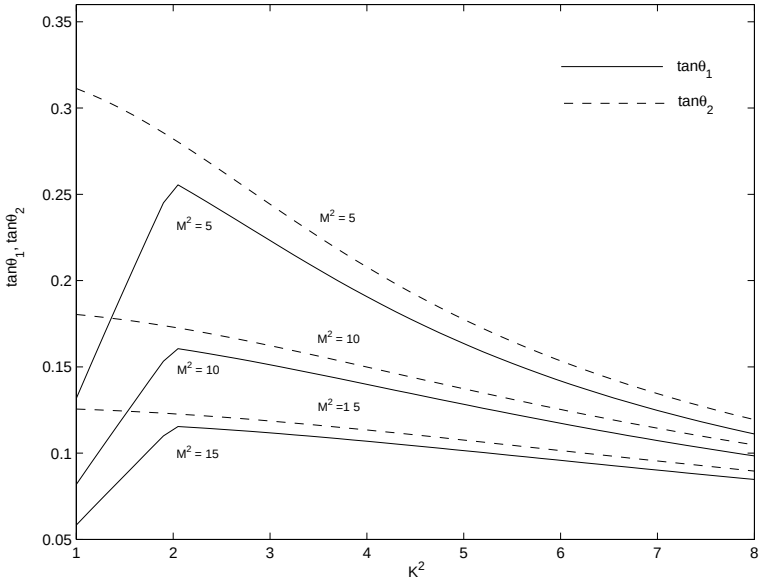

Figure 2.12: Variations of $\tan\theta_1$ and $\tan\theta_2$ for M^2 when $n = 4$, $\beta = 0.5$, $S = 0.5$ and $n\tau = \frac{\pi}{4}$.

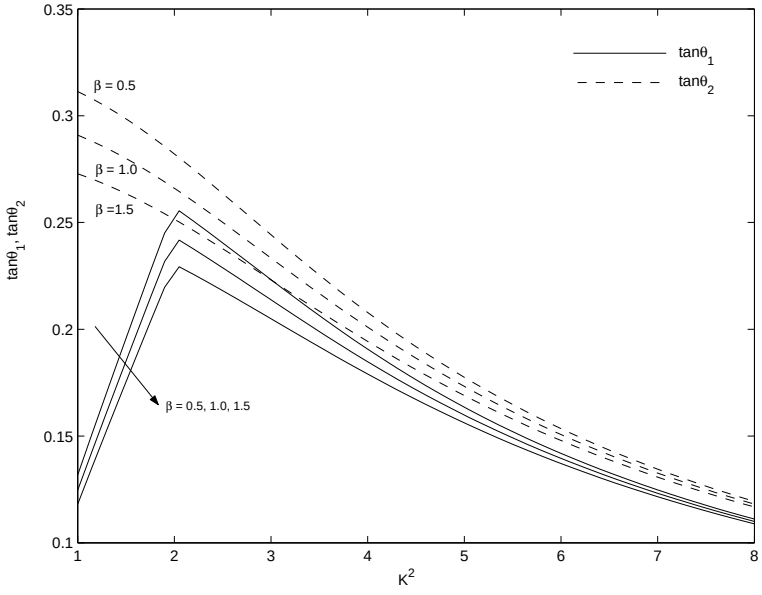

Figure 2.13: Variations of $\tan\theta_1$ and $\tan\theta_2$ for β when $n = 4$, $M^2 = 5$, $S = 0.5$ and $n\tau = \frac{\pi}{4}$.

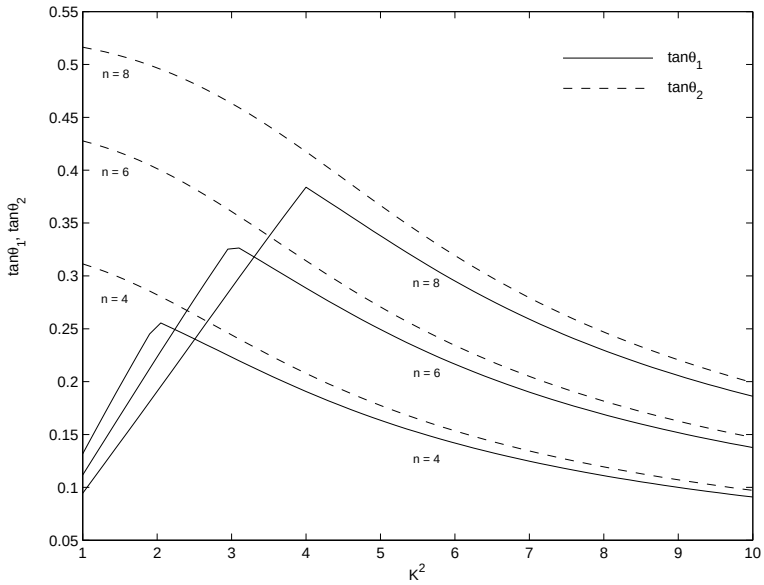

Figure 2.14: Variations of $\tan\theta_1$ and $\tan\theta_2$ for n when $M^2 = 5$, $\beta = 0.5$, $S = 0.5$ and $n\tau = \frac{\pi}{4}$.

2.4 Heat Transfer

We now discuss the temperature distribution in oscillating flow past a porous plate subject to uniform suction at the plate in the presence of a uniform magnetic field perpendicular to the flow field.

The equation of energy for the temperature distribution is

$$\rho c_p \left(\frac{\partial T}{\partial t} - v_0 \frac{\partial T}{\partial y} \right) = k \frac{\partial^2 T}{\partial y^2} + \mu \left[\left(\frac{\partial u}{\partial y} \right)^2 + \left(\frac{\partial w}{\partial y} \right)^2 \right] + \sigma B_0^2 \left(u^2 + w^2 \right), \qquad (2.25)$$

where k, μ, c_p and σ are respectively the thermal conductivity, coefficient of viscosity, specific heat of the fluid and electrical conductivity.

The last two terms within parenthesis are due to the viscous dissipation and Joule heating respectively.

The boundary conditions for temperature distribution are

$$T = T_w \text{ at } y = 0 \text{ and } T \to T_\infty \text{ as } y \to \infty, \qquad (2.26)$$

where T_∞ is the constant ambient temperature of the surrounding fluid and $T_w > T_\infty$. Introducing the non-dimensional variable

$$\theta = \frac{T - T_\infty}{T_w - T_\infty} \qquad (2.27)$$

and using equation (2.5), equation (2.25) reduced to

$$\frac{\partial\theta}{\partial t} - S\frac{\partial\theta}{\partial\eta} = \frac{1}{Pr}\frac{\partial^2\theta}{\partial\eta^2} + Ec\left[\left(\frac{\partial u_1}{\partial\eta}\right)^2 + \left(\frac{\partial w_1}{\partial\eta}\right)^2\right] + M^2\left(u_1^2 + w_1^2\right), \tag{2.28}$$

where $Ec = \frac{u_0^2}{c_p(T_w - T_\infty)}$ is the Eckert number and $Pr = \frac{\rho\, c_p\, \nu}{k}$ the Prandtl number.

The boundary conditions (2.26) become

$$\theta = 1 \text{ at } \eta = 0 \text{ and } \theta \to 0 \text{ as } \eta \to \infty. \tag{2.29}$$

Since the velocity field given by equations (2.19) and (2.20) has zero mean, we assume the solution for the temperature distribution as

$$\theta(\eta,\tau) = \theta_0(\eta)e^{2\beta\tau} + \theta_1(\eta)e^{2(\beta+in)\tau} + \overline{\theta}_1(\eta)e^{2(\beta-in)\tau}, \tag{2.30}$$

where $\theta_0(\eta)$ and $\theta_1(\eta)$ are the unknown functions of η with $\theta_0(\eta)$ represents the mean part and $\bar{\theta}_1(\eta)$ represents the complex conjugate of $\theta_1(\eta)$.

Substituting equation (2.30) in the equation (2.28) and equating the harmonic coefficients to zero, we get

$$\frac{d^2\theta_0}{d\eta^2} + SPr\frac{d\theta_0}{d\eta} = -EcPr\left[A_1 e^{-(S+2\alpha_1)\eta} + A_2 e^{-(S+2\alpha_2)\eta}\right], \tag{2.31}$$

$$\frac{d^2\theta_1}{d\eta^2} + SPr\frac{d\theta_1}{d\eta} - 2(\beta+in)Pr\theta_1 = -EcPr(c_r + ic_i)e^{-(\alpha_3+i\beta_3)\eta}, \tag{2.32}$$

$$\frac{d^2\bar{\theta}_1}{d\eta^2} + SPr\frac{d\bar{\theta}_1}{d\eta} - 2(\beta-in)Pr\bar{\theta}_1 = -EcPr(c_r - ic_i)e^{-(\alpha_3-i\beta_3)\eta}, \tag{2.33}$$

where

$$\begin{aligned}
A_1 &= \frac{1}{4}\left[\left(\frac{S}{2}+\alpha_1\right)^2 + {\beta_1}^2 + M^2\right], A_2 = \frac{1}{4}\left[\left(\frac{S}{2}+\alpha_2\right)^2 + {\beta_2}^2 + M^2\right], \\
c_r &= \frac{1}{4}\left[\left(\frac{S}{2}+\alpha_1\right)\left(\frac{S}{2}+\alpha_2\right) \pm \beta_1\beta_2 + M^2\right], \\
c_i &= \frac{1}{4}\left[\beta_1\left(\frac{S}{2}+\alpha_2\right) \mp \beta_2\left(\frac{S}{2}+\alpha_1\right)\right], \\
\alpha_3 &= S + \alpha_1 + \alpha_2, \\
\beta_3 &= \beta_1 \mp \beta_2.
\end{aligned} \tag{2.34}$$

with the upper sign in equation (2.34) for $n < 2K^2$ and the lower sign for $n > 2K^2$.

The boundary conditions for $\theta_0(\eta)$, $\theta_1(\eta)$ and $\bar{\theta_1}(\eta)$ become

$$\theta_0 = 1,\ \theta_1 = 0,\ \bar{\theta_1} = 0,\ \text{at } \eta = 0$$

and

$$\theta_0 \to 0,\ \theta_1 \to 0,\ \bar{\theta_1} \to 0 \text{ as } \eta \to \infty. \tag{2.35}$$

The solution of the equation (2.31) subject to the boundary conditions (2.35) is

$$\theta_0(\eta) = \begin{cases} e^{-SPr\,\eta} + Pr\,Ec\left[\frac{A_1\{e^{-(S+2\alpha_1)\eta} - e^{-SPr\eta}\}}{(S+2\alpha_1)(SPr-S-2\alpha_1)} + \frac{A_2\{e^{-(S+2\alpha_2)\eta} - e^{-SPr\eta}\}}{(S+2\alpha_2)(SPr-S-2\alpha_2)}\right] \\ \text{for } S+2\alpha_1 \neq SPr,\ \ S+2\alpha_2 \neq SPr \\ \\ e^{-SPr\,\eta} + Pr\,Ec\left[\frac{A_1}{SPr}\eta\, e^{-SPr\,\eta} + \frac{A_2\{e^{-(S+2\alpha_2)\eta} - e^{-SPr\eta}\}}{(S+2\alpha_2)(SPr-S-2\alpha_2)}\right] \\ \text{for } S+2\alpha_1 = SPr,\ \ S+2\alpha_2 \neq SPr \\ \\ e^{-SPr\,\eta} + Pr\,Ec\left[\frac{A_2}{SPr}\eta\, e^{-SPr\,\eta} + \frac{A_1\{e^{-(S+2\alpha_1)\eta} - e^{-SPr\eta}\}}{(S+2\alpha_1)(SPr-S-2\alpha_1)}\right] \\ \text{for } S+2\alpha_1 \neq SPr,\ \ S+2\alpha_2 = SPr \end{cases} \tag{2.36}$$

where α_1 and α_2 are given by equation (2.17).

The solution of the equation (2.32) subject to boundary conditions (2.35) is

$$\theta_1(\eta) = \frac{EcPr(c_r + ic_i)}{d_r + id_i}\left[e^{-(\alpha_4+i\beta_4)\eta} - e^{-(\alpha_3+i\beta_3)\eta}\right], \tag{2.37}$$

where

$$\begin{aligned} \alpha_4 &= \frac{1}{2\sqrt{2}}\left[\sqrt{2}SPr + \left\{\left[\left(S^2Pr^2 + 8\beta\,Pr\right)^2 + 64Pr^2n^2\right]^{\frac{1}{2}} + \left(S^2Pr^2 + 8\beta\,Pr\right)\right\}^{1/2}\right], \\ \beta_4 &= \frac{1}{2\sqrt{2}}\left\{\left[\left(S^2Pr^2 + 8\beta\,Pr\right)^2 + 64Pr^2n^2\right]^{\frac{1}{2}} - \left(S^2Pr^2 + 8\beta\,Pr\right)\right\}^{1/2}, \\ d_r &= \alpha_3^2 - SPr\,\alpha_3 - \beta_3^2 - 2\beta\,Pr,\ \ d_i = 2\alpha_3\beta_3 - SPr\beta_3 - 2nPr. \end{aligned} \tag{2.38}$$

Since the equation (2.33) is the complex conjugate of the equation (2.32) so the solution of the equation (2.33) is obtained on taking the complex conjugate of θ_1 in equation (2.37).

2.4.1 Effects of parameters on the temperature profiles

The effects of pertinent parameters such as magnetic parameter M^2, rotation parameter K^2, suction parameter S, frequency parameter n, accelerated parameter β and

time τ on the temperature distribution are presented graphically against η in **Figures 2.15-2.20**.

It is seen from **Figures 2.15-2.17** that the mean temperature $\theta_0(\eta)$ increases with an increase in either magnetic parameter M^2 or rotation parameter K^2 or frequency parameter n. It is seen from **Figure 2.18** that the mean temperature $\theta_0(\eta)$ increases near the plate and it decreases away from the plate with an increase in Prandtl number Pr.

The increase in Prandtl number Pr means that the thermal diffusivity decreases. So the temperature is decreased due to the decrease of thermal boundary layer. This characteristic indicates that the temperature dependent fluid viscosity plays a significant role in shifting the fluid away from the plate.

Further, **Figures 2.19-2.20** shows the mean temperature $\theta_0(\eta)$ decreases with an increase in either accelerated parameter β or suction parameter S.

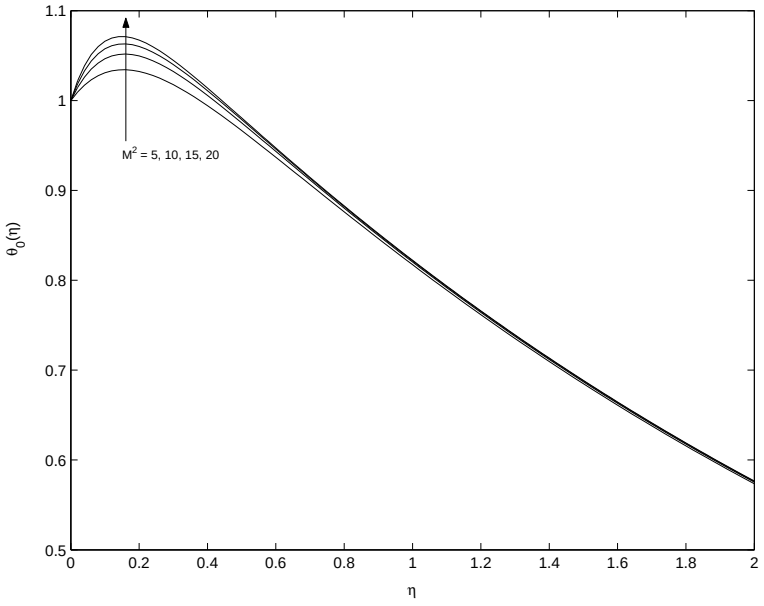

Figure 2.15: Variation of $\theta_0(\eta)$ for M^2 when $K^2 = 2$, $S = 1$, $\beta = 0.5$, $n = 4$ and $Pr = 0.71$.

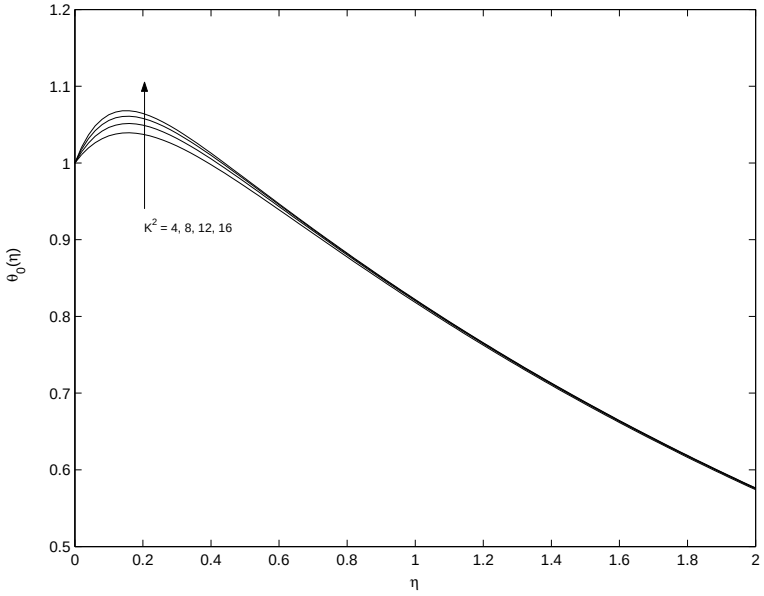

Figure 2.16: Variation of $\theta_0(\eta)$ for K^2 when $M^2 = 5$, $S = 1$, $\beta = 0.5$, $n = 4$ and $Pr = 0.71$.

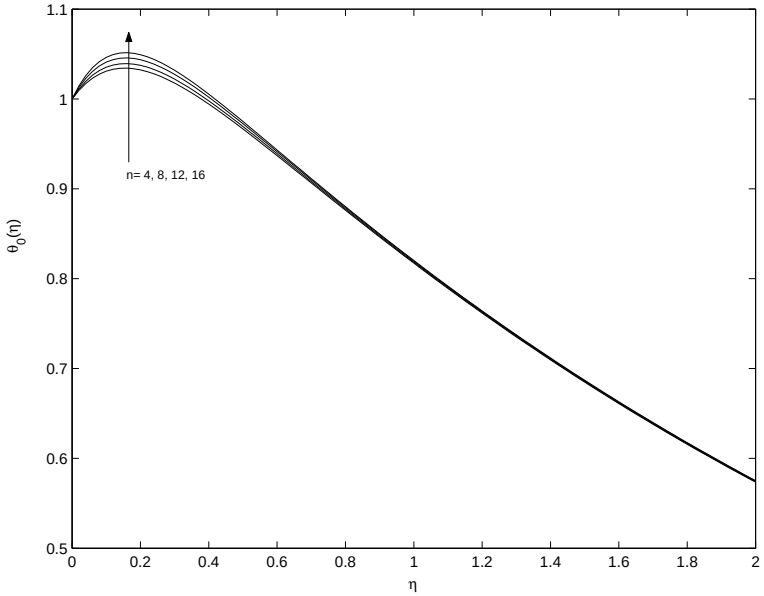

Figure 2.17: Variation of $\theta_0(\eta)$ for n when $K^2 = 2$, $S = 1$, $\beta = 0.5$, $M^2 = 5$ and $Pr = 0.71$.

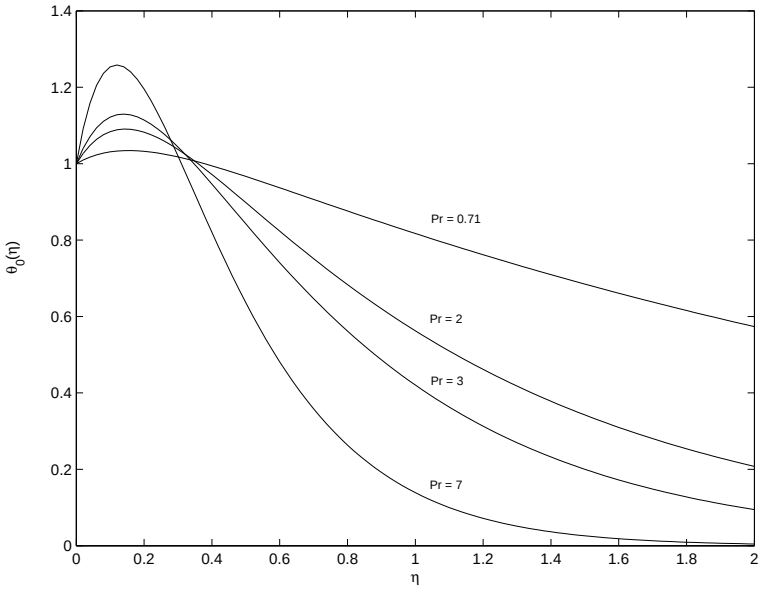

Figure 2.18: Variation of $\theta_0(\eta)$ for Pr when $K^2 = 2$, $S = 1$, $\beta = 0.5$, $n = 4$ and $M^2 = 5$.

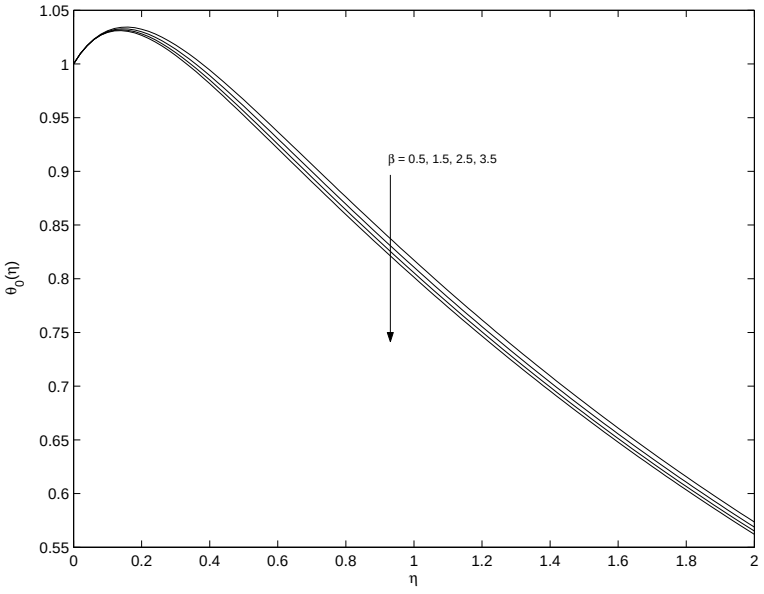

Figure 2.19: Variation of $\theta_0(\eta)$ for β when $K^2 = 2$, $S = 1$, $M^2 = 5$, $n = 4$ and $Pr = 0.71$.

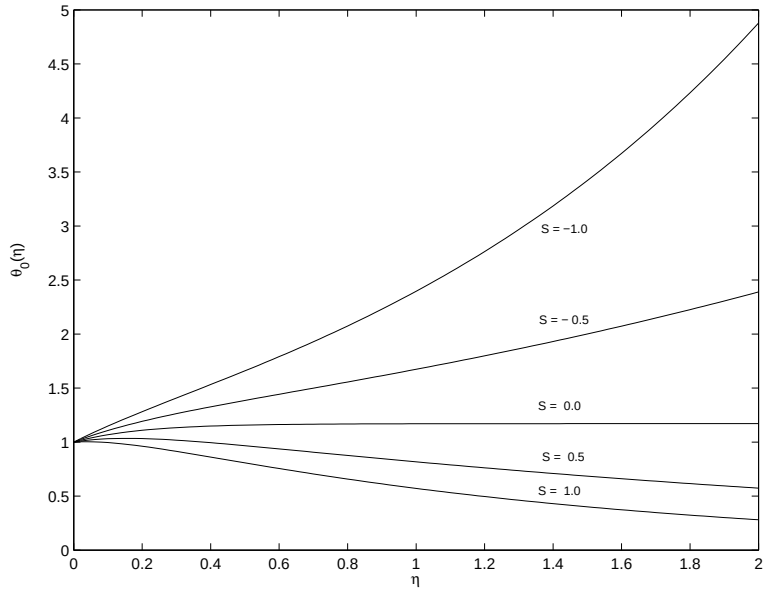

Figure 2.20: Variation of $\theta_0(\eta)$ for S when $K^2 = 2$, $M^2 = 5$, $\beta = 0.5$, $n = 4$ and $Pr = 0.71$.

2.4.2 Effects of parameters on the rate of heat transfer at the plate

The rate of heat transfer is important in the heat transfer studies, since it is directly related to the heat transfer coefficient.
The rate of heat transfer $\theta'(0,\tau)$ at the plate $\eta = 0$ is given by

$$\theta'(0,\tau) = \theta_0'(0) + 2EcPr\, R_3 \cos(2n\tau + \psi), \tag{2.39}$$

where

$$\begin{aligned} R &= d_r^2 + d_i^2, \\ X &= d_r(\alpha_3 - \alpha_4) + d_i(\beta_3 - \beta_4), \;\; Y = d_r(\beta_3 - \beta_4) - d_i(\alpha_3 - \alpha_4), \\ R_3^2 &= \left(\frac{c_r X - c_i Y}{R}\right)^2 + \left(\frac{c_i X + c_r Y}{R}\right)^2, \;\; \tan\psi = \frac{c_i X + c_r Y}{c_r X - c_i Y}. \end{aligned} \tag{2.40}$$

and

$$\theta_0'(0,\tau) = -SPr + Ec\,Pr\left(\frac{A_1}{S + 2\alpha_1} + \frac{A_2}{S + 2\alpha_2}\right), \tag{2.41}$$

whether $S + 2\alpha_1 \neq SPr$ and $S + 2\alpha_2 \neq SPr$ or $S + 2\alpha_1 = SPr$ and $S + 2\alpha_2 \neq SPr$ or $S + 2\alpha_1 \neq SPr$ and $S + 2\alpha_2 = SPr$.

The variation of amplitude of the rate of heat transfer oscillations R_3 and tangent of the phase angle of the rate of heat transfer oscillations $\tan\psi$ are shown in **Tables-I and -II** against K^2 for different values of Pr and n. It is found from **Table-I** that the amplitude R_3 increases with an increase in either rotation parameter K^2 or Prandtl number Pr while it decreases with an increase in frequency parameter n for fixed values of K^2. Farther, it is seen from **Table-II** that the magnitude of tangent of the phase angle $\tan\psi$ decreases with an increase in either rotation parameter K^2 or Prandtl number Pr while it increases with an increase in frequency parameter n for fixed values of K^2.

Table-I

Amplitude of the rate of heat transfer oscillations $10^{-3}R_3$ at the plate $\eta = 0$ for $M^2 = 5$, $n\tau = \frac{\pi}{4}$, $S = 0.5$, $\beta = 0.5$ and $Ec = 1$.

	Pr *with* $n = 10$				n *with* $Pr = 0.71$			
K^2	2	3	5	7	2	3	4	5
2	*0.73404*	*1.30662*	*2.62981*	*4.09991*	*0.08581*	*0.07295*	*0.06333*	*0.05243*
4	*0.86068*	*1.66219*	*3.56860*	*5.72213*	*0.22280*	*0.15159*	*0.11029*	*0.09011*
6	*1.09687*	*2.37460*	*5.54698*	*9.21527*	*0.61287*	*0.42904*	*0.30145*	*0.21324*
8	*1.23906*	*3.10512*	*8.01130*	*13.85063*	*1.40193*	*1.03917*	*0.77118*	*0.56806*

Table-II

The magnitude of tangent of the phase angle of the rate of heat transfer oscillations $\tan\psi$ at the plate $\eta = 0$ for $M^2 = 5$, $n\tau = \frac{\pi}{4}$, $S = 0.5$, $\beta = 0.5$ and $Ec = 1$.

	Pr *with* $n = 10$				n *with* $Pr = 0.71$			
K^2	5	7	9	11	2	3	4	5
2	*0.63530*	*0.54181*	*0.50338*	*0.48579*	*0.38746*	*0.67024*	*0.98702*	*1.29909*
4	*0.36693*	*0.27152*	*0.23503*	*0.21896*	*0.12769*	*0.27384*	*0.47076*	*0.74449*
6	*0.23659*	*0.12526*	*0.08797*	*0.07288*	*0.02516*	*0.09501*	*0.1816*	*0.30022*
8	*0.20780*	*0.06192*	*0.02223*	*0.00807*	*0.01479*	*0.02450*	*0.06783*	*0.12187*

2.5 Conclusions

The unsteady MHD flow and heat transfer of an incompressible viscous fluid bounded by an infinite heated porous flat plate in a rotating system have been studied. The effects of pertinent parameters such as magnetic parameter, rotation parameter, frequency parameter, suction parameter, phase angle and time are studied. It is found that with an increase in either magnetic parameter M^2 or suction parameter S the primary

velocity u_1 and the magnitude of secondary velocity w_1 of fluid decrease at a particular point in flow filed. This is due to the fact that variation of the magnetic parameter leads to the variation of the Lorentz force due to magnetic field and the Lorentz force produces more resistance to transport phenomena. The primary velocity u_1 and the magnitude of secondary velocity w_1 increase with an increase in either accelerated parameter β or frequency parameter n or time τ. It is found that the primary velocity u_1 decreases while the magnitude of secondary velocity w_1 first increases near the plate and it decreases away from the plate with an increase in rotation parameter K^2. It is found that both the amplitudes of shear stresses R_1 and R_2 due to primary and the secondary flow respectively decrease with an increase in either magnetic parameter M^2 or frequency parameter n. The mean wall temperature $\theta_0(\eta)$ as well as the rate of heat transfer $\theta'(0,\tau)$ are also obtained. It is found that with an increase in magnetic field intensity the mean temperature $\theta_0(\eta)$ increases at a particular point in flow filed. Further, it is found that the magnitude of tangent of the phase angle of the rate of heat transfer oscillations $\tan\psi$ decreases with an increase in either rotation parameter K^2 or Prandtl number Pr while it increases with an increase in frequency parameter n for fixed values of K^2. The effects of transverse magnetic field on a viscous incompressible conducting fluid is to suppress the velocity field which in turn causes the enhancement of the temperature field.

Bibliography

[1] Kakutani T, J. Phys. Soc. Jpn.: **13**(1958), pp.1504.

[2] Kakutani T, J. Phys. Soc. Jpn.: **15**(1960), pp.1316.

[3] Hide R and Roberts PH, Review of Modern Phys.: (1960), pp.799.

[4] Soundalgekar VM and Pop I, Bulletin Mathematique Roumanie: **14**(1970), pp.375.

[5] Debnath L, J. of Appl. Math. and Mech..: **52**(1972), pp.623.

[6] Datta N and Mazumdar BS, Rev. Roumanie Phys.: **22**(1977), pp.237.

[7] Bühler K and Zierep J, J. of Appl. Math. and Mech.: **70**(1990), pp.589.

[8] Turbatu S, Bühler K and Zierep J, Acta Mech.: **129**(1998), pp.25.

[9] Attia HA, Physica Scripta: **66**(2002), pp.470.

[10] Gupta AS, Misra JC, Reza M and Soundalgekar VM, Acta Mechanica: **165**(2003), pp.1.

[11] Gupta AS, Misra JC and Reza M, Fluid Dynamics Res.: **32**(2003), pp.283.

[12] Guria M and Jana RN, Magnetohydrodynamics: **43(1)**(2007), pp.53.

[13] Mohyuddin MR, Fakhar K and Ali F, Int. J. Dynamics of Fluids: **3(2)**(2007), pp.175.

[14] Akl MY, Computational Materials Sci.: **45(2)**(2009), pp.271.

Chapter 3

Radiation effects on unsteady MHD free convective Couette flow of heat generation/absorbing fluid*

3.1 Introduction

The research works on magnetohydrodynamics (MHD) have been advanced significantly during last three decades in natural sciences and engineering disciplines after the pioneer work of Hartmann (1937) in liquid metal duct flow under the influence of a strong external magnetic field. This fundamental investigation has provided basic knowledge for the development of several MHD devices such as MHD pumps, generators, breaks and flow meters. The study of flow for an electrically conducting fluid has many applications in engineering problems such as plasma studies, nuclear reactors, geothermal energy extraction and the boundary layer control in the field of aerodynamics. Recent advances and applications of MHD based microfluidic devices are extensively reviewed in the paper by Qian and Bau[1].

Some of these devices include MHD-based micro-pumps used for producing a mechanical force which sets the fluid into motion; MHD-based microfluidic networks used for transporting fluids and reagents across networks of conduits where the flow control typically requires the use of pumps and valves; MHD-based liquid chromatography used

* *Published in* **Int. J. of Computer Application (IJCA)**, *ISSN: 0975-8887, 39(3)(2012), pp.42-51.*

for the separation, purification and detection of various biochemicals. Although, some of these devices are fabricated with low temperature co-fired ceramic tapes, significant heat generation or radiative heat transfer occurs due to the induction of eddy currents in most of these engineering applications studied by Lemoff and Lee[2] and West et al.[3, 4]. Other examples are, high temperature phenomena or high-power radiation sources commonly encountered in solar physics-particularly in astrophysical studies represented by Bestman and Adjepong [5]. In combustion applications such as fires, furnaces, IC engines, in nuclear reactions such as in the sun or in nuclear explosions has been studied by Ghoshdastidar[6]. On the other hand, in compressors in ships and in gas flares from petrochemical industry have been examined by Peterson et al.[7].

For air, the contribution of radiation becomes significant when the wall temperature is in the range 6000 - 10,000K. This situation is encountered for re-entry space vehicles. Korycki[8] has described radiative heat transfer as an important fundamental phenomena existing in practical engineering such as those found in solar radiation in buildings, foundry engineering and solidification processes, die forging, chemical engineering, composite structures applied in industry. Another important feature that usually occurs in electronic devices over a period of continuous usage is the hotness of the surface. This means that a poor design could trap heat generated by the source of the power supply and could incapacitate the efficiency and durability of the systems. Therefore, the efficiency in the functioning of these systems is enhanced when they are subjected to external cooling devices like air conditioners, electric fans, and some others (e.g. laptop computers) inbuilt storage devices that store electrical energy for them to function for sometime even without external source of power supply have been studied by Gbaorun et al.[9]. The IC components of these electronic systems are thermally coupled to the surrounding via convection and radiation. Radiation has a significant role in heat transfer in low-flow applications where there exists a larger temperature gradient between the components and the surrounding. The Couette flow is one of the basic flow in fluid dynamics that refers to the laminar flow of a viscous fluid in the space between two parallel plates, one of which is moving relative to the other. The Couette flow is frequently used in physics and engineering to illustrate shear-driven fluid motion. The radiative free convection MHD Couette flows are frequently encountered in many scientific and environmental processes, such as astrophysical flows, heating and cooling of chambers and solar power technology. The heat transfer by simultaneous radiation and convection has applications in numerous technological problems including combustion, furnace design, the design of high temperature gas cooled nuclear reactors, nuclear reactor safety, fluidized bed heat exchanger, fire spreads, solar fans, solar

collectors natural convection in cavities, turbid water bodies, photo chemical reactors and many others.

Jha[10] has studied the natural convection in unsteady MHD Couette flow. The radiative heat transfer to magnetohydrodynamic Couette flow with variable wall temperature have been investigated by Ogulu and Motsa[11]. The effects of radiation on MHD Couette flow with heat transfer between two parallel plates has been examined by Mebine[12]. Jha and Ajibade[13] have made an analysis on the free convective flow of heat generating/ absorbing fluid between vertical porous plates with periodic heat input. Jha and Ajibade[14] have studied the unsteady free convective Couette flow of heat generating/absorbing fluid. The MHD oscillatory Couette flow of a radiating viscous fluid in a porous medium with periodic wall temperature have been examined by Israel-Cookey et al.[15]. The effects of thermal radiation and free convection currents on the unsteady Couette flow between two vertical parallel plates with constant heat flux at one boundary has been studied by Narahari[16]. Deka and Bhattacharya[17] have investigated the unsteady free convective Couette flow of heat generating/absorbing fluid in porous medium. The radiation and free convection effects on an MHD flow through a porous medium between infinite parallel plates with time-dependent suction have been described by Alagoa et al.[18]. Gbadeyan et al.[19] have discussed the radiation effect on electrohydrodynamic froth flow in vertical channel. The magnetic field and thermal radiation effects on steady hydromagnetic couette flow through a porous channel have been studied by Baoku et al.[20].

In this chapter, we investigate the radiation effects on free convection MHD Couette flow of a viscous incompressible heat generating fluid confined between vertical plates. An exact solution of the governing equations has been obtained. The effects of the dimensionless physical parameters characterizing the flow on the velocity, the temperature, the shear stress at the plate and the rate of heat transfer have been studied in detail.

3.2 Formulation of the problem and its solutions

Consider the unsteady free convective MHD Couette flow of a viscous incompressible radiative heat generating fluid between two infinite vertical parallel walls separated by a distance h. The flow is set up by the buoyancy force arising from the temperature gradient occurring as a result of asymmetric heating of the parallel plates as well as constant motion of one of the plates. Choose a Cartesian co-ordinate system with the x-axis along the plate in the vertically upward direction and the y- axis normal to

the plates [see **Figure 3.1**]. Initially, at time $t = 0$, both the plates and the fluid are assumed to be at the same temperature T_h and stationary. At time $t > 0$, the plate at $y = 0$ starts to move in its own plane with a velocity $U(t)$ and is heated with temperature T_0 whereas the plate at $y = h$ is stationary and maintained at a constant temperature T_h. A uniform magnetic field of strength B_0 is imposed perpendicular to the plates. It is also assumed that the radiative heat flux in the x-direction is negligible as compared to that in the y-direction. As the plates are infinitely long along the x-direction, the velocity field and temperature distribution are functions of y and t only.

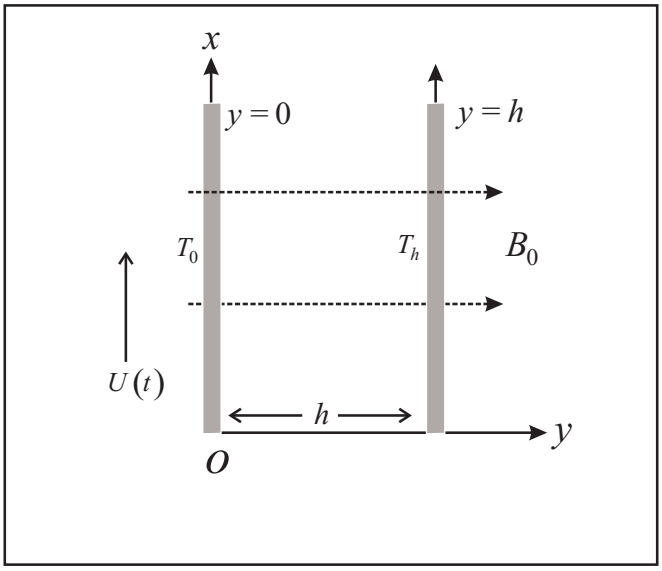

Figure 3.1: Geometry of the problem

The Boussinesq approximation is assumed to hold and for the evaluation of the gravitational body force, the density is assumed to depend on the temperature according to the equation of state

$$\rho = \rho_0 \left[1 - \beta(T - T_h)\right], \tag{3.1}$$

where T is the fluid temperature, ρ the fluid density, β the coefficient of thermal expansion and ρ_0 the density at the entrance of the channel.
Then the fully developed flow of a radiating gas is governed by the following set of equations

$$\frac{\partial u}{\partial t} = \nu \frac{\partial^2 u}{\partial y^2} + g\beta(T - T_h) - \frac{\sigma B_0^2}{\rho} u, \tag{3.2}$$

$$\rho c_p \frac{\partial T}{\partial t} = k\frac{\partial^2 T}{\partial y^2} - \frac{\partial q_r}{\partial y} - Q_0 (T - T_h), \tag{3.3}$$

where u is the velocity in the x-direction, g the acceleration due to gravity, ν the kinematic viscosity, ρ the fluid density, k the thermal conductivity, c_p the specific heat at constant pressure and q_r the radiative heat flux and Q_0 a constant.

The initial and boundary conditions for velocity field and temperature distribution are

$$\begin{aligned} &u = 0,\ T = T_h \ \text{ for } \ 0 \le y \le h \ \text{ and } \ t = 0, \\ &u = U,\ \ T = T_0 \ \text{ at } \ y = 0 \ \text{ for } \ t > 0, \\ &u = 0,\ T = T_h \ \text{ at } \ y = h \ \text{ for } \quad t > 0. \end{aligned} \tag{3.4}$$

It has been shown by Cogley et al.[21] that in the optically thin limit for a non-gray gas near equilibrium, the following relation holds

$$\frac{\partial q_r}{\partial y} = 4(T - T_h) \int_0^\infty K_{\lambda_h} \left(\frac{\partial e_{\lambda p}}{\partial T}\right)_h d\lambda, \tag{3.5}$$

where K_λ is the absorption coefficient, λ is the wave length, $e_{\lambda p}$ is the Plank's function and subscript $'0'$ indicates that all quantities have been evaluated at the temperature T_h which is the temperature of the plate at time $t = 0$. Thus our study is limited to small difference of plate temperature to the fluid temperature.
On the use of equation (3.5), equation (3.3) becomes

$$\rho c_p \frac{\partial T}{\partial t} = k\frac{\partial^2 T}{\partial y^2} - 4 (T - T_h) I - Q_0 (T - T_h), \tag{3.6}$$

where

$$I = \int_0^\infty K_{\lambda_h} \left(\frac{\partial e_{\lambda p}}{\partial T}\right)_h d\lambda. \tag{3.7}$$

Greif et al.[22] showed that, for an optically thin limit, the fluid does not absorb its own emitted radiation, this means that there is no self-absorption, but the fluid does absorb radiation emitted by the boundaries.
Introducing non-dimensional variables

$$\eta = \frac{y}{h},\ \ \tau = \frac{\nu t}{h^2},\ u_1 = \frac{u}{U},\ \theta = \frac{T - T_h}{T_0 - T_h} \tag{3.8}$$

equations (3.2) and (3.6) become

$$\frac{\partial u_1}{\partial \tau} = \frac{\partial^2 u_1}{\partial \eta^2} + Gr\,\theta - M^2 u_1, \tag{3.9}$$

$$Pr\,\frac{\partial \theta}{\partial \tau} = \frac{\partial^2 \theta}{\partial \eta^2} - (R + \phi)\ \theta, \tag{3.10}$$

where $M^2 = \frac{\sigma B_0^2 h^2}{\rho \nu}$ is the magnetic parameter, $R = \frac{4I h^2}{k}$ the radiation parameter, $\phi = \frac{Q_0 h^2}{k}$ the heat generation parameter, $Gr = \frac{g\beta(T_0 - T_h)h^2}{\nu U}$ the Grashof number and $Pr = \frac{\rho \nu c_p}{k}$ the Prandtl number.
The corresponding initial and boundary conditions for u_1 and θ are

$$\begin{aligned} &u_1 = 0,\ \theta = 0 \ \text{ for } \ 0 \le \eta \le 1 \ \text{ and } \ \tau = 0, \\ &u_1 = 1,\ \ \theta = 1 \ \text{ at } \ \eta = 0 \ \text{ for } \ \tau > 0, \\ &u_1 = 0,\ \theta = 0 \ \text{ at } \ \eta = 1 \ \text{ for } \ \tau > 0. \end{aligned} \tag{3.11}$$

3.2.1 General solution

To obtain the exact solution, on taking Laplace transformation of equations (3.9) and (3.10), we get

$$s\,\bar{u}_1 = \frac{d^2\bar{u}_1}{d\eta^2} + Gr\,\bar{\theta} - M^2\bar{u}_1, \tag{3.12}$$

$$Pr\,s\,\bar{\theta} = \frac{d^2\bar{\theta}}{d\eta^2} - (R+\phi)\,\bar{\theta}, \tag{3.13}$$

where

$$\bar{u}_1(\eta, s) = \int_0^\infty u_1(\eta, s)\, e^{-s\tau}\, d\tau \ \text{ and } \ \bar{\theta}(\eta, s) = \int_0^\infty \theta(\eta, s)\, e^{-s\tau}\, d\tau. \tag{3.14}$$

The corresponding boundary conditions for $\bar{u}_1$ and $\bar{\theta}$ are

$$\begin{aligned} &\bar{u}_1(0, s) = 0, \ \ \bar{\theta}(0, s) = \frac{1}{s}, \\ &\bar{u}_1(1, s) = 0, \ \ \bar{\theta}(1, s) = 0. \end{aligned} \tag{3.15}$$

The solution of equations (3.13) and (3.12) subject to the boundary conditions (3.15) can be easily obtained and are given by

$$\bar{\theta}(\eta, s) = \frac{1}{s}\frac{\sinh\sqrt{Pr(s+\alpha)}\,(1-\eta)}{\sinh\sqrt{Pr(s+\alpha)}}, \tag{3.16}$$

$$\begin{aligned} \bar{u}_1(\eta, s) &= \frac{1}{s}\frac{\sinh\sqrt{s+M^2}(1-\eta)}{\sinh\sqrt{s+M^2}} + \frac{Gr}{(Pr-1)s(s+b)} \\ &\times \left[\frac{\sinh\sqrt{s+M^2}\,(1-\eta)}{\sinh\sqrt{s+M^2}} - \frac{\sinh\sqrt{Pr(s+\alpha)}(1-\eta)}{\sinh\sqrt{Pr(s+\alpha)}}\right], \end{aligned} \tag{3.17}$$

where

$$\alpha = \frac{R+\phi}{Pr} \ \text{ and } \ b = \frac{\alpha\, Pr - M^2}{Pr - 1}. \tag{3.18}$$

The inverse transforms of (3.16) and (3.17) give the solution for the temperature distribution and velocity field as

$$\theta(\eta,\tau) = \begin{cases} \frac{\sinh\sqrt{\alpha\,Pr}(1-\eta)}{\sinh\sqrt{\alpha\,Pr}} - 2\pi\sum_{n=1}^{\infty}\frac{n\,e^{-\left(n^2\pi^2/Pr+\alpha\right)\tau}}{n^2\pi^2+\alpha\,Pr}\sin n\pi\eta & \text{for } Pr\neq 1, \\ \frac{\sinh\sqrt{R+\phi}(1-\eta)}{\sinh\sqrt{R+\phi}} - 2\pi\sum_{n=1}^{\infty}\frac{n\,e^{-\left(n^2\pi^2+R+\phi\right)\tau}}{n^2\pi^2+R+\phi}\sin n\pi\eta & \text{for } Pr=1 \end{cases} \tag{3.19}$$

$$u_1(\eta,\tau) = \begin{cases} \left[1+\frac{Gr}{b(Pr-1)}\right]\frac{\sinh M(1-\eta)}{\sinh M} - \frac{Gr}{b(Pr-1)}\frac{\sinh\sqrt{\alpha\,Pr}(1-\eta)}{\sinh\sqrt{\alpha\,Pr}} \\ -2\pi\sum_{n=1}^{\infty}\frac{n\,e^{-\left(n^2\pi^2+M^2\right)\tau}}{n^2\pi^2+M^2}\sin n\pi\eta \\ +\frac{2\pi\,Gr}{(Pr-1)}\sum_{n=1}^{\infty}n\left[\frac{e^{-\left(n^2\pi^2+M^2\right)\tau}}{(n^2\pi^2+M^2)(n^2\pi^2+M^2-b)}\right. \\ \left.-\frac{Pr\,e^{-\left(n^2\pi^2/Pr+\alpha\right)\tau}}{(n^2\pi^2+\alpha\,Pr)(n^2\pi^2+\alpha\,Pr-b\,Pr)}\right]\sin n\pi\eta & \text{for } Pr\neq 1, \\ \left(1+\frac{Gr}{R+\phi-M^2}\right)\left[\frac{\sinh M(1-\eta)}{\sinh M}\right. \\ \left.-2\pi\sum_{n=1}^{\infty}\frac{n\,e^{-\left(n^2\pi^2+M^2\right)\tau}}{n^2\pi^2+M^2}\sin n\pi\eta\right] \\ -\frac{Gr}{R+\phi-M^2}\left[\frac{\sinh\sqrt{R+\phi}(1-\eta)}{\sinh\sqrt{R+\phi}}\right. \\ \left.-2\pi\sum_{n=1}^{\infty}\frac{n\,e^{-\left(n^2\pi^2+R+\phi\right)\tau}}{n^2\pi^2+R+\phi}\sin n\pi\eta\right] & \text{for } Pr=1, \end{cases} \tag{3.20}$$

where α and b are given by equation (3.18).

3.2.2 Steady state solution

When the time $\tau\to\infty$, the temperature distribution and velocity field are obtained as

$$\theta(\eta) = \begin{cases} \frac{\sinh\sqrt{\alpha\,Pr}(1-\eta)}{\sinh\sqrt{\alpha\,Pr}} & \text{for } Pr\neq 1, \\ \frac{\sinh\sqrt{R+\phi}(1-\eta)}{\sinh\sqrt{R+\phi}} & \text{for } Pr=1 \end{cases} \tag{3.21}$$

$$u_1(\eta) = \begin{cases} \left[1+\frac{Gr}{b(Pr-1)}\right]\frac{\sinh M(1-\eta)}{\sinh M} \\ -\frac{Gr}{b(Pr-1)}\frac{\sinh\sqrt{\alpha\,Pr}(1-\eta)}{\sinh\sqrt{\alpha\,Pr}} & \text{for } Pr\neq 1, \\ \left(1+\frac{Gr}{R+\phi-M^2}\right)\frac{\sinh M(1-\eta)}{\sinh M} \\ -\frac{Gr}{R+\phi-M^2}\frac{\sinh\sqrt{R+\phi}(1-\eta)}{\sinh\sqrt{R+\phi}} & \text{for } Pr=1, \end{cases} \tag{3.22}$$

where α and b are given by equation (3.18).

3.3 Results and discussion

In order to understand the effects of different physical parameters, namely magnetic parameter M^2, radiation parameter R, heat generation parameter ϕ, Prandtl number Pr, Grashof number Gr and time τ on the nature of the flow computations are carried out for velocity, temperature, shear stress and rate of heat transfer. The computed results are presented graphically.

3.3.1 Effects of parameters on the velocity profiles

The effects of pertinent parameters on the velocity field u_1 are presented graphically against η in **Figures 3.2-3.11**. It is seen from **Figure 3.2** that the velocity u_1 decreases with an increase in magnetic parameter M^2. This observation can be explained by the fact that as M^2 increases, the Lorentz force which opposes the flow, increases and leads to enhanced deceleration of the flow. **Figure 3.3** reveals that the velocity u_1 decreases with an increase in radiation parameter R. This shows that there is a fall in velocity in the presence of high radiation.

It is seen from **Figure 3.4** that the velocity u_1 decreases with an increase in heat generation parameter ϕ. As ϕ increases, heat absorbing capacity of the fluid increases which decreases fluid temperature and hence the fluid velocity.

An increase in Prandtl number Pr leads to decrease the velocity u_1 near the moving plate and reverse result near stationary plate as shown in **Figure 3.5**.

Physically, this is true because the increase in the Prandtl number is due to increase in the viscosity of the fluid which makes the fluid thick and hence causes a decrease in the velocity of the fluid.

It is observed from **Figure 3.6** that an increase in Gr leads to increase in the values of velocity u_1. An increase in Grashof number leads to an increase in velocity, this is because, increase in Grashof number means more heating and less density. It is seen from **Figure 3.7** that the velocity u_1 increases with an increase in time τ.

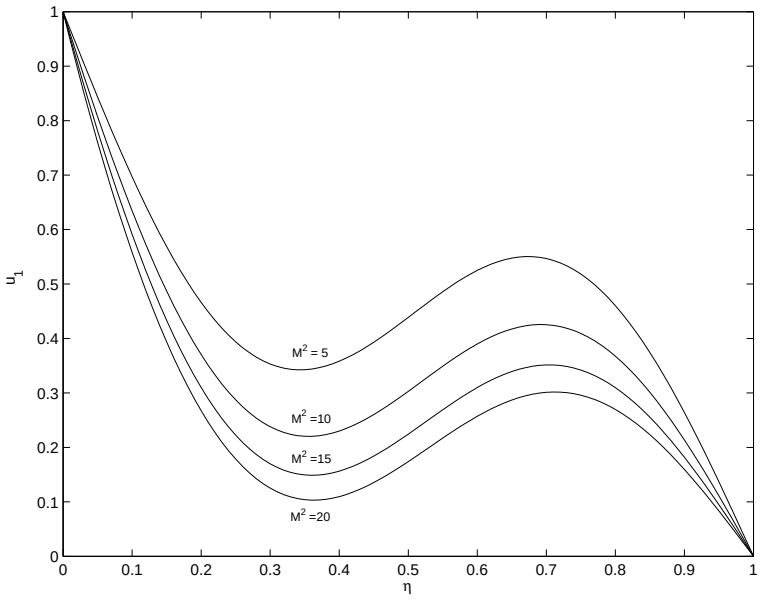

Figure 3.2: Velocity profile for M^2 when $R = 2$, $\phi = 2$, $Pr = 0.025$, $Gr = 5$ and $\tau = 0.0005$.

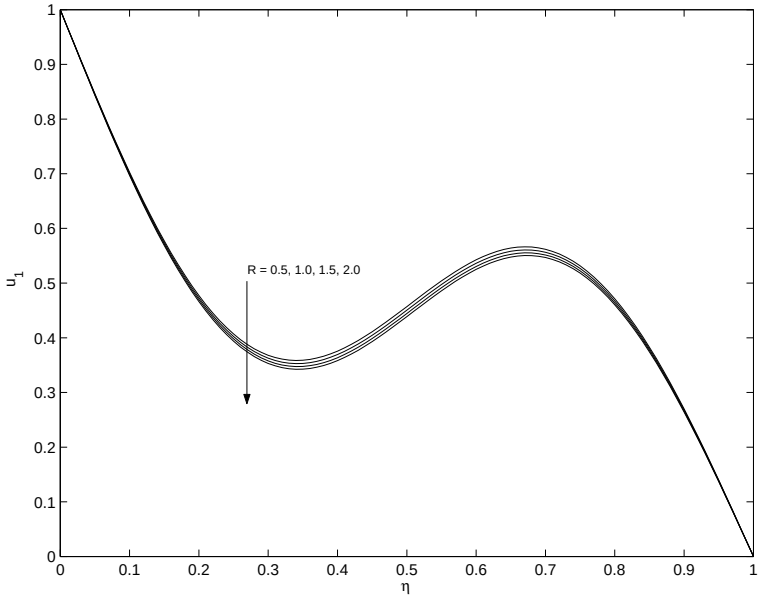

Figure 3.3: Velocity profile for R when $M^2 = 5$, $\phi = 2$, $Gr = 5$, $Pr = 0.025$ and $\tau = 0.0005$.

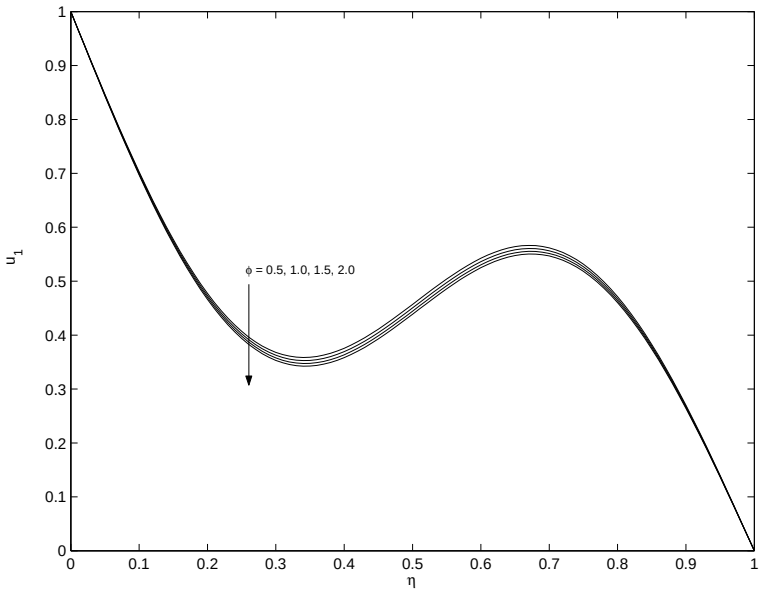

Figure 3.4: Velocity profile for ϕ when $M^2 = 5$, $R = 2$, $Gr = 5$, $Pr = 0.025$ and $\tau = 0.0005$.

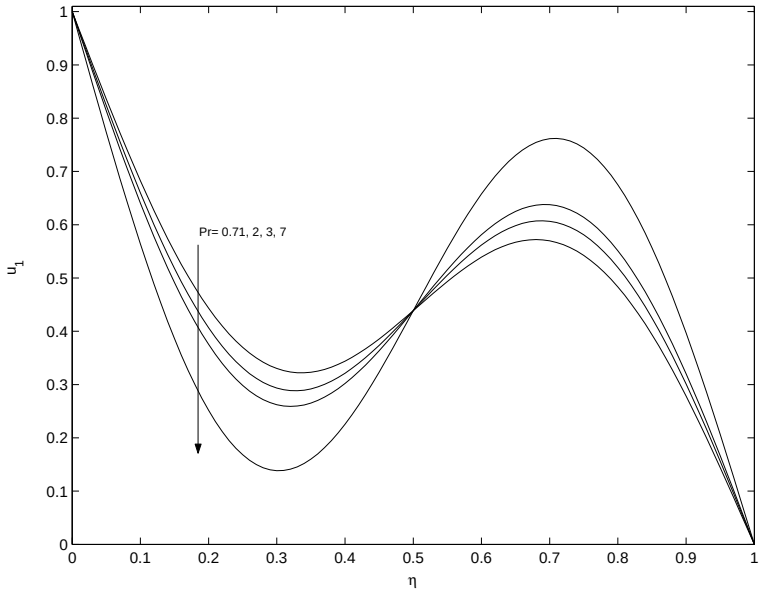

Figure 3.5: Velocity profile for Pr when $M^2 = 5$, $R = 2$, $Gr = 5$, $\phi = 2$ and $\tau = 0.0005$.

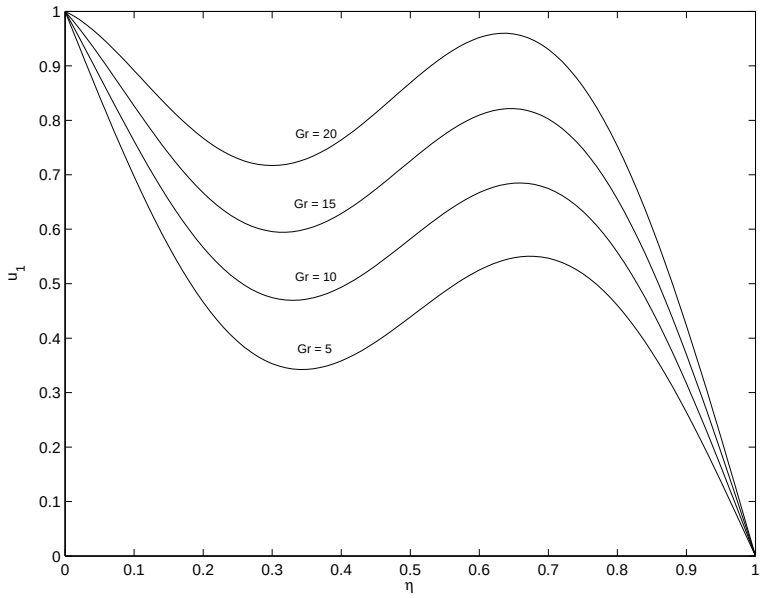

Figure 3.6: Velocity profile for Gr when $M^2 = 5$, $R = 2$, $\phi = 2$, $Pr = 0.025$ and $\tau = 0.0005$.

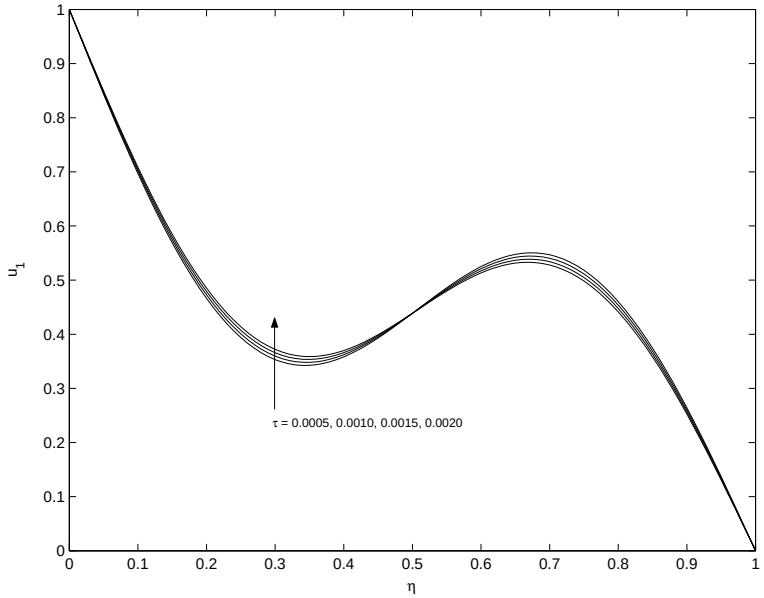

Figure 3.7: Velocity profile for time τ when $M^2 = 5$, $R = 2$, $Gr = 5$, $\phi = 2$ and $Pr = 0.025$.

3.3.2 Effects of parameters on the temperature profiles

The effects of pertinent parameters such as radiation parameter R, Prandtl number Pr, heat generation parameter ϕ and time τ on the temperature distribution are presented graphically in **Figures 3.8-3.11**. It is seen from **Figure 3.8** that the temperature θ decreases as the radiation parameter R increases. This is expected, since the effect of radiation is to decrease the rate of energy transport to the fluid, thereby decreasing the temperature of the fluid. It is seen from **Figure 3.9** that the temperature θ decreases as the heat generation parameter ϕ increases. This result agrees with expectations, as ϕ increases, heat absorbing capacity of the fluid increases and hence the fluid temperature decreases. It is observed from **Figure 3.10** that the temperature θ decreases with an increase in Prandtl number Pr. This implies that an increase in Prandtl number leads to fall the thermal boundary layer flow. This is because fluids with large Pr have low thermal diffusivity which causes low heat penetration resulting in reduced thermal boundary layer. **Figure 3.11** shows that the temperature θ increases with an increase in time τ. It is observed from **Figures 3.8-3.11** that temperature decreases gradually from highest value on the moving plate to a zero value on the stationary plate.

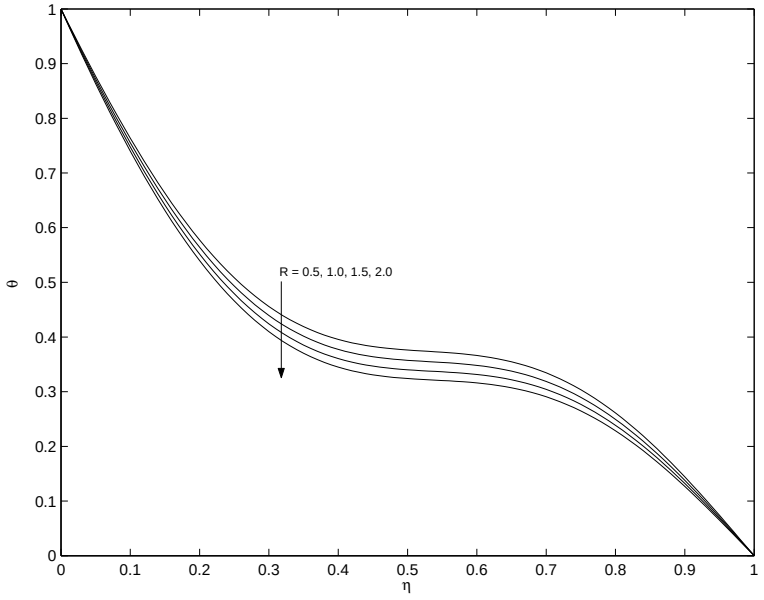

Figure 3.8: Temperature profile for R when $Pr = 0.025$, $\phi = 2$ and $\tau = 0.0005$.

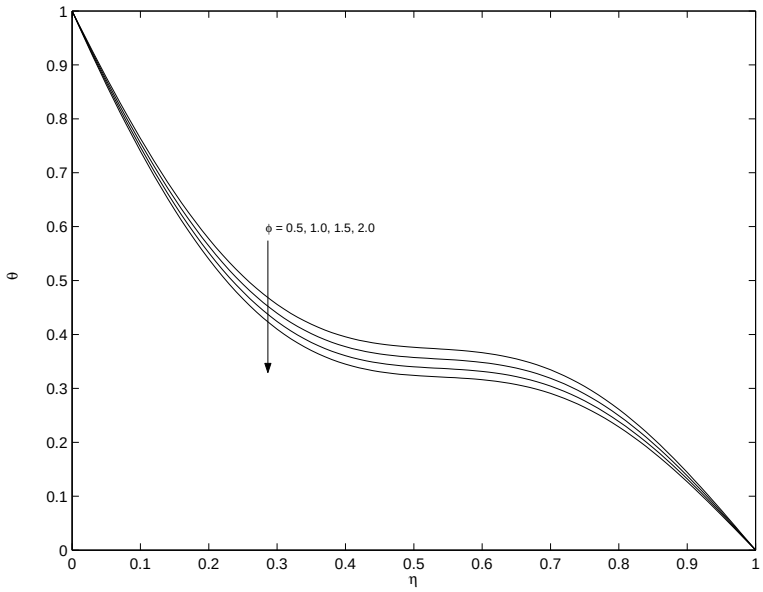

Figure 3.9: Temperature profile for ϕ when $R = 2$, $Pr = 0.025$ and $\tau = 0.5$.

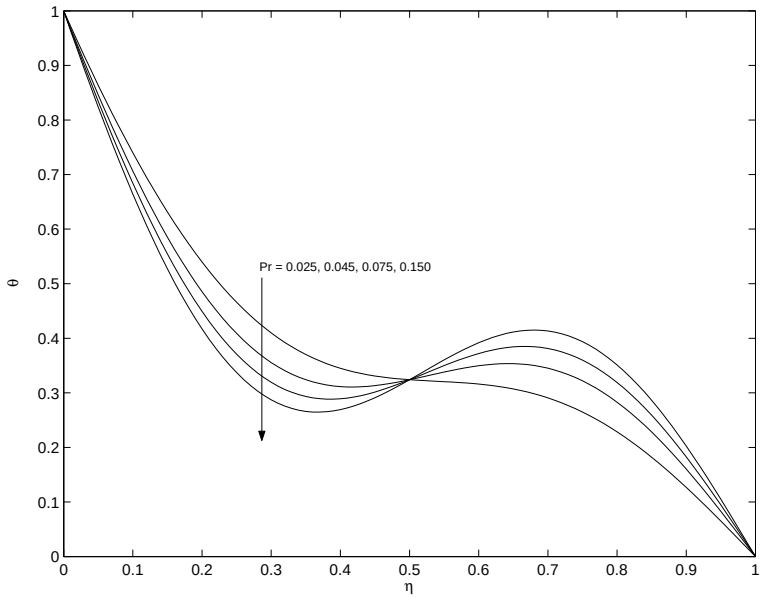

Figure 3.10: Temperature profile for Pr when $R = 2$, $\phi = 4$ and $\tau = 0.2$.

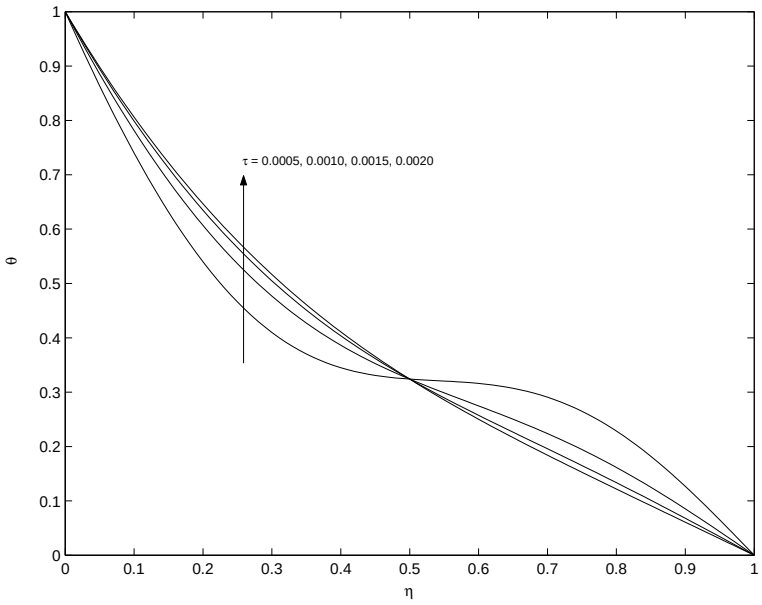

Figure 3.11: Temperature profile for τ when $Pr = 0.025$, $R = 2$ and $\phi = 2$.

3.3.3 Effects of parameters on the shear stress at the plate of the channel

For engineering purposes, one is usually interested to determine the values of the shear stress (or skin function). The increased shear stress is generally a disadvantage in the technical applications. From the physical point of view, it is necessary to know the shear stress at the plate $\eta = 0$. The non-dimensional shear stress at the plate $\eta = 0$ of the channel is denoted by

$$\tau_0 = \left(\frac{du_1}{d\eta}\right)_{\eta=0},$$

and defined as

$$\tau_0 = \begin{cases} -M\left[1+\frac{Gr}{b(Pr-1)}\right]\coth M - \frac{Gr\sqrt{\alpha\,Pr}}{b(Pr-1)}\coth\sqrt{\alpha\,Pr} \\ -2\pi^2\sum\limits_{n=1}^{\infty}\frac{n^2\,e^{-\left(n^2\pi^2+M^2\right)\tau}}{n^2\pi^2+M^2} \\ +\frac{2\pi^2\,Gr}{(Pr-1)}\sum\limits_{n=1}^{\infty}n^2\left[\frac{e^{-\left(n^2\pi^2+M^2\right)\tau}}{(n^2\pi^2+M^2)(n^2\pi^2+M^2-b)}\right. \\ \left.-\frac{Pr\,e^{-\left(n^2\pi^2/Pr+\alpha\right)\tau}}{(n^2\pi^2+\alpha\,Pr)(n^2\pi^2+\alpha\,Pr-b\,Pr)}\right] \qquad \text{for } Pr\neq 1, \end{cases} \tag{3.23}$$

$$\tau_0 = \begin{cases} -\left(1+\frac{Gr}{R+\phi-M^2}\right)[M\coth M \\ +2\pi^2\sum\limits_{n=1}^{\infty}\frac{n^2\,e^{-\left(n^2\pi^2+M^2\right)\tau}}{n^2\pi^2+M^2}\Bigg] \\ +\frac{Gr}{R+\phi-M^2}\left[\sqrt{R+\phi}\coth\sqrt{R+\phi}\right. \\ \left.+2\pi^2\sum\limits_{n=1}^{\infty}\frac{n^2\,e^{-\left(n^2\pi^2+R+\phi\right)\tau}}{n^2\pi^2+R+\phi}\right] \qquad \text{for } Pr=1, \end{cases} \tag{3.24}$$

where α and b are given by equation (3.18).

Numerical results of the non-dimensional shear stress τ_0 at the lower plate $\eta = 0$ are presented in **Figures 3.12-3.16** against magnetic parameter M^2 for various values of radiation parameter R, heat generation parameter ϕ, Prandtl number Pr, Grashof number Gr and time τ. **Figure 3.12** shows that the shear stress τ_0 decreases with an increase in magnetic parameter M^2 for fixed values of R, ϕ, Pr, Gr and τ. It is seen from **Figures 3.13-3.16** that for fixed values of M^2, the shear stress τ_0 decreases with an increase in either radiation parameter R or heat generation parameter ϕ or Prandtl number Pr while it increases with an increase in either Grashof number Gr or time τ.

These results are in agrement with the fact that the velocity decreases with an increase in R or ϕ or Pr while it increases with an increases in Gr or τ. A large Prandtl number implies more prominent viscous effects causing an enhanced frictional force.

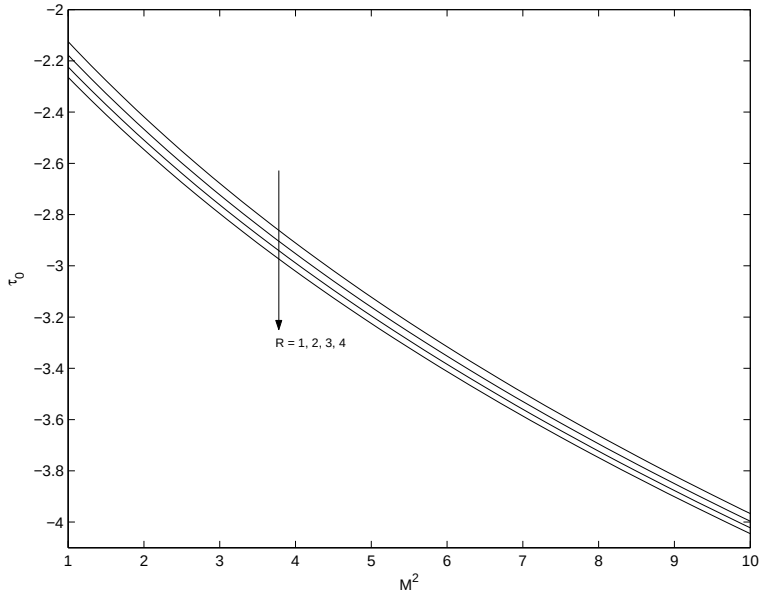

Figure 3.12: Shear stress τ_0 for R, $\phi = 2$, $Pr = 0.025$ and $\tau = 0.0005$.

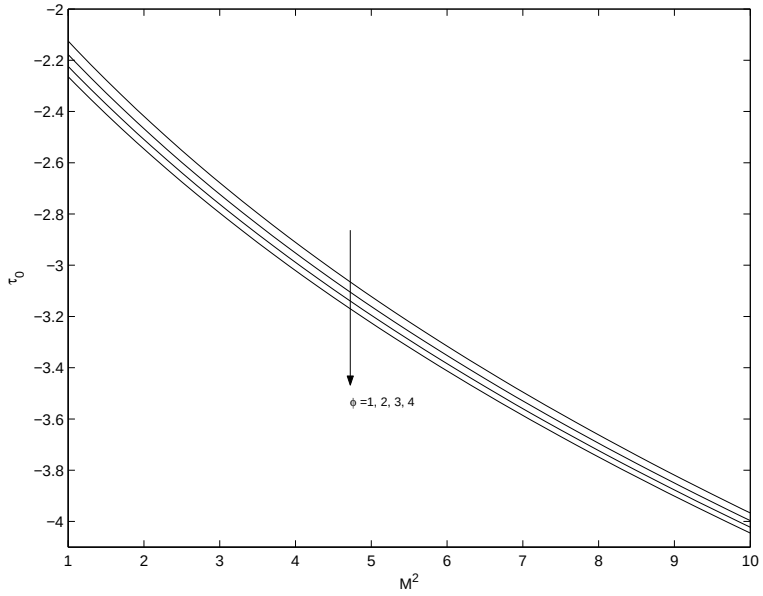

Figure 3.13: Shear stress τ_0 for ϕ when $R = 2$, $Pr = 0.025$ and $\tau = 0.0005$.

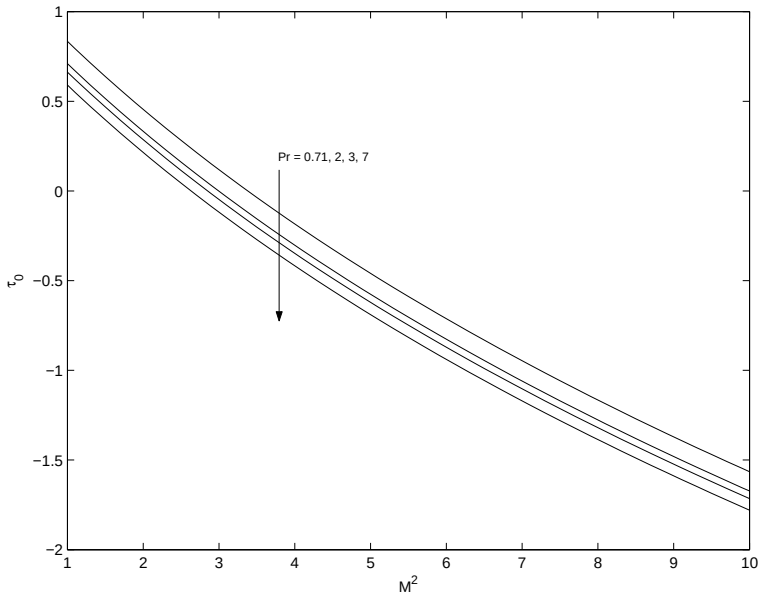

Figure 3.14: Shear stress τ_0 for Pr when $R = 2$, $\phi = 2$ and $\tau = 0.0005$.

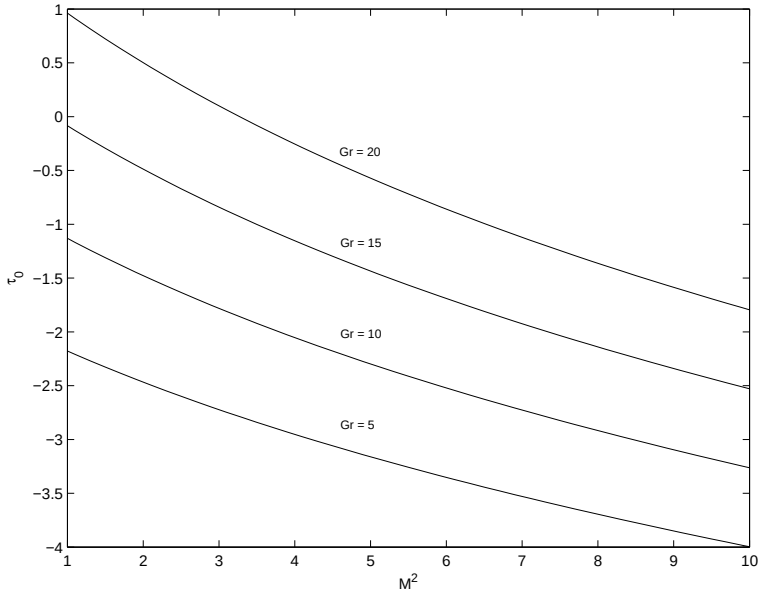

Figure 3.15: Shear stress τ_0 for Gr when $R = 2$, $\phi = 2$ and $\tau = 0.0005$.

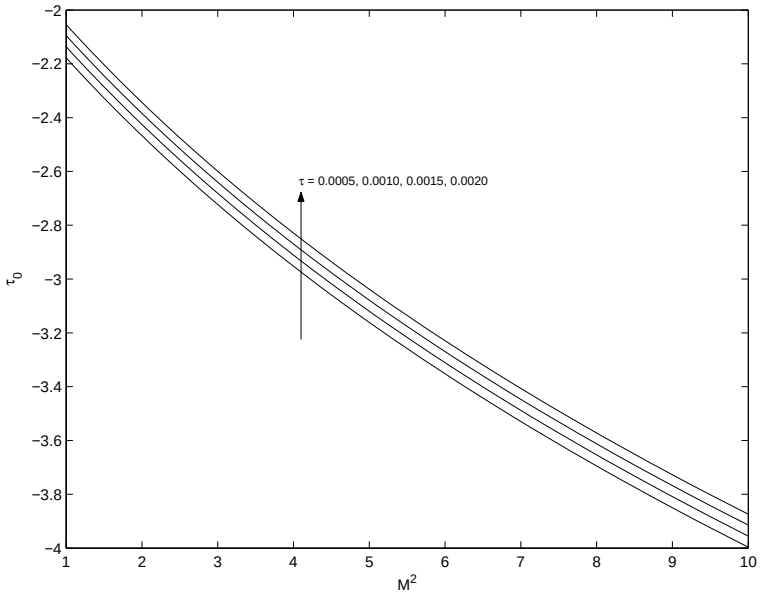

Figure 3.16: Shear stress τ_0 for time τ when $R = 2$, $\phi = 2$ and $Pr = 0.025$.

3.3.4 Vertical flow rate through the channel

The vertical flow rate Q through the channel is given by

$$Q = \int_0^1 u_1 d\eta,$$

and it is expressed as

$$Q = \begin{cases} M\left[1+\frac{Gr}{b(Pr-1)}\right]\frac{\cosh M-1}{M\sinh M}+\frac{Gr}{b(Pr-1)}\frac{1-\cosh\sqrt{\alpha\,Pr}}{\sqrt{\alpha\,Pr}\sinh\sqrt{\alpha\,Pr}} \\ -2\sum_{n=1}^{\infty}\left[1-(-1)^n\right]\frac{e^{-\left(n^2\pi^2+M^2\right)\tau}}{n^2\pi^2+M^2} \\ +\frac{2Gr}{(Pr-1)}\sum_{n=1}^{\infty}\left[1-(-1)^n\right]\left[\frac{e^{-\left(n^2\pi^2+M^2\right)\tau}}{(n^2\pi^2+M^2)(n^2\pi^2+M^2-b)}\right. \\ \left.-\frac{Pr\,e^{-\left(n^2\pi^2/Pr+\alpha\right)\tau}}{(n^2\pi^2+\alpha\,Pr)(n^2\pi^2+\alpha\,Pr-b\,Pr)}\right] \qquad \text{for } Pr \neq 1, \end{cases} \tag{3.25}$$

$$Q = \begin{cases} -\left(1+\frac{Gr}{R+\phi-M^2}\right)\left[\frac{1-\cosh M}{M\sinh M}\right. \\ \left. +2\sum\limits_{n=1}^{\infty}\left[1-(-1)^n\right]\frac{e^{-\left(n^2\pi^2+M^2\right)\tau}}{n^2\pi^2+M^2}\right] \\ +\frac{Gr}{R+\phi-M^2}\left[\frac{1-\cosh\sqrt{R+\phi}}{\sqrt{R+\phi}\sinh\sqrt{R+\phi}}\right. \\ \left. +2\sum\limits_{n=1}^{\infty}\left[1-(-1)^n\right]\frac{e^{-\left(n^2\pi^2+R+\phi\right)\tau}}{n^2\pi^2+R+\phi}\right] \quad \text{for } Pr=1. \end{cases} \tag{3.26}$$

Numerical results of the vertical flow rate Q through the channel against magnetic parameter M^2 are presented in the **Table-I** for various values of the radiation parameter R, heat generation parameter ϕ and time τ. **Table-I** shows that for fixed values of M^2, the vertical flow rate Q decreases with an increase in either radiation parameter R or heat generation parameter ϕ or time τ. Further, it is seen that for fixed value of R, ϕ and τ, the vertical flow rate Q decreases with an increase in M^2. We see that the vertical flow rate decreases with increasing radiation parameter and these variations are significant at lower values of time.

Table-I

Vertical flow rate Q with $Gr = 5$ and $Pr = 0.71$.

	R			ϕ			τ		
M^2	1	2	3	0.5	1	1.5	0.005	0.0010	0.0015
5	*0.42515*	*0.41762*	*0.31790*	*0.42938*	*0.42515*	*0.42124*	*0.41762*	*0.41949*	*0.42128*
10	*0.33069*	*0.32505*	*0.32017*	*0.33386*	*0.33069*	*0.32777*	*0.32505*	*0.32692*	*0.32870*
15	*0.27405*	*0.26954*	*0.26564*	*0.27657*	*0.27405*	*0.27171*	*0.26954*	*0.27140*	*0.27317*
20	*0.23622*	*0.23247*	*0.22922*	*0.23833*	*0.23622*	*0.23428*	*0.23247*	*0.23432*	*0.23608*

3.3.5 Critical Grashof number near the plates of the channel

The critical Grashof number for which there is no flow reversal near the plates $\eta = 0$ and $\eta = 1$ of the channel are respectively given by

$$Gr_0 = \frac{M\coth M - 2\pi^2\sum\limits_{n=1}^{\infty}\frac{n^2 e^{-\left(n^2\pi^2+M^2\right)\tau}}{n^2\pi^2+M^2}}{\frac{M}{b(Pr-1)}\coth M - \frac{\sqrt{\alpha\, Pr}}{b(Pr-1)}\coth\sqrt{\alpha\, Pr} + \frac{2\pi^2}{(Pr-1)}\sum\limits_{n=1}^{\infty} n^2 a_n}, \tag{3.27}$$

$$Gr_1 = \frac{M\,\mathrm{cosech} M - 2\pi^2\sum\limits_{n=1}^{\infty}\frac{n^2(-1)^n e^{-\left(n^2\pi^2+M^2\right)\tau}}{n^2\pi^2+M^2}}{\frac{M}{b(Pr-1)}\coth M - \frac{\sqrt{\alpha\, Pr}}{b(Pr-1)}\coth\sqrt{\alpha\, Pr} + \frac{2\pi^2}{(Pr-1)}\sum\limits_{n=1}^{\infty} n^2(-1)^n a_n} \tag{3.28}$$

where

$$a_n = \left[\frac{e^{-\left(n^2\pi^2+M^2\right)\tau}}{\left(n^2\pi^2+M^2\right)\left(n^2\pi^2+M^2-b\right)} - \frac{Pr\, e^{-\left(n^2\pi^2/Pr+\alpha\right)\tau}}{\left(n^2\pi^2+\alpha\, Pr\right)\left(n^2\pi^2+\alpha\, Pr-b\, Pr\right)}\right]. \quad (3.29)$$

The values of the critical Grashof number Gr_0 at the moving plate $\eta = 0$ and Gr_1 at the stationary plate $\eta = 1$ due to the flow are entered in the **Tables-II and -III** for various values of the radiation parameter R, heat generation parameter ϕ and time τ against magnetic parameter M^2. It is seen from the **Table-II and -III** that both the critical Grashof numbers Gr_0 and Gr_1 due to the flow increases with an increase in either R or ϕ while it decreases with an increase in time τ. On the other hand, with an increase in the magnetic parameter M^2, both Gr_0 and Gr_1 increase for fixed values of R, ϕ and τ.

Table-II

Critical Grashof number $10^{-2}Gr_0$ at the plate $\eta = 0$ with $Pr = 0.71$.

	R			ϕ			τ		
M^2	1	2	3	0.5	1	1.5	0.005	0.0010	0.0015
5	*0.18758*	*0.19555*	*0.21017*	*0.18343*	*0.18758*	*0.19162*	*0.19555*	*0.18541*	*0.17639*
10	*0.26678*	*0.27704*	*0.28677*	*0.26143*	*0.26678*	*0.27198*	*0.27704*	*0.26512*	*0.25451*
15	*0.34161*	*0.35372*	*0.36517*	*0.33528*	*0.34161*	*0.34775*	*0.35372*	*0.34030*	*0.32831*
20	*0.41350*	*0.42718*	*0.44009*	*0.40633*	*0.41350*	*0.42044*	*0.42718*	*0.41241*	*0.39921*

Table-III

Critical Grashof number $10^{-2}Gr_1$ at the plate $\eta = 1$ with $Pr = 0.71$.

	R			ϕ			τ		
M^2	1	2	3	0.5	1	1.5	0.005	0.0010	0.0015
5	*0.18631*	*0.20678*	*0.22505*	*0.17643*	*0.18631*	*0.19643*	*0.20678*	*0.17224*	*0.14170*
10	*0.31998*	*0.35899*	*0.40062*	*0.30141*	*0.31998*	*0.33917*	*0.35899*	*0.30600*	*0.25910*
15	*0.46915*	*0.53244*	*0.60144*	*0.43948*	*0.46915*	*0.50012*	*0.53244*	*0.45673*	*0.38964*
20	*0.63531*	*0.73001*	*0.83573*	*0.59166*	*0.63531*	*0.68137*	*0.73001*	*0.62654*	*0.53474*

3.3.6 Effects of parameters on the rate of heat transfer at the plate of the channel

The rate of heat transfer is important in the heat transfer studies, since it is directly related to the heat transfer coefficient. From the temperature distribution, we now study the rate of heat transfer at the plate $\eta = 0$, which is given in non-dimensional form as

$$-\theta'(0,\tau) = \begin{cases} \sqrt{\alpha\, Pr}\coth\sqrt{\alpha\, Pr} + 2\pi^2\sum\limits_{n=1}^{\infty}\frac{n^2\, e^{-\left(n^2\pi^2/Pr+\alpha\right)\tau}}{n^2\pi^2+\alpha\, Pr} & \text{for } Pr \neq 1, \\ \sqrt{R+\phi}\coth\sqrt{R+\phi} + 2\pi^2\sum\limits_{n=1}^{\infty}\frac{n^2\, e^{-\left(n^2\pi^2+R+\phi\right)\tau}}{n^2\pi^2+R+\phi} & \text{for } Pr = 1 \end{cases} \quad (3.30)$$

Numerical results of the rate of heat transfer $-\theta'(0,\tau)$ at the moving plate $\eta = 0$ against heat generation parameter ϕ are presented in the **Table-IV** for various values of the radiation parameter R, Prandtl number Pr and time τ. **Table-IV** shows that for fixed values of ϕ, the rate of heat transfer $-\theta'(0,\tau)$ increases with an increase R while it decreases with an increase in either Prandtl number Pr or time τ. This may be explained by the fact that frictional forces become dominant with increasing values of Pr and hence yield greater heat transfer rates. Further, it is seen that for fixed value of R, Pr and τ, the rate of heat transfer $-\theta'(0,\tau)$ increases with an increase in heat generation parameter ϕ. The negative value of $-\theta'(0,\tau)$ physically explains that their is heat flow from the plate to the fluid.

Table-IV

Rate of heat transfer $-10^{-1}\theta'(0)$ at the moving plate $\eta = 0$.

	R			Pr			τ		
ϕ	1	2	3	0.71	2	7	0.0020	0.0025	0.0030
0.5	*0.34897*	*0.36921*	*0.38735*	*0.36921*	*0.25677*	*0.19817*	*0.40746*	*0.40060*	*0.39395*
1.0	*0.35938*	*0.37851*	*0.39578*	*0.37851*	*0.26797*	*0.21016*	*0.41667*	*0.40982*	*0.40318*
1.5	*0.36921*	*0.38735*	*0.40384*	*0.38735*	*0.27867*	*0.22162*	*0.42542*	*0.41858*	*0.41195*
2.0	*0.37851*	*0.39578*	*0.41156*	*0.39578*	*0.28891*	*0.23261*	*0.43375*	*0.42693*	*0.42031*

3.4 Single vertical plate

In the limit $h \to \infty$, that is, when one of the plate $\eta = 1$ is placed at an infinite distance, then the problem is reduced to the flow past an vertical plate with variable temperature in the presence of heat generation. Equations (3.21) and (3.22) become

$$\theta(\eta,\tau) = e^{-\sqrt{R+\phi}\,\eta}, \tag{3.31}$$

$$u_1(\eta,\tau) = \left(1 + \frac{Gr}{R+\phi-M^2}\right) e^{-M\eta} - \frac{Gr}{R+\phi-M^2}\, e^{-\sqrt{R+\phi}\,\eta}, \tag{3.32}$$

It is evident from the equation (3.30) that there arises a single-deck thermal boundary layer of thickness of the order $\mathrm{O}(R+\phi)^{-\frac{1}{2}}$ near the plate $\eta = 0$. The thickness of this boundary layer decreases with an increase in either radiation parameter R or heat generation parameter ϕ. Further, equation (3.31) shows that there exists a double-deck boundary layer near the plate $\eta = 0$. Thicknesses of these boundary layers are of the order $\mathrm{O}(M)^{-1}$ and $\mathrm{O}(R+\phi)^{-\frac{1}{2}}$ which are decrease with an increase in either magnetic parameter or radiation parameter or heat generation parameter.

3.5 Conclusion

The radiation effects on transient MHD convective Couette flow confined between two infinite vertical walls have been studied. The dimensionless governing partial differential equations are solved by the Laplace transform technique. The effects of different parameters such as radiation

parameter, Grashof number, Prandtl number, heat generation parameter and time are studied. It is found that the velocity u_1 decreases with an increase in magnetic parameter M^2. This observation can be explained by the fact that as M^2 increases, the Lorentz force which opposes the flow, increases and leads to enhanced deceleration of the flow. It is also observed that the velocity u_1 increases with an increase in either heat generation parameter or Grashof number Gr or time τ for impulsive motion. An increase in either radiation parameter R or Prandtl number Pr leads to fall in the fluid temperature θ. It is seen that the fluid temperature θ decreases with an increase in heat generation parameter ϕ. Further, it is seen that the absolute value of the shear stress τ_0 at the moving plate increases with an increase in either Grashof number or time while it decreases with an increase in either radiation parameter or magnetic parameter. The rate of heat transfer $-\theta'(0,\tau)$ increases with an increase in either radiation parameter or ϕ. The vertical flow rate decreases with an increase in radiation parameter. Therefore, we may conclude that the interaction between the radiation, MHD effects, buoyancy forces and the heat generation induced by a vertical motion of one of the plates can affect the configuration of the flow field significantly.

Bibliography

[1] Qian S and Bau HH, Mech. Res. Communications: **36**(2009), pp.10.

[2] Lemoff AV and Lee APB, Sensors and Actuators: **63**(2000), pp.178.

[3] West J, Karamata B, Lillis B, Gleeson JP, Alderman J, Collins JK, Lane W, Mathewson A and Berney H, Lab on a Chip.: **2**(2002), pp. 224.

[4] West J, Gleeson JP, Alderman J, Collins JK, Berney H. and Structuring B., Sensors and Actuators: **96**(2003), pp.190.

[5] Bestman AR and Adjepong SN, Space Sci.: **143**(1988), pp.73.

[6] Ghoshdastidar PS: Heat Transfer, Oxford University Press, UK: (2004).

[7] Peterson J, Tuttle N, Cooper H and Baukal C, Hydrocarbon Processing: (2007), pp.111.

[8] Korycki R, Int. J. Heat Mass Trans.: **49**(2006), pp.2033.

[9] Gbaorun FK, Ikyo B, Iyorzor B and Okanigbun R, J. of NAMP: **12**(2008), pp.201.

[10] Jha BK, Heat and Mass Trans.: **37**(2001), pp.329.

[11] Ogulu A and Motsa S, Physica Scripta: **71**(2005), pp.336.

[12] Mebine P, Global J. Pure and Appl. Math.: **3(2)**(2007), pp.1.

[13] Jha BK and Ajibade AO, Int. Comm. Heat and Mass Trans.: **36**(2009), pp.624.

[14] Jha BK and Ajibade AO, Int. J. Energy and Tech.: **2(12)**(2010), pp.1.

[15] Israel-Cookey C, Amos E and Nwaigwe C, American J. Sci. Indust. Res.: **1(2)**(2010), pp.326.

[16] Narahari M, WSEAS Transactions on Heat and Mass Trans.: **5(1)**(2010), pp.21.

[17] Deka RK and Bhattacharya A, Int. J. Math. Arch.: **2(6)**(2011), pp.853.

[18] Alagoa KD, Tay G and Abbey TM, Astro. Space Sci.: **260**(1999), pp.455.

[19] Gbadeyan JA, Daniel S and Kefas EG, J. Math. Associ. Nigeria: **32(2B)**(2005), pp.388.

[20] Baoku IG, Israel-Cookey C and Olajuwon BI, Surveys in Mathematics and its Appl.: **5**(2010), pp.215.

[21] Cogley ACL, Vincentine WC and Gilles SE, Am. Inst. Aeronat. Astronaut., J.: **6**(1968), pp.551.

[22] Grief R, Habib IS and Lin JC, J. Fluid Mech.: **46**(1970), pp.513.

Chapter 4

Hall effects on unsteady hydromagnetic flow past an accelerated porous plate in a rotating system*

4.1 Introduction

In recent years, considerable interest has been given to the theory of rotating fluids due to its application in cosmic and geophysical sciences. The rotating flow of an electrically conducting fluid in the presence of a magnetic field is encountered in cosmical and geophysical fluid dynamics. It is also important in the solar physics involved in the sunspot development, the solar cycle and the structure of rotating magnetic stars. It is well known that a number of astronomical bodies posses fluid interiors and magnetic fields. Changes in the rotation rate of such objects suggest the possible importance of hydromagnetic spin-up.

The hydromagnetic flow of a viscous incompressible electrically conducting fluid induced by a porous plate in the presence of rotating system is of considerable interest in the technical field due to its frequent occurrence in industrial and technological applications. The mechanism of conduction in ionized gases in the presence of strong magnetic field is different from that in metallic substance. The electric current in ionized gases is generally carried by electrons, which undergo successive collisions with other charged or neutral particles. In the ionized gases, the current is not proportional to the applied potential except when the field is very weak in an ionized gas where the density is low and the magnetic field is very strong, the conductivity normal to the magnetic field is reduced due to the free spiraling of electrons and ions about the

* *Published in* **J. of Applied Fluid Mech. (JAFM)**, *ISSN: 1735-3572, IF: 0.89, 8(3)(2015), pp.409-417.*

magnetic lines of force before suffering collisions and a current is induced in a direction normal to both electric and magnetic fields. This phenomenon, well known in the literature, is called the Hall effects.

The Hall effects are commonly used in distributors for ignition timing (and in some types of crank and camshaft position sensors for injection pulse timing, speed sensing, etc.). The Hall effects are used as a direct replacement for the mechanical breaker points used in earlier automotive applications in automotive ignition and fuel injection. The Hall effects devices when appropriately packaged are immune to dust, dirt, mud and water. These characteristics make Hall effects devices better for position sensing than alternative means such as optical and electromechanical sensing. The Hall effects sensors may be used in various sensors such as rotating speed sensors (bicycle wheels, gearteeth, automotive speedometers, electronic ignition systems), fluid flow sensors, current sensors, and pressure sensors. The common applications are often found where a robust and contactless switch or potentiometer is required. These include: electric airsoft guns, triggers of electropneumatic paintball guns, gocart speed controls, smart phones and some global positioning systems.

The study of hydromagnetic viscous flows with Hall currents has important engineering applications in problems of magnetohydrodynamic generators and of Hall accelerators as well as in flight magnetohydrodynamics. The unsteady hydromagnetic flow of an incompressible electrically conducting viscous fluid induced by a porous plate is of considerable interest in the technical field due to its frequent occurrence in industrial and technological applications. It is well known that a number of astronomical bodies posses fluid interiors and magnetic fields. It is also important in the solar physics involved in the sunspot development, the solar cycle and the structure of magnetic stars. The hydromagnetic flow near an accelerated plate in presence of a magnetic field has been examined by Soundalgekar[1]. Katagiri[2] has discussed the effects of Hall current on the boundary layer flow past a semi-infinite flat plate. The Hall effects on hydromagnetic flow near a porous plate has been studied by Pop[3]. Pop and Soundalgekar[4] have investigated the effects of Hall currents on hydromagnetic flow near a porous plate. Gupta[5] have studied the effects of Hall current on the steady magnetohydrodynamic flow of an electrically conducting fluid past an infinite porous flat plate. The oscillatory magnetohydrodynamic flow past a flat plate with Hall effects have been described by Datta and Jana[6]. Debnath et al.[7] have examined the effects of Hall current on unsteady hydromagnetic flow past a porous plate in a rotating system. Raptis and Ram[8] have presented the effects of Hall current and rotation on electrically conducting fluid past an infinite porous plate. The effect of Hall currents on hydromagnetic free convective flow near an accelerated porous plate have been investigated by Hossain and Mohammad[9]. Pop and Watanabe[10] have studied the Hall effects on magnetohydrodynamic free convection about a semi-infinite vertical flat plate. Takhar et al.[11] has discussed the MHD flow over a moving plate in a rotating fluid with magnetic field, Hall currents and free stream velocity. Hayat and Abbas[12] have studied the fluctuating rotating flow of second grade fluid past a porous heated plate with variable suction and Hall current. Hayat et al.[13] have also analyzed the effects of Hall Current and heat transfer on the flow in a porous medium with slip condition. Deka[14] has studied the Hall effects on MHD flow past an

accelerated plate. The Hall effects on hydromagnetic flow on an oscillatory porous plate have been described by Maji et al.[15]. Gupta et al.[16] have examined the Hall effects on MHD shear flow past an infinite porous flat plate with suction and blowing at the plate. Resently, Deka and Das[17] have presented the Hall effects on radiating MHD flow past an accelerated plate in a rotating fluid. In a recent paper, Deka[14] has made an exact solution of the Hall effects on an MHD flow past an accelerated plate in a rotating system. On a keen perusal into Deka's work, we have observed that his solution is incorrect due to wrongly written the equations of motion (1) and (2). He has shown that for a given value of Hall parameter m , the transverse velocity v_1 vanishes when $\Omega = \frac{mM^2}{1+m^2}$, which does not actually happen where Ω is the rotation parameter, M^2 the magnetic parameter and m the Hall parameter. He got this result due to error in Eqs. (1) and (2).

In this chapter, we have examined the effects of Hall current and rotation on a hydromagnetic flow of a viscous incompressible electrically conducting fluid past an accelerated porous flat plate in the presence of a uniform transverse magnetic field. It is assumed that the magnetic Reynolds number is small enough to neglect induced magnetic fields. The effects of governing parameters on the fluid velocity components, and the shear stresses at the plate are presented graphically and tabulated.

4.2 Mathematical formulation and its solution

Consider the unsteady hydromagnetic flow of a viscous incompressible electrically conducting fluid past an accelerated porous flat plate in the presence of a uniform transverse magnetic field in a rotating system. Choose a Cartesian co-ordinate system with x-axis along the plate in the direction of the flow, z-axis is normal to the plate and y-axis is perpendicular to the xz-plane [see **Figure 4.1**]. Initially, at time $t = 0$, both the plate and the fluid are assumed to be at rest. At time $t > 0$, the plate at $z = 0$ starts to move in its own plane with the velocity at, where t is the time and a being a constant. A uniform magnetic field of strength B_0 is imposed perpendicular to the plate. The effects of Hall current and rotation give rise to a force in y-direction, which induces a cross flow in that direction. Since the plate is infinitely long along x and y-directions and is electrically non-conducting, the velocity field and temperature distribution are functions of z and t only. Also, no applied or polarized voltages exist, so the effects of polarization of fluid is negligible. This corresponds to the case where no energy is added or extracted from the fluid by electrical means. It is assumed that the induced magnetic field generated by fluid motion is negligible in comparison to the applied one. This assumption is justified because magnetic Reynolds number is very small for partially ionized fluids which are commonly used in industrial applications. The equation of continuity $\nabla \cdot \vec{q} = 0$ gives $w = -w_0$, where u,v and w_0 being the velocity components along the coordinate axes. Here $w_0 > 0$ for suction and $w_0 < 0$ for blowing/injection at the plate.

The equations of momentum in a rotating frame of reference is

$$\frac{\partial \vec{q}}{\partial t} + (\vec{q}.\vec{\nabla})\vec{q} + 2\vec{\Omega} \times \vec{q} \;\; = \;\; -\frac{1}{\rho}\vec{\nabla} p_0 + \nu \nabla^2 \vec{q} + \frac{1}{\rho}(\vec{j} \times \vec{B}), \tag{4.1}$$

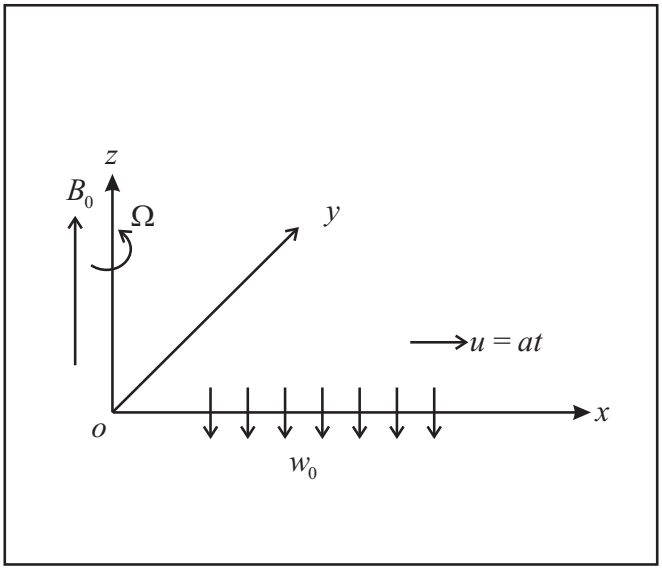

Figure 4.1: Geometry of the problem

where p_0, $\vec{q}$, ρ, ν, $\vec{j}$ and $\vec{B}$ are respectively the fluid pressure including centrifugal force, the fluid velocity vector, the fluid density, the kinematic viscosity, the current density vector and magnetic field vector.
The initial and boundary conditions for the velocity fields are

$$\begin{aligned} t = 0: &\qquad u = v = 0 \ \text{ for all } \ z \geq 0, \\ t > 0: &\qquad u = a\,t, \ v = 0 \ \text{ at } \ z = 0, \\ t > 0: &\qquad u \to 0, \ \ v \to 0 \ \text{ as } \ z \to \infty, \end{aligned} \tag{4.2}$$

where a is a constant.
The generalized Ohm's law, on taking Hall currents into an account and neglecting ion-slip and thermo-electric effects, is (see Cowling[19])

$$\vec{j} + \frac{\omega_e \tau_e}{B_0}\left(\vec{j} \times \vec{B}\right) = \sigma\left(\vec{E} + \mu_e \vec{q} \times \vec{B}\right), \tag{4.3}$$

where $\vec{E}$ the electric field vector, ω_e the cyclotron frequency, σ the electrical conductivity of the fluid and τ_e the collision time of electron and μ_e the magnetic permeability.

The solenoidal relation $\nabla \cdot \vec{B} = 0$ for the magnetic field gives $B_z = B_0 =$ constant everywhere in the fluid where $\vec{B} \equiv (0, 0, B_0)$. Further, if (j_x, j_y, j_z) be the components of the current density $\vec{j}$, then the equation of the conservation of the charge $\nabla \cdot \vec{j} = 0$ gives $j_z =$ constant. This constant is zero since $j_z = 0$ at the plate which is electrically non-conducting. Thus $j_z = 0$ everywhere in the flow. Since the induced magnetic field is neglected, the Maxwell's equation $\nabla \times \vec{E} = -\mu_e \frac{\partial \vec{B}}{\partial t}$ becomes $\nabla \times \vec{E} = 0$ which gives $\frac{\partial E_x}{\partial z} = 0$ and $\frac{\partial E_y}{\partial z} = 0$. This implies that $E_x =$ constant and $E_y =$ constant everywhere in the flow.

In view of the above assumption, equation (4.3) gives

$$j_x + mj_y = \sigma(E_x + vB_0), \tag{4.4}$$

$$j_y - mj_x = \sigma(E_y - uB_0), \tag{4.5}$$

where $m = \omega_e\tau_e$ is the Hall parameter. For positive values of m, B_0 is upwards and the electrons of the conducting fluid gyrate in the same sense as the rotating system. For negative values of m, B_0 is downwards and the electrons gyrate in an opposite sense to the rotating system.
At infinity, the magnetic field is uniform so that there is no current and hence, we have

$$j_x \to 0,\ j_y \to 0 \ \text{ as } \ \mathrm{z} \to \infty. \tag{4.6}$$

On the use of equation (4.6), equations (4.4) and (4.5) yield

$$E_x = 0,\ \ E_y = 0, \tag{4.7}$$

everywhere in the flow.
Substituting the above values of E_x and E_y in equations (4.4) and (4.5) and solving for j_x and j_y, we get

$$j_x = \frac{\sigma B_0}{1+m^2}(v + mu), \tag{4.8}$$

$$j_y = \frac{\sigma B_0}{1+m^2}(mv - u). \tag{4.9}$$

On the use of equations (4.8) and (4.9), the momentum equations of (4.1) along x- and y-directions become

$$\frac{\partial u}{\partial t} - w_0\frac{\partial u}{\partial z} - 2\Omega v = \nu\frac{\partial^2 u}{\partial z^2} - \frac{\sigma B_0^2}{\rho(1+m^2)}(u - mv), \tag{4.10}$$

$$\frac{\partial v}{\partial t} - w_0\frac{\partial v}{\partial z} + 2\Omega u = \nu\frac{\partial^2 v}{\partial z^2} - \frac{\sigma B_0^2}{\rho(1+m^2)}(v + mu), \tag{4.11}$$

where w_0 is the normal velocity of suction or injection at the plate according as $w_0 > 0$ or $w_0 < 0$, respectively and $w_0 = 0$ represents the case of non-permeable plate.

Introducing non-dimensional variables

$$(u_1, v_1) = \frac{(u, v)}{(a\nu)^{\frac{1}{3}}},\ \ \eta = z\left(\frac{a}{\nu}\right)^{\frac{1}{3}}, \tau = t\left(\frac{a^2}{\nu}\right)^{\frac{1}{3}} \tag{4.12}$$

equations (4.10) and (4.11) become

$$\frac{\partial u_1}{\partial \tau} - S\frac{\partial u_1}{\partial \eta} - 2K^2 v_1 = \frac{\partial^2 u_1}{\partial \eta^2} - \frac{M^2}{1+m^2}(u_1 - mv_1), \tag{4.13}$$

$$\frac{\partial v_1}{\partial \tau} - S\frac{\partial v_1}{\partial \eta} + 2K^2 u_1 = \frac{\partial^2 v_1}{\partial \eta^2} - \frac{M^2}{1+m^2}(mu_1 + v_1), \tag{4.14}$$

where $M^2 = \frac{\sigma {B_0}^2 \left(\frac{\nu}{a^2}\right)^{\frac{1}{3}}}{\rho}$ is the magnetic parameter, $K^2 = \Omega \left(\frac{\nu}{a^2}\right)^{\frac{1}{3}}$ the rotation parameter and $S = \frac{w_0}{(a\nu)^{\frac{1}{3}}}$ the suction parameter.

The initial and boundary conditions (4.2) become

$$\begin{aligned} \tau = 0 \quad &: \quad u_1 = v_1 = 0 \ \text{ for all } \ \eta \geq 0, \\ \tau > 0 \quad &: \quad u_1 = \tau, \ v_1 = 0 \ \text{ at } \ \eta = 0, \\ \tau > 0 \quad &: \quad u_1 \to 0, \ v_1 \to 0 \ \text{ as } \ \eta \to \infty. \end{aligned} \tag{4.15}$$

Combining equations (4.13) and (4.14), we get

$$\frac{\partial F}{\partial \tau} - S\frac{\partial F}{\partial \eta} = \frac{\partial^2 F}{\partial \eta^2} - \left[2iK^2 + \frac{M^2(1+im)}{1+m^2}\right] F \tag{4.16}$$

where

$$F = u_1 + iv_1 \ \ and \ \ i = \sqrt{-1}. \tag{4.17}$$

The initial and boundary conditions for $F(\eta, \tau)$ are

$$F(\eta, 0) = 0, \quad F(0, \tau) = \tau, \quad F(\infty, \tau) = 0. \tag{4.18}$$

4.2.1 General solution

Taking the Laplace transform of equation (4.16), we have

$$\frac{d\bar{F}}{d\tau} + S\frac{d\bar{F}}{d\eta} - \left[s + 2iK^2 + \frac{M^2(1+im)}{1+m^2}\right] \bar{F} = 0, \tag{4.19}$$

where

$$\bar{F}(\eta, s) = \int_0^\infty F(\eta, \tau)\, e^{-s\tau}\, d\tau \tag{4.20}$$

and $s(> 0)$ is the Laplace parameter.
The corresponding boundary conditions for $\bar{F}$ are

$$\bar{F}(0, s) = \frac{1}{s^2}, \quad \bar{F}(\infty, s) = 0. \tag{4.21}$$

The solution of equation (4.19) subject to the boundary conditions (4.21) is

$$\overline{F}(\eta, s) = \frac{1}{s^2}\, e^{-\frac{S}{2}\,\eta} e^{-\sqrt{\lambda + s}\,\eta}, \tag{4.22}$$

where

$$\lambda = \left[2iK^2 + \frac{M^2(1+im)}{1+m^2}\right] + \frac{S^2}{4}. \tag{4.23}$$

On the use of inverse Laplace transform, equation (4.22) becomes

$$\begin{aligned} F(\eta,\tau) &= \frac{1}{2}\Bigg[\left\{\tau+\frac{\eta}{2(\alpha+i\beta)}\right\} e^{\{(\alpha+i\beta)-\frac{S}{2}\}\,\eta}\,\mathrm{erfc}\left\{\frac{\eta}{2\sqrt{\tau}}+(\alpha+i\beta)\sqrt{\tau}\right\} \\ &+ \left\{\tau-\frac{\eta}{2(\alpha+i\beta)}\right\} e^{-\{(\alpha+i\beta)+\frac{S}{2}\}\,\eta}\,\mathrm{erfc}\left\{\frac{\eta}{2\sqrt{\tau}}-(\alpha+i\beta)\sqrt{\tau}\right\}\Bigg], \end{aligned} \tag{4.24}$$

where

$$\begin{aligned} \alpha,\ \beta &= \frac{1}{\sqrt{2}}\left[\left\{\left(\frac{M^2}{1+m^2}+\frac{S^2}{4}\right)^2+\left(2K^2+\frac{M^2}{1+m^2}\right)^2\right\}^{\frac{1}{2}}\right. \\ &\left.\pm\left(\frac{M^2}{1+m^2}+\frac{S^2}{4}\right)\right]^{1/2}. \end{aligned} \tag{4.25}$$

Equation (4.24) does not coincident with the Eq.(15) of Deka[14] when $S = 0$ due to the mathematical error in Eqs.(1) and (2) of his paper (as discussed in the introduction).

4.2.2 Small time solution

To get some physical insight into the flow pattern, we shall examine the solution (4.24) for small and large times τ. For small times τ , the method given by Carslaw and Jaeger[18] is very useful where small time corresponds to large s. For small times, equation (4.22) can be rewritten as

$$\bar{F}(\eta,p) = e^{-(\frac{S}{2}\,\eta+\lambda\tau)}\sum_{n=0}^{\infty}(n+1)\lambda^n\frac{e^{-\sqrt{s}\,\eta}}{s^{n+2}}, \tag{4.26}$$

where λ is given by equation (4.23).
Taking the inverse Laplace transform of equation (4.26), we have

$$\begin{aligned} F(\eta,\tau) &= e^{-\{\frac{S}{2}\eta+(\alpha+i\beta)^2\,\tau\}} \\ &\times\sum_{n=0}^{\infty}(n+1)(\alpha+i\beta)^{2n}(4\tau)^{n+1}\,i^{2n+2}\mathrm{erfc}\left(\frac{\eta}{2\sqrt{\tau}}\right). \end{aligned} \tag{4.27}$$

On the use of equation (4.17), equation (4.27) yields

$$\begin{aligned} u_1(\eta,\tau) &= e^{-\{\frac{S}{2}\eta+(\alpha^2-\beta^2)\,\tau\}} \\ &\times\left[\cos 2\alpha\beta\tau\left\{(4\tau)T_2+2(\alpha^2-\beta^2)(4\tau)^2T_4+\cdots\right\}\right. \\ &\left.+\sin 2\alpha\beta\tau\left\{4\alpha\beta(4\tau)^2T_4+12\alpha\beta(\alpha^2-\beta^2)(4\tau)^3T_6+\cdots\right\}\right], \end{aligned} \tag{4.28}$$

$$\begin{aligned} v_1(\eta,\tau) &= e^{-\{\frac{S}{2}\eta+(\alpha^2-\beta^2)\,\tau\}} \\ &\times\left[\cos 2\alpha\beta\tau\left\{4\alpha\beta(4\tau)^2T_4+12\alpha\beta(\alpha^2-\beta^2)(4\tau)^3T_6+\cdots\right\}\right. \\ &\left.-\sin 2\alpha\beta\tau\left\{(4\tau)T_2+2(\alpha^2-\beta^2)(4\tau)^2T_4+\cdots\right\}\right], \end{aligned} \tag{4.29}$$

where α and β are given by equation (4.25) and

$$T_{2n+2} = j^{2n+2}\text{erfc}\left(\frac{\eta}{2\sqrt{\tau}}\right),\ j^n\text{erfc}(\eta) = j^{n-1}\text{erfc}(\eta),\ j^0\text{erfc}(\eta) = \text{erfc}(\eta). \quad (4.30)$$

Equations (4.28) and (4.29) show that the Hall effects become important only when terms of order τ is taken into an account.

4.2.3 Solution for large time

For large times, equation (4.24) can be written in the following form

$$\begin{aligned} u_1 + iv_1 &= e^{-\frac{S}{2}\eta}\left[2\left(\frac{\tau}{2} - \frac{\eta}{4(\alpha+i\beta)}\right)e^{-(\alpha+i\beta)\eta}\right. \\ &+ \left(\frac{\tau}{2} + \frac{\eta}{4(\alpha+i\beta)}\right)e^{(\alpha+i\beta)\eta}\ \text{erfc}\left\{(\alpha+i\beta)\sqrt{\tau} + \frac{\eta}{2\sqrt{\tau}}\right\} \\ &- \left.\left(\frac{\tau}{2} - \frac{\eta}{4(\alpha+i\beta)}\right)e^{-(\alpha+i\beta)\eta}\text{erfc}\left\{(\alpha+i\beta)\sqrt{\tau} - \frac{\eta}{2\sqrt{\tau}}\right\}\right]. \quad (4.31) \end{aligned}$$

For $\eta \ll 2\sqrt{\tau}$ and $\tau \gg 1$, equation (4.31) approximates to

$$\begin{aligned} u_1(\eta,\tau) &= \tau e^{-(\frac{S}{2}+\alpha)\eta}\cos\beta\eta + \sqrt{\frac{\tau}{\pi}}\,\frac{e^{-\{\frac{S}{2}\eta+(\alpha^2-\beta^2)\tau\}}}{\alpha^2+\beta^2} \\ &\times [\alpha(\cos 2\alpha\beta\tau\sinh\alpha\eta\cos\beta\eta + \sin 2\alpha\beta\tau\cosh\alpha\eta\sin\beta\eta) \\ &+ \beta(\cos 2\alpha\beta\tau\cosh\alpha\eta\sin\beta\eta - \sin 2\alpha\beta\tau\sinh\alpha\eta\cos\beta\eta)] \quad (4.32) \end{aligned}$$

$$\begin{aligned} v_1(\eta,\tau) &= -\tau e^{-(\frac{S}{2}+\alpha)\eta}\sin\beta\eta + \sqrt{\frac{\tau}{\pi}}\,\frac{e^{-\{\frac{S}{2}\eta+(\alpha^2-\beta^2)\tau\}}}{\alpha^2+\beta^2} \\ &\times [\alpha(\cos 2\alpha\beta\tau\cosh\alpha\eta\sin\beta\eta - \sin 2\alpha\beta\tau\sinh\alpha\eta\cos\beta\eta) \\ &- \beta(\cos 2\alpha\beta\tau\sinh\alpha\eta\cos\beta\eta + \sin 2\alpha\beta\tau\cosh\alpha\eta\sin\beta\eta)] \quad (4.33) \end{aligned}$$

The second term in each of the equation (4.32) and (4.33) represents the inertial oscillations on the fluid velocity which decay exponentially with time τ and the frequency of these oscillations is $\omega = 2\alpha\beta = 1 + \frac{mM^2}{1+m^2}$. This equation shows that the frequency is independent of suction/blowing at the plate. Further, the frequency ω increases with an increase in magnetic parameter M^2 while with an increase in Hall parameter m, ω first increases steadily, reaches a maximum and then decreases.

4.3 Result and Discussion

In order to get a physical insight into the problem, a parametric study is performed and the obtained numerical results are elucidated with the help of graphical illustrations. We have presented the non-dimensional velocity and shear stresses for several values of magnetic parameter M^2, Hall parameter m, rotation parameter K^2, suction parameter S and time τ.

4.3.1 Effects of parameters on the velocity profiles

The effects of pertinent parameters on the primary as well as the secondary velocities are presented graphically against η in **Figures 4.2-4.6**.

It is seen from **Figure 4.2** that both the primary velocity u_1 and the magnitude of the secondary velocity v_1 decrease with an increase in magnetic parameter M^2. The imposition of the transverse magnetic field tends to retard the fluid flow. This phenomenon has an excellent agreement with the physical fact that the Lorentz force generated in present flow model due to interaction of the transverse magnetic field and the fluid velocity acts as a resistive force to the fluid flow which serves to decelerate the flow. The reduction of the boundary layer velocity due to the imposition of the transverse magnetic field causes the pressure gradient to drop and as a consequence the boundary layer separation is prevented to some extent. It also resists the transition from laminar to turbulent flow which causes the viscous drag to increase and as a result the flow is stabilized. As such the magnetic field is an effective regulatory mechanism for the flow regime. **Figure 4.3** illustrate that the primary velocity u_1 as well as the magnitude of the secondary velocity v_1 increase with an increase in Hall parameter m. Hall currents tend to accelerate secondary fluid velocity which is consistent with the fact that Hall currents induce secondary flow in the flow field. This is a new phenomenon, which appears as a result of including the Hall term. The case $m = 0$ corresponds to the neglect of the Hall effects.

It is found from **Figure 4.4** that the primary velocity u_1 decreases while the magnitude of the secondary velocity v_1 increases with an increase in rotation parameter K^2. This implies that rotation tends to retard primary fluid velocity. Although rotation induces the secondary fluid velocity in the flow field by suppressing the primary fluid velocity, its accelerating effects is prevalent only in the region near to the plate. This is due to the reason that Coriolis force is dominant in the region near to the axis of rotation. An increase in suction parameter S leads to decrease both the primary velocity u_1 and the magnitude of the secondary velocity v_1 as shown in **Figure 4.5**. It is observed that the suction/blowing exerts a strong influence on the velocity profiles. It is observed from **Figure 4.6** that both the primary velocity u_1 and the magnitude of the secondary velocity v_1 increase with an increase in time τ. This implies that primary and secondary fluid velocities are getting accelerated with the progress of time.

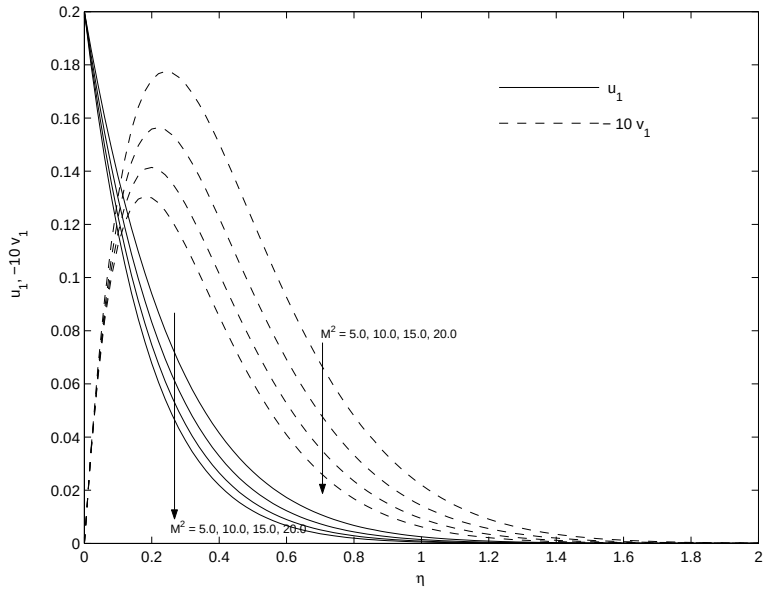

Figure 4.2: Velocity profiles for M^2 when $K^2 = 3, S = 0.5, m = 0.2$ and $\tau = 0.2$.

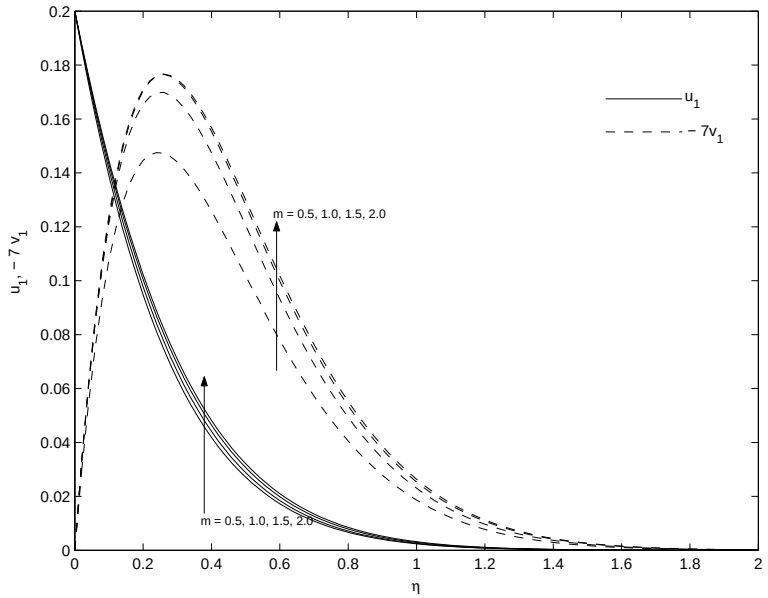

Figure 4.3: Velocity profiles for m when $K^2 = 3, S = 0.5, M^2 = 5$ and $\tau = 0.2$.

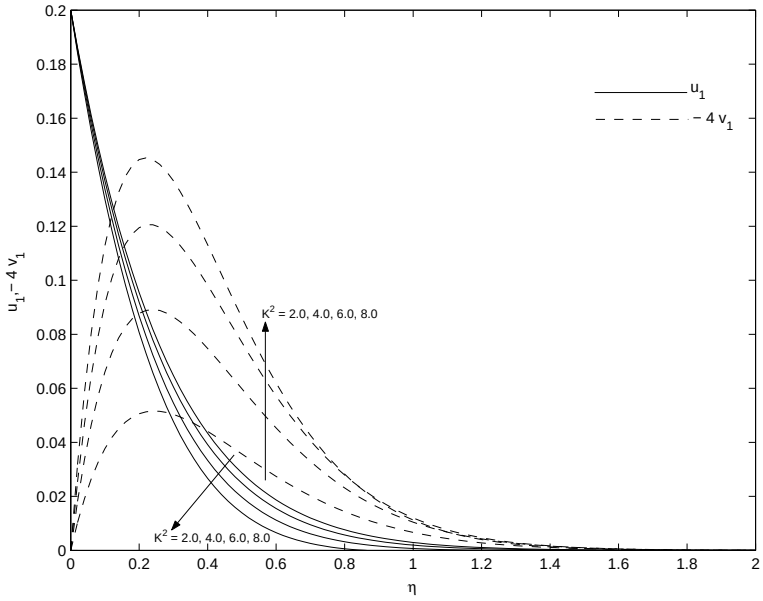

Figure 4.4: Velocity profiles for K^2 when $M^2 = 5, S = 0.5, m = 0.2$ and $\tau = 0.2$.

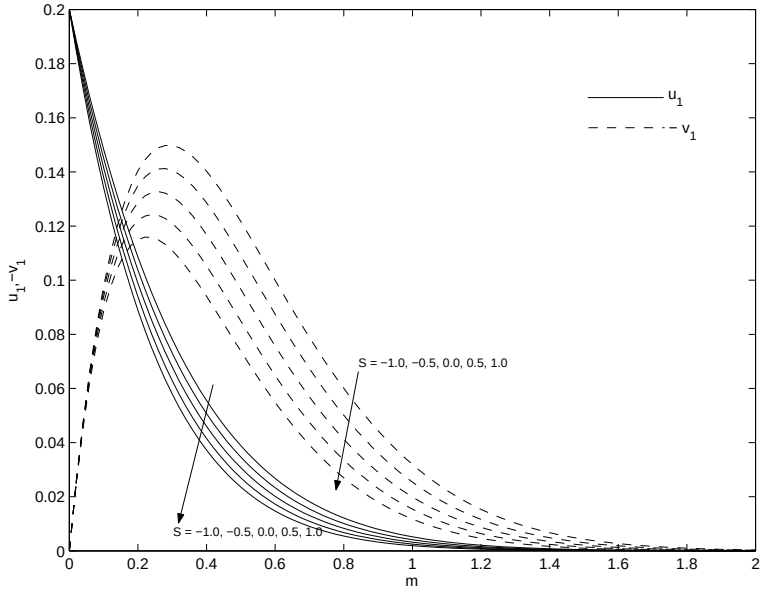

Figure 4.5: Velocity profiles for S when $K^2 = 3, M^2 = 5, m = 0.2$ and $\tau = 0.2$.

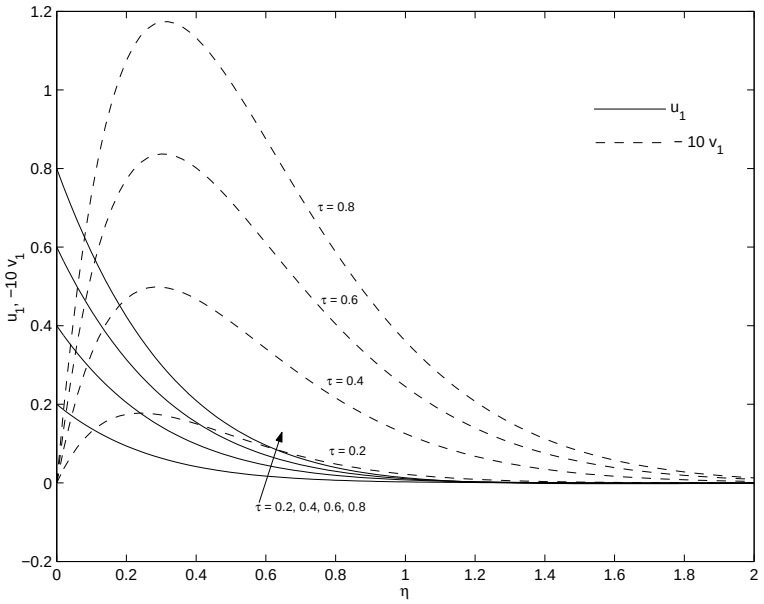

Figure 4.6: Velocity profiles for τ when $K^2 = 3, S = 0.5, m = 0.2$ and $M^2 = 5$.

4.3.2 Comparison between general time and small time solution

For small values of time, we have drawn the primary velocity u_1 and the secondary velocity v_1 on using the exact solution given by the equation (4.24) and the series solution given by equations (4.28) and (4.29) in **Figures 4.7 and 4.8** respectively.

It is seen from **Figures 4.7 and 4.8** that the series solution given by equations (4.28) and (4.29) converges more quickly than the exact solution given by equation (4.24) for small times. Hence, we conclude that for small times, the numerical values of the velocity components u_1 and v_1 can be computed from equations (4.28) and (4.29) instead of equation (4.24).

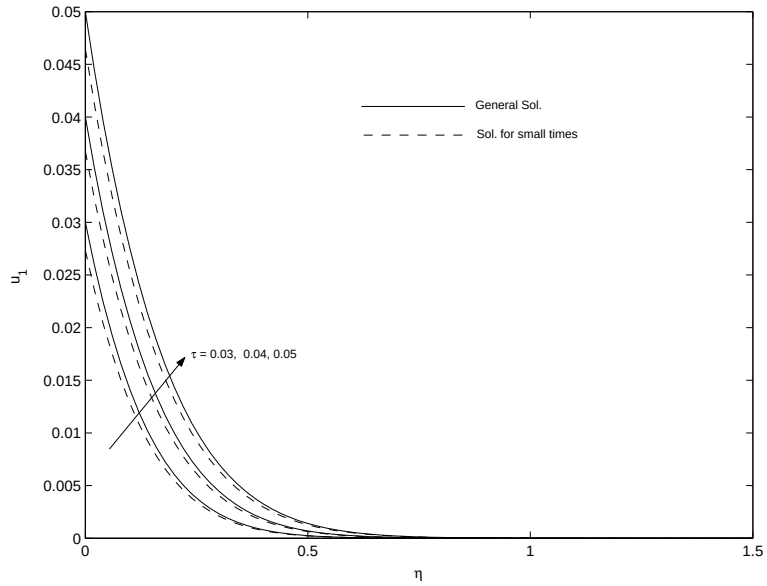

Figure 4.7: Variation of u_1 for general and small time solutions when $M^2 = 5, K^2 = 3, m = 0.2$ and $S = 0.5$.

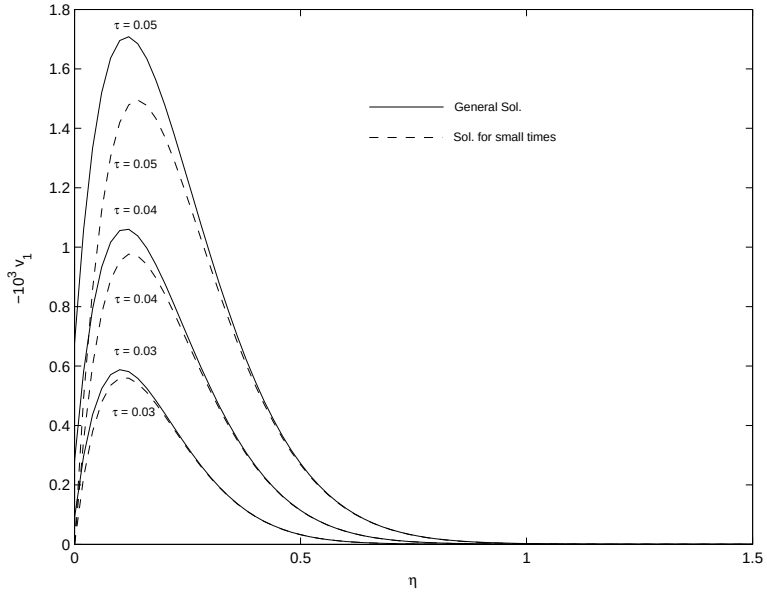

Figure 4.8: Variation of v_1 for general and small time solutions when $M^2 = 5, K^2 = 3, m = 0.2$ and $S = 0.5$.

4.3.3 Effects of parameters on the shear stresses at the plate

For engineering purposes, one is usually interested to determine the values of the shear stresses (or skin functions). The increased shear stresses is generally a disadvantage in the technical applications.
The non-dimensional shear stresses τ_x and τ_y due to the primary and the secondary flows at the plate $\eta = 0$ respectively obtained from equation (4.24) are

$$\tau_x + i\tau_y = -\frac{S\tau}{2} - \frac{1}{2\,(\alpha + i\beta)}\{1 + 2(\alpha + i\beta)^2\tau\}\left\{\mathrm{erf}\sqrt{(\alpha + i\beta)\tau}\right\} - \sqrt{\frac{\tau}{\pi}}\, e^{-(\alpha+i\beta)^2\tau}, \quad (4.34)$$

where α and β are given by equation (4.25).

The numerical results of the non-dimensional shear stresses τ_x and τ_y at the plate $\eta = 0$ for several values of rotation parameter K^2, magnetic parameter M^2 , suction parameter S and time τ against the Hall parameter m are presented in **Figures 4.9-4.12**. **Figure 4.9** shows that the absolute values of the shear stresses τ_x and τ_y increase with an increase in rotation parameter K^2. Rotation tends to enhance both the shear stresses at the plate. On the other hand, the absolute value of the shear stress τ_x decreases whereas the absolute value of the shear stress τ_y increases with an increase in Hall parameter m. This implies that, the Hall currents have tendency to reduce the shear stress due to the primary flow whereas these physical quantities have reverse effects on the shear stress due to secondary flow. It is seen from **Figure 4.10** that the absolute value of the shear stress τ_x increases while the absolute value of the shear stress τ_y decreases for $m \leq 0.2$ and it increases for $m > 0.2$ for increasing magnetic parameter M^2. **Figure 4.11** displays that the absolute value of the shear stress τ_x increases whereas the absolute value of the shear stress τ_y decreases with an increase in suction parameter S. It is found from **Figure 4.12** that the absolute values of the shear stresses τ_x and τ_y decrease with an increase in time τ.

4.3.4 Shear stresses at the plate for small time

For small time, the non-dimensional shear stresses τ_x due to the primary flow and τ_y due to the secondary flow at the plate $\eta = 0$ are obtained as

$$\tau_x = -e^{(\alpha^2-\beta^2)\tau}\left[\frac{S}{2}\, A_1(0,\tau) + \frac{1}{2\sqrt{\tau}}\, A_2(0,\tau)\right], \quad (4.35)$$

$$\tau_y = -e^{(\alpha^2-\beta^2)\tau}\left[\frac{S}{2}\, B_1(0,\tau) + \frac{1}{2\sqrt{\tau}}\, B_2(0,\tau)\right], \quad (4.36)$$

where

$$\begin{aligned}
A_1(\eta,\tau) &= \cos 2\alpha\beta\tau\left\{(4\tau)T_2 + 2(\alpha^2-\beta^2)(4\tau)^2T_4 + \cdots\right\} \\
&+ \sin 2\alpha\beta\tau\left\{4\alpha\beta(4\tau)^2T_4 + 12\alpha\beta(\alpha^2-\beta^2)(4\tau)^3T_6 + \cdots\right\} \\
B_1(\eta,\tau) &= \cos 2\alpha\beta\tau\left\{4\alpha\beta(4\tau)^2T_4 + 12\alpha\beta(\alpha^2-\beta^2)(4\tau)^3T_6 + \cdots\right\} \\
&- \sin 2\alpha\beta\tau\left\{(4\tau)T_2 + 2(\alpha^2-\beta^2)(4\tau)^2T_4 + \cdots\right\}
\end{aligned}$$

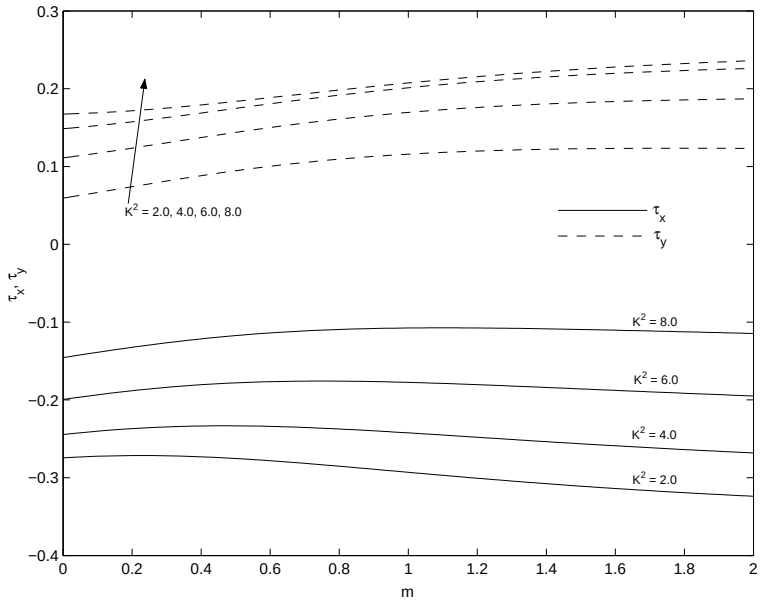

Figure 4.9: Shear stresses τ_x and τ_y for K^2 when $M^2 = 5, S = 0.5$ and $\tau = 0.2$.

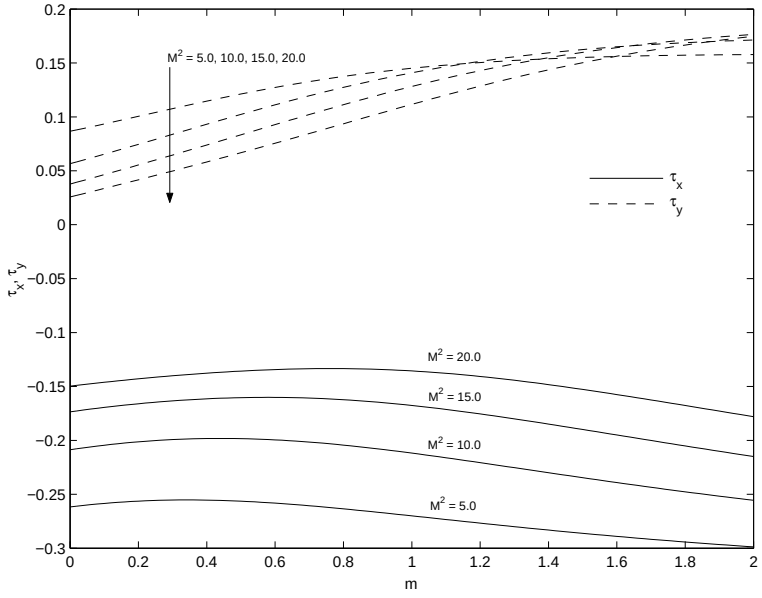

Figure 4.10: Shear stresses τ_x and τ_y for M^2 when $K^2 = 3, S = 0.5$ and $\tau = 0.2$.

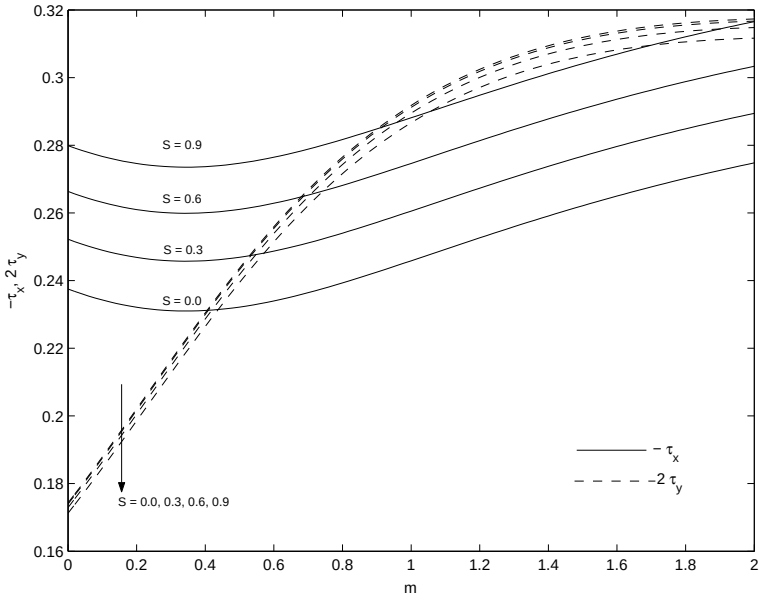

Figure 4.11: Shear stresses τ_x and τ_y for S when $M^2 = 5, K^2 = 3$ and $\tau = 0.2$.

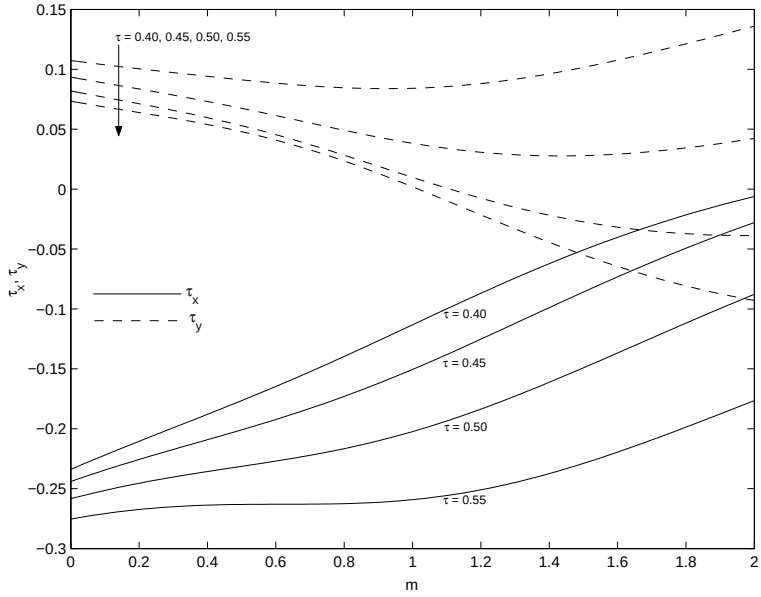

Figure 4.12: Shear stresses τ_x and τ_y for τ when $M^2 = 5, S = 0.5$ and $K^2 = 3$.

$$
\begin{aligned}
A_2(\eta,\tau) &= \cos 2\alpha\beta\tau\left\{(4\tau)Y_1 + 2(\alpha^2-\beta^2)(4\tau)^2Y_3 + \cdots\right\} \\
&+ \sin 2\alpha\beta\tau\left\{4\alpha\beta(4\tau)^2Y_3 + 12\alpha\beta(\alpha^2-\beta^2)(4\tau)^3Y_5 + \cdots\right\} \\
B_2(\eta,\tau) &= \cos 2\alpha\beta\tau\left\{4\alpha\beta(4\tau)^2Y_3 + 12\alpha\beta(\alpha^2-\beta^2)(4\tau)^3Y_5 + \cdots\right\} \\
&- \sin 2\alpha\beta\tau\left\{(4\tau)Y_1 + 2(\alpha^2-\beta^2)(4\tau)^2Y_3 + \cdots\right\} \\
Y_{2n+1} &= j^{2n+1}\mathrm{erfc}\left(\eta/2\sqrt{\tau}\right),\ j^{-1}\mathrm{erfc}\left(\eta/2\sqrt{\tau}\right) = \frac{2}{\sqrt{\pi}}\,e^{-z^2}. \qquad (4.37)
\end{aligned}
$$

The numerical results of the non-dimensional shear stress τ_x due to the primary flow and the shear stress τ_y due to the secondary flow at the plate $\eta = 0$ for the general solution and the solution for small time calculated from the equations (4.34), (4.35) and (4.36) respectively are given in **Tables-I and II** for several values of Hall parameter m and time τ. It is observed from **Tables-I and II** that for small time solution, the shear stresses calculated from equations (4.35) and (4.36) give better result than that calculated from equation (4.34).

Table-I

Shear stress τ_x at the plate $\eta = 0$ when $M^2 = 5$, $K^2 = 3$ and $S = 0.5$

	$-10\tau_x$ (For general solution)			*$-10\tau_x$ (Solution for small times)*		
m/τ	*0.001*	*0.002*	*0.003*	*0.001*	*0.002*	*0.003*
0.2	*0.35991*	*0.51127*	*0.62856*	*0.35992*	*0.51131*	*0.62867*
0.4	*0.35985*	*0.51111*	*0.62825*	*0.35986*	*0.51117*	*0.62844*
0.6	*0.35977*	*0.51089*	*0.62786*	*0.35979*	*0.51098*	*0.62811*
0.8	*0.35970*	*0.51068*	*0.62748*	*0.35972*	*0.51078*	*0.62776*

Table-II

Shear stress τ_y at the plate $\eta = 0$ when $M^2 = 5$, $K^2 = 3$ and $S = 0.5$

	$-10^3\tau_y$ (For general solution)			*$-10^3\tau_y$ (Solution for small times)*		
m/τ	*0.001*	*0.002*	*0.003*	*0.001*	*0.002*	*0.003*
0.2	*0.08258*	*0.23365*	*0.42893*	*0.08272*	*0.23367*	*0.42869*
0.4	*0.09165*	*0.25929*	*0.47606*	*0.09178*	*0.25930*	*0.47572*
0.6	*0.09737*	*0.27553*	*0.50594*	*0.09752*	*0.27553*	*0.50554*
0.8	*0.10015*	*0.28342*	*0.52051*	*0.10030*	*0.28343*	*0.52008*

It is seen from **Table-I** that the magnitude of the shear stress τ_x due to the primary flow decreases with an increase in Hall parameter m whereas it increases with an increase in time τ for both general solution and solution for small times. **Table-II** depicted that for both general solution and small time solution the magnitude of the shear stress τ_y due to the secondary flow increases with an increase in either Hall parameter m or time τ.

4.4 Conclusion

An investigation of the effects of Hall current and rotation on unsteady hydromagnetic flow of a viscous incompressible electrically conducting fluid past an accelerated porous plate in a rotating system have been carried out. The dimensionless governing partial differential equations are solved by the Laplace transform technique. The effects of different parameters such as magnetic parameter, Hall parameter, rotation parameter, suction parameter and time are studied. It is seen that Hall current tends to accelerate the primary and secondary fluid velocities. Rotation has tendency to retard primary fluid velocity and tends to accelerate secondary fluid velocity. The primary and secondary fluid velocities are getting accelerated with the progress of time. It is also found that both the primary velocity u_1 and the magnitude of the secondary velocity v_1 decrease with an increase in magnetic parameter M^2. The imposition of the transverse magnetic field tends to retard the fluid flow. This phenomenon has an excellent agreement with the physical fact that the Lorentz force generated in present flow model due to interaction of the transverse magnetic field and the fluid velocity acts as a resistive force to the fluid flow which serves to decelerate the flow. The reduction of the boundary layer velocity due to the imposition of the transverse magnetic field causes the pressure gradient to drop and as a consequence the boundary layer separation is prevented to some extent. Rotation tends to enhance both the shear stresses at the plate. On the other hand, the absolute value of the shear stress τ_x due to the primary flow decreases whereas the absolute value of the shear stress τ_y due to the secondary flow increases with an increase in Hall parameter m. This implies that, the Hall currents have a tendency to reduce the shear stress due to the primary flow whereas these physical quantities have reverse effects on the shear stress due to secondary flow. It is interesting to note that for small times, the series solution converges more rapidly than the general solution. The effects of Hall current in rotating environment will be useful in dealing with real engineering problems.

Bibliography

[1] Soundalgekar VM, Appl. Sci. Res.: **12(1)**(1965), pp.151.

[2] Katagiri T, J. Phys. Soc. Jpn.: **27**(1969), pp.1051.

[3] Pop I, J. Math. Phys. Sci.: **5**(1971), pp.375.

[4] Pop I and Soundalgekar VM, Acta Mechanica: **20**(1974), pp.316.

[5] Gupta AS, Acta Mechanica: **22**(1975), pp.281.

[6] Datta N and Jana RN, J. Phys. Soc. Jpn.: **40**(1976), pp.1469.

[7] Debnath L, Ray SC and Chatterjee AK, Z. Angew. Math. Mech.: **59**(1979), pp.469.

[8] Raptis A and Ram PC, Astrophys. Space Sci.: **106**(1984), pp.257.

[9] Hossain MA and Mohammad K, Jpn. J. Appl. Phys.: **27(8)**(1988), pp.1531.

[10] Pop I and Watanabe T, Int. J. Engg. Sci.: **32**(1994), pp.1903.

[11] Takhar HS, Chamkha AJ and Nath G, Int. J. Eng. Sci.: **40**(2002), pp.1511.

[12] Hayat T and Abbas Z, J. Porous Medium: **10**(2007), pp.35.

[13] Hayat T, Wang Y and Hutter K, Int. J. Non-linera Mech.: **39**(2004), pp.1027.

[14] Deka RK, Theoret. Appl. Mech.: **35(4)**(2008), pp.333.

[15] Maji SL, Kanch AK, Guria M and Jana RN, Appl. Math. Mech.: **30(4)**(2009), pp.503.

[16] Gupta AS, Guria M and Jana RN, Int. J. Non-Linear Mech.: **46**(2011), pp.1057.

[17] Deka RK and Das SK, Fluids and Heat Trans.: **7**(2013), pp.2641.

[18] Carslaw HS and Jaeger JC, Conduction of heat in solids, Oxford Univ. Press, Oxford: (1959)

[19] Cowling TG, Magnetohydrodynamics, Intersci. Publisher, Inc, New York: (1957)

[20] Cramer KR and Pai SI, Magnetofluid Dynamics for Engineers and appl. physicists. McGraw Hill Book Company, NY: (1973)

Chapter 5

Effects of Hall current and radiation on unsteady MHD flow past a heated moving vertical plate*

5.1 Introduction

The combined effects of Hall current and radiation on the magnetohydrodynamic flows continue to attract the attention of engineering science and applied mathematics researchers owing to extensive applications of such flows in the context of ionized aerodynamics (see Soundalgekar and Takhar[1]). The nuclear energy systems control have been improved by Soundalgekar et al.[2]. Ram and Takhar [3] have improved designs in aerospace MHD energy systems. The manufacture of advanced aerospace materials etc have been developed by Takhar and Nath[4]. Both analytical and computational solutions have been presented to a wide spectrum of problems. Helliwell and Mosa[5] have reported on thermal radiation effects in buoyancy-driven hydromagnetic flow in a horizontal channel flow with an axial temperature gradient in the presence of Joule and viscous heating. The Hall current and surface temperature oscillation effects on natural convection magnetohydrodynamic heat-generating flow have been considered by Takhar and Ram[6]. Alagoa et al.[7] have studied the magnetohydrodynamic optically-transparent free-convection flow, with radiative heat transfer in porous medium with time-dependent suction using an asymptotic approximation, showing that thermal radiation exerts a significant effects on the flow dynamics. The magnetohydrodynamic free convection heat and mass transfer of a heat generating fluid past an impulsively started infinite vertical porous plate with Hall current

* *Published in* **J. of Applied Fluid Mech. (JAFM)**, *ISSN: 1735-3572, IF: 0.89, 7(4)(2014), pp.683-692.*

and radiation absorption have been studied by Kinyanjui et al.[8]. Aboeldahab and Elbarbary[9] have presented the effects of Hall current on magnetohydrodynamic free convection flow past a semi-infinite vertical plate with mass transfer. Cookey et al.[10] have investigated the influence of viscous dissipation and radiation on unsteady MHD free convection flow past an infinite heated vertical plate in a porous media with time dependent suction. Aboeldahab and El-Aziz[11] have studied the viscous dissipation and Joule heating effects on MHD free convection from a vertical plate with power-law variation in surface temperature in the presence of Hall and ion-slip currents. The thermal radiation interaction with unsteady MHD flow past a vertical porous plate immersed in a porous medium have been investigated by Samad and Rahman[12]. Chaudhary and Jain[13] have studied the unsteady hydromagnetic flow of a viscoelastic fluid from a radiative vertical porous plate. The effects of thermal radiation and Hall current on magnetohydrodynamic free-convective flow and mass transfer over a stretching sheet with variable viscosity in the presence of heat generation/absorption have been investigated by Shit and Haldar [14]. Israel-Cookey et al.[15] have studied the MHD oscillatory Couette flow of a radiating viscous fluid in a porous medium with periodic wall temperature. The effects of thermal radiation, Hall currents, Soret and Dufour on MHD flow by mixed convection over a vertical surface in porous mediaum have been described by Shateyi et al. [16]. Aurangzaib[17] has studied the effects of Soret and Dufour on unsteady MHD flow by mixed convection over a vertical surface in porous mediaum with internal heat generation, chemical reaction and Hall current. Singh and Pathak[18] have discussed the effects of rotation and Hall current on mixed convection MHD flow through a porous medium in a vertical channel in the presence of thermal radiation. Jain and Singh[19] have observed Hall and thermal radiation effects on an unsteady rotating free convection slip-flow. Recently, Chaudhary et al.[20] have presented the effects of Hall current and thermal radiation on an unsteady free convection slip-flow along a vertical plate embedded in a porous medium with constant heat and mass flux.

In this chapter, we study the effects of Hall current and radiation on MHD flow of a viscous incompressible electrically conducting fluid past a moving vertical plate with variable temperature in the presence of a uniform transverse magnetic filed. The governing equations are solved by the Laplace transform technique to obtain the analytical results for velocity, temperature, rate of heat transfer and shear stresses. The effects of physical parameters on the velocity, temperature, rate of heat transfer and shear stresses are analyzed in detail.

5.2 Formulation of the problem and its solution

Consider the unsteady hydromagnetic viscous incompressible electrically conducting fluid past a moving vertical plate with variable plate temperature. Choose a Cartesian co-ordinate system with x- axis along the plate in the direction of the flow, z-axis is normal to the plate and y-axis is perpendicular to the xz-plane [see **Figure 5.1**]. Initially, at time $t = 0$, both the plate and the fluid are assumed to be at the same temperature T_∞ and stationary. At time $t > 0$, the plate at $z = 0$ starts to move in its own plane with a uniform velocity U_0 and is heated with temperature $T_\infty + (T_w - T_\infty)\,\frac{t}{t_0}$, where T_w is the plate temperature. A uniform magnetic field

of strength B_0 is imposed perpendicular to the plate. It is also assumed that the radiative heat flux in the x-direction is negligible as compared to that in the z- direction. Since the plate is infinitely long along x and y-directions, the velocity field and temperature distribution are functions of z and t only. The equation of continuity $\nabla \cdot \vec{q} = 0$ gives $w = 0$ everywhere in the fluid, where $\vec{q} \equiv (u, v, w)$.

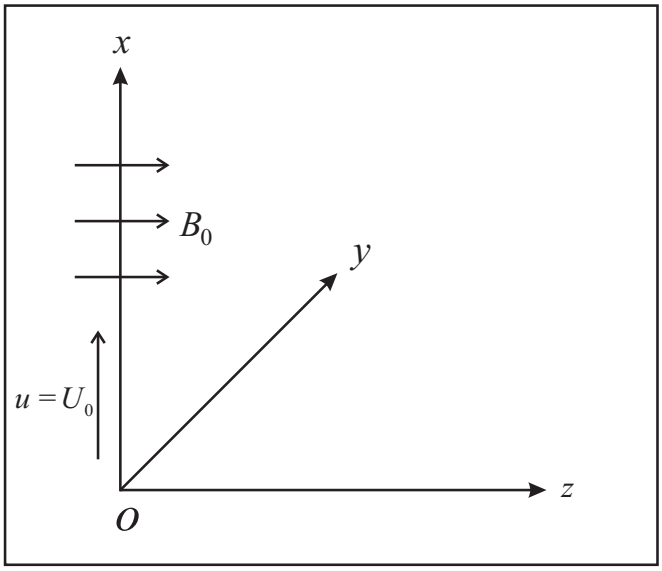

Figure 5.1: Geometry of the problem

The Boussinesq approximation is assumed to hold and for the evaluation of the gravitational body force, the density is assumed to be dependent on the temperature according to the equation of state

$$\rho = \rho_0 \left[1 - \beta(T - T_\infty)\right], \tag{5.1}$$

where T is the fluid temperature, ρ the fluid density, β the coefficient of thermal expansion and ρ_0 the reference fluid density.

Using Boussinesq approximation, the momentum equations of motion along x and y-directions are

$$\frac{\partial u}{\partial t} = -\frac{1}{\rho}\frac{\partial p}{\partial x} + \nu\frac{\partial^2 u}{\partial z^2} + g\beta(T - T_\infty) + \frac{B_0}{\rho}\, j_y, \tag{5.2}$$

$$\frac{\partial v}{\partial t} = -\frac{1}{\rho}\frac{\partial p}{\partial y} + \nu\frac{\partial^2 v}{\partial z^2} - \frac{B_0}{\rho}\, j_x, \tag{5.3}$$

where ν, p and j_x, j_y are the kinematic viscosity, fluid pressure and components of current density along x, y-directions respectively.

Neglecting ion-slip and thermoelectric effects, the generalised Ohm's law for partially ionized

gas is (see Cowling [21])

$$\vec{j} + \frac{\omega_e \tau_e}{B_0}(\vec{j} \times \vec{B}) \quad = \quad \sigma(\vec{E} + \vec{q} \times \vec{B}), \tag{5.4}$$

where $\vec{B}$, $\vec{E}$, $\vec{q}$, $\vec{j}$, σ, ω_e and τ_e are respectively, the magnetic field vector, the electric field vector, the fluid velocity vector, the current density vector, the conductivity of the fluid, the cyclotron frequency and the electron collision time.

We shall assume that the magnetic Reynolds number for the flow is small so that the induced magnetic field can be neglected. This assumption is justified since the magnetic Reynolds number is generally very small for partially ionized gases (Shereliff [22]). The solenoidal relation $\nabla.\vec{B} = 0$ for the magnetic field gives $B_z = B_0 =$ constant everywhere in the fluid where $\vec{B} \equiv (0, B_y, 0)$. The equation of the conservation of the charge $\nabla \cdot \vec{j} = 0$ gives $j_z =$constant. This constant is zero since $j_z = 0$ at the plate which is electrically non-conducting. Thus $j_z = 0$ everywhere in the flow. Since the induced magnetic field is neglected, the Maxwell's equation $\nabla \times \vec{E} = -\frac{\partial \vec{B}}{\partial t}$ becomes $\nabla \times \vec{E} = 0$ which gives $\frac{\partial E_x}{\partial z} = 0$ and $\frac{\partial E_y}{\partial z} = 0$. This implies that $E_x =$ constant and $E_y =$ constant everywhere in the flow.
In view of the above assumption, equation (5.4) gives

$$j_x + m j_y = \sigma(E_x + v B_0), \tag{5.5}$$

$$j_y - m j_x = \sigma(E_y - u B_0), \tag{5.6}$$

where $m = \omega_e \tau_e$ is the Hall parameter.
Solving equations (5.5) and (5.6) for j_x and j_y, we get

$$j_x \quad = \quad \frac{\sigma}{1+m^2}[(E_x + v B_0) - m(E_y - u B_0)], \tag{5.7}$$

$$j_y \quad = \quad \frac{\sigma}{1+m^2}[m(E_x + v B_0) + (E_y - u B_0)]. \tag{5.8}$$

On the use of equations (5.7) and (5.8), equations (5.2) and (5.3)become

$$\frac{\partial u}{\partial t} \quad = \quad -\frac{1}{\rho}\frac{\partial p}{\partial x} + \nu \frac{\partial^2 u}{\partial z^2} + g\beta(T - T_\infty) + \frac{\sigma B_0^2}{\rho(1+m^2)}[m(E_x + v B_0) + (E_y - u B_0)], \tag{5.9}$$

$$\frac{\partial v}{\partial t} \quad = \quad -\frac{1}{\rho}\frac{\partial p}{\partial y} + \nu \frac{\partial^2 v}{\partial z^2} - \frac{\sigma B_0^2}{\rho(1+m^2)}[(E_x + v B_0) - m(E_y - u B_0)]. \tag{5.10}$$

The energy equation is

$$\rho c_p \frac{\partial T}{\partial t} \quad = \quad k\frac{\partial^2 T}{\partial y^2} - \frac{\partial q_r}{\partial y}, \tag{5.11}$$

where k is the thermal conductivity, c_p the specific heat at constant pressure and q_r the radiative heat flux. The heat due to viscous and Joule dissipations are neglected for small velocities in the energy equation (5.11).

The initial and boundary conditions for velocity field and temperature distribution are

$$\begin{aligned} &u = 0,\ v = 0,\ \ T = T_\infty \ \text{ for all } \ z \ \text{ and } \ t = 0, \\ &u = U_0,\ \ v = 0,\ \ T = T_\infty + (T_w - T_\infty)\,\frac{t}{t_0} \ \text{ at } \ z = 0 \ \text{ for } \ t > 0, \\ &u \to 0,\ \ v \to 0,\ \ T \to T_\infty \ \text{ as } \ z \to \infty \ \text{ for } \quad t > 0. \end{aligned} \tag{5.12}$$

It has been shown by Cogley et al.[23] that in the optically thin limit for a non-gray gas near equilibrium, the following relation holds

$$\frac{\partial q_r}{\partial y} = 4(T - T_\infty)\int_0^\infty K_{\lambda_w}\left(\frac{\partial e_{\lambda p}}{\partial T}\right)_w d\lambda, \tag{5.13}$$

where K_λ is the absorption coefficient, λ is the wave length, $e_{\lambda p}$ is the Planck's function and subscript $'w'$ indicates that all quantities have been evaluated at the temperature T_∞ which is the temperature of the plate at time $t = 0$. Thus our study is limited to small difference of plate temperature to the fluid temperature.
On the use of equation (5.13), equation (5.11) becomes

$$\rho c_p \frac{\partial T}{\partial t} = k\frac{\partial^2 T}{\partial y^2} - 4\,(T - T_\infty)\,I, \tag{5.14}$$

where

$$I = \int_0^\infty K_{\lambda_w}\left(\frac{\partial e_{\lambda p}}{\partial T}\right)_w d\lambda. \tag{5.15}$$

Using infinity conditions, equations (5.9) and (5.10) yield

$$-\frac{1}{\rho}\frac{\partial p}{\partial x} + \frac{\sigma B_0}{\rho}(m\,E_x + E_y) = 0, \tag{5.16}$$

$$-\frac{1}{\rho}\frac{\partial p}{\partial y} - \frac{\sigma B_0}{\rho}(E_x - mE_y) = 0. \tag{5.17}$$

On the use of equations (5.16) and (5.17), equations (5.9) and (5.10) become

$$\frac{\partial u}{\partial t} = g\beta(T - T_\infty) + \nu\frac{\partial^2 u}{\partial z^2} - \frac{\sigma\,B_0^2}{\rho}(m\,v - u), \tag{5.18}$$

$$\frac{\partial v}{\partial t} = \nu\frac{\partial^2 u}{\partial z^2} - \frac{\sigma\,B_0^2}{\rho}(v + m\,u). \tag{5.19}$$

Introducing non-dimensional variables

$$\eta = \frac{z\,U_0}{\nu},\ \ \tau = \frac{\nu t}{U_0},\ u_1 = \frac{u}{U_0},\ v_1 = \frac{v}{U_0},\ \theta = \frac{T - T_\infty}{T_w - T_\infty} \tag{5.20}$$

equations (5.18), (5.19) and (5.14) become

$$\frac{\partial u_1}{\partial \tau} = \frac{\partial^2 u_1}{\partial \eta^2} - M^2(u_1 - m\,v_1) + Gr\,\theta, \tag{5.21}$$

$$\frac{\partial v_1}{\partial \tau} = \frac{\partial^2 v_1}{\partial \eta^2} - M^2(v_1 + m\,u_1), \tag{5.22}$$

$$Pr\,\frac{\partial \theta}{\partial \tau} = \frac{\partial^2 \theta}{\partial \eta^2} - \ R\,\theta, \tag{5.23}$$

where $M^2 = \frac{\sigma B_0^2 \nu}{\rho U_0^2}$ is the magnetic parameter, $R = \frac{4I h^2}{k}$ the radiation parameter, $Gr = \frac{g \beta \nu (T_w - T_\infty)}{U_0^3}$ the Grashof number and $Pr = \frac{\rho \nu c_p}{k}$ the Prandtl number.

The corresponding initial and boundary conditions for u_1, v_1 and θ are

$$\begin{aligned} &u_1 = 0, \;\; v_1 = 0, \;\; \theta = 0 \;\text{ for all }\; \eta \;\text{ and }\; \tau = 0, \\ &u_1 = 1, \;\; v_1 = 0, \;\; \theta = \tau \;\;\text{ at }\; \eta = 0 \;\text{ for }\; \tau > 0, \\ &u_1 \to 0, \;\; v_1 \to 0, \;\; \theta \to 0 \;\text{ as }\; \eta \to 0 \;\text{ for }\; \tau > 0. \end{aligned} \tag{5.24}$$

Combining equations (5.21) and (5.22), we have

$$\frac{\partial F}{\partial \tau} = \frac{\partial^2 F}{\partial \eta^2} - \frac{M^2(1 + i\,m)}{1 + m^2} + Gr\,\theta, \tag{5.25}$$

where

$$F = u_1 + i\,v_1, \;\; i = \sqrt{-1}. \tag{5.26}$$

The corresponding initial and boundary conditions for F and θ are

$$\begin{aligned} &F = 0, \;\; \theta = 0 \;\text{ for all }\; \eta \;\text{ and }\; \tau = 0, \\ &F = 1, \;\; \theta = \tau \;\;\text{ at }\; \eta = 0 \;\text{ for }\; \tau > 0, \\ &F \to 0, \;\; \theta \to 0 \;\text{ as }\; \eta \to 0 \;\text{ for }\; \tau > 0. \end{aligned} \tag{5.27}$$

Taking Laplace transformation and on using initial conditions for $F(\eta, \tau)$ and $\theta(\eta, \tau)$, equations (5.25) and (5.23) become

$$\frac{d^2 \bar{F}}{d\eta^2} - \left[s + \frac{M^2(1 + i\,m)}{1 + m^2} \right] \bar{F} = -\,Gr\,\bar{\theta}, \tag{5.28}$$

$$\frac{d^2 \bar{\theta}}{d\eta^2} - (s\,Pr + R)\bar{\theta} = 0, \tag{5.29}$$

where

$$\bar{F}(\eta, s) = \int_0^\infty F(\eta, \tau)\, e^{-s\tau}\, d\tau \;\text{ and }\; \bar{\theta}(\eta, s) = \int_0^\infty \theta(\eta, \tau)\, e^{-s\tau}\, d\tau. \tag{5.30}$$

The corresponding boundary conditions for $\bar{F}$ and $\bar{\theta}$ are

$$\begin{aligned} &\bar{F}(0, s) = \frac{1}{s}, \;\; \bar{\theta}(0, s) = \frac{1}{s^2}, \\ &\bar{F} \to 0, \;\; \bar{\theta} \to 0 \;\text{ as }\; \eta \to 0. \end{aligned} \tag{5.31}$$

The solution of equations (5.29) and (5.28) subject to the boundary conditions (5.31) can be easily obtained and are given by

$$\bar{\theta}(\eta, s) \;\; = \;\; \begin{cases} \frac{1}{s^2}\, e^{-\sqrt{s\,Pr + R}\,\eta} & \text{for }\; Pr \neq 1 \\ \\ \frac{1}{s^2}\, e^{-\sqrt{s + R}\,\eta} & \text{for }\; Pr = 1, \end{cases} \tag{5.32}$$

$$\bar{F}(\eta,s) = \begin{cases} \left(\frac{1}{s}+\frac{G_1}{b^2\,s}+\frac{G_1}{b\,s^2}\right)\,e^{-\sqrt{s+r^2}\,\eta} \\ -G_1\left(\frac{1}{b^2\,s}+\frac{1}{b\,s^2}\right)\,e^{-\sqrt{Pr(s+a)}\,\eta} \\ +\frac{G_1}{b^2(s-b)}\,e^{-\sqrt{Pr(s+a)}\,\eta}-\frac{G_1}{b^2(s-b)}\,e^{-\sqrt{s+r^2}\,\eta} & \text{for } Pr\neq 1 \\ \\ \left(\frac{1}{s}-\frac{G_2}{s^2}\right)\,e^{-\sqrt{s+r^2}\,\eta}+\frac{G_2}{s^2}\,e^{-\sqrt{s+R}\,\eta} & \text{for } Pr=1, \end{cases} \tag{5.33}$$

where

$$a=\frac{R}{Pr}, G_1=\frac{Gr}{1-Pr}, G_2=\frac{Gr}{r^2-R} \text{ and } r^2=\frac{M^2(1+i\,m)}{1+m^2}. \tag{5.34}$$

The inverse Laplace transforms of equations (5.32) and (5.33) give the solution for temperature distribution and the velocity field as

$$\theta(\eta,\tau) = \begin{cases} \frac{1}{2}\left[\left(\tau+\frac{\eta\sqrt{Pr}}{2\sqrt{a}}\right)e^{\eta\sqrt{a\,Pr}}\,\text{erfc}\left(\frac{\eta\sqrt{Pr}}{2\sqrt{\tau}}+\sqrt{a\,\tau}\right)\right. \\ \left.+\left(\tau-\frac{\eta\sqrt{Pr}}{2\sqrt{a}}\right)e^{-\eta\sqrt{a\,Pr}}\,\text{erfc}\left(\frac{\eta\sqrt{Pr}}{2\sqrt{\tau}}-\sqrt{a\,\tau}\right)\right] & \text{for } Pr\neq 1 \\ \\ \frac{1}{2}\left[\left(\tau+\frac{\eta}{2\sqrt{a}}\right)e^{\eta\sqrt{a}}\,\text{erfc}\left(\frac{\eta}{2\sqrt{\tau}}+\sqrt{a\,\tau}\right)\right. \\ \left.+\left(\tau-\frac{\eta}{2\sqrt{a}}\right)e^{-\eta\sqrt{a}}\,\text{erfc}\left(\frac{\eta}{2\sqrt{\tau}}-\sqrt{a\,\tau}\right)\right] & \text{for } Pr=1, \end{cases} \tag{5.35}$$

$$F(\eta,\tau) = \begin{cases} \frac{1}{2}\left(1+\frac{G_1}{b^2}+\frac{G_1\,\tau}{b}+\frac{G_1\,\eta}{2b\,r}\right)e^{r\,\eta}\,\text{erfc}\left(\frac{\eta}{2\sqrt{\tau}}+r\sqrt{\tau}\right) \\ +\frac{1}{2}\left(1+\frac{G_1}{b^2}+\frac{G_1\,\tau}{b}-\frac{G_1\,\eta}{2b\,r}\right)e^{-r\,\eta}\,\text{erfc}\left(\frac{\eta}{2\sqrt{\tau}}-r\sqrt{\tau}\right) \\ -\frac{G_1}{2b}\left(\tau+\frac{\eta\sqrt{Pr}}{2\sqrt{a}}+\frac{1}{b}\right)e^{\eta\sqrt{a\,Pr}}\,\text{erfc}\left(\frac{\eta\sqrt{Pr}}{2\sqrt{\tau}}+\sqrt{a\,\tau}\right) \\ -\frac{G_1}{2b}\left(\tau-\frac{\eta\sqrt{Pr}}{2\sqrt{a}}+\frac{1}{b}\right)e^{-\eta\sqrt{a\,Pr}}\,\text{erfc}\left(\frac{\eta\sqrt{Pr}}{2\sqrt{\tau}}-\sqrt{a\,\tau}\right) \\ -\frac{G_1e^{b\tau}}{2b^2}\left[e^{\eta\sqrt{r^2+b}}\,\text{erfc}\left(\frac{\eta}{2\sqrt{\tau}}+\sqrt{(r^2+b)\,\tau}\right)\right. \\ \left.+\,e^{-\eta\sqrt{r^2+b}}\,\text{erfc}\left(\frac{\eta}{2\sqrt{\tau}}-\sqrt{(r^2+b)\,\tau}\right)\right] \\ +\frac{G_1e^{b\tau}}{2b^2}\left[e^{\eta\sqrt{Pr(a+b)}}\,\text{erfc}\left(\frac{\eta\sqrt{Pr}}{2\sqrt{\tau}}+\sqrt{(a+b)\,\tau}\right)\right. \\ \left.+\,e^{-\eta\sqrt{Pr(a+b)}}\,\text{erfc}\left(\frac{\eta\sqrt{Pr}}{2\sqrt{\tau}}-\sqrt{(a+b)\,\tau}\right)\right] & \text{for } Pr\neq 1 \\ \\ \\ \frac{1}{2}\left(1-G_2\tau-\frac{G_2\,\eta}{2\,r}\right)e^{r\,\eta}\,\text{erfc}\left(\frac{\eta}{2\sqrt{\tau}}+r\sqrt{\tau}\right) \\ +\frac{1}{2}\left(1-G_2\tau+\frac{G_2\,\eta}{2\,r}\right)e^{-r\,\eta}\,\text{erfc}\left(\frac{\eta}{2\sqrt{\tau}}-r\sqrt{\tau}\right) \\ +\frac{1}{2}G_2\left[\left(\tau+\frac{\eta}{2\sqrt{R}}\right)e^{\eta\sqrt{R}}\,\text{erfc}\left(\frac{\eta}{2\sqrt{\tau}}+\sqrt{R\,\tau}\right)\right. \\ \left.+\left(\tau-\frac{\eta}{2\sqrt{R}}\right)e^{-\eta\sqrt{R}}\,\text{erfc}\left(\frac{\eta}{2\sqrt{\tau}}-\sqrt{R\,\tau}\right)\right] & \text{for } Pr=1 \end{cases} \tag{5.36}$$

where erfc(.) is the complementary error function.

5.3 Results and discussion

In order to look into the physical insight of the problem, the expressions obtained in previous section are studied with help of graphs. The effects of various physical parameters such as magnetic parameter M^2, radiation parameter R, Hall parameter m, Prandtl number Pr, Grashof number Gr and time τ are studied numerically by choosing suitable values.

5.3.1 Effects of parameters on the velocity profiles

The effects of pertinent parameters on the primary as well as the secondary velocities are presented graphically against η in **Figures 5.2-5.7**.

It is seen from **Figure 5.2** that the primary velocity u_1 decreases where as the magnitude of the secondary velocity v_1 increases with an increase in magnetic parameter M^2. The application of the transverse magnetic field plays the role of a resistive type force (Lorentz force) similar to drag force (that acts in the opposite direction of the fluid motion) which tends to resist the flow thereby reducing its velocity. The effect of radiation parameter on the velocity field is shown in **Figure 5.3**. It is observed that both the primary velocity u_1 and the magnitude of the secondary velocity v_1 decrease with an increase in radiation parameter R. This means that there is a fall in velocity in the presence of radiation. It is seen from **Figure 5.4** that both the primary velocity u_1 and the magnitude of the secondary velocity v_1 increase with an increase in Hall parameter m.

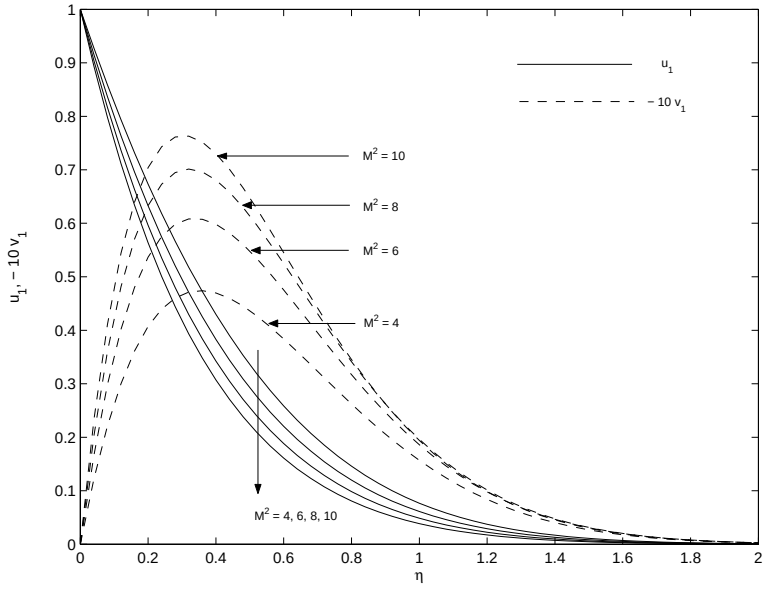

Figure 5.2: Velocity profiles for M^2 when $R = 4$, $m = 0.5$, $Pr = 0.71$, $Gr = 5$ and $\tau = 0.5$.

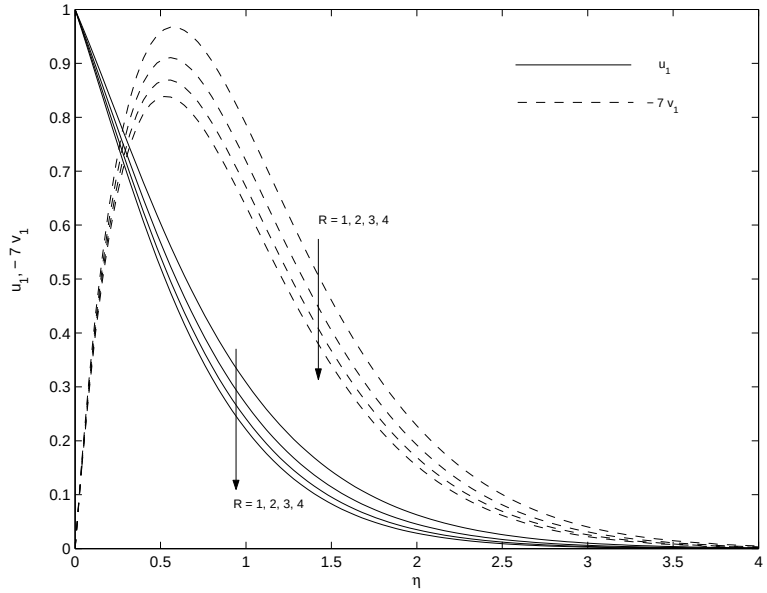

Figure 5.3: Velocity profiles for R when $M^2 = 5$, $Gr = 5$, $Pr = 0.71$, $m = 0.5$ and $\tau = 0.5$.

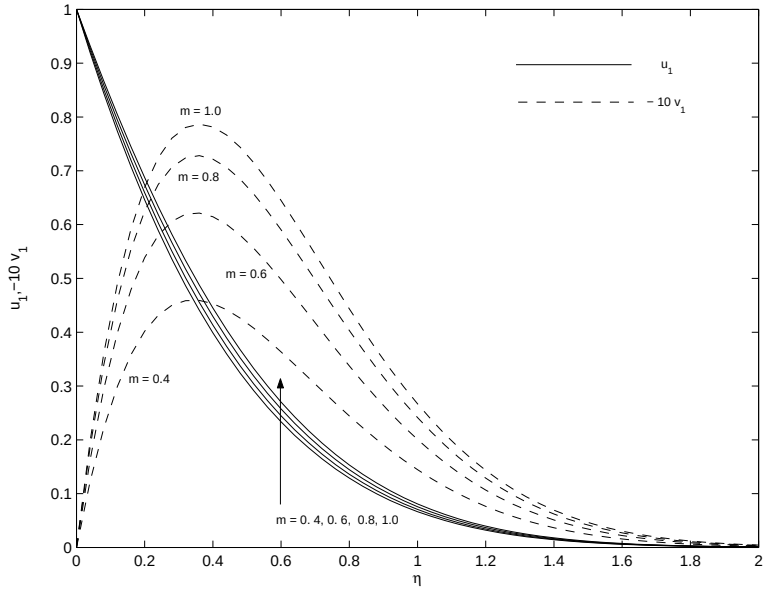

Figure 5.4: Velocity profiles for m when $M^2 = 5$, $R = 4$, $Gr = 5$, $Pr = 0.71$ and $\tau = 0.5$.

Figure 5.5 illustrates that both the primary velocity u_1 and the magnitude of the secondary velocity v_1 decrease with an increase in Prandtl number Pr. Physically, this is true because the increase in the Prandtl number is due to increase in the viscosity of the fluid which makes the fluid thick and hence causes a decrease in the velocity of the fluid. It is observed from **Figure 5.6** that an increase in Gr leads to rise in the both values of the primary velocity u_1 and the magnitude of the secondary velocity v_1. An increase in Grashof number leads to an increase in velocity, this is because, increase in Grashof number means more heating and less density. It is seen from **Figure 5.7** that the both the primary velocity u_1 and the magnitude of the secondary velocity v_1 increase with an increase in time τ.

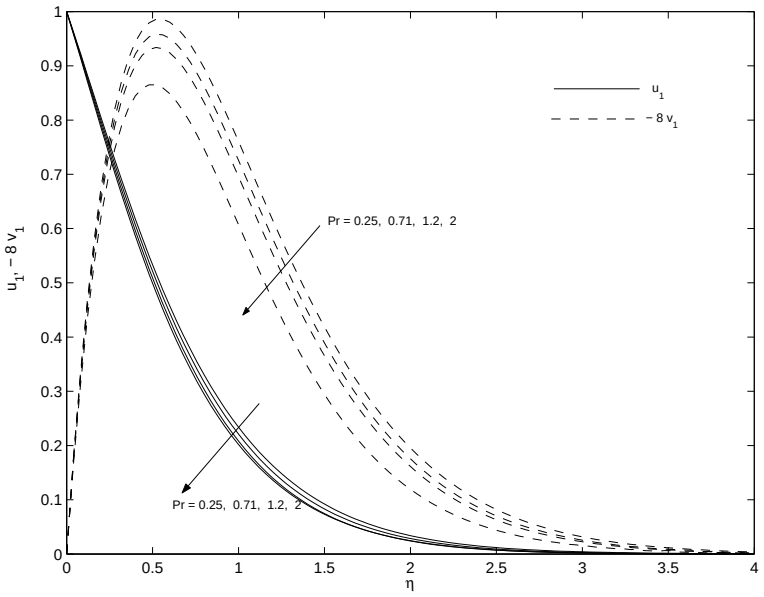

Figure 5.5: Velocity profiles for Pr when $M^2 = 5$, $R = 4$, $Gr = 5$, $m = 0.5$ and $\tau = 0.5$.

5.3.2 Effects of parameters on the temperature profiles

The effects of pertinent parameters such as radiation parameter R, prandtl number Pr and time τ on the temperature distribution are presented graphically against η in **Figures 5.8-5.10**. It is seen from **Figure 5.8** that the temperature θ decreases with an increase in radiation parameter R. This result qualitatively agrees with expectations, since the effects of radiation is to decrease the rate of energy transport to the fluid, thereby decreasing the temperature of the fluid. **Figure 5.9** shows that the temperature θ decreases with an increase in Pr. This implies that an increase in Prandtl number leads to fall the thermal boundary layer flow. This is because fluids with large Pr have low thermal diffusivity which causes low heat penetration resulting in reduced thermal boundary layer. **Figure 5.10** reveals that the temperature θ increases with an increase in τ. The trend shows that the temperature increases with an increase in time.

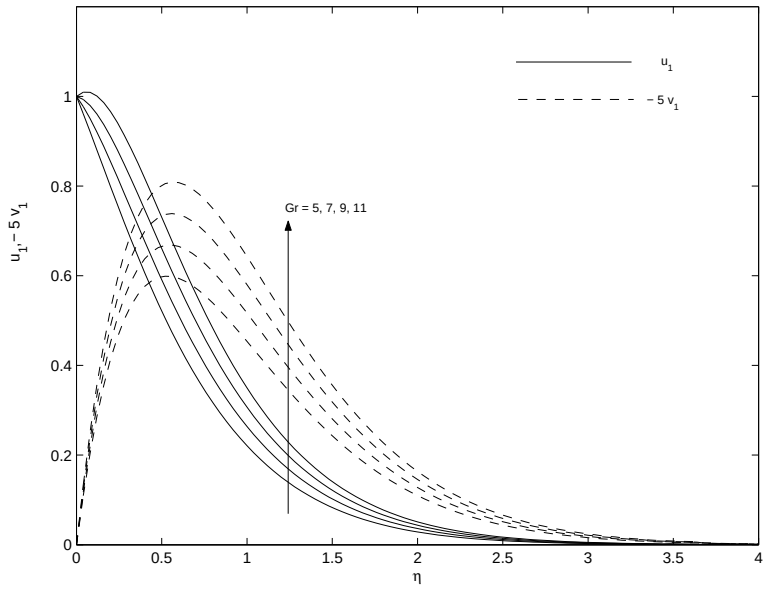

Figure 5.6: Velocity profiles for Gr when $M^2 = 5$, $R = 4$, $Pr = 0.71$, $m = 0.5$ and $\tau = 0.5$.

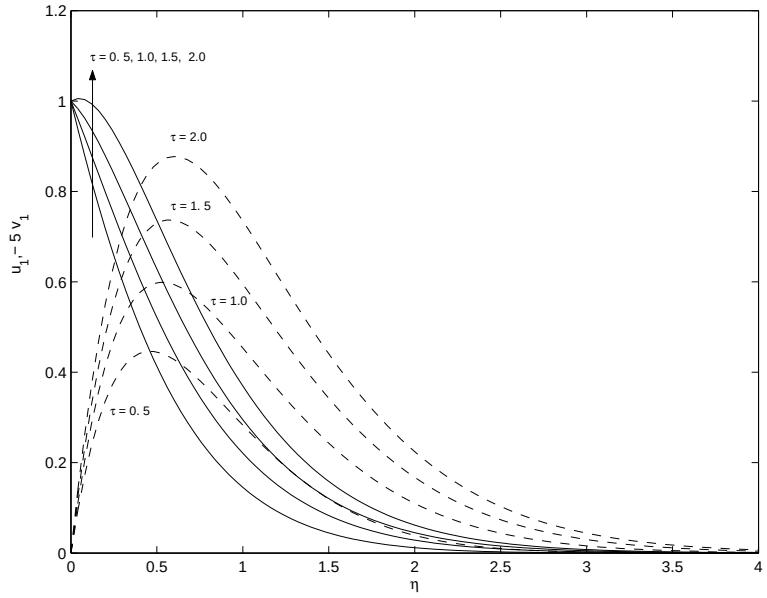

Figure 5.7: Velocity profiles for τ when $M^2 = 5$, $R = 4$, $Gr = 5$, $m = 0.5$ and $Pr = 0.71$.

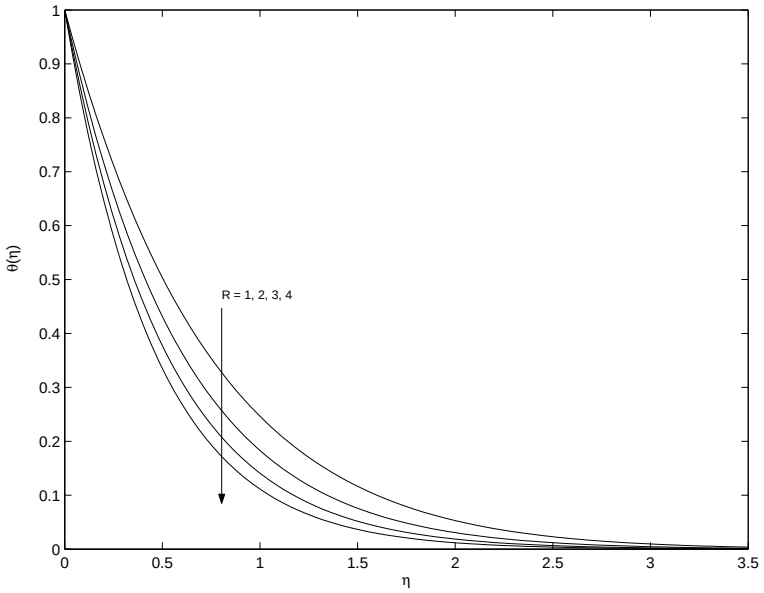

Figure 5.8: Temperature profile for$R$ when $Pr = 0.71$ and $\tau = 0.5$.

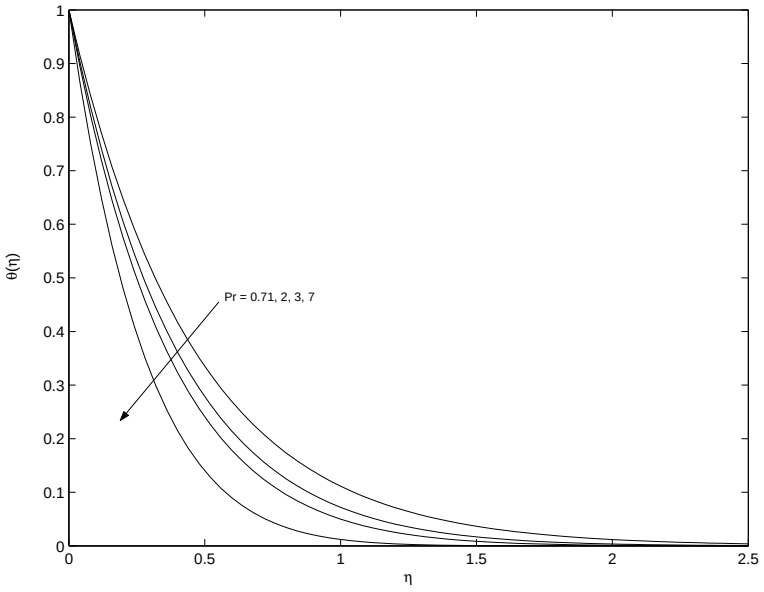

Figure 5.9: Temperature profile for Pr when $R = 4$ and $\tau = 0.2$.

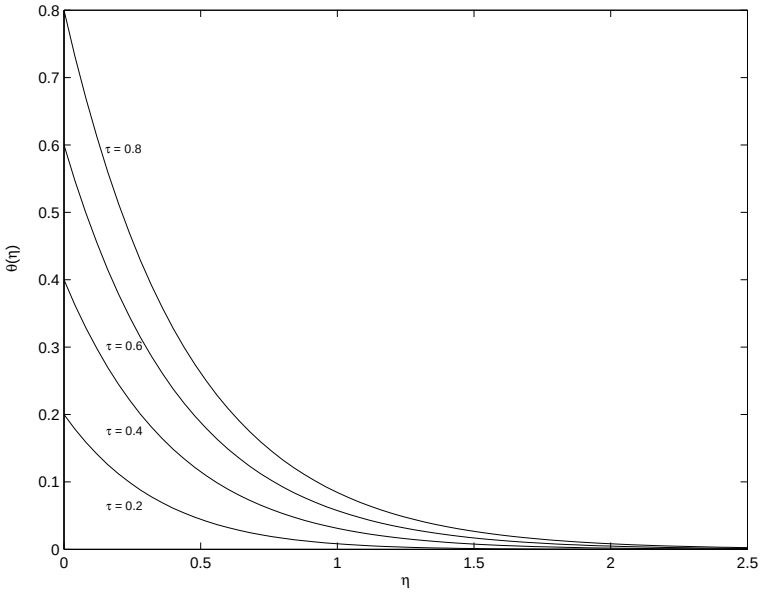

Figure 5.10: Temperature profile for τ when $Pr = 0.71$ and $R = 4$.

5.3.3 Effects of parameters on the shear stresses at the plate

From the physical point of view, it is necessary to know the shear stresses at the moving plate. The non-dimensional shear stresses at the plate $\eta = 0$ is

$$\tau_x + i\,\tau_y = \left(\frac{\partial F}{\partial \eta}\right)_{\eta=0}$$

$$= \begin{cases} -\left[\frac{G_1}{2b\,r} + \left(1 + \frac{G_1}{b^2} + \frac{G_1\,\tau}{b}\right)\right]\,\mathrm{erf}\,(r\sqrt{\tau}) \\ -\frac{1}{\sqrt{\pi\,\tau}}\left(1 + \frac{G_1}{b^2} + \frac{G_1\,\tau}{b}\right)e^{-r^2\,\eta} \\ +\left[\frac{G_1}{2b}\sqrt{\frac{Pr}{a}} + \frac{G_1}{b}\left(\tau + \frac{1}{b}\right)\right]\,\mathrm{erf}\,(\sqrt{a\,\tau}) \\ -\frac{G_1}{b}\sqrt{\frac{Pr}{\pi\,\tau}}\left(\tau + \frac{1}{b}\right)e^{-a\,\tau} \\ +\frac{G_1 e^{b\tau}}{b^2}\left[\sqrt{r^2+b}\,\mathrm{erf}\left(\sqrt{(r^2+b)\,\tau}\right)\right. \\ \left. -\sqrt{Pr(a+b)}\,\mathrm{erf}\left(\sqrt{Pr(a+b)\,\tau}\right)\right] \\ +\frac{G_1\,e^{b\tau}}{2b^2\sqrt{\pi\,\tau}}\left[e^{-(r^2+b)\tau} - \sqrt{Pr}\,e^{-(a+b)\tau}\right] \qquad \text{for } Pr \neq 1 \\ \\ \left[\frac{G_2}{2\,r} - (1 - G_2\,\tau)\right]\,\mathrm{erf}\,(r\sqrt{\tau}) - \frac{(1-G_2\,\tau)}{\sqrt{\pi\,\tau}}\,e^{-r^2\,\tau} \\ -G_2\left(\frac{1}{2\sqrt{R}} + \tau\sqrt{R}\right)\,\mathrm{erf}\left(\sqrt{R\,\tau}\right) - G_2\sqrt{\frac{\tau}{\pi}}\,e^{-R\,\tau} \quad \text{for } Pr = 1, \end{cases} \qquad ,(5.37)$$

where a, G_1, G_2 and r are given by equation (5.34).

Numerical results of the shear stresses τ_x due to the primary flow and τ_y due to the secondary flow at the plate ($\eta = 0$) are presented in **Figures 5.11-5.14** against Hall parameter m for several values of magnetic parameter M^2, radiation parameter R, Prandtl number Pr and time τ. **Figure 5.11** illustrates that the absolute value of the shear stress τ_x increases whereas the absolute value of the shear stress τ_y decreases with an increase in magnetic parameter M^2 for the fixed value of Hall parameter m. It is seen that the absolute value of the shear stress τ_x decreases while the absolute value of the shear stress τ_y increases with an increase in Hall parameter m for fixed value of the magnetic parameter M^2. These results are in agrement with the fact that the primary velocity decreases and the secondary increases with an increase in Hall parameter m. It is seen from **Figure 5.12** that the absolute value of the shear stress τ_x increases whereas the absolute value of the shear stress τ_y decreases with an increase in radiation parameter R.

Figure 5.13 reveals that the absolute value of shear stress τ_x decreases whereas the absolute value of the shear stress τ_y increases near the plate with an increase in Prandtl number Pr. Further, it is revealed from **Figure 5.14** that the absolute value of the shear stress τ_x decreases while the absolute value of the shear stress τ_y increases with an increase in time τ for the fixed value of Hall parameter m.

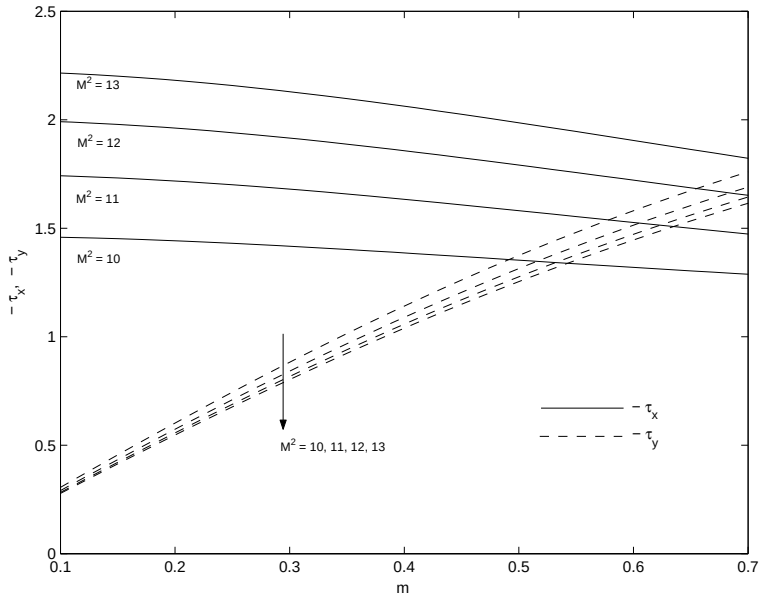

Figure 5.11: Shear stresses $-\tau_x$ and $-\tau_y$ for M^2 when $R = 4$, $Pr = 0.71$, $Gr = 5$ and $\tau = 0.5$.

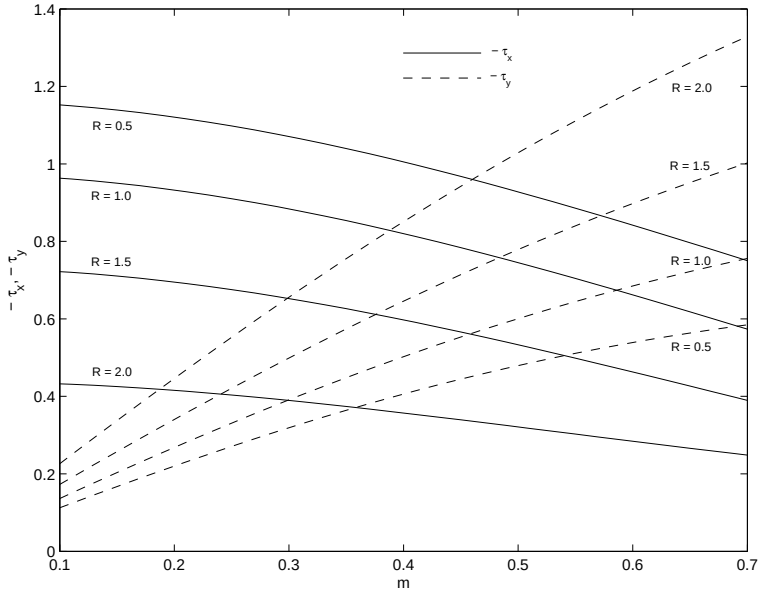

Figure 5.12: Shear stresses $-\tau_x$ and $-\tau_y$ for R when $M^2 = 5$, $Pr = 0.71$, $Gr = 5$ and $\tau = 0.5$.

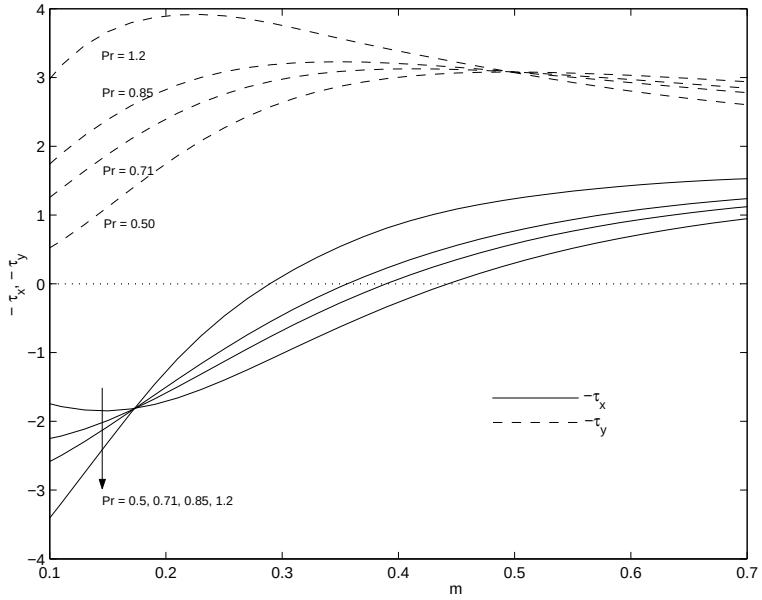

Figure 5.13: Shear stresses $-\tau_x$ and $-\tau_y$ for Pr when $M^2 = 5$, $R = 4$, $Gr = 5$ and $\tau = 0.5$.

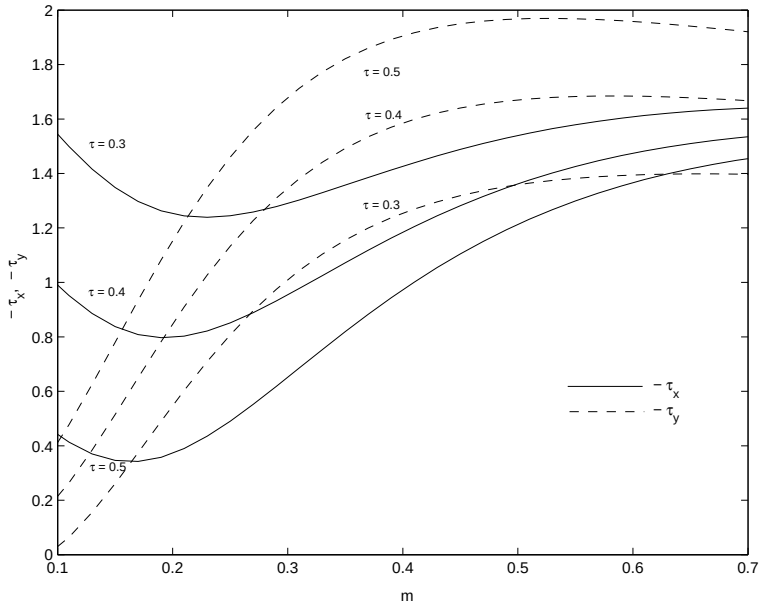

Figure 5.14: Shear stresses $-\tau_x$ and $-\tau_y$ for τ when $M^2 = 5$, $R = 4$, $Gr = 5$ and $Pr = 0.71$.

5.3.4 Effects of parameters on the rate of heat transfer at the plate

The rate of heat transfer is important in the heat transfer studies, since it is directly related to the heat transfer coefficient. The rate of heat transfer at the moving plate $\eta = 0$ is given by

$$-\left(\frac{\partial\theta}{\partial\eta}\right)_{\eta=0} = \begin{cases} \left(\tau\sqrt{R} + \frac{1}{2}\sqrt{\frac{Pr^2}{R}}\right) \text{ erf}\left(\sqrt{\frac{R\tau}{Pr}}\right) + \sqrt{\frac{\tau Pr}{\pi}}\, e^{-\frac{R\tau}{Pr}} & \text{for } Pr \neq 1 \\ \left(\tau\sqrt{\frac{R}{Pr}} + \frac{1}{2}\sqrt{\frac{Pr}{R}}\right) \text{ erf}\left(\sqrt{\frac{R\tau}{Pr}}\right) + \sqrt{\frac{\tau}{\pi}}\, e^{-\frac{R\tau}{Pr}} & \text{for } Pr = 1. \end{cases} \tag{5.38}$$

Numerical results of the rate of heat transfer $-\left(\frac{\partial\theta}{\partial\eta}\right)_{\eta=0}$ at the moving plate ($\eta = 0$) against the radiation parameter R are presented in the **Table-I** for several values of radiation parameter R, Prandtl number Pr and time τ. **Table-I** shows that for the fixed value of radiation parameter R, the rate of heat transfer $-\left(\frac{\partial\theta}{\partial\eta}\right)_{\eta=0}$ increases with an increase in either Prandtl number Pr or time τ. This may be explained by the fact that frictional forces become dominant with increasing values of Pr and hence yield greater heat transfer rates. Further, it is seen that for fixed values of Pr and τ, the rate of heat transfer $-\left(\frac{\partial\theta}{\partial\eta}\right)_{\eta=0}$ increases with an increase in radiation parameter R.

Table-I
Rate of heat transfer $-\left(\frac{\partial\theta}{\partial\eta}\right)_{\eta=0}$ at the plate $\eta = 0$.

	Pr				τ			
R	*0.71*	*2*	*3*	*7*	*0.2*	*0.4*	*0.6*	*0.8*
2	*0.78575*	*0.93166*	*1.14519*	*1.87743*	*0.29814*	*0.60353*	*0.98504*	*1.42837*
4	*0.99997*	*0.91905*	*1.05290*	*1.70618*	*0.33859*	*0.75278*	*1.27002*	*1.87238*
6	*1.16851*	*0.96373*	*1.03091*	*1.58148*	*0.37827*	*0.87221*	*1.49389*	*2.22458*
8	*1.31126*	*1.02273*	*1.04219*	*1.49154*	*0.41138*	*0.97210*	*1.68518*	*2.52734*

5.4 Conclusion

The effects of Hall current and radiation on MHD flow of a viscous incompressible electrically conducting fluid past a moving vertical plate with variable plate temperature in the presence of a uniform transverse magnetic field have been investigated. The dimensionless governing partial differential equations are solved by the Laplace transform technique. The effects of pertinent parameters such as Hall parameter, radiation parameter, Grashof number, Prandtl number, magnetic parameter and time are studied. It is found that the Hall parameter m accelerates the primary velocity u_1 as well as the magnitude of the secondary velocity v_1. An increase in radiation parameter R leads to fall in the primary velocity u_1 as well as the magnitude of the secondary velocity v_1. Both the primary velocity u_1 and the magnitude of the secondary velocity v_1 increase when time τ is progressed. It is also found that an increase in Grashof number Gr leads to rise in the both the values of primary velocity u_1 and the magnitude of the secondary velocity v_1. An increase in Grashof number leads to an increase in velocity, this is because, increase in Grashof number means more heating and less density. The temperature θ reduces with an increase in radiation parameter R. This result qualitatively agrees with expectations, since the effects of radiation is to decrease the rate of energy transport to the fluid, thereby decreasing the temperature of the fluid. Further, the absolute value of the shear stress τ_x due to the primary flow at the moving plate ($\eta = 0$) decreases whereas the absolute value of the shear stress τ_y due to the secondary flow at the moving plate ($\eta = 0$) increases with an increase in Hall parameter m. The rate of heat transfer $-\left(\frac{\partial\theta}{\partial\eta}\right)_{\eta=0}$ increases with an increase in either Prandtl number Pr or radiation parameter R or time τ.

Bibliography

[1] Soundalgekar VM and Takhar HS, AIAA J.: **15**(1977), pp.457.

[2] Soundalgekar VM, Patil MR and Takhar HS, Nuclear Engg. and Design: **64**(1981), pp.43.

[3] Ram PC and Takhar HS, Int. J. Non-Linear Mech., **29**(1994): pp.775.

[4] Takhar HS and Nath G, Zeitschrift fur Angewwandte Mathematik und Physik, ZAMP: **49**(1998), pp.989.

[5] Helliwell JB and Mosa MF, Int. J. Heat Mass Trans.: **22**(1979), pp.657.

[6] Takhar HS and Ram PC, Astrophysics and Space Sci.: **183**(1991), pp.193.

[7] Alagoa KD, Tay G and Abbey TM, Astrophysics and Space Sci.: **260(4)**(1998), pp.455.

[8] Kinyanjui M, Kwanza JK and Uppal SM, Energy Conversion and Management: **42(8)**(2001), pp.917.

[9] Aboeldahab EM and Elbarbary EME, Int. J. of Engg. Sci.: **39(14)**(2001), pp.1641.

[10] Cookey CA, Ogolu A and Omubopepple VB, Int. J. of Heat and Mass Trans.: **13**(2003), pp.2305.

[11] Aboeldahab EM and El-Aziz MA, Appl. Mathematical Model.: **29(6)**(2005), pp.579.

[12] Samad MA and Rahman MM, J. Naval Architecture and Marine Engg.: **3**(2006), pp.7.

[13] Chaudhary RC and Jain P, UUR J. Phys.: **52(10)**(2007), pp.110.

[14] Shit GC and Haldar R, Phys. Fluid-dynamics, ar XIv: 1008.0165v1.

[15] Israel-Cookey C, Amos E and Nwaigwe C, American J Sci. Indust. Res.: **1(2)**(2010), pp.326.

[16] Shateyi S, Mosta SS and Sibanda P, Mathematical Problems in Engg.: (2010)

[17] Aurangzaib SS, Canadian J. Sci. Engg. Math.: **2(4)**(2011), pp.153.

[18] Singh KD and Pathak R, Indian J. Pure and Appl. Phys.: **50**(2012), pp.77.

[19] Jain NC and Singh H, Int. J. of Appl. Mech. And Engg.: **17(1)**(2012), pp.53.

[20] Chaudhary D, Singh H and Jain NC, Appl. Math. and Phys.: **1(2)**(2013), pp.11.

[21] Cowling TG, Magnetohydrodynamics, Intersci. Publisher, Inc, New York: (1957)

[22] Shereliff JA, A text book of Magnetohydrodynamic-1st ed. London, Pergamon Press: (1965)

[23] Cogley ACL, Vincentine WC and Gilles SE, Am. Inst. Aeronat. Astronaut., J.: **6**(1968), pp.551.

Chapter 6

Combined effects of Hall current and rotation on unsteady MHD Couette flow in a porous channel*

6.1 Introduction

The Hall effects is important when the magnetic field is strong or when the collision frequency is low, causing the Hall parameter to be significant (see Sutton and Sherman[1]). The effects of Hall current on the fluid flow in rotating channels have many engineering applications in flows of laboratory plasmas, in MHD power generation, in MHD accelerators, and in several astrophysical and geophysical situations. The effects of Hall current and rotaion on MHD flow through a channel have been investigated by many researchers. Chandran et al.[2], Katagiri et al.[3], Ghosh and Pop [4], Ghosh[5], Gubanov and Lunkin[6] and Jana and Datta[7] have studied the MHD Couette flow between two parallel plates channel in a rotating system with Hall effects. Reddy and Bathaiah[8] have considered the Hall effects on MHD Couette flow through a porous horizontal channel. Das et al.[9] have investigated the unsteady MHD Couette flow in a rotating system. The combined effects of free and forced convection on MHD flow in a rotating porous channel have been investigated by Prasad-Rao et al.[10]. Mandal and Mandal[11] have studied the effects of Hall current on MHD Couette flow between thick arbitrarily conducting plates in a rotating system. The Hall effects on unsteady MHD free and forced convection flow in a porous channel have been studied by Sivaprasad et al.[12].

In this chapter, we have studied the combined effects of Hall current and rotation on MHD Couette flow of a viscous incompressible electrically conducting fluid between two infinite horizontal parallel porous plates channel in a rotating system when one of the plate is moving with uniform velocity and the other one held at rest. Solutions for the velocity fields as well as the

*Published in **World J. of Mech. (WJM)**, ISSN: 2160-049X, 1(3)(2011), pp.87-99.*

shear stresses have been obtained for general times and small times by the use of Laplace transformation technique. Here, we assume that the plates are electrically non-conducting. Also, we neglecting the ion-slip and thermoelectric effects. The effects of pertinent parameters on the velocity field and shear stresses at the plate are illustrate and discussed in detail.

6.2 Mathematical formulation and its solution

Consider the unsteady MHD Couette flow of a viscous incompressible electrically conducting fluid between two infinite horizontal parallel porous plates separated by a distance h when both the fluid and channel are rotate in unison about an axis normal to the plates with a uniform angular velocity Ω. Choose a Cartesian co-ordinate system with x-axis along the lower stationary plate in the direction of flow, z-axis is normal to the plates and y-axis is perpendicular to the zx-plane. A uniform magnetic field of strength B_0 is imposed perpendicular to the plates. The flow within the channel is induced due to the movement of the upper plate ($z = h$) parallel to itself in x-direction with a uniform velocity U_0. Initially, at time $t = 0$, both the fluid and the plates of the channel are assumed to be at rest. At time $t > 0$, the upper plate ($z = h$) suddenly starts to move with uniform velocity U_0 along x-direction in its own plane while the lower plate ($z = 0$) is held at rest [see **Figure 6.1**]. Since the plates of the channel are infinitely long along x and y-directions and are electrically non-conducting, all the physical quantities, except pressure, will be the functions of z and t only. Suction/injection of the fluid takes place through the porous plates of the channel with uniform velocity w_0 which is $w_0 > 0$ for suction and is $w_0 < 0$ for blowing/injection. The equation of continuity $\nabla \cdot \vec{q} = 0$ gives $w = -w_0$ everywhere in the fluid, where $\vec{q} \equiv (u, v, w)$.

Neglecting ion-slip and thermoelectric effects, the generalised Ohm's law for partially ionized gas is [see Cowling[13]]

$$\vec{j} + \frac{\omega_e \tau_e}{B_0}(\vec{j} \times \vec{B}) \quad = \quad \sigma(\vec{E} + \vec{q} \times \vec{B}), \tag{6.1}$$

where $\vec{B}$, $\vec{E}$, $\vec{q}$, $\vec{j}$, σ, ω_e and τ_e are respectively, the magnetic field vector, the electric field vector, the fluid velocity vector, the currents density vector, the conductivity of the fluid, the cyclotron frequency and the electron collision time.

We shall assume that the magnetic Reynolds number for the flow is small so that the induced magnetic field can be neglected in comparison to the applied one. This assumption is justified since the magnetic Reynolds number is generally very small for metallic liquids and partially ionized fluids. The solenoidal relation $\nabla.\vec{B} = 0$ for the magnetic field gives $B_z = B_0 =$ constant everywhere in the fluid where $\vec{B} \equiv (0, 0, B_z)$. The equation of conservation of charge $\nabla \cdot \vec{j} = 0$ gives $j_z =$constant. This constant is zero since the plates are electrically non-conducting. Thus $j_z = 0$ everywhere in the flow. Since the induced magnetic field is neglected, the Maxwell's equation $\nabla \times \vec{E} = -\frac{\partial \vec{B}}{\partial t}$ becomes $\nabla \times \vec{E} = 0$ which gives $\frac{\partial E_x}{\partial z} = 0$ and $\frac{\partial E_y}{\partial z} = 0$. This implies that $E_x =$ constant and $E_y =$ constant everywhere in the flow.

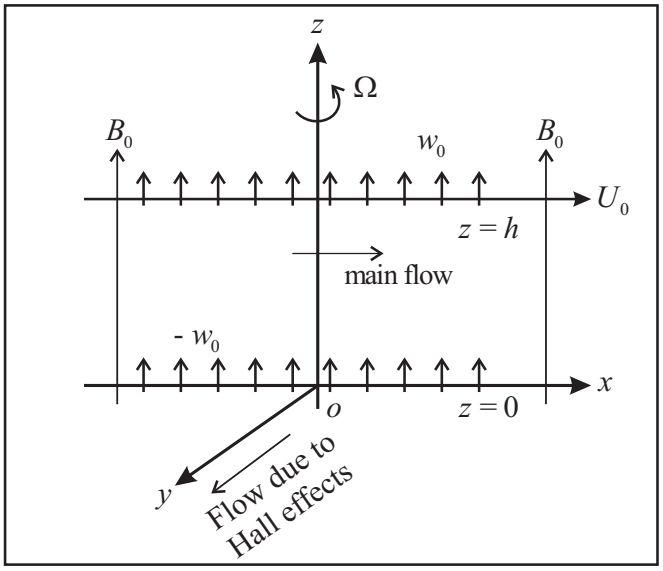

Figure 6.1: Geometry of the problem

In view of the above assumption and on taking $E_x = E_y = 0$, equation (6.1) gives

$$j_x + mj_y = \sigma B_0 v, \tag{6.2}$$

$$j_y - mj_x = -\sigma B_0 u, \tag{6.3}$$

where $m = \omega_e \tau_e$ is the Hall parameter.
Solving equations (6.2) and (6.3) for j_x and j_y, we get

$$j_x = \frac{\sigma B_0}{1+m^2}(v + mu), \tag{6.4}$$

$$j_y = -\frac{\sigma B_0}{1+m^2}(u - mv). \tag{6.5}$$

On the use of equations (6.4) and (6.5), the equation of motion along x, y and z-directions are respectively

$$\frac{\partial u}{\partial t} - w_0 \frac{\partial u}{\partial z} - 2\Omega v = \nu \frac{d^2 u}{dz^2} - \frac{\sigma B_0^2}{\rho(1+m^2)}(u - mv), \tag{6.6}$$

$$\frac{\partial v}{\partial t} - w_0 \frac{\partial v}{\partial z} + 2\Omega u = \nu \frac{d^2 v}{dz^2} - \frac{\sigma B_0^2}{\rho(1+m^2)}(v + mu), \tag{6.7}$$

$$0 = -\frac{1}{\rho}\frac{\partial p}{\partial z}, \tag{6.8}$$

where ρ, ν and p are respectively the fluid density, the kinematic viscosity and the modified fluid pressure including centrifugal force.

The initial and boundary conditions for the velocity fields are

$$\begin{aligned} &u = v = 0 \ \text{ for } \ 0 \le z \le h, \ \ t = 0, \\ &u = v = 0 \ \text{ at } \ z = 0, \ \text{ for } \ t > 0, \\ &u = U_0, \ v = 0 \ \text{ at } \ z = h, \ \text{ for } \ t > 0. \end{aligned} \tag{6.9}$$

Introducing the non-dimensional variables

$$\eta = \frac{z}{h}, \ u_1 = \frac{u}{U_0}, \ v_1 = \frac{v}{U_0}, \tau = \frac{\nu\, t}{h^2}, \tag{6.10}$$

equations (6.6) and (6.7) become

$$\frac{\partial u_1}{\partial \tau} - Re\frac{\partial v_1}{\partial \eta} - 2K^2 v_1 = \frac{\partial^2 u_1}{\partial \eta^2} - \frac{M^2}{1+m^2}(u_1 - m v_1), \tag{6.11}$$

$$\frac{\partial v_1}{\partial \tau} - Re\frac{\partial v_1}{\partial \eta} + 2K^2 u_1 = \frac{\partial^2 v_1}{\partial \eta^2} - \frac{M^2}{1+m^2}(v_1 + m u_1), \tag{6.12}$$

where $M^2 = \frac{\sigma B_0^2 h^2}{\rho\nu}$ is the magnetic parameter, $K^2 = \frac{\Omega h^2}{\nu}$ the rotation parameter and $Re = \frac{w_0\, h}{\nu}$ the Reynolds number.
Combing equations (6.11) and (6.12), we have

$$\frac{\partial q}{\partial \tau} - Re\frac{\partial q}{\partial \eta} - 2\,i\,K^2 q = \frac{\partial^2 q}{\partial \eta^2} - \frac{M^2(1 + i\,m)}{1+m^2} q, \tag{6.13}$$

where

$$q = u_1 + i\, v_1, \ i = \sqrt{-1}. \tag{6.14}$$

The initial and boundary conditions for $q(\eta, \tau)$ are

$$q(\eta, 0) = 0 \ \text{ for } \ 0 \le \eta \le 1 \ \text{ and } \ \tau = 0, \tag{6.15}$$

$$q(0, \tau) = 0 \ \text{ and } \ q(0, \tau) = 1 \ \text{ for } \ \tau > 0. \tag{6.16}$$

6.2.1 General solution

For general solution, the method given in Batchelor[15] can be used. The solution of the equation (6.13) subject to the conditions (6.15) and (6.16) can be written in the following form

$$q(\eta, \tau) = \frac{\sinh(\alpha + i\,\beta)\,\eta}{\sinh(\alpha + i\,\beta)}\, e^{\frac{1}{2}Re(1-\eta)} + F_1(\eta, \tau), \tag{6.17}$$

where first term on the right hand side is the steady-state solution, $F_1(\eta, \tau)$ shows the departure from the steady-state and

$$\begin{aligned} \alpha &= \frac{1}{\sqrt{2}}\left[\left\{\left(\frac{Re^2}{4} + \frac{M^2}{1+m^2}\right)^2 + \left(2K^2 + \frac{mM^2}{1+m^2}\right)^2\right\}^{\frac{1}{2}} + \left(\frac{Re^2}{4} + \frac{M^2}{1+m^2}\right)\right]^{\frac{1}{2}}, \\ \beta &= \frac{1}{\sqrt{2}}\left[\left\{\left(\frac{Re^2}{4} + \frac{M^2}{1+m^2}\right)^2 + \left(2K^2 + \frac{mM^2}{1+m^2}\right)^2\right\}^{\frac{1}{2}} - \left(\frac{Re^2}{4} + \frac{M^2}{1+m^2}\right)\right]^{\frac{1}{2}}. \end{aligned} \tag{6.18}$$

Now, $F_1(\eta,\tau)$ satisfies the following differential equation

$$\frac{\partial F_1}{\partial \tau} - Re\,\frac{\partial F_1}{\partial \tau} + \left[\frac{M^2(1+i\,m)}{1+m^2} + 2iK^2\right] F_1 = \frac{\partial^2 F_1}{\partial \eta^2}, \tag{6.19}$$

with

$$F_1(0,\tau) = 0, F_1(1,\tau) = 0, F_1(\eta,0) = -\frac{\sinh(\alpha+i\,\beta)\,\eta}{\sinh(\alpha+i\,\beta)}\, e^{\frac{1}{2}Re(1-\eta)}. \tag{6.20}$$

Taking Laplace's transform of the equation (6.19), we get

$$\frac{d^2\bar{F}_1}{d\eta^2} + \frac{d^2\bar{F}_1}{d\eta^2} - \left[s + \frac{M^2(1+i\,m)}{1+m^2} + 2iK^2\right]\bar{F}_1 = \frac{\sinh(\alpha+i\,\beta)\,\eta}{\sinh(\alpha+i\,\beta)}\, e^{\frac{1}{2}Re(1-\eta)}, \tag{6.21}$$

where

$$\bar{F}_1 = \int_0^\infty F_1 e^{-s\tau} d\tau. \tag{6.22}$$

The corresponding boundary conditions for $\bar{F}_1(\eta,s)$ are

$$\bar{F}_1(0,s) = 0 \text{ and } \bar{F}_1(1,s) = 0 \tag{6.23}$$

The solution of the equation (6.21) subject to the boundary conditions (6.23) is

$$\bar{F}_1(\eta,s) = \left[\frac{1}{s}\frac{\sinh\gamma\,\eta}{\sinh\gamma} - \frac{1}{s}\frac{\sinh(\alpha+i\,\beta)\,\eta}{\sinh(\alpha+i\,\beta)}\right] e^{\frac{1}{2}Re(1-\eta)}, \tag{6.24}$$

where

$$\gamma = \left[\frac{Re^2}{4} + s + \frac{M^2(1+i\,m)}{1+m^2} + 2iK^2\right]^{1/2}. \tag{6.25}$$

Taking inverse Laplace's transform of the equation (6.24), we have

$$F_1(\eta,\tau) = \sum_{n=1}^{\infty} \frac{2n\pi(-1)^n e^{-\lambda_n^2\tau}\,\sin(n\pi\eta)}{n^2\pi^2 + (\alpha+i\,\beta)^2}\, e^{\frac{1}{2}Re(1-\eta)}. \tag{6.26}$$

On the use of (6.17), we have

$$q(\eta,\tau) = \left[\frac{\sinh(\alpha+i\beta)\eta}{\sinh(\alpha+i\beta)} + \sum_{n=1}^{\infty}\frac{2n\pi(-1)^n e^{-\lambda_n^2\tau}}{n^2\pi^2+(\alpha+i\,\beta)^2}\sin(n\pi\eta)\right] e^{\frac{1}{2}Re(1-\eta)}, \tag{6.27}$$

where

$$\lambda_n^2 \;=\; n^2\pi^2 + (\alpha+i\,\beta)^2. \tag{6.28}$$

On separating into a real and imaginary parts and using the equation (6.14), we get

$$u_1 \;=\; e^{\frac{1}{2}Re(1-\eta)}\Big[\frac{S(\eta)S(1)+C(\eta)C(1)}{S^2(1)+C^2(1)}$$

$$
\begin{aligned}
&+ \quad 2\sum_{n=1}^{\infty} \frac{n\pi(-1)^n \sin(n\pi\eta)}{(n^2\pi^2+\alpha^2-\beta^2)^2+4\alpha^2\beta^2} \\
&\times \quad \left\{(n^2\pi^2+\alpha^2-\beta^2)\cos 2\alpha\beta\tau - 2\alpha\beta \sin 2\alpha\beta\tau\right\} e^{-(n^2\pi^2+\alpha^2-\beta^2)\tau}\Big], \qquad (6.29)\\
v_1 \quad &= \quad e^{\frac{1}{2}Re(1-\eta)}\Big[\frac{C(\eta)S(1)-S(\eta)C(1)}{S^2(1)+C^2(1)} \\
&- \quad 2\sum_{n=1}^{\infty} \frac{n\pi(-1)^n \sin(n\pi\eta)}{(n^2\pi^2+\alpha^2-\beta^2)^2+4\alpha^2\beta^2} \\
&\times \quad \left\{2\alpha\beta\cos 2\alpha\beta\tau + (n^2\pi^2+\alpha^2-\beta^2)\sin 2\alpha\beta\tau\right\} e^{-(n^2\pi^2+\alpha^2-\beta^2)\tau}\Big], \qquad (6.30)
\end{aligned}
$$

where

$$
\begin{aligned}
S(\eta) &= \sinh\eta\cos\eta, \qquad C(\eta) = \cosh\eta\sin\eta, \\
S(1) &= \sinh\alpha\cos\alpha, \qquad C(1) = \cosh\alpha\sin(\alpha), \qquad (6.31)
\end{aligned}
$$

and α, β are given by equation (6.18).

The solution given by the equations (6.29) and (6.30) exists for both $Re < 0$ (corresponding to $w_0 < 0$ for the blowing at the plates) and $Re > 0$(corresponding to $w_0 > 0$ for the suction at the plates). If $Re = 0$ and $m = 0$, then the above equations (6.29) and (6.30) are identical with equations (26) and (27) of Das et al.[9].

6.2.2 Small time solution

Following Carslaw and Jaeger[16], for small time, the solution of (6.13) subject to the boundary conditions (6.15) and (6.16) is obtained by Laplace transformation technique in the following form

$$
\begin{aligned}
q(\eta,\tau) &= e^{-(c+i\,d)\tau} e^{\frac{1}{2}Re(1-\eta)} \sum_{k=0}^{\infty}\sum_{n=0}^{\infty} (c+i\,d)^n (4\tau)^n \\
&\times \quad \left[\left\{i^{2n}\mathrm{erfc}\left(\frac{a}{2\sqrt{\tau}}\right) - i^{2n}\mathrm{erfc}\left(\frac{b}{2\sqrt{\tau}}\right)\right\}\right. \\
&- \quad \left.\frac{Re^2}{4}\sqrt{\tau}\left\{a\, i^{2n+1}\mathrm{erfc}\left(\frac{a}{2\sqrt{\tau}}\right) - b\, i^{2n+1}\mathrm{erfc}\left(\frac{b}{2\sqrt{\tau}}\right)\right\}\right], \qquad (6.32)
\end{aligned}
$$

where

$$
\begin{aligned}
c &= \frac{M^2}{1+m^2}, \quad d = 2\,K^2 + \frac{mM^2}{1+m^2}, \quad a = 2k+1-\eta, \quad b = 2k+1+\eta, \\
i^n\mathrm{erfc}(x) &= \int_x^{\infty} i^{n-1}\mathrm{erfc}(\xi)d\xi, \\
i\mathrm{erfc}(x) &= \int_x^{\infty} \mathrm{erfc}(\xi)d\xi, \qquad (6.33)\\
i^0\mathrm{erfc}(x) &= \mathrm{erfc}(x).
\end{aligned}
$$

The solution (6.32) can be written as

$$
q(\eta,\tau) = e^{-(c+i\,d)\tau} e^{\frac{1}{2}Re(1-\eta)} \sum_{k=0}^{\infty} (c+i\,d)^n (4\tau)^n T_r, \quad r = 0,2,4,6,\cdots, \qquad (6.34)
$$

where

$$T_r = \sum_{k=0}^{\infty}\left[\left\{i^r\mathrm{erfc}\left(\frac{a}{2\sqrt{\tau}}\right)-i^r\mathrm{erfc}\left(\frac{b}{2\sqrt{\tau}}\right)\right\}-\frac{Re^2}{4}\sqrt{\tau}\left\{a\,i^{r+1}\mathrm{erfc}\left(\frac{a}{2\sqrt{\tau}}\right)\right.\right.$$
$$\left.\left.- \quad b\,i^{r+1}\mathrm{erfc}\left(\frac{b}{2\sqrt{\tau}}\right)\right\}\right],\ r=0,2,4,6,\cdots \tag{6.35}$$

On separating into real and imaginary parts and using equation (6.14), we get the velocity fields for the primary and the secondary flows as

$$\begin{aligned} u_1 &= e^{\frac{1}{2}Re(1-\eta)}\left[\left\{T_0+c(4\tau)T_2+(c^2-d^2)(4\tau)^2T_4\right.\right.\\ &+ \left.(c^3-3cd^2)(4\tau)^3T_6+\cdots\right\}\cos 2d\tau\\ &+ \left\{d(4\tau)T_2+2cd(4\tau)^2T_4\right.\\ &+ \left.\left.(3c^2d-d^3)(4\tau)^3T_6+\cdots\right\}\sin d\tau\right]e^{-c\tau}, \end{aligned}\tag{6.36}$$

$$\begin{aligned} v_1 &= e^{\frac{1}{2}Re(1-\eta)}\left[\left\{d(4\tau)T_2+2cd(4\tau)^2T_4\right.\right.\\ &+ \left.(3c^2d-d^3)(4\tau)^3T_6+\cdots\right\}\cos d\tau\\ &- \left\{T_0+c(4\tau)T_2+(c^2-d^2)(4\tau)^2T_4\right.\\ &+ \left.\left.(c^3-3cd^2)(4\tau)^3T_6+\cdots\right\}\sin d\tau\right]e^{-c\tau}. \end{aligned}\tag{6.37}$$

The equations (6.36) and (6.37) describe the fluid velocities for small time. If $m = 0$ and $Re = 0$, the equations (6.36) and (6.37) coincide with equations (17) and (18) of Das et al.[9].

6.3 Steady state solution

When the time is very large, i.e., the time $\tau \to \infty$, we obtained the solution for steady state from equations (6.29) and (6.30) as

$$u_1 = e^{\frac{1}{2}Re(1-\eta)}\left[\frac{\sinh\eta\cos\eta\sinh\alpha\cos\alpha+\cosh\eta\sin\eta\cosh\alpha\sin(\alpha)}{\sinh^2\alpha\cos^2\alpha+\cosh^2\alpha\sin^2(\alpha)}\right], \tag{6.38}$$

$$v_1 = e^{\frac{1}{2}Re(1-\eta)}\left[\frac{\cosh\eta\sin\eta\sinh\alpha\cos\alpha-\sinh\eta\cos\eta\cosh\alpha\sin(\alpha)}{\sinh^2\alpha\cos^2\alpha+\cosh^2\alpha\sin^2(\alpha)}\right]. \tag{6.39}$$

We shall now discuss the asymptotic behavior of solutions (6.38) and (6.39) for small and large values of M^2, K^2 and Re in three different cases.

Case(i): When $K^2 \gg 1$, $M^2 \ll 1$ and $Re \ll 1$.

When K^2 is large, M^2 and Re are of small order of magnitude, the flow becomes boundary layer type. For the boundary layer flow near the moving plate $\eta = 1$, introducing the boundary layer coordinate $\xi = 1-\eta$, we obtain the velocity distributions from (6.38) and (6.39) as

$$u_1 = e^{-(-\frac{Re}{2}+\alpha)\xi}\cos\beta\xi, \tag{6.40}$$

$$v_1 = -e^{-(-\frac{Re}{2}+\alpha)\xi}\sin\beta\xi, \tag{6.41}$$

where

$$\begin{aligned}\alpha &= K\left[1+\frac{M^2(1+m)}{4K^2(1+m^2)}+\frac{Re^2}{16K^2}\right],\\ \beta &= K\left[1+\frac{M^2(1-m)}{4K^2(1+m^2)}-\frac{Re^2}{16K^2}\right].\end{aligned} \tag{6.42}$$

It is evident from equations (6.40)and (6.41) that there arises a single-deck boundary layer of thickness of the order $\mathrm{O}(-\frac{Re}{2}+\alpha)^{-1}$ near the moving plate ($\eta=1$) of the channel, where α is given by equation (6.42). The thickness of this boundary layer increases with an increase in either Hall parameter m or rotation parameter K^2 since α decreases with increase in either m or K^2. On the other hand, it decreases with an increase in either magnetic parameter M^2 or Re as α increases with an increase in either M^2 or Re.

Case(ii): When $M^2 \gg 1$, $K^2 \ll 1$ and $Re \ll 1$.

In this case, the velocity distributions are obtained from the equations (6.38) and (6.39) as

$$u_1 = e^{-(-\frac{Re}{2}+\alpha)\xi}\cos\beta\xi, \tag{6.43}$$

$$v_1 = -e^{-(-\frac{Re}{2}+\alpha)\xi}\sin\beta\xi, \tag{6.44}$$

where

$$\begin{aligned}\alpha &= \frac{M}{\sqrt{1+m^2}}\left[1+\frac{Re^2(1+m^2)}{8M^2}\right],\\ \beta &= \frac{\sqrt{1+m^2}}{2M}\left(2K^2+\frac{m\,M^2}{1+m^2}\right).\end{aligned} \tag{6.45}$$

The equations (6.43) and (6.44) reveal that there appears a single-decker boundary layer of thickness of the order $\mathrm{O}(-\frac{Re}{2}+\alpha)^{-1}$ adjacent to the moving plate ($\eta=1$) of the channel, where α is given by equation (6.45). The thicknesses of the layer increases with an increase in either Hall parameter m or Reynolds number Re while it decreases with an increase in magnetic parameter M^2. It is interesting to note that for large values of M^2, the boundary layer thickness is independent of the rotation parameter.

Case(iii): When $Re \gg 1$, $K^2 \ll 1$ and $M^2 \ll 1$.

In this case, equations (6.38) and (6.39) become

$$u_1 = e^{-(-\frac{Re}{2}+\alpha)\xi}\cos\beta\xi, \tag{6.46}$$

$$v_1 = -e^{-(-\frac{Re}{2}+\alpha)\xi}\sin\beta\xi, \tag{6.47}$$

where

$$\begin{aligned}\alpha &= \frac{Re}{2}\left[1+\frac{2M^2}{Re^2(1+m^2)}\right],\\ \beta &= \frac{1}{Re}\left(2K^2+\frac{mM^2}{1+m^2}\right).\end{aligned} \tag{6.48}$$

It is seen from equations (6.46)and (6.47) that there exists a single-deck boundary layer of thickness of the order $\mathrm{O}(-\frac{Re}{2}+\alpha)^{-1}$, where α is given by equation (6.48). It is seen that

the thickness of this boundary layer increases with an increase in either Hall parameter m or Reynolds number Re since α decreases with an increase in either m or Re. On the other hand, it decreases with an increase in magnetic parameter M^2 as α increases with increase in M^2.

6.4 Results and discussion

In order to gain a clear physical insight of the problem, we examine the effects of magnetic parameter M^2, the rotation parameter K^2, Hall parameter m, Reynolds number Re and time τ on the velocity and shear stresses at the plate. The default values of the pertinent parameters are presented in the respective figures.

6.4.1 Effects of parameters on the velocity profiles

The effects of pertinent parameters on the primary as well as the secondary velocities are presented graphically against η in **Figures 6.2-6.6**. It is seen from **Figure 6.2** that both the primary velocity u_1 and the magnitude of the secondary velocity v_1 decreases with an increase in magnetic parameter M^2 as expected since the magnetic field has a retarding influence on the flow.

This observation can be explained by the following fact. As the magnetic parameter M^2 increases, the Lorentz force which opposes the flow, also increases and leads to the enhanced deceleration of the flow. It reveals that magnetic field tends to decelerate the fluid velocity.

Figure 6.3 reveals that the primary velocity u_1 decreases with increase in K^2. On the other hand, the magnitude of the secondary velocity v_1 increases with an increase in K^2. It is observed from **Figure 6.4** that both the primary velocity u_1 and the magnitude of the secondary velocity v_1 increase with an increase in Hall parameter m.

In the physical point of view this figure indicates that flow field quickly gets stabilized owing to the effects of the Hall currents, because the electrical conductivity of the fluid $\frac{\sigma}{1+m^2}$ decreases with an increase in Hall parameter m which ultimately reduces the magnetic damping force, as a result the fluid velocity increases.

Figure 6.5 shows that the primary velocity u_1 increases while the magnitude of the secondary velocity v_1 decreases with an increase in Reynolds number Re. It is observed from **Figure 6.6** that both the primary velocity u_1 and the magnitude of the secondary velocity v_1 increase with an increase in time τ.

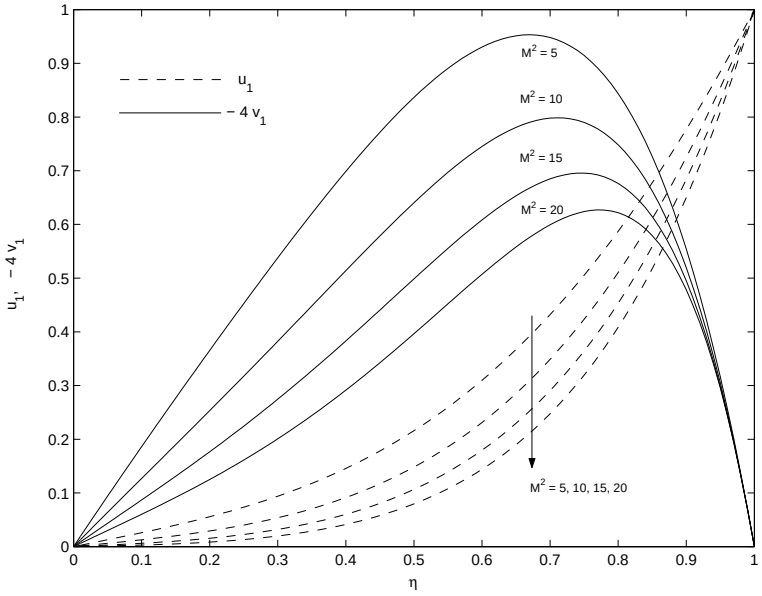

Figure 6.2: Variations of u_1 and v_1 for M^2 when $K^2 = 4$, $m = 0.5$, $Re = 0.5$, and $\tau = 0.2$.

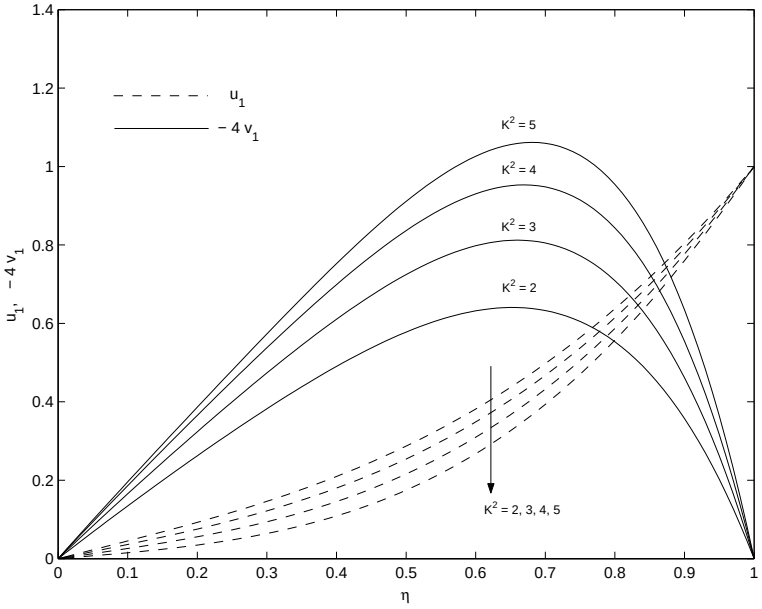

Figure 6.3: Variations of u_1 and v_1 for K^2 when $M^2 = 5$, $m = 0.5$, $Re = 0.5$, and $\tau = 0.2$.

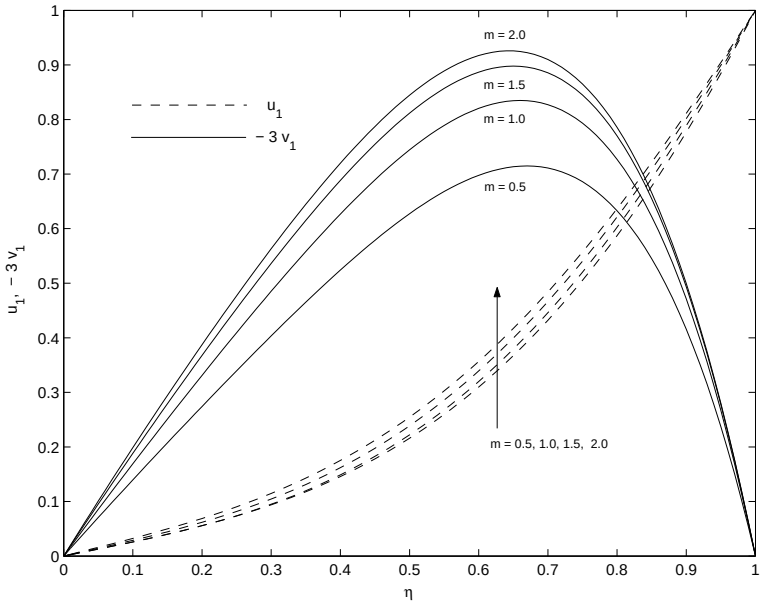

Figure 6.4: Variations of u_1 and v_1 for m when $M^2 = 5$, $K^2 = 4$, $Re = 0.5$ and $\tau = 0.2$.

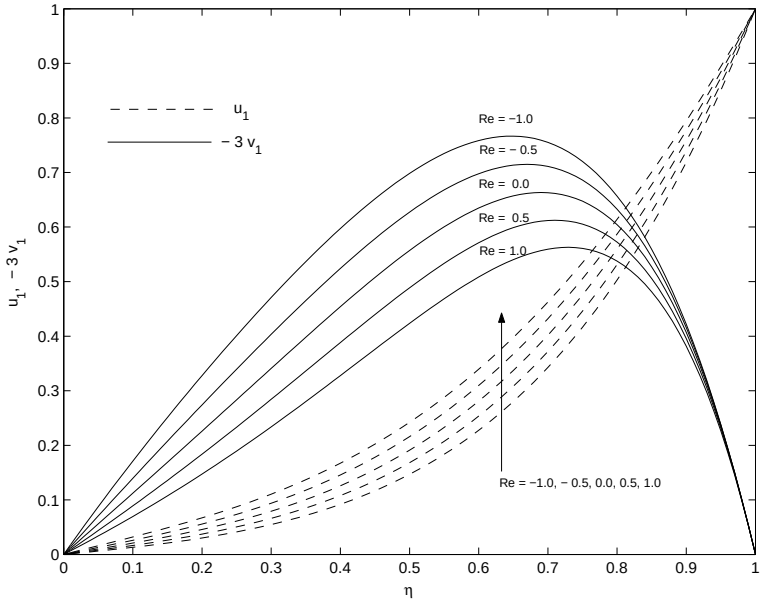

Figure 6.5: Variations of u_1 and v_1 for Re when $M^2 = 5$, $K^2 = 4$, $m = 0.5$ and $\tau = 0.2$.

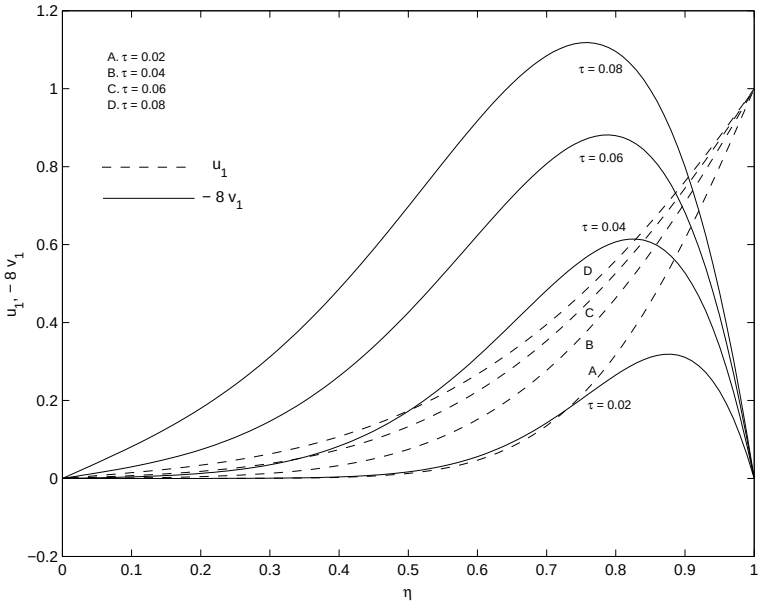

Figure 6.6: Variations of u_1 and v_1 for τ when $M^2 = 5$, $K^2 = 4$, $m = 0.5$ and $Re = 0.5$.

6.4.2 Comparison between general solution and small time solution

For small values of time, we have drawn the velocity components u_1 and v_1 on using the solution given by equations (6.36) and (6.37) and the general solution given by equations (6.29) and (6.30) in **Figures 6.7 and 6.8**.

It is seen that the solution for small time given by the equations (6.36) and (6.37) converges more rapidly than the general solution given by equation (6.29) and (6.30). Hence, we conclude that for small times, the numerical values of the velocity components can be evaluated from the equations (6.36) and (6.37) instead of equations (6.29) and (6.30).

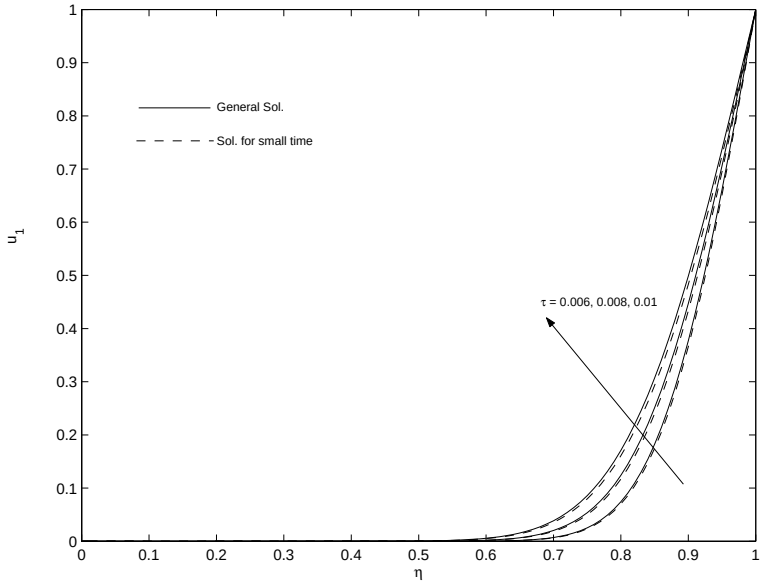

Figure 6.7: Variation of u_1 for the general solution and small time solution with $m = 0.5,\ M^2 = 5,\ K^2 = 4,\ Re = 0.5$.

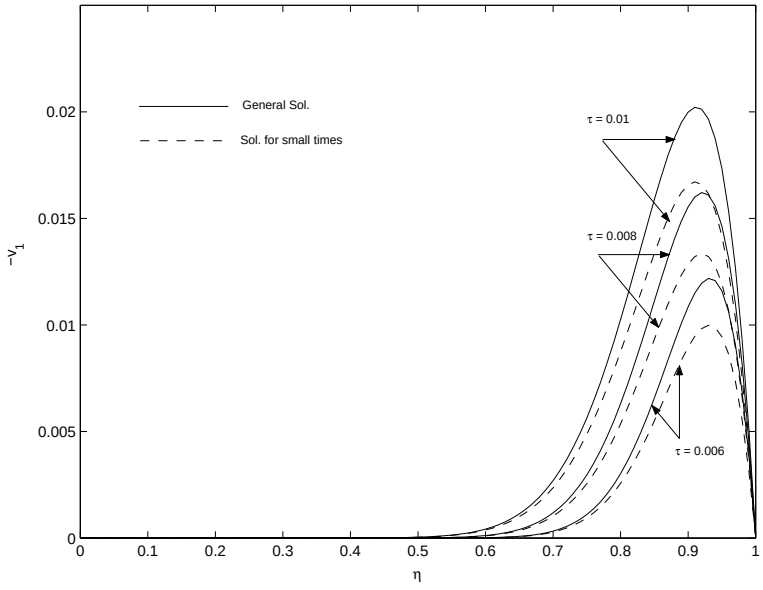

Figure 6.8: Variation of v_1 for the general solution and small time solution with $m = 0.5,\ M^2 = 5,\ K^2 = 4,\ Re = 0.5$.

6.4.3 Effects of parameters on the shear stresses at the plate

For engineering purposes, one is usually interested to determine the values of the shear stresses (or skin functions). The increased shear stresses is generally a disadvantage in the technical applications. For general solution, the non-dimensional shear stresses due to the primary and the secondary flows at the stationary plate $\eta = 0$ are given by

$$\left(\frac{\partial q}{\partial \eta}\right)_{\eta=0} = e^{\frac{1}{2}Re}\left[\frac{(\alpha + i\,\beta)}{\sinh(\alpha + i\,\beta)} + \sum_{n=1}^{\infty}\frac{2n^2\pi^2(-1)^n e^{-\{n^2\pi^2+(\alpha+i\,\beta)^2\}\tau}}{n^2\pi^2+(\alpha+i\,\beta)^2}\right]. \tag{6.49}$$

On separating into a real and imaginary parts, we get the shear stress components due to the primary and secondary flows at the stationary plate ($\eta = 0$)as

$$\begin{aligned}\tau_{x_0} &= e^{\frac{1}{2}Re}\left[\frac{2(\alpha\,\sinh\alpha\cos\beta + \beta\cosh\alpha\sin\beta)}{\cosh 2\alpha - \cos 2\beta}\right.\\ &+ \sum_{n=1}^{\infty}\frac{2n^2\pi^2(-1)^n}{(n^2\pi^2+\alpha^2-\beta^2)^2+4\alpha^2\beta^2}\\ &\times \left.\{(n^2\pi^2+\alpha^2-\beta^2)\cos 2\alpha\beta\tau - 2\alpha\beta\sin 2\alpha\beta\tau)\}e^{-(n^2\pi^2+\alpha^2-\beta^2)\tau}\right],\end{aligned} \tag{6.50}$$

$$\begin{aligned}\tau_{y_0} &= e^{\frac{1}{2}Re}\left[\frac{2(\beta\,\sinh\alpha\cos\beta - \alpha\cosh\alpha\sin\beta)}{\cosh 2\alpha - \cos 2\beta}\right.\\ &- \sum_{n=1}^{\infty}\frac{2n^2\pi^2(-1)^n}{(n^2\pi^2+\alpha^2-\beta^2)^2+(2K^2)^2}\\ &\times \left.\{2\alpha\beta\cos 2\alpha\beta\tau + (n^2\pi^2+\alpha^2-\beta^2)\sin 2\alpha\beta\tau)\}e^{-(n^2\pi^2+\alpha^2-\beta^2)\tau}\right],\end{aligned} \tag{6.51}$$

where α and β are given by equation (6.18).

The numerical values of τ_{x_0} and τ_{y_0} are presented in **Figures 6.9-6.12** against Hall parameter m for various values of M^2, K^2, Re and τ.

It is seen from **Figure 6.9** that both the shear stress τ_{x_0} and the magnitude of the shear stress τ_{y_0} decrease with an increase in M^2 when m is fixed, while τ_{x_0} first decreases, reaches a minimum and then increases and the magnitude of τ_{y_0} increases with an increase in m when M^2 is fixed. **Figure 6.10** displays that both the shear stress τ_{x_0} and the magnitude of the shear stress τ_{y_0} decrease with increase in K^2 when m is fixed. It is seen from **Figure 6.11** that both the shear stress τ_{x_0} and the magnitude of τ_{y_0} increase with an increase in Re when m is fixed, while τ_{x_0} first decreases, reaches a minimum and then increases and the magnitude of τ_{y_0} first increases, reaches a maximum and then decreases with an increase in m when Re is fixed. It is also seen from **Figure 6.12** that for fixed values of τ, τ_{x_0} first decreases, reaches a minimum and then increases and the magnitude of τ_{y_0} increases with an increase in m. On the other hand, for fixed values of m, τ_{x_0} decreases and the magnitude of τ_{y_0} increases with an increase in τ.

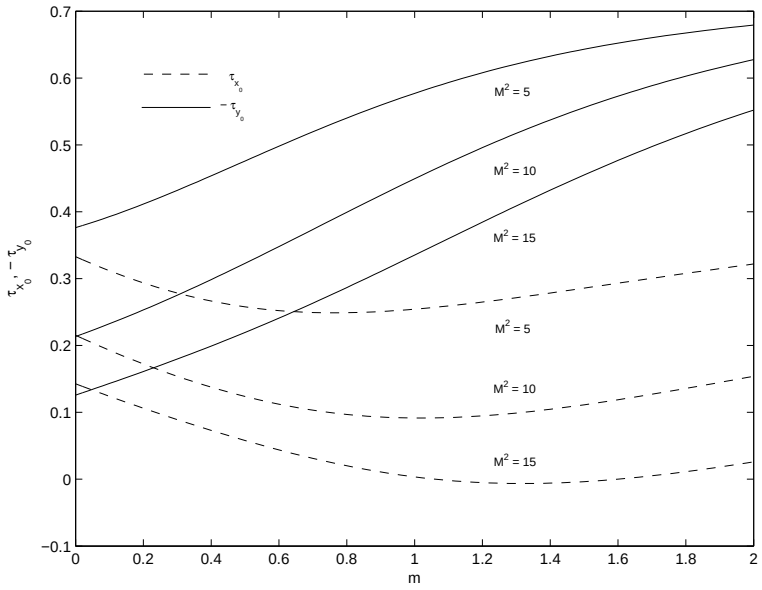

Figure 6.9: Variations of τ_{x_0} and $-\tau_{y_0}$ for M^2 when $K^2 = 4$, $Re = 0.5$, and $\tau = 0.2$.

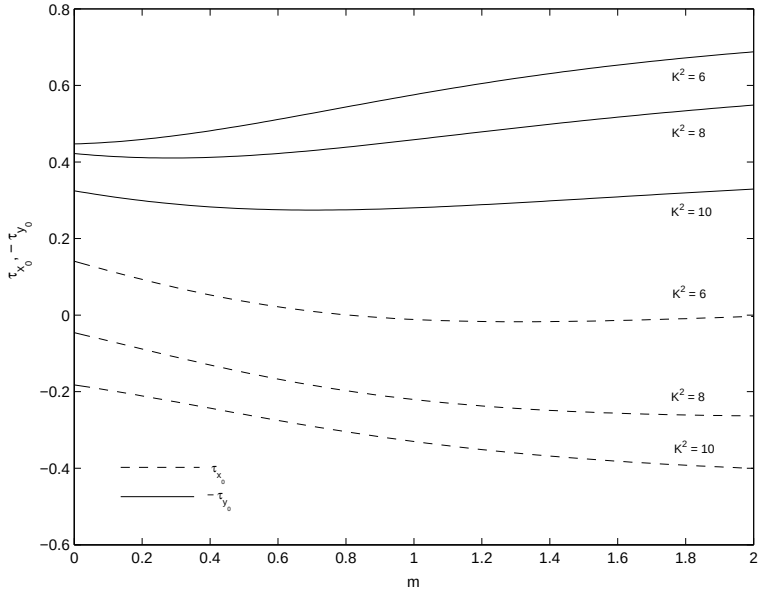

Figure 6.10: Variations of τ_{x_0} and $-\tau_{y_0}$ for K^2 when $M^2 = 5$, $Re = 0.5$ and $\tau = 0.2$.

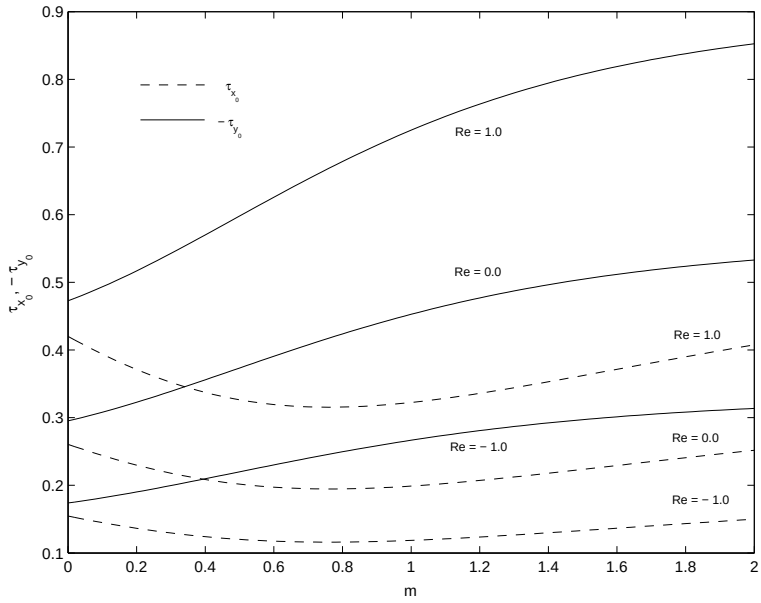

Figure 6.11: Variations of τ_{x_0} and $-\tau_{y_0}$ for Re when $K^2 = 4$, $M^2 = 5$ and $\tau = 0.2$.

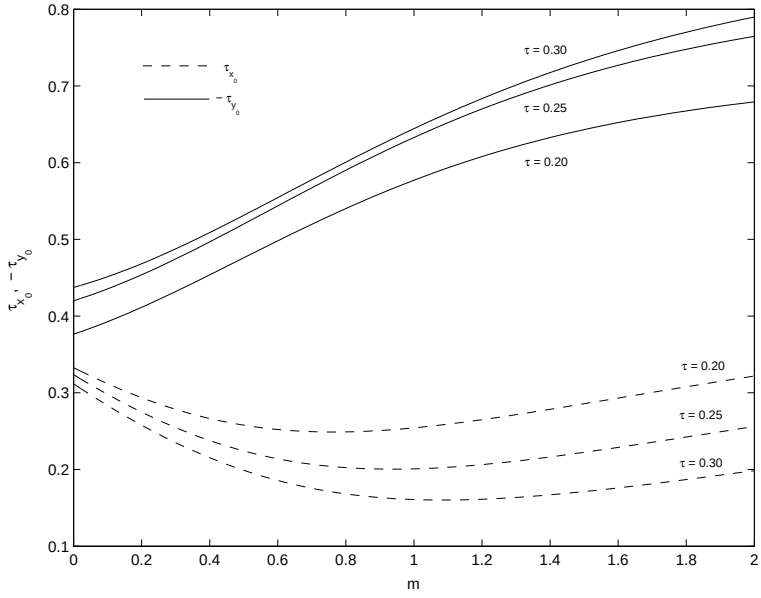

Figure 6.12: Variations of τ_{x_0} and $-\tau_{y_0}$ for τ when $K^2 = 4$, $M^2 = 5$ and $Re = 0.5$.

6.5 Conclusions

The combined effects of Hall current and rotation on MHD Couette flow of a viscous incompressible electrically conducting fluid between two infinitely long horizontal parallel porous plates channel in a rotating system in the presence of uniform transverse magnetic field have been investigated. The dimensionless governing partial differential equations are solved by the Laplace transformation technique. The effects of pertinent parameters such as magnetic parameter, Hall parameter, rotation parameter, Reynolds number and time are studied. It is found that the primary velocity u_1 and the magnitude of the secondary velocity v_1 decrease with an increase in Hall parameter m. It is also found that the primary velocity u_1 decreases while the magnitude of the secondary velocity v_1 increases with an increase in rotation parameter K^2. It is seen that the solution for small time converges more rapidly than the general solution. The asymptotic behavior of the solution is analyzed for small as well as large values of magnetic parameter M^2 , rotation parameter K^2 and Reynolds number Re. It is observed that a thin boundary layer is formed near the moving plate and the thickness of the layer increases with an increase in either Hall parameter m or Reynolds number Re, while it decreases with an increase in magnetic parameter M^2 as expected since the magnetic field has a retarding influence on the flow. It is interesting to note that for large values of M^2, the boundary layer thickness is independent of the rotation parameter. The expression for the shear stresses at the stationary plate due to the primary and secondary velocities are obtained. It is found that both the shear stress τ_{x_0} due to the primary flow and magnitude of the shear stress τ_{y_0} due to secondary flow decrease with an increase in M^2 when m is fixed while τ_{x_0} first decreases, reaches a minimum and then increases and the magnitude of τ_{y_0} increases with an increase in m when M^2 is fixed.

Bibliography

[1] Sutton GW and Sherman A, Engg. Magnetohydrodynamics, McGraw-Hill, New York: (1965)

[2] Chandran P, Sacheti NC and Singh AK, Astrophysics and Space Sci.: **202(1)**(1993), pp.1.

[3] Katagiri M, Seth GS and Ansari MS, Int. J. Theory and Application Mechanism: **4**(2009), pp.205.

[4] Ghosh SK and Pop I, Int. J. Appl. Mech. and Engg.: **9(2)**(2004), pp.293.

[5] Ghosh SK, Czechoslovak J. Phys.: **52(1)**(2002), pp.51.

[6] Gubanov AI and Lunkin PT, Soviet Physics-Technical Phys.: **5**(1961), pp.984.

[7] Jana RN and Datta N, Czechoslovak J. Phys.: **30**(1980), pp.659.

[8] Reddy NB and Bathaiah D, Defense Sci. J.: **32**(1982), pp.313.

[9] Das S, Maji SL, Guria M and Jana RN, Mathe. and Com. Model.: **50**(2009), pp.1211.

[10] Prasad-Rao DRV, Krishna DV and Debnath L, Int. J. Mathematics and Mathematical Sci.: **5**(1982), pp.165.

[11] Mandal G and Mandal KK, J. the Physical Society of Jpn.: **52**(1983), pp.470.

[12] Sivaprasad R, Prasad-Rao DRV and Krishna DV, Indian J. Pure and Appl. Math.: **19(7)**(1988), pp.688.

[13] Cowling TG, Magnetohydrodynamics, Intersci., New York: (1957)

[14] Pai SI, Magnetogasdynamics and Plasma Dynamics, Springer-Verlag, Viena; Prentice Hall, Englewood cliffs: (1962)

[15] Batchelor GK, An Introduction to Fluid Dynamics, Ist ed., Cambridge Press, Cambridge, U. K.: (1967), pp.200.

[16] Carslaw HS and Jaeger JC, Conduction of Heat in solids, Oxford University Press, Oxford: (1959)

Chapter 7

Combined effects of Hall current and radiation on MHD free convective flow in a vertical channel with an oscillatory wall temperature*

7.1 Introduction

The radiative convective flows are frequently encountered in many scientific and environmental processes, such as astrophysical flows, water evaporation from open reservoirs, heating and cooling of chambers, and solar power technology. The unsteady hydromagnetic flow of a viscous incompressible electrically conducting fluid through a vertical channel is of considerable interest in the technical field due to its frequent occurrence in industrial and technological applications. The Hall effects on the flow of ionized gas between parallel plates under transverse magnetic field has been studied by Sato[1]. Miyatake and Fujii[2] have discussed the free convection flow between vertical plates - one plate isothermally heated and other thermally insulated. The natural convection flow between two vertical parallel plates, one plate with a uniform heat flux and the other thermally insulated have been investigated by Tanaka et al.[3]. Gupta and Gupta[4] have studied the effects of radiation on hydromantic convection in a vertical channel. The Hall effects on the hydromagnetic convective flow through a channel with conducting walls have been investigated by Dutta and Jana[5]. The unsteady hydromagnetic free convective flow with radiative heat transfer in a rotating fluid have been described by Bestman and Adjepong[6].

*Published in **Open J. of Fluid Dynamics (OJFD)**, ISSN: 2165-3852, 3(1)(2013), pp.9-22.*

Joshi[7] has studied the transient effects in natural convection cooling of vertical parallel plates. Singh[8] has described the natural convection in unsteady Couette motion. Singh et al.[9] have studied the unsteady free convective flow between two vertical parallel plates. The natural convection in unsteady MHD Couette flow with heat and mass transfers has been analyzed by Jha[10]. Narahari et al.[11] have studied the unsteady free convective flow between long vertical parallel plates with constant heat flux at one boundary. The unsteady free convective flow in a vertical channel due to symmetric heating have been described by Jha et al.[12]. Singh and Paul[13] have analysed the unsteady natural convective flow between two vertical walls heated/cooled asymmetrically. Sanyal and Adhikari[14] have studied the effects of radiation on MHD vertical channel flow. The effects of radiation on MHD Couette flow with heat transfer between two parallel plates has presented by Mebine[15]. Grosan and Pop[16] have considered the effects thermal radiation on the fully developed mixed convective flow in a vertical channel. Guria and Jana[17] have discussed the Hall effects on the hydromagnetic convective flow through a rotating channel under general wall conditions. Jha and Ajibade[18] have examined the unsteady free convective Couette flow of heat generating/absorbing fluid. The effects of thermal radiation and free convection current on unsteady Couette flow between two vertical parallel plates with constant heat flux at one boundary has been studied by Narahari[19]. Rajput and Sahu[20] have considered the unsteady free convection MHD flow between two long vertical parallel plates with constant temperature and variable mass diffusion. Das et al.[21] have investigated the radiation effects on free convection MHD Couette flow started exponentially with variable wall temperature in presence of heat generation. The effects of radiation on transient natural convection flow between two vertical walls have been described by Mandal et al.[22]. The effects of radiation on MHD free convective Couette flow in a rotating system have been carried out by Sarkar et al.[23]. Sarkar et al.[24] have also presented an oscillatory MHD free convective flow between two vertical walls in a rotating system.

The aim of this chapter, is to study the combined effects of Hall current and radiation on the unsteady MHD free convective flow of a viscous incompressible electrically conducting fluid in a vertical channel with an oscillatory wall temperature of one of the channel walls. A uniform transverse magnetic field of strength B_0 is applied normal to the channel walls. Here we assume that the flow is laminar and the pressure gradient term in the momentum equation can be neglected. The governing differential equations for both velocity and temperature are solved by the Laplace transformation technique. The effects of physical variables, involving in this study, on velocity, temperature, shear stresses and rate of heat transfer are presented graphically and in tabular form.

7.2 Formulation of the problem and its solutions

Consider the unsteady MHD flow of a viscous incompressible electrically conducting radiative fluid between two infinitely long vertical parallel walls separated by a distance h. The flow is set up by the buoyancy force arising from the temperature gradient. Choose a Cartesian co-ordinate system with x- axis along the channel wall in the vertically upward direction, z-

axis perpendicular to the channel walls and y-axis is normal to the xz-plane [see **Figure 7.1**]. Initially, at time $t = 0$, both the walls and the fluid are assumed to be at the same temperature T_h and stationary. At time $t > 0$, the wall at $z = 0$ starts to move in its own plane with a velocity $U(t)$ and its temperature raised to $T_h + (T_0 - T_h)\cos\omega t$ whereas the wall at $z = h$ is stationary and maintained at a constant temperature T_h, where ω is the frequency of the temperature oscillations. A uniform transverse magnetic field of strength B_0 is applied perpendicular to the channel walls. We assume that the flow is laminar and the pressure gradient term in the momentum equation can be neglected. Here we also neglect the viscous and Joule dissipations. It is also assumed that the radiative heat flux in the x-direction is negligible as compared to that in the z-direction. As the channel walls are infinitely long along x and y-directions, the velocity field and temperature distribution are functions of z and t only.

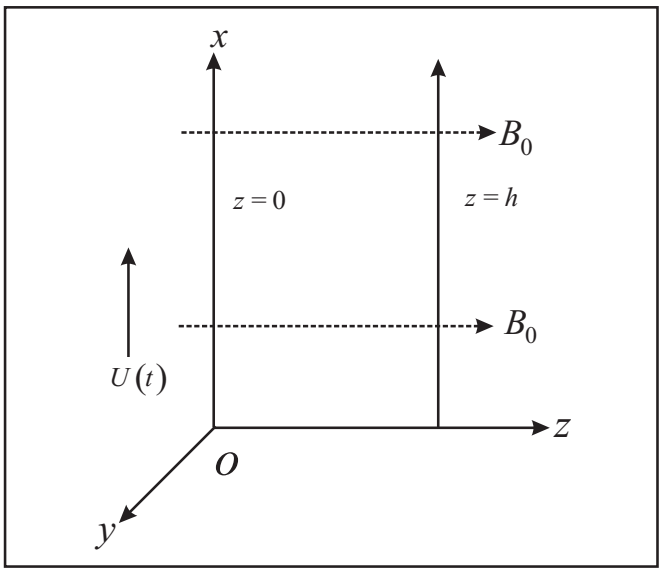

Figure 7.1: Geometry of the problem

Under the usual Boussinesq approximation, the flow is governed by the Navier-Stokes equations

$$\frac{\partial u}{\partial t} = \nu\frac{\partial^2 u}{\partial z^2} + g\beta(T - T_h) + \frac{B_0}{\rho}j_y, \tag{7.1}$$

$$\frac{\partial v}{\partial t} = \nu\frac{\partial^2 v}{\partial z^2} - \frac{B_0}{\rho}j_x, \tag{7.2}$$

$$\rho\, c_p\frac{\partial T}{\partial t} = k^*\frac{\partial^2 T}{\partial z^2} - \frac{\partial q_r}{\partial z}, \tag{7.3}$$

where ρ is the fluid density, T the fluid temperature, ν the kinematic viscosity, u and v are fluid velocity components, g the acceleration due to gravity, k^* the thermal conductivity, c_p the specific heat at constant pressure, q_r the radiative heat flux and j_x, j_y the components of current density along x, y-directions respectively.

The initial and boundary conditions for the velocity field and temperature distributions are

$$\begin{aligned} &t = 0: \quad u = v = 0, \;\; T = T_h \;\text{ for }\; 0 \le y \le h, \\ &t > 0: \quad u = U(t), \;\; v = 0, \;\; T = T_h + (T_0 - T_h)\cos\omega t \;\text{ at }\; y = 0, \\ &t > 0: \quad u = v = 0, \;\; T = T_h \;\text{ at }\; y = h. \end{aligned} \tag{7.4}$$

It has been shown by Cogley et al.[25] that in the optically thin limit for a non-gray gas near equilibrium, the following relation holds

$$\frac{\partial q_r}{\partial z} = 4(T - T_h)\int_0^\infty K_{\lambda_h}\left(\frac{\partial e_{\lambda p}}{\partial T}\right)_h d\lambda, \tag{7.5}$$

where K_{λ_h} is the absorption coefficient, λ is the wave length, $e_{\lambda p}$ is the Planck's function and subscript $'h'$ indicates that all quantities have been evaluated at the temperature T_h which is the temperature of the wall at time $t = 0$. Thus, our study is limited to small difference of wall temperatures to the fluid temperature.

On the use of equation (7.5), equation (7.3) becomes

$$\rho c_p \frac{\partial T}{\partial t} = k^* \frac{\partial^2 T}{\partial z^2} - 4\,(T - T_h)\,I, \tag{7.6}$$

where

$$I = \int_0^\infty K_{\lambda_h}\left(\frac{\partial e_{\lambda p}}{\partial T}\right)_h d\lambda. \tag{7.7}$$

The generalized Ohm's law, on taking Hall currents into account and neglecting ion-slip and thermo-electric effects, is (see Cowling[26])

$$\vec{j} + \frac{\omega_e \tau_e}{B_0}\left(\vec{j} \times \vec{B}\right) = \sigma\left(\vec{E} + \vec{q} \times \vec{B}\right), \tag{7.8}$$

where $\vec{j}$ is the current density vector, $\vec{B}$ the magnetic field vector, $\vec{E}$ the electric field vector, ω_e the cyclotron frequency, σ the electrical conductivity of the fluid and τ_e the collision time of electron.

We shall assume that the magnetic Reynolds number for the flow is small so that the induced magnetic field can be neglected. This assumption is justified since the magnetic Reynolds number is generally very small for partially ionized gases. The solenoidal relation $\nabla \cdot \vec{B} = 0$ for the magnetic field gives $B_z = B_0 =$ constant everywhere in the fluid where $\vec{B} \equiv (0, 0, B_0)$. Further, if (j_x, j_y, j_z) be the components of the current density $\vec{j}$, then the equation of the conservation of the current density $\nabla \cdot \vec{j} = 0$ gives $j_z =$ constant. This constant is zero since $j_z = 0$ at the walls which are electrically non-conducting. Thus $j_z = 0$ everywhere in the flow. Since the induced magnetic field is neglected, the Maxwell's equation $\nabla \times \vec{E} = -\frac{\partial \vec{B}}{\partial t}$ becomes $\nabla \times \vec{E} = 0$ which gives $\frac{\partial E_x}{\partial z} = 0$ and $\frac{\partial E_y}{\partial z} = 0$. This implies that $E_x =$ constant and $E_y =$ constant everywhere in the flow. We choose this constants equal to zero, i.e. $E_x = E_y = 0$.

In view of the above assumption, the equation (7.8) gives

$$j_x + mj_y = \sigma v B_0, \tag{7.9}$$

$$j_y - mj_x = -\sigma u B_0, \tag{7.10}$$

where $m = \omega_e \tau_e$ is the Hall parameter.
Solving equations (7.9) and (7.10) for j_x and j_y, we have

$$j_x = \frac{\sigma B_0}{1+m^2}(v + mu), \tag{7.11}$$

$$j_y = \frac{\sigma B_0}{1+m^2}(mv - u). \tag{7.12}$$

On the use of equations (7.11) and (7.12), the momentum equations (7.1) and (7.2) along x- and y-directions become

$$\frac{\partial u}{\partial t} = \nu \frac{\partial^2 u}{\partial y^2} + g\beta(T - T_h) - \frac{\sigma B_0^2}{\rho(1+m^2)}(u - mv), \tag{7.13}$$

$$\frac{\partial v}{\partial t} = \nu \frac{\partial^2 v}{\partial y^2} - \frac{\sigma B_0^2}{\rho(1+m^2)}(v + mu). \tag{7.14}$$

Introducing non-dimensional variables

$$(u_1, v_1) = \frac{(u,v)}{U_0}, \;\; \eta = \frac{z}{h}, \;\; \tau = \frac{\nu t}{h^2}, \;\; \theta = \frac{T - T_h}{T_0 - T_h}, \;\; U(t) = U_0 f(\tau) \tag{7.15}$$

equations (7.13), (7.14) and (7.3) become

$$\frac{\partial u_1}{\partial \tau} = \frac{\partial^2 u_1}{\partial \eta^2} + Gr\theta - \frac{M^2}{1+m^2}(u_1 - mv_1), \tag{7.16}$$

$$\frac{\partial v_1}{\partial \tau} = \frac{\partial^2 v_1}{\partial \eta^2} - \frac{M^2}{1+m^2}(v_1 + mu_1), \tag{7.17}$$

$$Pr\frac{\partial \theta}{\partial \tau} = \frac{\partial^2 \theta}{\partial \eta^2} - R\theta, \tag{7.18}$$

where $M^2 = \frac{\sigma {B_0}^2 h^2}{\rho \nu}$ is the magnetic parameter, $Gr = \frac{g\beta(T_0 - T_h)h^2}{\nu^2}$ the Grashof number, $Pr = \frac{\rho\, c_p\, \nu}{k^*}$ the Prandtl number and $R = \frac{4Ih^2}{k^*}$ the radiation parameter.
The initial and boundary conditions (7.4) become

$$\begin{aligned} &\tau = 0: \;\; u_1 = v_1 = 0, \;\; \theta = 0 \;\text{ for }\; 0 \le \eta \le 1, \\ &\tau > 0: \;\; u_1 = f(\tau), \; v_1 = 0, \;\; \theta = \cos n\tau \;\text{ at }\; \eta = 0, \\ &\tau > 0: \;\; u_1 = v_1 = 0, \;\; \theta = 0 \;\text{ at }\; \eta = 1, \end{aligned} \tag{7.19}$$

where $n = \frac{\omega h^2}{\nu}$ is the temperature frequency parameter.
Combining equations (7.16) and (7.17), we get

$$\frac{\partial F}{\partial \tau} = \frac{\partial^2 F}{\partial \eta^2} + Gr\;\theta - \frac{(1+im)\,M^2}{1+m^2}F, \tag{7.20}$$

where

$$F = u_1 + i\, v_1 \ \text{ and } \ i = \sqrt{-1}. \tag{7.21}$$

The initial and boundary conditions for $F(\eta, \tau)$ are

$$\begin{aligned} &\tau = 0: \ \ F = 0 \ \text{ for } \ 0 \le \eta \le 1, \\ &\tau > 0: \ \ F = f(\tau) \ \text{ at } \ \eta = 0, \\ &\tau > 0: \ \ F = 0 \ \text{ at } \ \eta = 1. \end{aligned} \tag{7.22}$$

Taking the Laplace transform of equations (7.20) and (7.18) and on the use of (7.19) and (7.22), we have

$$\frac{d^2\bar{F}}{d\eta^2} - (a+s)\bar{F} = -Gr\ \bar{\theta}, \tag{7.23}$$

$$\frac{d^2\bar{\theta}}{d\eta^2} - (R + sPr)\bar{\theta} = 0, \tag{7.24}$$

where

$$a = \frac{M^2(1+im)}{1+m^2}. \tag{7.25}$$

The boundary conditions for $\bar{F}(\eta, s)$ and $\bar{\theta}(\eta, s)$ are

$$\begin{aligned} &\bar{F}(0,s) = \bar{f}(s), \ \ \bar{F}(1,s) = 0, \\ &\bar{\theta}(0,s) = \frac{1}{2}\left(\frac{1}{s - i\,n} + \frac{1}{s + i\,n}\right), \ \ \bar{\theta}(1,s) = 0. \end{aligned} \tag{7.26}$$

Solution of equations (7.24) and (7.23) subject to the boundary conditions (7.26) are given by

$$\bar{\theta}(\eta, s) = \begin{cases} \frac{s}{s^2+n^2}\,\frac{\sinh\sqrt{R+sPr}(1-\eta)}{\sinh\sqrt{R+sPr}} & \text{for } \ Pr \neq 1 \\ \\ \frac{s}{s^2+n^2}\,\frac{\sinh\sqrt{R+s}(1-\eta)}{\sinh\sqrt{R+s}} & \text{for } \ Pr = 1, \end{cases} \tag{7.27}$$

$$\bar{F}(\eta, s) = \begin{cases} \bar{f}(s)\,\frac{\sinh\sqrt{a+s}(1-\eta)}{\sinh\sqrt{a+s}} \\ \quad + \frac{s\,Gr}{(Pr-1)(s+\alpha)(s^2+n^2)}\left\{\frac{\sinh\sqrt{a+s}(1-\eta)}{\sinh\sqrt{a+s}} - \frac{\sinh\sqrt{R+sPr}(1-\eta)}{\sinh\sqrt{R+sPr}}\right\} & \text{for } \ Pr \neq 1 \\ \\ \bar{f}(s)\,\frac{\sinh\sqrt{a+s}(1-\eta)}{\sinh\sqrt{a+s}} \\ \quad + \frac{s\,Gr}{(R-a)(s^2+n^2)}\left\{\frac{\sinh\sqrt{a+s}(1-\eta)}{\sinh\sqrt{a+s}} - \frac{\sinh\sqrt{R+s}(1-\eta)}{\sinh\sqrt{R+s}}\right\} & \text{for } \ Pr = 1, \end{cases} \tag{7.28}$$

Now, we shall considered the following two cases.

(i) When the wall at $\eta = 0$ started impulsively:

In this case $f(\tau) = 1$, i.e. $f(s) = \frac{1}{s}$. Then the inverse Laplace transforms of equations (7.27) and (7.28) give the solution for the temperature distribution and the velocity fields as

$$\theta(\eta,\tau) = \begin{cases} \frac{1}{2}\left[e^{in\tau}\frac{\sinh\sqrt{R+inPr}(1-\eta)}{\sinh\sqrt{R+inPr}} + e^{-in\tau}\frac{\sinh\sqrt{R-inPr}(1-\eta)}{\sinh\sqrt{R-inPr}}\right] \\ +\frac{2\pi}{Pr}\sum_{k=1}^{\infty}\frac{k\,s_1 e^{s_1\tau}}{s_1^2+n^2}\,\sin k\pi\eta \qquad \text{for } Pr \neq 1 \\ \\ \frac{1}{2}\left[e^{in\tau}\frac{\sinh\sqrt{R+in}(1-\eta)}{\sinh\sqrt{R+in}} + e^{-in\tau}\frac{\sinh\sqrt{R-in}(1-\eta)}{\sinh\sqrt{R-in}}\right] \\ +2\pi\sum_{k=1}^{\infty}\frac{k\,s_3\,e^{s_3\tau}}{s_3^2+n^2}\,\sin k\pi\eta \qquad \text{for } Pr = 1, \end{cases} \tag{7.29}$$

$$F(\eta,\tau) = \begin{cases} \frac{\sinh\sqrt{a}(1-\eta)}{\sinh\sqrt{a}} + 2\pi\sum_{k=1}^{\infty}\frac{k\,e^{s_2\tau}}{s_2}\,\sin k\pi\eta \\ +\frac{Gr}{2(Pr-1)}\left[\frac{e^{in\tau}}{(\alpha+in)}\left\{\frac{\sinh\sqrt{a+in}(1-\eta)}{\sinh\sqrt{a+in}} - \frac{\sinh\sqrt{R+inPr}(1-\eta)}{\sinh\sqrt{R+inPr}}\right\}\right. \\ +\frac{e^{-in\tau}}{\alpha-in}\left\{\frac{\sinh\sqrt{a-in}(1-\eta)}{\sinh\sqrt{a-in}} - \frac{\sinh\sqrt{R-inPr}(1-\eta)}{\sinh\sqrt{R-inPr}}\right\} \\ \left.+4\pi\sum_{k=1}^{\infty}k\left\{\frac{s_2 e^{s_2\tau}}{(s_2+\alpha)(s_2^2+n^2)} - \frac{s_1\,e^{s_1\tau}}{Pr(s_1+\alpha)(s_1^2+n^2)}\right\}\sin k\pi\eta\right] \qquad \text{for } Pr \neq 1 \\ \\ \frac{\sinh\sqrt{a}(1-\eta)}{\sinh\sqrt{a}} + 2\pi\sum_{k=1}^{\infty}\frac{k\,e^{s_2\tau}}{s_2}\,\sin k\pi\eta \\ +\frac{Gr}{2(R-a)}\left[e^{in\tau}\left\{\frac{\sinh\sqrt{a+in}(1-\eta)}{\sinh\sqrt{a+in}} - \frac{\sinh\sqrt{R+in}(1-\eta)}{\sinh\sqrt{R+in}}\right\}\right. \\ +e^{-in\tau}\left\{\frac{\sinh\sqrt{a-in}(1-\eta)}{\sinh\sqrt{a-in}} - \frac{\sinh\sqrt{R-in}(1-\eta)}{\sinh\sqrt{R-in}}\right\} \\ \left.+4\pi\sum_{k=1}^{\infty}\left\{\frac{s_2\,e^{s_2\tau}}{(s_2^2+n^2)} - \frac{s_3\,e^{s_3\tau}}{(s_3^2+n^2)}\right\}k\sin k\pi\eta\right] \qquad \text{for } Pr = 1, \end{cases} \tag{7.30}$$

where

$$s_1 = -\frac{1}{Pr}(R+k^2\pi^2),\;\; s_2 = -\left[\frac{M^2(1+im)}{1+m^2} + k^2\pi^2\right],\;\; s_3 = -(R+k^2\pi^2) \text{ and } \alpha = \frac{R-a}{Pr-1} \tag{7.31}$$

(ii) When the wall at $\eta = 0$ started acceleratedly:

In this case $f(\tau) = \tau$, i.e. $f(s) = \frac{1}{s^2}$. Then the inverse Laplace transforms of equations (7.27) and (7.28) give the solution for the temperature distribution and the velocity field as

$$\theta(\eta,\tau) = \begin{cases} \frac{1}{2}\left[e^{in\tau}\frac{\sinh\sqrt{R+inPr}(1-\eta)}{\sinh\sqrt{R+inPr}} + e^{-in\tau}\frac{\sinh\sqrt{R-in\,Pr}(1-\eta)}{\sinh\sqrt{R-in\,Pr}}\right] \\ +\frac{2\pi}{Pr}\sum_{k=1}^{\infty}\frac{k\,s_1 e^{s_1\tau}}{s_1^2+n^2}\,\sin k\pi\eta \qquad \text{for } Pr \neq 1 \\ \\ \frac{1}{2}\left[e^{in\tau}\frac{\sinh\sqrt{R+inPr}(1-\eta)}{\sinh\sqrt{R+inPr}} + e^{-in\tau}\frac{\sinh\sqrt{R-in\,Pr}(1-\eta)}{\sinh\sqrt{R-in\,Pr}}\right] \\ +2\pi\sum_{k=1}^{\infty}\frac{k\,s_3 e^{s_3\tau}}{s_3^2+n^2}\,\sin k\pi\eta \qquad \text{for } Pr = 1, \end{cases} \tag{7.32}$$

$$
F(\eta,\tau) = \begin{cases}
\frac{\tau\sinh\sqrt{a}(1-\eta)}{\sinh\sqrt{a}} + 2\pi\sum_{k=1}^{\infty}\frac{k\,e^{s_2\tau}}{s_2^2}\sin k\pi\eta \\
+\frac{1}{2\sqrt{a}\sinh^2\sqrt{a}}\left[(1-\eta)\sinh\sqrt{a}\cosh\sqrt{a}(1-\eta)\right. \\
\left.-\cosh\sqrt{a}\sinh\sqrt{a}(1-\eta)\right] \\
+\frac{Gr}{2(Pr-1)}\left[\frac{e^{in\tau}}{(\alpha+in)}\left\{\frac{\sinh\sqrt{a+in}(1-\eta)}{\sinh\sqrt{a+in}}-\frac{\sinh\sqrt{R+inPr}(1-\eta)}{\sinh\sqrt{R+inPr}}\right\}\right. \\
+\frac{e^{-in\tau}}{(\alpha-in)}\left\{\frac{\sinh\sqrt{a-in}(1-\eta)}{\sinh\sqrt{a-in}}-\frac{\sinh\sqrt{R-inPr}(1-\eta)}{\sinh\sqrt{R-inPr}}\right\} \\
\left.+4\pi\sum_{k=1}^{\infty}k\left\{\frac{s_2e^{s_2\tau}}{(s_2+\alpha)(s_2^2+n^2)}-\frac{s_1e^{s_1\tau}}{Pr(s_1+\alpha)(s_1^2+n^2)}\right\}\sin k\pi\eta\right] & \text{for } Pr\neq 1 \\
 & \\
\frac{\tau\sinh\sqrt{a}(1-\eta)}{\sinh\sqrt{a}} + 2\pi\sum_{k=1}^{\infty}\frac{k\,e^{s_2\tau}}{s_2^2}\sin k\pi\eta \\
+\frac{1}{2\sqrt{a}\sinh^2\sqrt{a}}\left[(1-\eta)\sinh\sqrt{a}\cosh\sqrt{a}(1-\eta)\right. \\
\left.-\cosh\sqrt{a}\sinh\sqrt{a}(1-\eta)\right] \\
+\frac{Gr}{2(R-a)}\left[e^{in\tau}\left\{\frac{\sinh\sqrt{a+in}(1-\eta)}{\sinh\sqrt{a+in}}-\frac{\sinh\sqrt{R+in}(1-\eta)}{\sinh\sqrt{R+in}}\right\}\right. \\
+e^{-in\tau}\left\{\frac{\sinh\sqrt{(a-in)}(1-\eta)}{\sinh\sqrt{a-in}}-\frac{\sinh\sqrt{R-in}(1-\eta)}{\sinh\sqrt{R-in}}\right\} \\
\left.+4\pi\sum_{k=1}^{\infty}\left\{\frac{s_2e^{s_2\tau}}{s_2^2+n^2}-\frac{s_3e^{s_3\tau}}{s_3^2+n^2}\right\}k\sin k\pi\eta\right] & \text{for } Pr=1,
\end{cases} \tag{7.33}
$$

where s_1, s_2, s_3, α and a are given by equations (7.31) and (7.25) respectively.

7.3 Results and discussion

In order to get a physical insight into the problem, a representative set of numerical results are discuss graphically, to illustrate the influence of physical quantities such as Hall parameter m, radiation parameter R, Prandtl number Pr, frequency parameter n, Grashof number Gr and time τ on velocity, temperature, shear stresses and rate of heat transfer.

7.3.1 Effects of parameters on the velocity profiles

The effects of pertinent parameters on the primary as well as the secondary velocities are presented graphically against η in **Figures 7.2-7.13**. It is seen from **Figures 7.2 and 7.3** that the primary velocity u_1 and the magnitude of the secondary velocity v_1 increase with an increase in Hall parameter m for both the impulsive as well as accelerated motions of one of the channel walls. **Figures 7.4 and 7.5** show that the primary velocity u_1 and the magnitude of the secondary velocity v_1 decrease with an increase in radiation parameter R for both the impulsive and accelerated motions of one of the channel walls. It is illustrated from **Figures 7.6 and 7.7** that the primary velocity u_1 and the magnitude of the secondary velocity v_1 decrease with an increase in Prandtl number Pr for both the impulsive as well as accelerated motions of one of the channel walls. This is due to the fact that the fluids with high Prandtl number have greater viscosity which makes the fluid thick and hence move slowly.

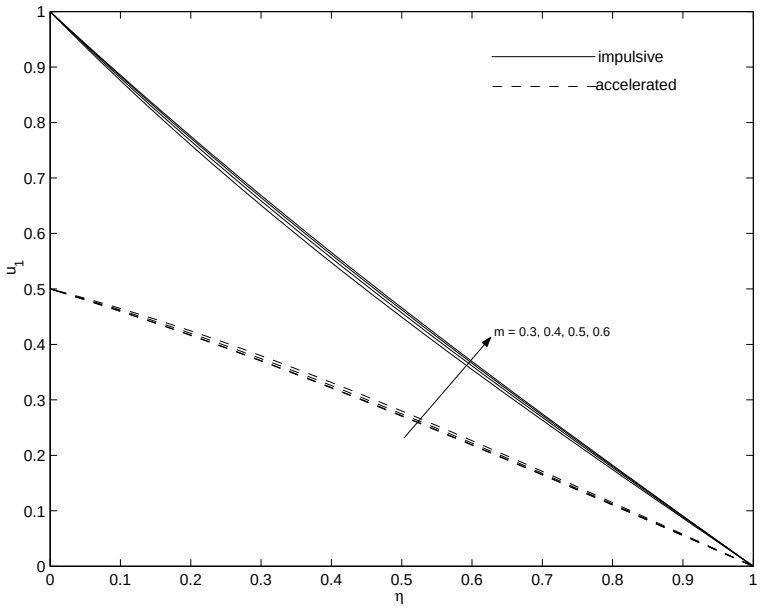

Figure 7.2: Primary velocity u_1 for different m when $R = 2$, $Pr = 0.71$, $n = 2$, $Gr = 5$ and $\tau = 0.5$.

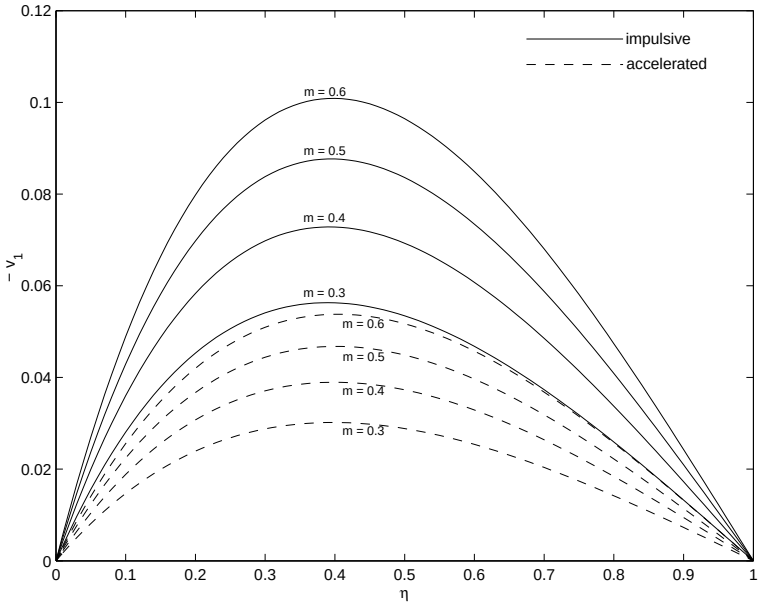

Figure 7.3: Secondary velocity v_1 for different m when $R = 2$, $Pr = 0.71$, $n = 2$, $Gr = 5$ and $\tau = 0.5$.

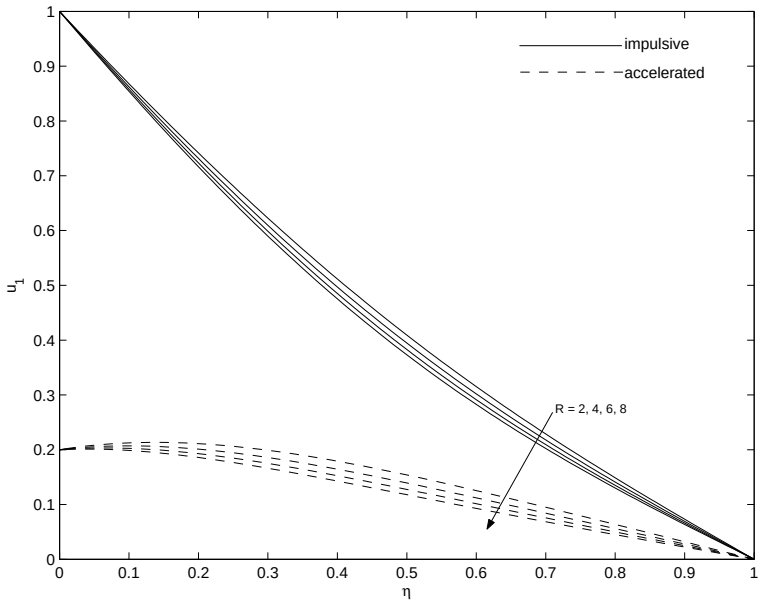

Figure 7.4: Primary velocity u_1 for different R when $m = 0.5$, $Pr = 0.71$, $n = 2$, $Gr = 5$ and $\tau = 0.2$.

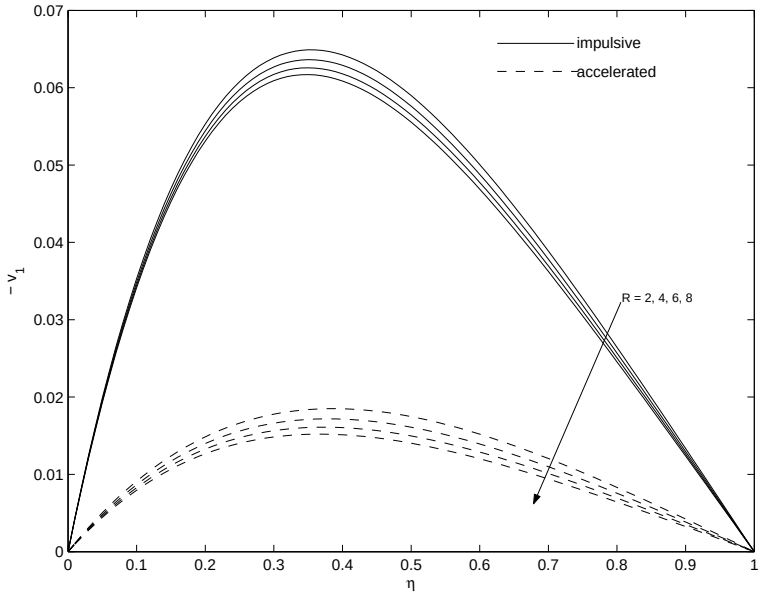

Figure 7.5: Secondary velocity v_1 for different R when $m = 0.5$, $Pr = 0.71$, $n = 2$, $Gr = 5$ and $\tau = 0.2$.

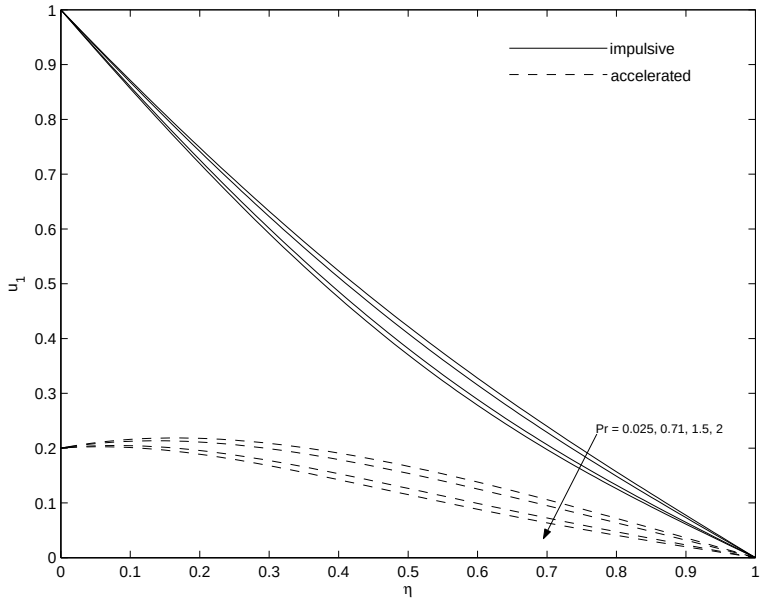

Figure 7.6: Primary velocity u_1 for different Pr when $m = 0.5$, $R = 2$, $n = 2$, $Gr = 5$ and $\tau = 0.2$.

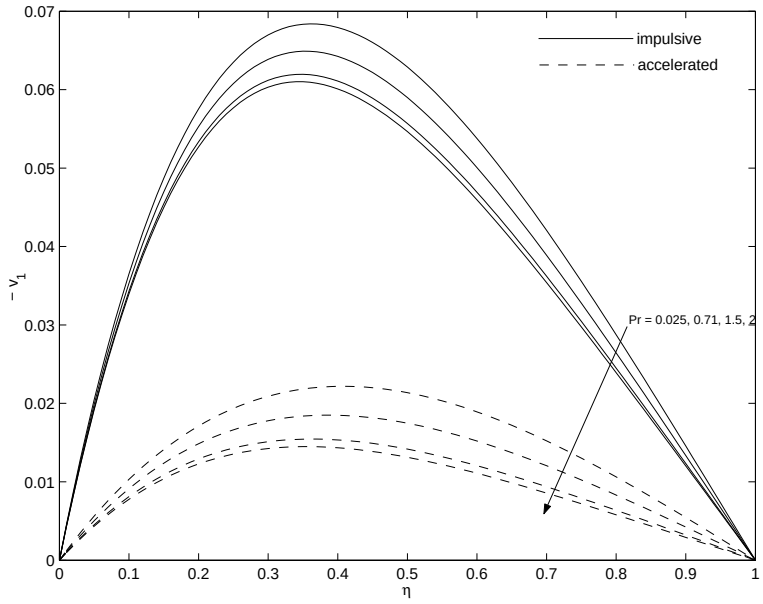

Figure 7.7: Secondary velocity v_1 for different Pr when $m = 0.5$, $R = 2$, $n = 2$, $Gr = 5$ and $\tau = 0.2$.

Figures 7.8 and 7.9 show that both the primary velocity u_1 and the magnitude of the secondary velocity v_1 decrease with an increase in frequency parameter n for both the impulsive and accelerated motions of one of the channel walls.

An increase in Grashof number Gr leads to increase the primary velocity u_1 and the magnitude of the secondary velocity v_1 for both the impulsive and accelerated motions of one of the channel walls shown in **Figures 7.10 and 7.11**.

Physically this is due to fact that as the Grashof number Gr increases, the contribution from the buoyancy force near the plate becomes significant and hence a rise in the velocity near the plate as observed.

It is seen form **Figures 7.12 and 7.13** that the primary velocity u_1 and the magnitude of the secondary velocity v_1 increase with an increase in time τ for both the impulsive and accelerated motions of one of the channel walls. **Figures 7.2-7.13** show that the primary and the secondary velocities is larger in case of the impulsive motion than the accelerated motion.

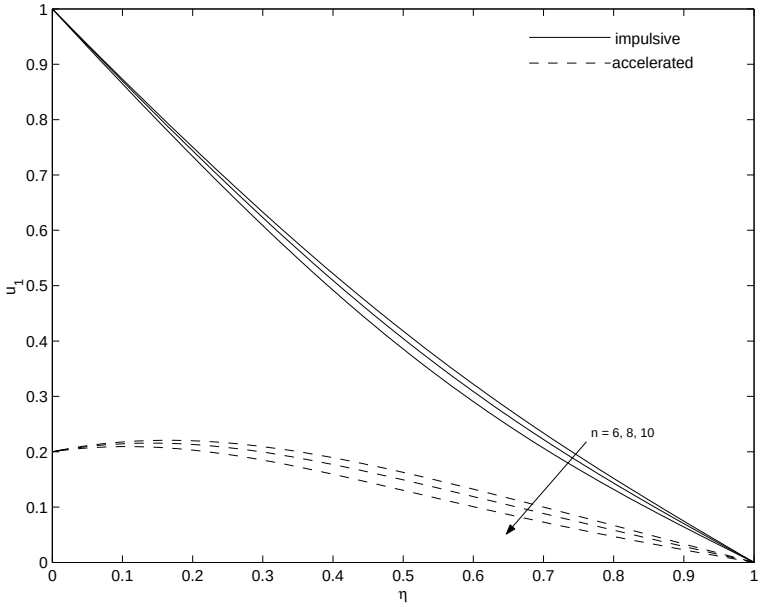

Figure 7.8: Primary velocity u_1 for different n when $m = 0.5$, $R = 2$, $Pr = 0.71$, $Gr = 5$ and $\tau = 0.2$.

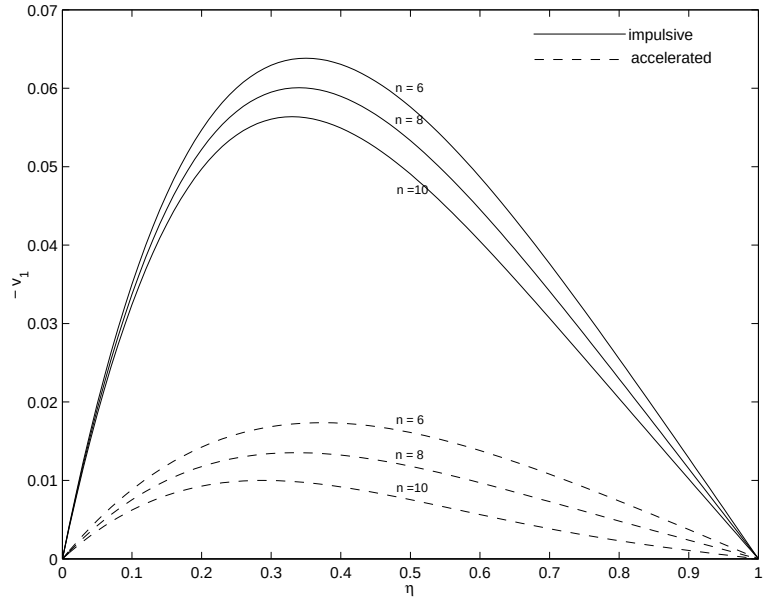

Figure 7.9: Secondary velocity v_1 for different n when $m = 0.5$, $R = 2$, $Pr = 0.71$, $Gr = 5$ and $\tau = 0.2$.

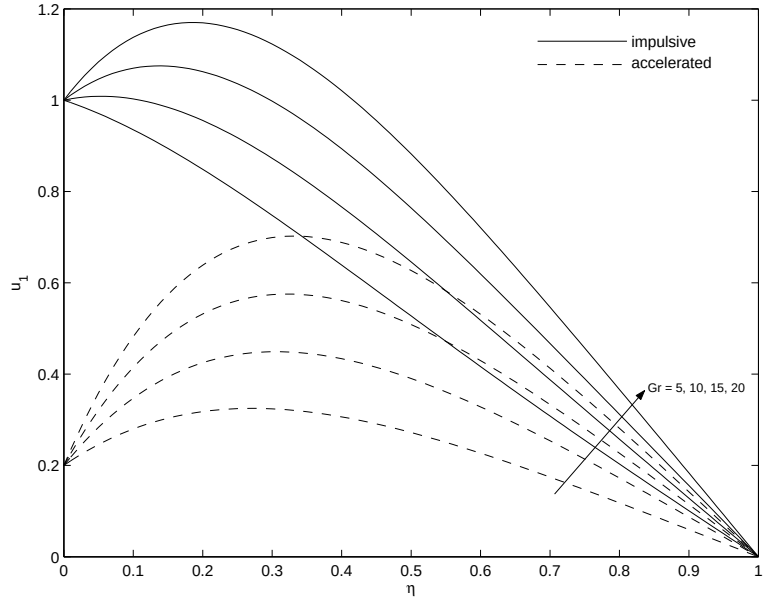

Figure 7.10: Primary velocity u_1 for different Gr when $m = 0.5$, $R = 2$, $Pr = 0.71$, $n = 2$ and $\tau = 0.2$.

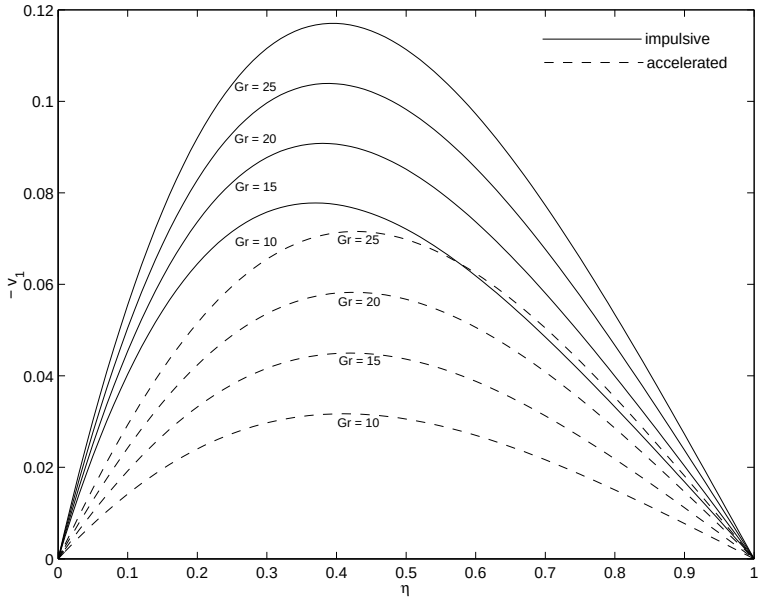

Figure 7.11: Secondary velocity v_1 for different Gr when $m = 0.5$, $R = 2$, $Pr = 0.71$, $n = 2$ and $\tau = 0.2$.

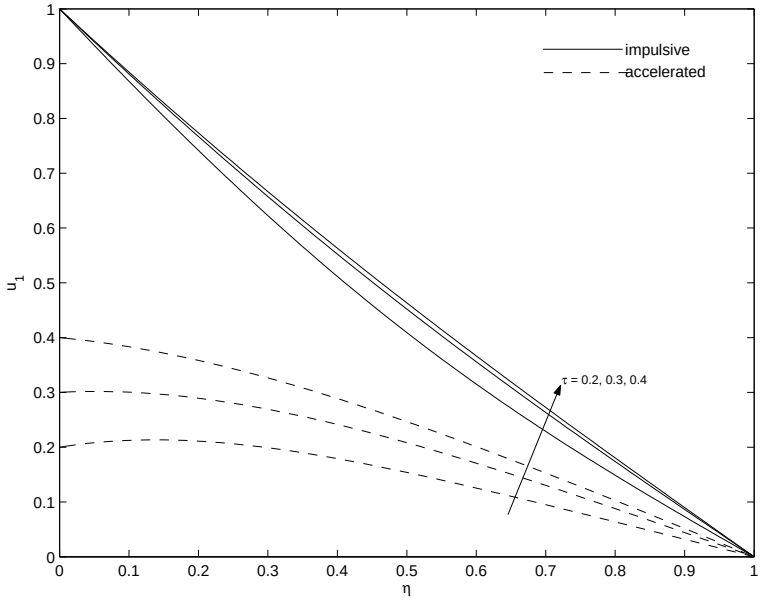

Figure 7.12: Primary velocity u_1 for different τ when $m = 0.5$, $R = 2$, $Pr = 0.71$, $n = 2$ and $M^2 = 5$.

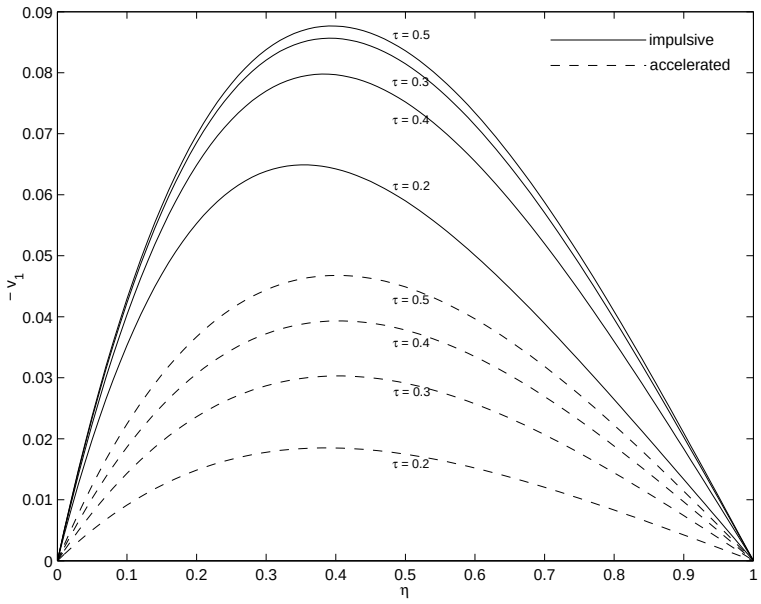

Figure 7.13: Secondary velocity v_1 for different τ when $m = 0.5$, $R = 2$, $Pr = 0.71$, $n = 2$ and $M^2 = 5$.

7.3.2 Effects of parameters on temperature profiles

The effects of pertinent parameters such as frequency parameter n, radiation parameter R, prandtl number Pr and time τ on the temperature distribution are presented graphically against η in **Figures 7.14-7.17**.

The influence of the thermal radiation on the fluid temperature is depicted in **Figure 7.14**. It is seen from **Figure 7.14** that the fluid temperature θ decreases with an increase in radiation parameter R. Therefore, an increase in the value of radiation parameter R lead to decrease in the thermal boundary layer thickness. In the presence of radiation in the fluid, the thermal boundary layer is always found to thicken. The reason for this is that radiation provides an additional means to diffuse energy. It is observed from **Figure 7.15** that the fluid temperature θ increases with an increase in Prandtl number Pr. This is in agreement with the physical fact that the thermal boundary layer thickness decreases with increasing Pr.

Figure 7.16 shows that the fluid temperature θ decreases with an increase of frequency parameter n. **Figure 7.17** shows that the fluid temperature θ increases when time τ progresses.

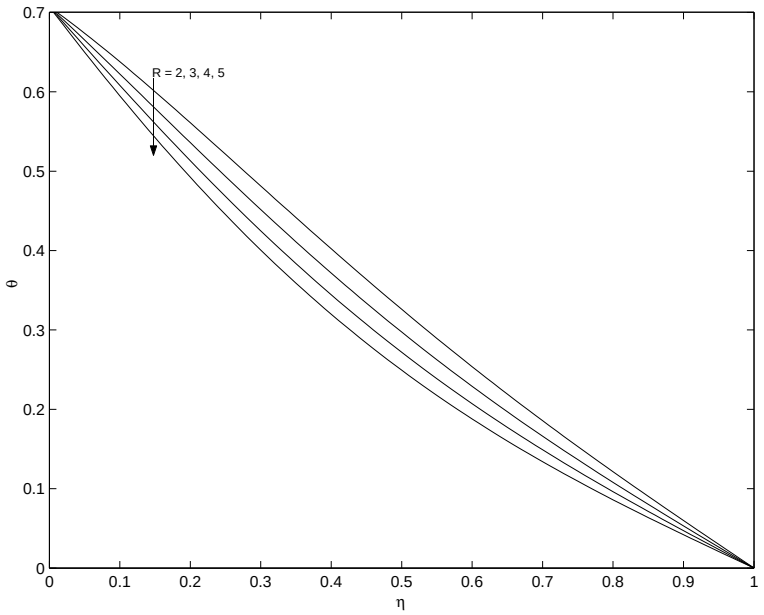

Figure 7.14: Temperature θ for different R when $Pr = 0.71$, $n = 2$ and $\tau = 0.2$.

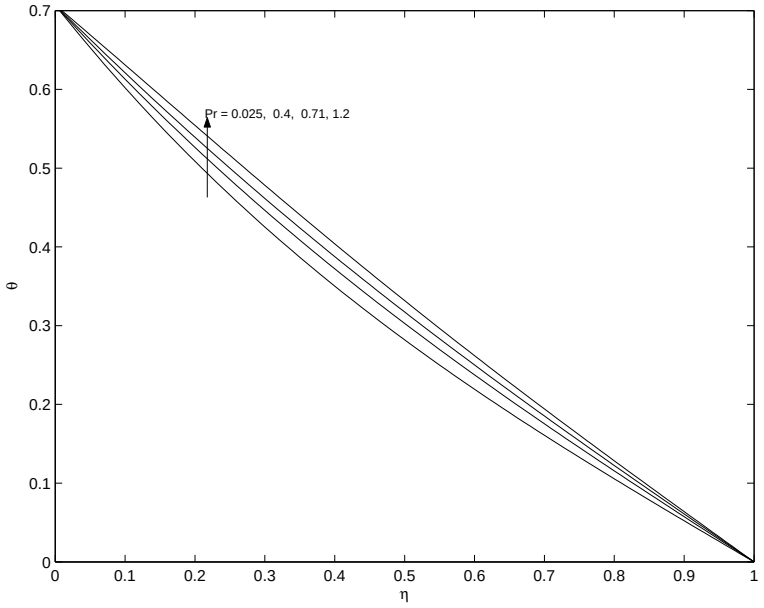

Figure 7.15: Temperature θ for different Pr when $R = 2$, $n = 2$ and $\tau = 0.2$.

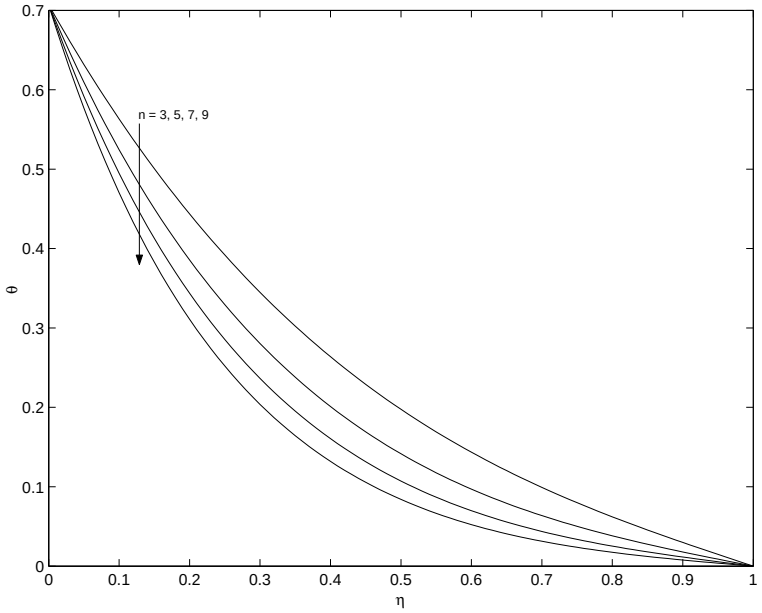

Figure 7.16: Temperature θ for different n for $Pr = 0.71$, $R = 2$ and $\tau = 0.2$.

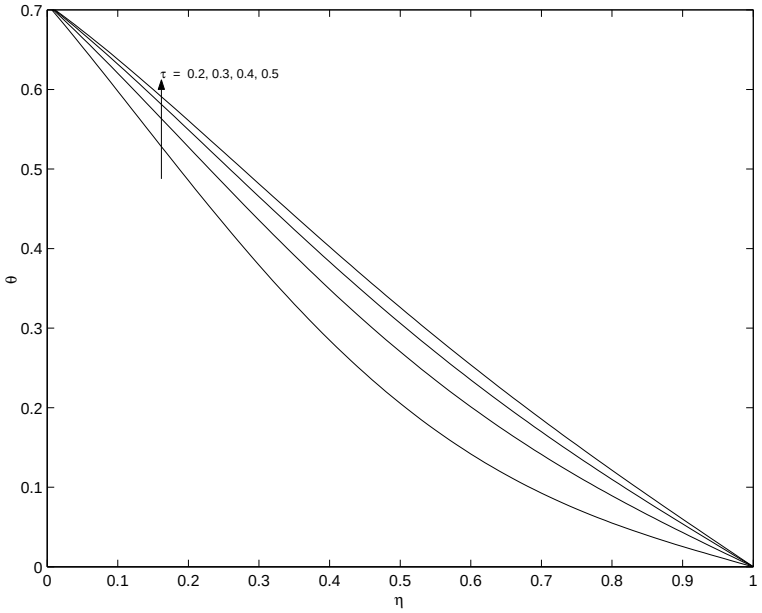

Figure 7.17: Temperature θ for different τ for $Pr = 0.71$, $n = 2$ and $R = 2$.

7.3.3 Effects of parameters on the shear stresses at the channel wall

In this chapter, we obtained the shear stresses at the wall $\eta = 0$ for the impulsive as well as accelerated motion. For the impulsive motion, the non-dimensional shear stresses at the wall $\eta = 0$ is denoted by

$$\tau_x + i\tau_y = \left(\frac{\partial F}{\partial \eta}\right)_{\eta=0}$$

and defined as

$$\tau_x + i\tau_y = \begin{cases} -\sqrt{a}\,\coth\sqrt{a} + 2\pi^2 \sum\limits_{k=1}^{\infty} \frac{k^2 e^{s_2\tau}}{s_2} \\ -\frac{Gr}{2(Pr-1)}\left[\frac{e^{in\tau}}{(\alpha+in)}\left\{\sqrt{a+in}\,\coth\sqrt{a+in}\right.\right. \\ \left. -\sqrt{R+inPr}\,\coth\sqrt{R+inPr}\right\} \\ -\frac{e^{-in\tau}}{(\alpha-in)}\left\{\sqrt{a-in}\,\coth\sqrt{a-in}\right. \\ \left. -\sqrt{R-inPr}\,\coth\sqrt{R-inPr}\right\} \\ \left. +\sum\limits_{k=1}^{\infty} 4k^2\pi^2\left\{\frac{s_2 e^{s_2\tau}}{(s_2+\alpha)(s_2^2+n^2)} - \frac{s_1 e^{s_1\tau}}{Pr(s_1+\alpha)(s_1^2+n^2)}\right\}\right] \quad \text{for } Pr \neq 1 \\ -\sqrt{a}\,\coth\sqrt{a} + 2\pi^2 \sum\limits_{k=1}^{\infty} \frac{k^2 e^{s_2\tau}}{s_2} \\ -\frac{Gr}{2(R-a)}\left[e^{in\tau}\left\{\sqrt{a+in}\,\coth\sqrt{a+in}\right.\right. \\ \left. -\sqrt{R+in}\,\coth\sqrt{R+in}\right\} \\ -e^{-in\tau}\left\{\sqrt{a-in}\,\coth\sqrt{a-in}\right. \\ \left. -\sqrt{R-in}\,\coth\sqrt{R-in}\right\} \\ \left. +\sum\limits_{k=1}^{\infty} 4k^2\pi^2\left\{\frac{s_2 e^{s_2\tau}}{(s_2^2+n^2)} - \frac{s_3 e^{s_3\tau}}{(s_3^2+n^2)}\right\}\right] \quad \text{for } Pr = 1, \end{cases} \tag{7.34}$$

For the accelerated motion, the non-dimensional shear stresses at the wall $\eta = 0$ is also denoted by $\tau_x + i\tau_y = \left(\frac{\partial F}{\partial \eta}\right)_{\eta=0}$ and defined as

$$\tau_x + i\tau_y = \begin{cases} -\tau\sqrt{a}\,\coth\sqrt{a} \\ +2\pi^2 \sum\limits_{k=1}^{\infty} \frac{k^2 e^{s_2\tau}}{s_2^2} - \frac{\sinh\sqrt{a}\cosh\sqrt{a}-\sqrt{a}}{2\sqrt{a}\sinh^2\sqrt{a}} \\ -\frac{Gr}{2(Pr-1)}\left[\frac{e^{in\tau}}{(\alpha+in)}\left\{\sqrt{a+in}\,\coth\sqrt{a+in}\right.\right. \\ \left. -\sqrt{R+inPr}\,\coth\sqrt{R+inPr}\right\} \\ -\frac{e^{-in\tau}}{(\alpha-in)}\left\{\sqrt{a-in}\,\coth\sqrt{a-in}\right. \\ \left.\left. -\sqrt{R-inPr}\,\coth\sqrt{R-inPr}\right\}\right. \\ \left. +\sum\limits_{k=1}^{\infty} 4k^2\pi^2\left\{\frac{s_2 e^{s_2\tau}}{(s_2+\alpha)(s_2^2+n^2)} - \frac{s_1 e^{s_1\tau}}{Pr(s_1+\alpha)(s_1^2+n^2)}\right\}\right] \quad \text{for } Pr \neq 1 \\ -\tau\sqrt{a}\,\coth\sqrt{a} \\ +2\pi^2 \sum\limits_{k=1}^{\infty} \frac{k^2 e^{s_2\tau}}{s_2^2} - \frac{\sinh\sqrt{a}\cosh\sqrt{a}-\sqrt{a}}{2\sqrt{a}\sinh^2\sqrt{a}} \\ -\frac{Gr}{2(R-a)}\left[e^{in\tau}\left\{\sqrt{a+in}\,\coth\sqrt{a+in}\right.\right. \\ \left. -\sqrt{R+in}\,\coth\sqrt{R+in}\right\} \\ -e^{-in\tau}\left\{\sqrt{a-in}\,\coth\sqrt{a-in}\right. \\ \left.\left. -\sqrt{R-in}\,\coth\sqrt{R-in}\right\}\right. \\ \left. +\sum\limits_{k=1}^{\infty} 4k^2\pi^2\left\{\frac{s_2 e^{s_2\tau}}{(s_2^2+n^2)} - \frac{s_3 e^{s_3\tau}}{(s_3^2+n^2)}\right\}\right] \quad \text{for } Pr = 1, \end{cases} \tag{7.35}$$

where s_1, s_2, s_3, α and a are given by equations (7.31) and (7.25) respectively.

Numerical results of the non-dimensional shear stresses τ_x and τ_y at the wall ($\eta = 0$) due to the primary and the secondary flows are presented in **Figures 7.18-7.27** against Hall parameter m for several values of radiation parameter R, Prandtl number Pr, frequency parameter n, Grashof number Gr and time τ when $M^2 = 5$ and $n\tau = \frac{\pi}{4}$.

Figures 7.18 and 7.19 shows that the shear stress τ_x due to primary flow and the magnitude of the shear stress τ_y due to secondary flow decrease for both the impulsive as well as accelerated motions of one of the channel walls with an increase in radiation parameter R. It is seen from **Figures 7.20 and 7.21** that for the impulsive and accelerated motions of one of the channel walls the shear stress τ_x and the magnitude of the shear stress τ_y increase with an increase of Prandtl number Pr. **Figures 7.22 and 7.23** show that the shear stress τ_x and the magnitude of the shear stress τ_y decrease with an increase in frequency parameter n for the impulsive as well as accelerated motions of one of the channel walls. An increase of Grashof number Gr leads to increase in the shear stress τ_x while the magnitude of the shear stress τ_y decreases for $m \leq 0.3$ and increases for $m > 0.3$ for both the impulsive and accelerated motions of one of the channel walls show in **Figures 7.24 and 7.25**. **Figures 7.26 and 7.27** show that for both the impulsive and accelerated motions of one of the channel walls, the magnitude of the share stress τ_x decreases whereas the magnitude of the share stress τ_y increases with an increase in time τ.

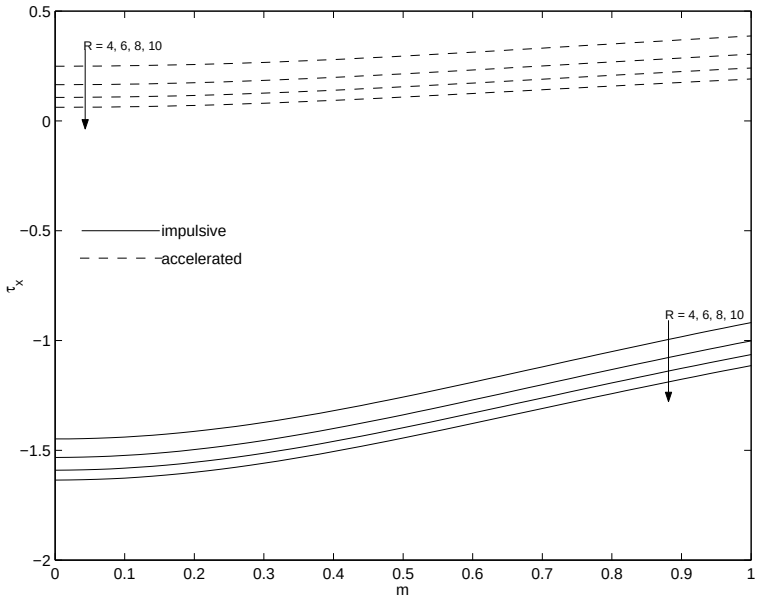

Figure 7.18: Shear stress τ_x for different R when $Gr = 5$, $Pr = 0.71$, $n = 2$ and $\tau = 0.2$.

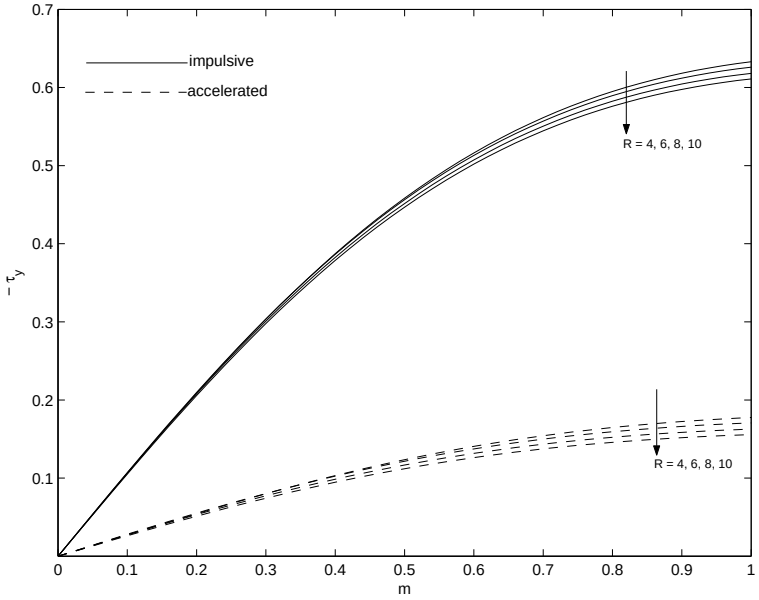

Figure 7.19: Shear stress τ_y for different R when $Pr = 0.71$, $n = 2$, $Gr = 5$ and $\tau = 0.2$.

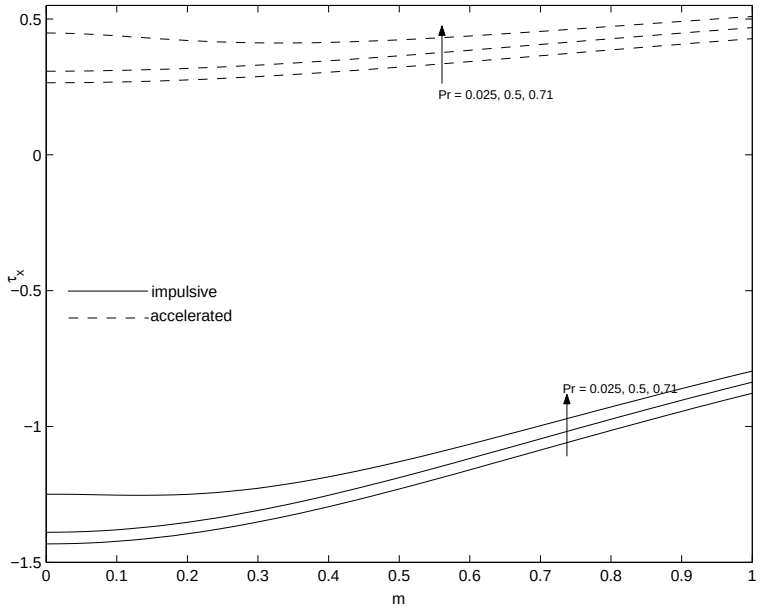

Figure 7.20: Shear stress τ_x for different Pr when $R = 2$, $n = 2$, $Gr = 5$ and $\tau = 0.2$.

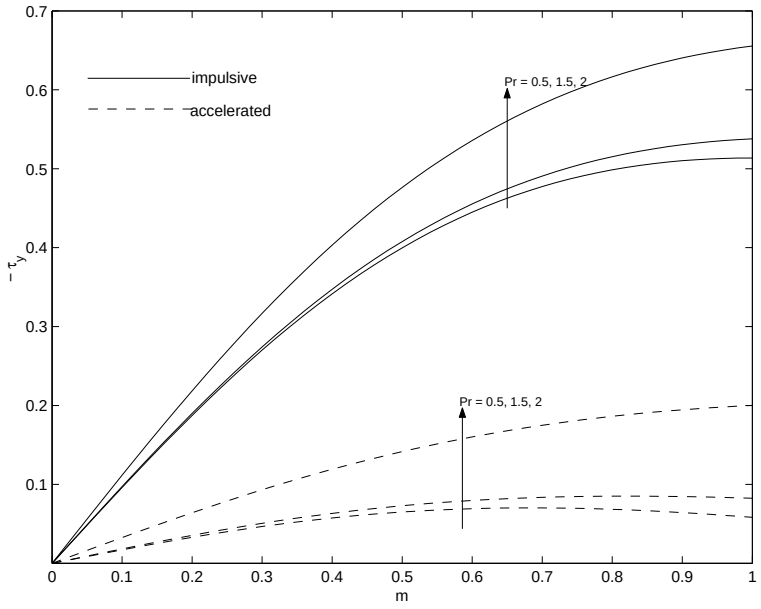

Figure 7.21: Shear stress τ_y for different Pr when $R = 2$, $n = 2$, $\tau = 0.2$ and $Gr = 5$.

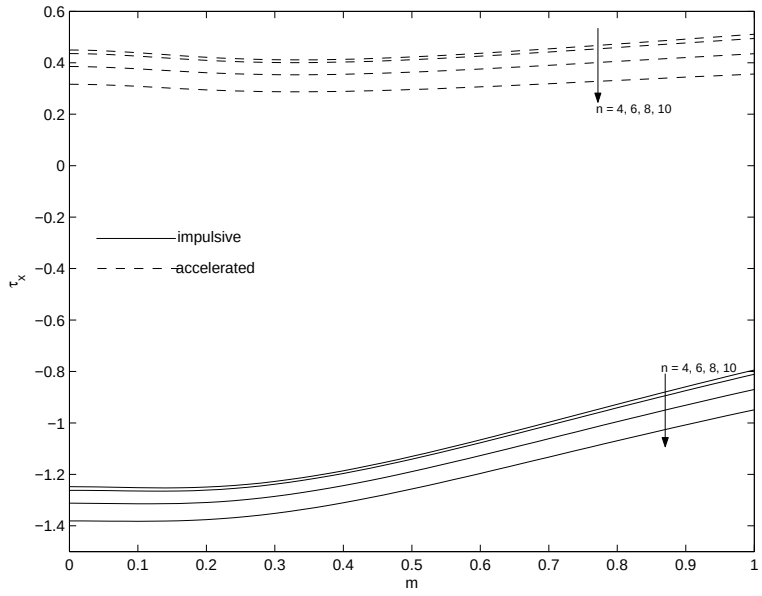

Figure 7.22: Shear stress τ_x for different n when $R = 2$, $Pr = 0.71$, $Gr = 5$ and $\tau = 0.2$.

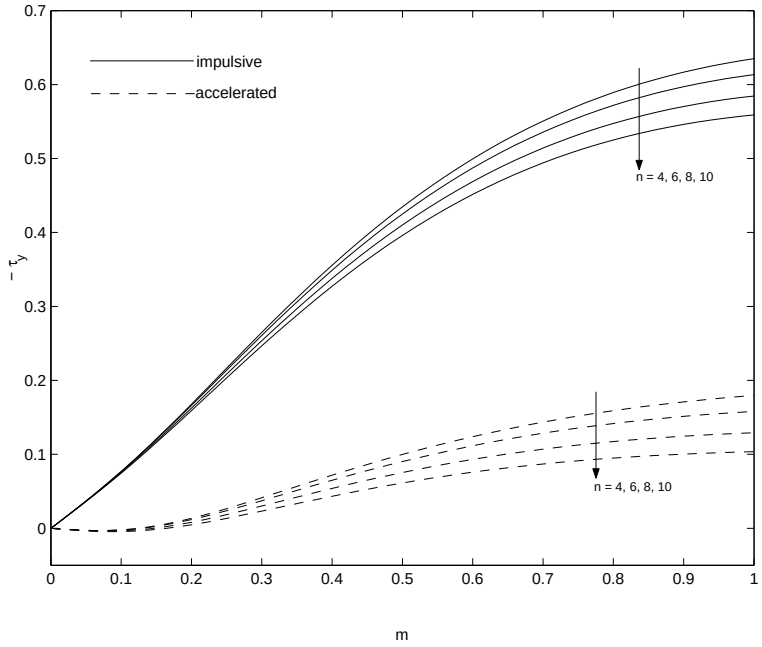

Figure 7.23: Shear stress τ_y for different n when $R = 2$, $\tau = 0.2$, $Pr = 0.71$ and $Gr = 5$.

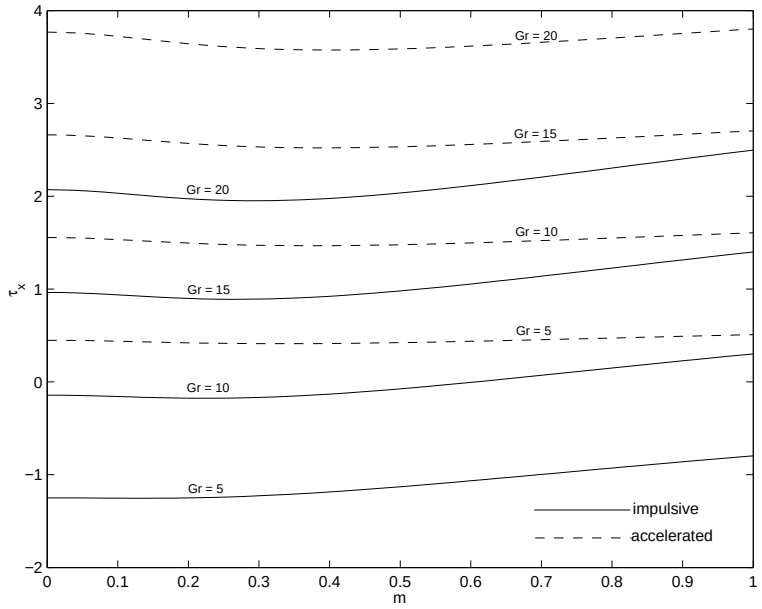

Figure 7.24: Shear stress τ_x for different Gr when $R = 2$, $Pr = 0.71$, $n = 2$ and $\tau = 0.2$.

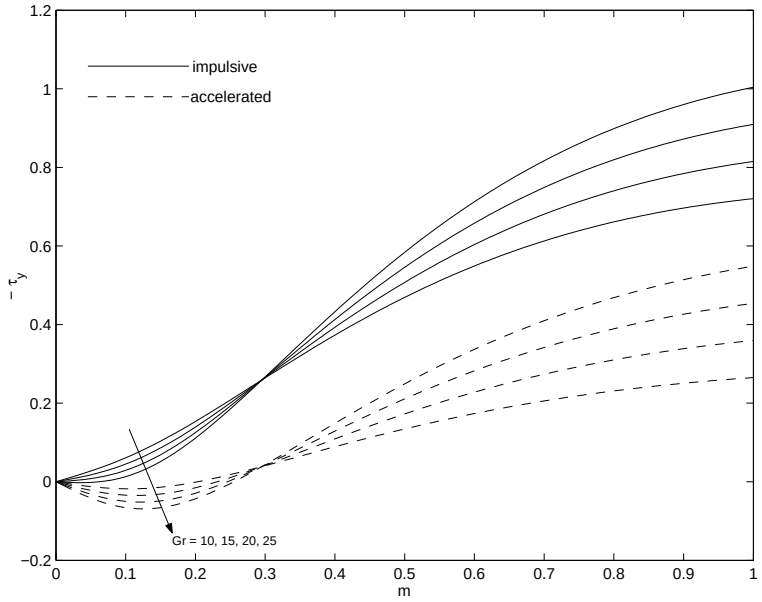

Figure 7.25: Shear stress τ_y for different Gr when $\tau = 0.2$, $Pr = 0.71$, $n = 2$ and $R = 2$.

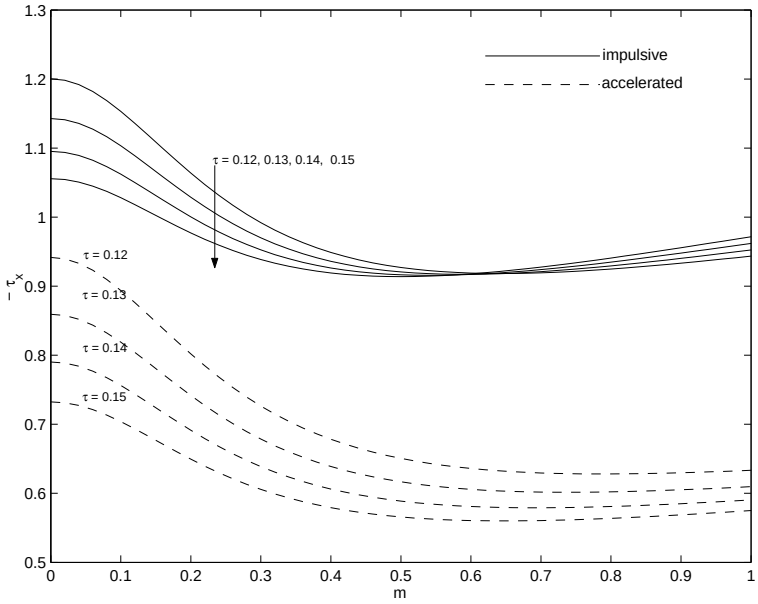

Figure 7.26: Shear stress τ_x for different τ when $R = 2$, $Pr = 0.71$, $n = 2$ and $Gr = 5$

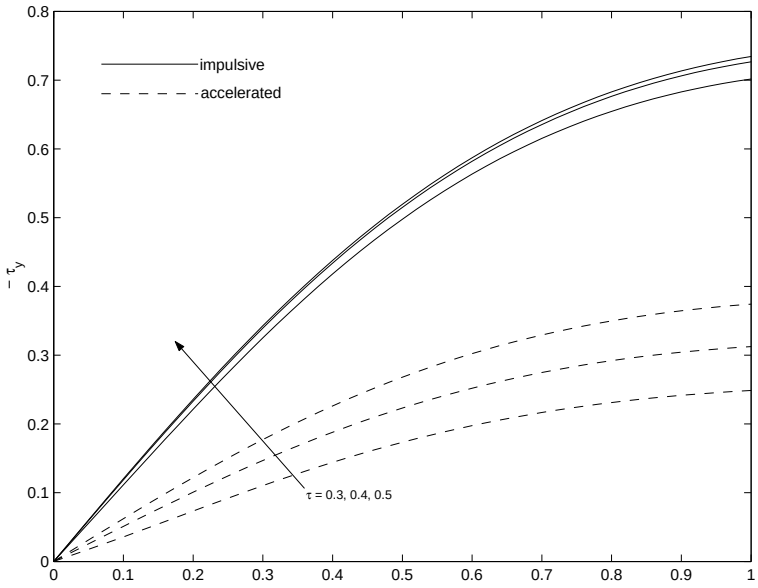

Figure 7.27: Shear stress τ_y for different τ when $R = 2$, $Pr = 0.71$, $n = 2$ and $Gr = 5$.

7.3.4 Effects of parameters on the rate of heat transfer at the channel walls

The rate of heat transfer at the channel walls $\eta = 0$ and $\eta = 1$ are respectively $\theta'(0,\tau)\left[=\left(\frac{\partial\theta}{\partial\eta}\right)_{\eta=0}\right]$ and $\theta'(1,\tau)\left[=\left(\frac{\partial\theta}{\partial\eta}\right)_{\eta=1}\right]$ and are given by

$$-\theta'(0,\tau) = \begin{cases} \frac{1}{2}\left[e^{in\tau}\sqrt{R+inPr}\,\coth\sqrt{R+inPr}\right. \\ \left.+\,e^{-in\tau}\sqrt{R-inPr}\,\coth\sqrt{R-inPr}\right] \\ -\frac{2\pi^2}{Pr}\sum\limits_{k=1}^{\infty}\frac{k^2 s_1\, e^{s_1\tau}}{s_1^2+n^2} & \text{for } Pr \neq 1 \\ \\ \frac{1}{2}\left[e^{in\tau}\sqrt{R+inPr}\,\coth\sqrt{R+in}\right. \\ \left.+\,e^{-in\tau}\sqrt{R-in}\,\coth\sqrt{R-in}\right] \\ -2\pi^2\sum\limits_{k=1}^{\infty}\frac{k^2 s_3\, e^{s_3\tau}}{s_3^2+n^2} & \text{for } Pr = 1, \end{cases} \tag{7.36}$$

$$-\theta'(1,\tau) = \begin{cases} \frac{1}{2}\left[e^{in\tau}\sqrt{R+inPr}\,\mathrm{cosech}\sqrt{R+inPr}\right. \\ \left.+\,e^{-in\tau}\sqrt{R-inPr}\,\mathrm{cosech}\sqrt{R-inPr}\right] \\ -\frac{2\pi^2}{Pr}\sum\limits_{k=1}^{\infty}(-1)^k\,\frac{k^2 s_1\, e^{s_1\tau}}{s_1^2+n^2} & \text{for } Pr \neq 1 \\ \\ \frac{1}{2}\left[e^{in\tau}\sqrt{R+in}\,\mathrm{cosech}\sqrt{R+in}\right. \\ \left.+\,e^{-in\tau}\sqrt{R-in}\,\mathrm{cosech}\sqrt{R-in}\right] \\ -2\pi^2\sum\limits_{k=1}^{\infty}(-1)^k\,\frac{k^2 s_3\, e^{s_3\tau}}{s_3^2+n^2} & \text{for } Pr = 1, \end{cases} \tag{7.37}$$

where s_1, s_2 and s_3 are given by equation (7.31).

Numerical results of the rate of heat transfer at the channel walls $\eta = 0$ and $\eta = 1$ are respectively $-\theta'(0,\tau)$ and $-\theta'(1,\tau)$ which are presented in the **Tables-I through -III** for several values of Prandtl number Pr, time τ, frequency parameter n when $n\tau = \frac{\pi}{4}$.

Table-I shows that the rate of heat transfer $-\theta'(0,\tau)$ decreases while the rate of heat transfer $-\theta'(1,\tau)$ increases with an increase in Prandtl number Pr.

Table-II shows that the rate of heat transfer $-\theta'(0,\tau)$ at the wall $\eta = 0$ decreases whereas the rate of heat transfer $-\theta'(1,\tau)$ at the wall $\eta = 1$ increases when time τ progresses.

It is seen from **Table-III** that the rate of heat transfers $-\theta'(0,\tau)$ and $-\theta'(1,\tau)$ decrease with an increase in frequency parameter n.

Table-I

Rate of heat transfer $-\theta'(0,\tau)$ and $-\theta'(1,\tau)$ when $n = 2$ and $\tau = 0.5$.

	$-\theta'(0,\tau)$				$-\theta'(1,\tau)$			
$R\backslash Pr$	*0.025*	*0.50*	*0.71*	*1.5*	*0.025*	*0.50*	*0.71*	*1.5*
0.5	*0.81019*	*0.61501*	*0.53916*	*0.35855*	*0.65667*	*0.74367*	*0.77283*	*0.78451*
1.0	*0.91808*	*0.73317*	*0.66030*	*0.47547*	*0.60637*	*0.68479*	*0.71169*	*0.73004*
1.5	*1.01988*	*0.84411*	*0.77404*	*0.58682*	*0.56124*	*0.63216*	*0.65695*	*0.68005*
2.0	*1.11631*	*0.94872*	*0.88126*	*0.69306*	*0.52058*	*0.58492*	*0.60777*	*0.63414*

Table-II

Rate of heat transfer $-\theta'(0,\tau)$ and $-\theta'(1,\tau)$ when $n = 2$ and $Pr = 2$.

	$-\theta'(0,\tau)$				$-\theta'(1,\tau)$			
$R\backslash\tau$	*0.1*	*0.2*	*0.3*	*0.4*	*0.1*	*0.2*	*0.3*	*0.4*
0.5	*1.47365*	*0.82218*	*0.55322*	*0.40750*	*0.09949*	*0.29145*	*0.49835*	*0.63567*
1.0	*1.53123*	*0.89769*	*0.64202*	*0.50682*	*0.08631*	*0.27539*	*0.47252*	*0.59998*
1.5	*1.58644*	*0.97084*	*0.72809*	*0.60282*	*0.07517*	*0.26086*	*0.44838*	*0.56653*
2.0	*1.63963*	*1.04186*	*0.81162*	*0.69566*	*0.06571*	*0.24763*	*0.42577*	*0.53517*

Table-III

Rate of heat transfer $-\theta'(0,\tau)$ and $-\theta'(1,\tau)$ when $\tau = 0.5$ and $Pr = 2$.

	$-\theta'(0,\tau)$				$-\theta'(1,\tau)$			
$R\backslash n$	*2*	*3*	*4*	*5*	*2*	*3*	*4*	*5*
0.5	*0.32266*	*0.18085*	*0.11582*	*0.09219*	*0.71936*	*0.67272*	*0.56856*	*0.44258*
1.0	*0.43004*	*0.28113*	*0.20490*	*0.17048*	*0.67574*	*0.63838*	*0.54692*	*0.43254*
1.5	*0.53342*	*0.37888*	*0.29290*	*0.24863*	*0.63501*	*0.60540*	*0.52516*	*0.42146*
2.0	*0.63301*	*0.47408*	*0.37966*	*0.32643*	*0.59701*	*0.57386*	*0.50352*	*0.40961*

7.4 Conclusion

The combined effects of Hall current and radiation on the unsteady MHD free convective flow in a vertical channel with an oscillatory wall temperature have been investigated. The dimensionless governing partial differential equations are solved by the usual Laplace transformation technique. The effects of pertinent parameters such as Hall parameter, radiation parameter, frequency parameter, Prandtl parameter, Grashof number and time are studied. It is observed that the primary velocity u_1 and the magnitude of the secondary velocity v_1 decrease with an increase in either radiation parameter R or frequency parameter n or Prandtl number Pr for both the impulsive as well as accelerated motions of one of the channel walls. The primary velocity u_1 and the magnitude of the secondary velocity v_1 increase with an increase in either Hall parameter m or Grashof number Gr or time τ for both the impulsive as well as accelerated motions of one of the channel walls. The fluid temperature θ increases with an increase in Prandtl number Pr whereas it decreases with an increase in either radiation parameter R or frequency parameter n. Further, the shear stress τ_x due to the primary flow and the absolute value of the shear stress τ_y due to the secondary flow at the wall $\eta = 0$ decrease with an increase in either radiation parameter R or frequency parameter n or Prandtl number Pr for both the impulsive as well as accelerated motions of one of the channel walls. It is also seen that both the rate of heat transfers $-\theta'(0,\tau)$ and $-\theta'(1,\tau)$ increase with an increase in radiation parameter R while they decrease with an increase in either frequency parameter n or time τ.

Bibliography

[1] Sato H, J. Phys. Soc. Jpn.: **16**(1961), pp.14.

[2] Miyatake O and Fujii T, Heat Trans. Jpn. Res.: **1**(1972), pp.30.

[3] Tanaka H, Miyatake O, Fujii T and Fujii M, Heat Trans. Jpn. Res.: **2**(1973), pp.25.

[4] Gupta PS and Gupta AS, Int. J. Heat Mass Trans.: **17**(1974), pp.1437.

[5] Datta N and Jana RN, Int. J. Engg. Sci.: **15**(1977), pp.561.

[6] Bestman AR and Adjepong SN, Space Sci.: **143**(1988), pp.73.

[7] Joshi HM, Int. Comm. Heat and Mass Trans.: **15**(1988), pp.227.

[8] Singh AK, Defense Sci. J.: **38(1)**(1988), pp.35.

[9] Singh AK, Gholami HR and Soundalgekar VM, Heat and Mass Trans.: **31**(1996), pp.329.

[10] Jha BK, Heat and Mass Trans.: **37**(2001), pp.329.

[11] Narahari M, Sreenadh S and Soundalgekar VM, J. Thermophysics and Aeromechanics: **9(2)**(2002), pp.287.

[12] Jha BK, Singh AK and Takhar HS, Int. J. Appl. Mech. Engg.: **8(3)**(2003), pp.497.

[13] Singh AK and Paul T, Int. J. Appl. Mech. Engg.: **11(1)**(2006), pp.143.

[14] Sanyal DC and Adhikari A, Bull. Cal. Math. Soc.: **98(5)**(2006), pp.487.

[15] Mebine P, Global J. Pure and Appl. Math.: **3(2)**(2007), pp.191.

[16] Grosan T and Pop I, Technische Mechanik: **27(1)**(2007), pp.37.

[17] Guria M and Jana RN, Magnetohydrodynamics: **43(3)**(2007), pp.287.

[18] Jha BK and Ajibade AO, Int. J. Energy and Tech.: **2(12)**(2010), pp.1.

[19] Narahari M, WSEAS Transactions on Heat and Mass Trans.: **5(1)**(2010), pp.21.

[20] Rajput US and Sahu PK, Int. J. Math. Analysis: **34(5)**(2011), pp.1665.

[21] Das S, Sarkar BC and Jana RN, Open J. Fluid Dynamics: **2**(2012), pp.14.

[22] Mandal C, Das S and Jana RN, Int. J. Appl. Inf. Systems: **2(2)**(2012), pp.49.

[23] Sarkar BC, Das S and Jana RN, Int. J. Engg. Res. and Appl.: **2(4)**(2012), pp.2346.

[24] Sarkar BC, Das S and Jana RN, Adv. in Appl. Sci. Res.: **3(5)**(2012), pp.3311.

[25] Cogley ACL, Vincentine WC and Gilles SE, Am. Inst. Aeronat. Astronaut., J.: **6**(1968), pp.551.

[26] Cowling TG, Magnetohydrodynamics, New York, Intersscience: (1957)

Chapter 8

Hall effects on hydromagnetic free convection in a heated vertical channel in the presence of inclined magnetic field and thermal radiation*

8.1 Introduction

The hydromagnetic fluid dynamics continues to attract the attention of the applied mathematics and engineering sciences communities owing to considerable practical applications of such flows in plasma aerodynamics see Takenouchi[1]. The MHD energy systems have been developed by Hardianto et al.[2]. The nuclear engineering control has been studied by Narasimhan[3]. Takhar and Ram[4] have analyzed the astrophysical fluid dynamics. The mechanical engineering manufacturing processes have been examined by Ryabinin and Khozhainov[5] and Barmin and Uspenskii[6]. Often such flows may occur from very low Reynolds numbers to high speed supersonic flows and also simultaneously with electro-magneto-fluid dynamic effects (Hall currents, ion-slip, Alfven waves etc.) and thermophysical phenomena which can exert a substantial influence on velocity evolution and in the case of induction problems and magnetic field distributions. Magnetohydrodynamic (MHD) convective flow has many important en-

* *Published in* **Turkish J. of Engg. and Environmental Sci. (TJEES)**, *ISSN: 1300-0160, 38(3)(2014), pp.434-454.*

gineering applications in the design of power generators, heat exchangers, pumps and flow meters, in solving space vehicle propulsion, control and re-entry problems; in designing communications and radar system; in creating novel power generating systems; in developing confinement schemes for controlled fusion and in design of nuclear cooling reactors and MHD accelerators.

The Hall effects are important when the magnetic field is high or when the collision frequency is low (see Sutton and Sherman[7]). Mazumder et al.[8] have examined the Hall effects on combined free and forced convective hydromagnetic flow through a channel. The Hall currents and surface temperature oscillations effects on natural convection magnetohydrodynamic heat-generating flow have been considered by Takhar and Ram[9]. Gourla and Katoch[10] have presented the unsteady free convection MHD flow between heated vertical plates. Borkakati and Chakrabarty[11] have studied the unsteady free convection MHD flow between two heated vertical parallel plates in the presence of magnetic field. Jha[12] has examined the unsteady MHD natural convective Couette flow. Singh and Pathak[13] have analyzed the effects of rotation and Hall current on mixed convection MHD flow through a porous medium filled in a vertical channel in the presence of thermal radiation. Das et al.[14] have investigated the radiation effects on free convective MHD Couette flow started exponentially with variable wall temperature in the presence of heat generation. The effects of radiation on transient natural convection flow between two vertical walls have been discussed by Mandal et al.[15]. Recently, Sarkar et al.[16] have considered the effects of radiation on MHD free convective Couette flow in a rotating system. Seth and Ghosh[17] have presented the unsteady hydromagnetic flow in a rotating channel in the presence of inclined magnetic field. Pop et al.[18] have examined the effects of the Hall current on free and forced convection flows in a rotating channel in the presence of an inclined magnetic field. Kalita and Lahkar[19] have carried out the effects of magnetic field on unsteady free convection MHD flow between two heated vertical plates.

In this chapter, we have studied the combined effects of Hall current and radiation on a hydromagnetic free convective flow of a viscous incompressible electrically conducting fluid in the presence of an inclined applied magnetic field. The temperature of the fluid motion is assumed to be changing with time exponentially. The magnetic Reynolds number is assumed to be small enough so that the induced magnetic field can be neglected. It is also assumed that there is no applied voltage, which implies the absence of an electrical field. The analytical solutions for velocity field, temperature distribution, shear stresses and the rate of heat transfer at the plates of the channel are obtained and the effects of pertinent parameters are presented graphically.

8.2 Formulation of the problem and its solutions

Consider the unsteady hydromagnetic free convective flow of a viscous incompressible electrically conducting fluid between two infinite vertical parallel plates separated by a distance $2h$. The channel plates are electrically nonconducting. Choose a Cartesian co-ordinate system with the x-axis along vertically upward direction, z-axis normal to the plates and y-axis is perpendicular to the xz-plane [see **Figure 8.1**]. Initially, at time $t = 0$, both the plates and the fluid are assumed to be at the same temperature T_h. At time $t > 0$, the plate at $(z = -h)$ is heated with the variable temperature $T_h + (T_0 - T_h)(1 - e^{-n\tau})$, where T_0 is the temperature at the plate at $z = h$ and $n(> 0)$,a real number, denotes the decay factor. The plate at $z = h$ is thermally insulated. A uniform magnetic field of strength B_0 is imposed at an angle ϕ to the x-axis. It is also assumed that the radiative heat flux in the x-direction is negligible in comparison with that in the z- direction. As the plates are infinitely long along the x and y directions, the velocity field and temperature distribution are functions of z and t only. In accordance with the Boussinesq approximation, we assume that all fluid properties are constant, except the density, which varies with temperature only in the body force term.

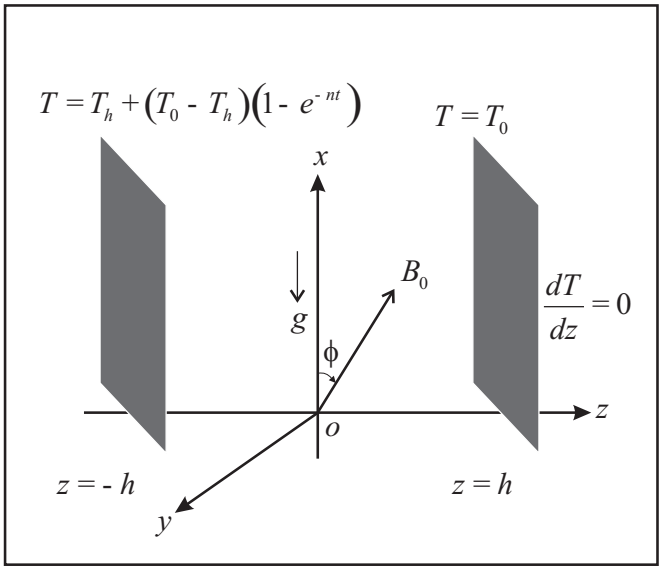

Figure 8.1: Geometry of the problem

The Navier-Stokes MHD momentum equations under the Boussinesq approximation for the transient magnetohydrodynamic channel flow with inclined magnetic field can

be written in component form as

$$\frac{\partial u}{\partial t} = \nu\frac{\partial^2 u}{\partial z^2} + g\beta(T - T_h) + \frac{B_0}{\rho}\, j_y \cos\phi, \tag{8.1}$$

$$\frac{\partial v}{\partial t} = \nu\frac{\partial^2 v}{\partial z^2} - \frac{B_0}{\rho}\, j_x \cos\phi, \tag{8.2}$$

where u, v are the velocity components, ν the kinematic viscosity, ρ the fluid density, g the acceleration due to gravity and j_x, j_y the components of current density along x, y-directions respectively.
The energy equation is

$$\rho c_p \frac{\partial T}{\partial t} = k\frac{\partial^2 T}{\partial z^2} - \frac{\partial q_r}{\partial z}, \tag{8.3}$$

where T is the temperature of the fluid, β the coefficient of thermal expansion, k the thermal conductivity, c_p the specific heat at constant pressure and q_r the radiative heat flux. The effects of viscous and Joule's dissipation is assumed to be negligible in the energy equation as small velocity is usually encountered in free convection flows.
The initial and boundary conditions for the velocity field and temperature distribution are

$$\begin{aligned} &u = 0 = v, \;\; T = T_h \;\text{ for }\; -h \le z \le h \;\text{ and }\; t = 0, \\ &u = 0 = v, \;\; T = T_h + (T_0 - T_h)\,(1 - e^{-n\,t}) \;\text{ at }\; z = -h \;\text{ for }\; t > 0, \\ &u = 0 = v, \;\; \frac{dT}{dz} = 0 \;\text{ at }\; z = h \;\text{ for }\; t > 0. \end{aligned} \tag{8.4}$$

The generalized Ohm's law on taking Hall currents into account is (Cowling[20])

$$\vec{j} + \frac{\omega_e\,\tau_e}{B_0}\left(\vec{j} \times \vec{B}\right) = \sigma\left(\vec{E} + \vec{q} \times \vec{B}\right), \tag{8.5}$$

where $\vec{q}$, $\vec{B}$, $\vec{E}$, $\vec{j}$, σ, ω_e and τ_e are respectively the velocity vector, the magnetic field vector, the electric field vector, the current density vector, the electric conductivity, the cyclotron frequency and electron collision time.

It is assumed that the magnetic Reynolds number Re_m for the flow is small so that the induced magnetic field can be neglected. This assumption is justified since the magnetic Reynolds number is generally very small for the partially ionized gases. Thus, it can be assumed that due to the low magnetic Reynolds number the applied magnetic field is unaffected by the effects of the motion of the conducting fluid i.e. the applied magnetic field will guide the flow. Whereas, the effects of the magnetic field on the fluid motion manifests itself in the form $\frac{1}{\rho}(\vec{j} \times \vec{B})$, which is known as the Lorentz

force. The Lorentz force will be a linear function of velocity when $Re_m \ll 1$. If the strength of the magnetic field is high, then one cannot neglect the Hall current. This is rather important case for some practical engineering problems. The electron-atom collision frequency is assumed to be relatively high, so that the Hall effects cannot be neglected (see Sutton and Sherman[7]).

The equation of continuity $\nabla \cdot \vec{q} = 0$ with no-slip condition at the plate gives $w = 0$ everywhere in the flow where $\vec{q} \equiv (u, v, w)$, u, v and w are respectively the velocity components along the coordinate axes. The solenoidal relation $\nabla \cdot \vec{B} = 0$ gives $B_z = \text{constant} = B_0$ everywhere in the flow where $\vec{B} \equiv (0, 0, B_z)$. The conservation of electric current $\nabla \cdot \vec{j} = 0$ yields $j_z = \text{constant}$ where $\vec{j} \equiv (j_x, j_y, j_z)$. This constant is zero since $j_z = 0$ at the plates which are electrically non-conducting. Hence, $j_z = 0$ everywhere in the flow. As the induced magnetic field is neglected, the Maxwell's equation $\nabla \times \vec{E} = -\frac{\partial \vec{B}}{\partial t}$ becomes $\nabla \times \vec{E} = 0$ which gives $\frac{\partial E_x}{\partial z} = 0$ and $\frac{\partial E_y}{\partial z} = 0$ where $\vec{E} \equiv (E_x, E_y, E_z)$. This implies that $E_x = \text{constant}$ and $E_y = \text{constant}$ everywhere in the flow. Since there is no electrical field applied in the current regime under consideration, the polarization voltage is neglected. Therefore it follows that $E_x = 0$ and $E_y = 0$ as indicated by Meyer[21].
In view of the above assumption, equation (8.5) yields

$$j_x + m\, j_y \cos\phi = \sigma\, v\, B_0 \cos\phi, \tag{8.6}$$

$$j_y - m\, j_x \cos\phi = -\sigma\, u\, B_0 \cos\phi, \tag{8.7}$$

where $m = \omega_e\, \tau_e$ is the Hall parameter which can take positive or negative values. Positive values of m mean that B_0 is upward. For negative values of m, B_0 is downward.

Solving for j_x and j_y from equations (8.6) and (8.7), we have

$$j_x = \frac{\sigma B_0 \cos\phi}{1 + m^2 \cos^2\phi} \left(v + mu \cos\phi\right), \tag{8.8}$$

$$j_y = \frac{\sigma B_0 \cos\phi}{1 + m^2 \cos^2\phi} \left(mv \cos\phi - u\right). \tag{8.9}$$

On the use of equations (8.8) and (8.9), equations (8.1) and (8.2) become

$$\frac{\partial u}{\partial t} = \nu \frac{\partial^2 u}{\partial z^2} + g\beta(T - T_h) + \frac{\sigma B_0^2 \cos\phi}{1 + m^2 \cos^2\phi} \left(mv \cos\phi - u\right), \tag{8.10}$$

$$\frac{\partial v}{\partial t} = \nu \frac{\partial^2 v}{\partial z^2} - \frac{\sigma B_0^2 \cos\phi}{1 + m^2 \cos^2\phi} \left(v + mu \cos\phi\right). \tag{8.11}$$

It has been shown by Cogley et al.[22] that in the optically thin limit for a non-gray

gas near equilibrium, the following relation holds

$$\frac{\partial q_r}{\partial z} = 4(T - T_h) \int_0^\infty K_{\lambda_h^*} \left(\frac{\partial e_{\lambda^* p}}{\partial T} \right)_h d\lambda^*, \tag{8.12}$$

where K_λ^* is the absorption coefficient, λ^* is the wave length, $e_{\lambda^* p}$ is the Planck's function and subscript $'h'$ indicates that all quantities have been evaluated at the temperature T_h which is the temperature of the wall at time $t = 0$. Thus, our study is limited to small difference of plate temperature to the fluid temperature. Grief et al.[23] showed that for an optically thin limit, the fluid does not absorb its own emitted radiation, this means that there is no self-absorption, but the fluid does absorb radiation emitted by the boundaries. Treatments to the radiative heating are either in the limit where photon mean free paths are very small, called optically thick, or very long, called optically thin. At high temperature the presence of thermal radiation alters the distribution of temperature in the boundary layer, which in turn affects the heat transfer at the channel walls.

On the use of the equation (8.12), equation (8.3) becomes

$$\rho c_p \frac{\partial T}{\partial t} = k \frac{\partial^2 T}{\partial z^2} - 4\,(T - T_h)\, I, \tag{8.13}$$

where

$$I = \int_0^\infty K_{\lambda_h^*} \left(\frac{\partial e_{\lambda^* p}}{\partial T} \right)_h d\lambda^*. \tag{8.14}$$

Introducing non-dimensional variables

$$\eta = \frac{z}{h}, \quad \tau = \frac{\nu\, t}{h^2}, \quad (u_1, v_1) = \frac{h}{\nu}\,(u, v), \quad \theta = \frac{T - T_h}{T_0 - T_h} \tag{8.15}$$

equations (8.10), (8.11) and (8.13) become

$$\frac{\partial u_1}{\partial \tau} = \frac{\partial^2 u_1}{\partial \eta^2} + Gr\,\theta + \frac{M^2 \cos\phi}{1 + m^2 \cos^2\phi}\,(m v_1 \cos\phi - u_1)\,, \tag{8.16}$$

$$\frac{\partial v_1}{\partial \tau} = \frac{\partial^2 v_1}{\partial \eta^2} - \frac{M^2 \cos\phi}{1 + m^2 \cos^2\phi}\,(v_1 + m u_1 \cos\phi)\,, \tag{8.17}$$

$$Pr\,\frac{\partial \theta}{\partial \tau} = \frac{\partial^2 \theta}{\partial \eta^2} - \,R\,\theta, \tag{8.18}$$

where $M^2 = \frac{\sigma\, B_0^2 h^2}{\rho\, \nu}$ is the magnetic parameter that represents the ratio of the magnetic field strength to the viscous force, $R = \frac{4I\,h^2}{k}$ the radiation parameter, $Gr = \frac{g\,\beta\,(T_0 - T_h) h^3}{\nu^2}$

the Grashof number that approximates the ratio of the buoyancy force to the viscous force acting on a fluid and $Pr = \frac{\rho\,\nu\,c_p}{k}$ the Prandtl number which measures the ratio of momentum diffusivity to the thermal diffusivity.
The corresponding initial and boundary conditions for u_1, v_1 and θ are

$$\begin{aligned} &u_1 = 0 = v_1,\ \theta = 0 \ \text{ for } \ -1 \le \eta \le 1 \ \text{ and } \ \tau = 0, \\ &u_1 = 0 = v_1,\ \ \theta = 1 - e^{-\omega\,\tau} \ \text{ at } \ \eta = -1 \ \text{ for } \ \tau > 0, \\ &u_1 = 0 = v_1,\ \ \frac{d\theta}{d\eta} = 0 \ \text{ at } \ \eta = 1 \ \text{ for } \ \tau > 0, \end{aligned} \tag{8.19}$$

where $\omega = \frac{n\,h^2}{\nu}$ is the non-dimensional decay factor.
Combining equations (8.16) and (8.17), we get

$$\frac{\partial F}{\partial \tau} = \frac{\partial^2 F}{\partial \eta^2} + Gr\,\theta - a\,F, \tag{8.20}$$

where

$$F = u_1 + i\,v_1,\ \ a = \frac{M^2\cos^2\phi}{1 + m^2\cos^2\phi}(1 - i\,m\cos\phi) \ \text{ and } \ i = \sqrt{-1}. \tag{8.21}$$

The corresponding boundary conditions for F and θ are

$$\begin{aligned} &F = 0,\ \theta = 0 \ \text{ for } \ -1 \le \eta \le 1 \ \text{ and } \ \tau = 0, \\ &F = 0,\ \ \theta = 1 - e^{-\omega\,\tau} \ \text{ at } \ \eta = -1 \ \text{ for } \ \tau > 0, \\ &F = 0,\ \ \frac{d\theta}{d\eta} = 0 \ \text{ at } \ \eta = 1 \ \text{ for } \ \tau > 0. \end{aligned} \tag{8.22}$$

8.2.1 General solution

In order to obtain the exact solution of equations (8.20) and (8.18) subject to the boundary conditions (8.22), we will use the Laplace transformation technique.
On the use of Laplace transformation, equations (8.20) and (8.18) become

$$s\,\bar{F} = \frac{d^2\bar{F}}{d\eta^2} + Gr\,\bar{\theta} - a\,\bar{F}, \tag{8.23}$$

$$Pr\,s\,\bar{\theta} = \frac{d^2\bar{\theta}}{d\eta^2} - R\,\bar{\theta}, \tag{8.24}$$

where

$$\bar{F}(\eta, s) = \int_0^\infty F(\eta,\tau)\,e^{-s\tau}\,d\tau \ \text{ and } \ \bar{\theta}(\eta, s) = \int_0^\infty \theta(\eta,\tau)\,e^{-s\tau}\,d\tau. \tag{8.25}$$

The corresponding boundary conditions for $\bar{F}$ and $\bar{\theta}$ are

$$\bar{F}(-1,s)=0,\ \ \bar{\theta}(-1,s)=\frac{1}{s}-\frac{1}{s+\omega},$$
$$\bar{F}(1,s)=0,\ \ \frac{d\bar{\theta}}{d\eta}(1,s)=0. \tag{8.26}$$

The solution of equations (8.24) and (8.23) subject to the boundary conditions (8.26) are given by

$$\bar{\theta}(\eta,s) = \frac{\omega}{s(s+\omega)}\,\frac{\cosh\sqrt{s\,Pr+R}\,(1-\eta)}{\cosh 2\sqrt{s\,Pr+R}}, \tag{8.27}$$

$$\bar{F}(\eta,s) = \begin{cases} \frac{\omega\,Gr}{(1-Pr)\,s\,(s+\omega)\,(s+b)}\left[\frac{\cosh\sqrt{s\,Pr+R}(1-\eta)}{\cosh 2\sqrt{s\,Pr+R}}\right. \\ \left. -\ \frac{\sinh\sqrt{s+a}(1-\eta)}{\sinh 2\sqrt{s+a}}-\frac{\sinh\sqrt{s+a}\,(1+\eta)}{\sinh 2\sqrt{s+a}\cosh 2\sqrt{s\,Pr+R}}\right] & \text{for } Pr\neq 1 \\ \frac{\omega\,Gr}{(a-R)\,s\,(s+\omega)}\left[\frac{\cosh\sqrt{s+R}(1-\eta)}{\cosh 2\sqrt{s+R}}\right. \\ \left. -\ \frac{\sinh\sqrt{s+a}(1-\eta)}{\sinh 2\sqrt{s+a}}-\frac{\sinh\sqrt{s+a}\,(1+\eta)}{\sinh 2\sqrt{s+a}\cosh 2\sqrt{s+R}}\right] & \text{for } Pr=1, \end{cases} \tag{8.28}$$

where $b=\frac{a-R}{1-Pr}$ and a is given by equation (8.21).
The inverse Laplace transform of equations (8.27) and (8.28) give the solution for the temperature distribution and the velocity field respectively as

$$\theta(\eta,\tau) = \frac{\cosh\sqrt{R}(1-\eta)}{\cosh 2\sqrt{R}}-\frac{\cosh\sqrt{R-\omega\,Pr}\,(1-\eta)}{\cosh 2\sqrt{R-\omega\,Pr}}\,e^{-\omega\,\tau} + \sum_{k=0}^{\infty}\frac{\pi(2k+1)\,(-1)^k\,e^{s_1\tau}}{4s_1(s_1+\omega)\,Pr}\,\cos(2k+1)\frac{\pi}{4}(1-\eta), \tag{8.29}$$

$$F(\eta,\tau) = \begin{cases} \frac{Gr}{(1-Pr)}\left[\frac{1}{b}\left\{\frac{\cosh\sqrt{R}\,(1-\eta)}{\cosh 2\sqrt{R}}-\frac{\sinh\sqrt{a}\,(1-\eta)}{\sinh 2\sqrt{a}}-\frac{\sinh\sqrt{a}\,(1+\eta)}{\sinh 2\sqrt{a}\cosh 2\sqrt{R}}\right\}\right. \\ -\ \frac{e^{-\omega\,\tau}}{b-\omega}\left\{\frac{\cosh\sqrt{R-\omega\,Pr}\,(1-\eta)}{\cosh 2\sqrt{R-\omega\,Pr}}-\frac{\sinh\sqrt{a-\omega}\,(1-\eta)}{\sinh 2\sqrt{a-\omega}}\right. \\ \left.\left. -\ \frac{\sinh\sqrt{a}\,(1+\eta)}{\sinh 2\sqrt{a-\omega}\cosh 2\sqrt{R-\omega\,Pr}}\right\}\right. \\ +\ \sum_{k=0}^{\infty}\frac{(2k+1)\,\pi\,e^{s_1\tau}}{4s_1(s_1+\omega)(s_1+b)\,Pr} \\ \times\ (-1)^k\left\{\cos(2k+1)\frac{\pi}{4}\,(1-\eta)-\frac{\sinh\sqrt{s_1+a}\,(1-\eta)}{\sinh 2\sqrt{s_1+a}}\right\} \\ +\ \sum_{k=0}^{\infty}\frac{\pi\,k\,e^{s_2\tau}}{2s_2(s_2+\omega)(s_2+b)} \\ \left.\times\ (-1)^k\left\{\sin\frac{k\pi}{2}\,(1-\eta)+\frac{\sinh\frac{k\pi}{2}(1+\eta)}{\cosh 2\sqrt{s_2Pr+R}}\right\}\right] & \text{for } Pr\neq 1 \end{cases} \tag{8.30}$$

$$F(\eta,\tau) = \begin{cases} \frac{Gr}{(a-R)}\left[\left\{\frac{\cosh\sqrt{R}\,(1-\eta)}{\cosh 2\sqrt{R}} - \frac{\sinh\sqrt{a}\,(1-\eta)}{\sinh 2\sqrt{a}} - \frac{\sinh\sqrt{a}\,(1+\eta)}{\sinh 2\sqrt{a}\cosh 2\sqrt{R}}\right\}\right. \\ - e^{-\omega\tau}\left\{\frac{\cosh\sqrt{R-\omega}\,(1-\eta)}{\cosh 2\sqrt{R-\omega}} - \frac{\sinh\sqrt{a-\omega}\,(1-\eta)}{\sinh 2\sqrt{a-\omega}}\right. \\ \left. - \frac{\sinh\sqrt{a}\,(1+\eta)}{\sinh 2\sqrt{a-\omega}\cosh 2\sqrt{R-\omega}}\right\} \\ + \sum_{k=0}^{\infty}\frac{(2k+1)\,\pi\, e^{s_3\tau}}{4s_3(s_3+\omega)} \\ \times(-1)^k\left\{\cos(2k+1)\tfrac{\pi}{4}\,(1-\eta) - \frac{\sinh\sqrt{s_3+a}\,(1-\eta)}{\sinh 2\sqrt{s_3+a}}\right\} \\ + \sum_{k=0}^{\infty}\frac{\pi\, k\, e^{s_2\tau}}{2s_2(s_2+\omega)(s_2+b)} \\ \left.\times(-1)^k\left\{\sin\tfrac{k\pi}{2}\,(1-\eta) + \frac{\sinh\frac{k\pi}{2}(1+\eta)}{\cosh 2\sqrt{s_2+R}}\right\}\right] & \text{for } Pr=1, \end{cases} \tag{8.31}$$

where

$$s_1 = -\frac{1}{Pr}\left[R + (2k+1)^2\frac{\pi^2}{16}\right],$$
$$s_2 = -\left[a + \frac{k^2\pi^2}{4}\right],\quad s_3 = -\left[R + (2k+1)^2\frac{\pi^2}{16}\right]. \tag{8.32}$$

In the absence of Hall currents ($m = 0$), equations (8.29) and (8.30) are reduced to that obtained by Kalita and Lahkar[19].

8.2.2 Steady state solution

When the time τ is very large ($\tau \to \infty$), then the steady state solution for temperature distribution and velocity field are respectively given by

$$\theta(\eta,\tau) = \frac{\cosh\sqrt{R}(1-\eta)}{\cosh 2\sqrt{R}}, \tag{8.33}$$

$$F(\eta,\tau) = \begin{cases} \frac{Gr}{(1-Pr)b}\left[\frac{\cosh\sqrt{R}\,(1-\eta)}{\cosh 2\sqrt{R}} - \frac{\sinh\sqrt{a}\,(1-\eta)}{\sinh 2\sqrt{a}} - \frac{\sinh\sqrt{a}\,(1+\eta)}{\sinh 2\sqrt{a}\cosh 2\sqrt{R}}\right] & \text{for } Pr\neq 1 \\ \\ \frac{Gr}{(a-R)}\left[\frac{\cosh\sqrt{R}\,(1-\eta)}{\cosh 2\sqrt{R}} - \frac{\sinh\sqrt{a}\,(1-\eta)}{\sinh 2\sqrt{a}} - \frac{\sinh\sqrt{a}\,(1+\eta)}{\sinh 2\sqrt{a}\cosh 2\sqrt{R}}\right] & \text{for } Pr=1, \end{cases} \tag{8.34}$$

where $b = \frac{a-R}{1-Pr}$ and a is given by equation (8.21).

8.3 Results and discussion

In order to get physical insight into the problem, the numerical values of the velocity, temperature, shear stresses and rate of heat transfer at the plate are computed as functions of time for different values of magnetic parameter M^2, Hall parameter

m, radiation parameter R, Grashof number Gr, Prandlt number Pr, magnetic field inclination ϕ, non-dimensional decay factor ω and time τ. The default values of the parameters are mentioned in the description of the respective figures.

8.3.1 Effects of parameters on the velocity profiles

The effects of pertinent parameters on the primary as well as the secondary velocities are presented graphically against η in **Figures 8.2-8.8**. It is seen from **Figure 8.2** that both the primary velocity u_1 and the secondary velocity v_1 decrease with an increase in magnetic parameter M^2. This is because the presence of a magnetic field in an electrically conducting fluid introduces a Lorentz force (a resistive force similar to the drag force) which acts against the flow. This resistive force tends to slow down the fluid flow and hence the fluid velocity components decrease with an increase in magnetic parameter. This trend is consistent with many classical studies on magneto-convection flow. **Figure 8.3** reveals that both the primary velocity u_1 and the secondary velocity v_1 increase with an increase in Hall parameter m. Since the magnetic field is strong, therefore the electromagnetic force becomes very large, which results in the phenomenon of the Hall currents. The Hall currents cause an increase in the secondary velocity. The secondary velocity is totally dependent on the Hall currents. Thus, the secondary velocity can be manipulated by increasing or decreasing the Hall parameter. The Hall parameter m has a marked effect on the velocity profiles. It is observed that an increasing value of m increases the velocity profiles until they reach the hydrodynamic values. This is because the effective conductivity $\frac{\sigma \cos\phi}{1+m^2\cos^2\phi}$ decreases as m increases for the fixed value of ϕ. Since the fluid is assumed to be weakly ionized, we can consider the value of the Hall parameter m lees than unity (see Sutton and Sherman[7]).

It is seen from **Figure 8.4** that an increase in radiation parameter R leads to a decrease in the primary velocity u_1 and the secondary velocity v_1. The radiation parameter arises only in the energy equation in the thermal diffusion term and via coupling of the temperature field with the buoyancy terms in the momentum equation, the fluid velocity is indirectly influenced by thermal radiation effects. An increase in radiation parameter implies less interaction of radiation with the momentum boundary layer and hence, the flow becomes decelerated. We focus on the positive values of buoyancy parameter i.e. Grashof number Gr which corresponding to the cooling problem. The cooling problem is often encountered in engineering applications.

Figure 8.5 reveals that both the primary velocity u_1 and the secondary velocity v_1 increase with an increase in Grashof number Gr. The Grashof number signifies the relative effects of the thermal buoyancy force to the viscous hydrodynamic force

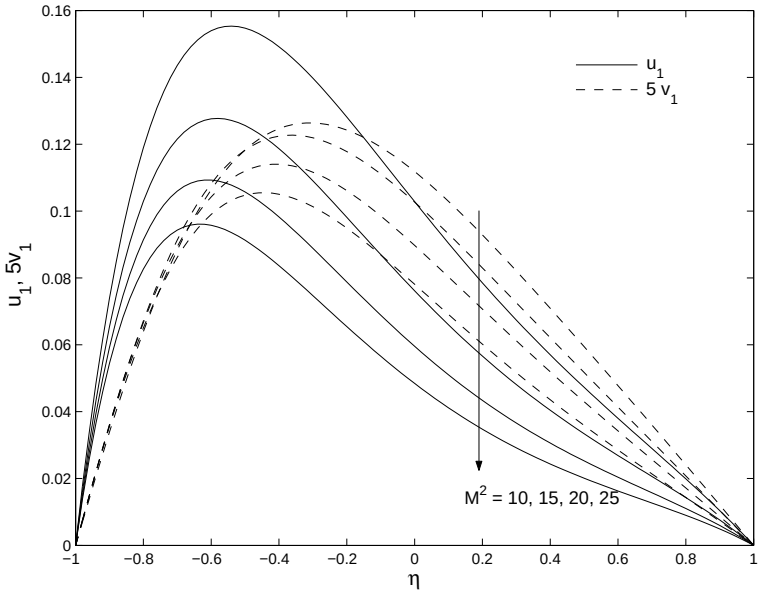

Figure 8.2: Primary and secondary velocities for M^2 when $m = 0.5$, $Gr = 5$, $\omega = 3$, $R = 2$, $Pr = 0.025$, $\tau = 1$ and $\phi = \frac{\pi}{4}$.

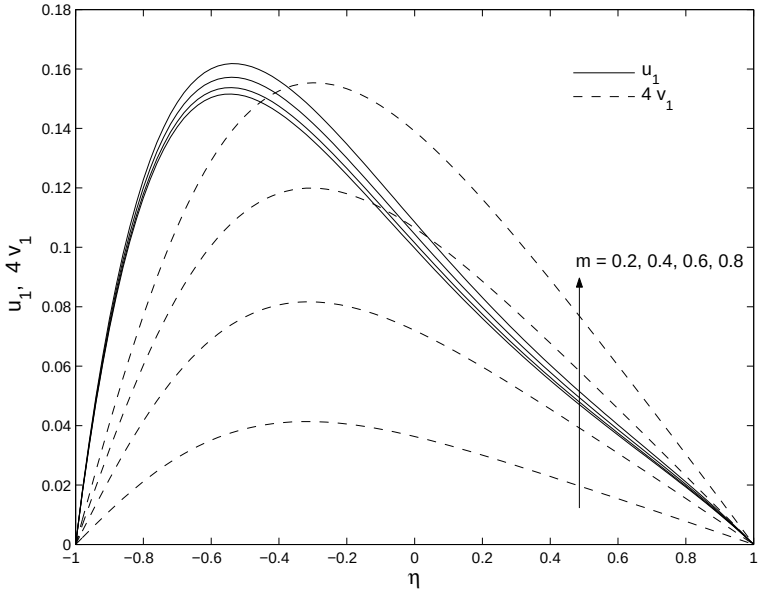

Figure 8.3: Primary and secondary velocities for m when $M^2 = 10$, $Gr = 5$, $\omega = 3$, $R = 2$, $Pr = 0.025$, $\tau = 1$ and $\phi = \frac{\pi}{4}$.

in the boundary layer. As expected, it is observed that there is a rise in the velocity components due to the enhancement of thermal buoyancy force. The maximum of the velocity profiles shifts toward the left half of the channel due to the greater buoyancy force in this part of the channel due to the presence of the hotter plate. In the left half there lies the hot plate at $\eta = -1$ and heat is transferred from the hot plate to the fluid and consequently the buoyancy force enhances the flow velocity further.

Figure 8.6 shows that both the primary velocity u_1 and the secondary velocity v_1 decrease with an increase in Prandlt number Pr. Prandtl number Pr then provides a measure of relative effectiveness of momentum and energy transport of diffusion in the velocity and thermal boundary layers respectively, e.g. in case of gases Pr is nearly equal to unity therefore energy and momentum transfer by diffusion are comparable whereas for liquid metals $Pr < 1$ and energy diffusion rate greatly exceeds the momentum diffusion rate.

On the other hand, in case of oils $Pr > 1$. From this interpretation it implies that value of Pr influences the growth of the velocity and thermal boundary layer. Thus the Prandtl number acts as the conducting link between the velocity field and the temperature field since it involves momentum transfer that consequently yields heat transfer.

Physically, this is true because the increase in the Prandtl number is due to increase in the viscosity of the fluid which makes the fluid thick and hence causes a decrease in the velocity of the fluid. It is worth mentioning that present investigation deals with those functional fluids which act as liquid metals in many engineering applications because of their ability to reduce the temperature of the system. For instance, liquid metals are used in nuclear power plants and mercury, sodium, alloys, lead-bismuth and bismuth are extensively utilized as coolant.

It is seen from **Figure 8.7** that the primary velocity u_1 is accelerated whereas the secondary velocity v_1 is retarded with an increase in magnetic field inclination ϕ. As magnetic field inclination ϕ increases, the hydromagnetic drag force decreases. In consistency with this, it is observed that a rise in inclination clearly accelerates the primary flow and decelerates the secondary flow. **Figure 8.8** demonstrates that both the primary velocity u_1 and the secondary velocity v_1 decrease with an increase in non-dimensional decay factor ω.

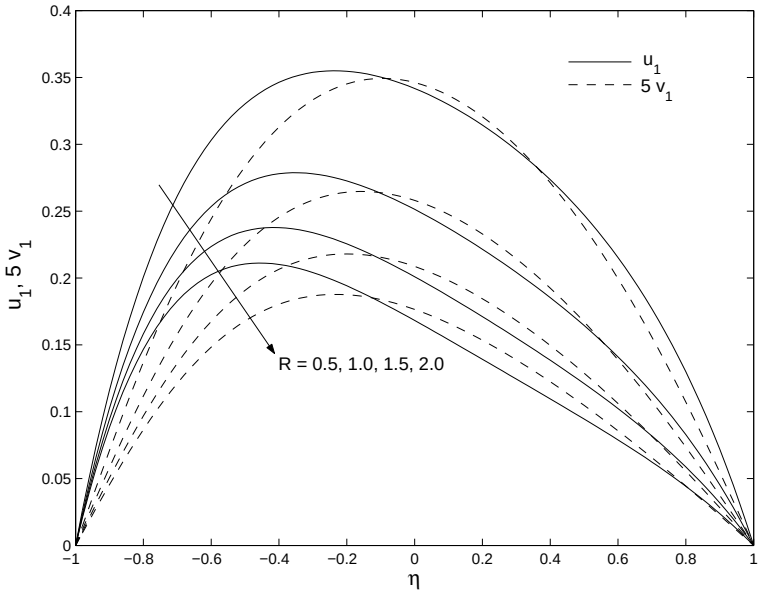

Figure 8.4: Primary and secondary velocities for R when $M^2 = 10$, $Gr = 5$, $\omega = 3$, $m = 0.5$, $Pr = 0.025$, $\tau = 1$ and $\phi = \frac{\pi}{4}$.

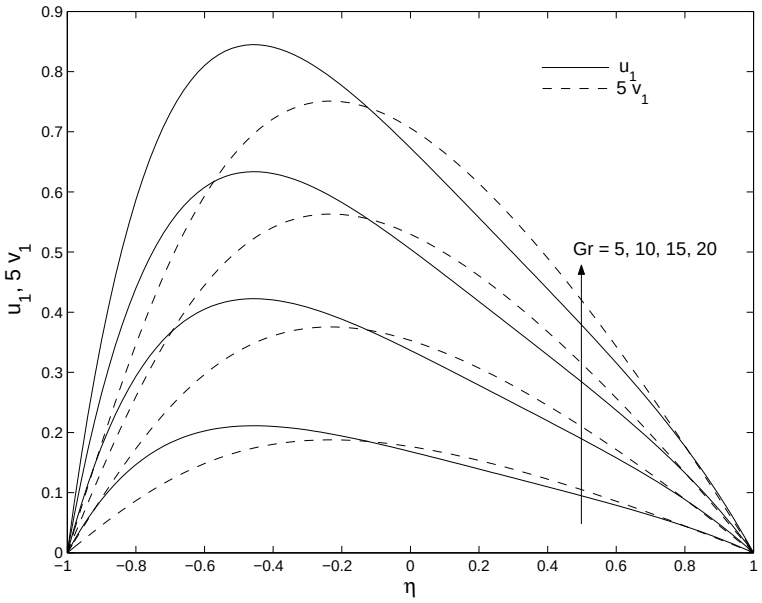

Figure 8.5: Primary and secondary velocities for Gr when $M^2 = 10$, $R = 2$, $\omega = 3$, $m = 0.5$, $Pr = 0.025$, $\tau = 1$ and $\phi = \frac{\pi}{4}$.

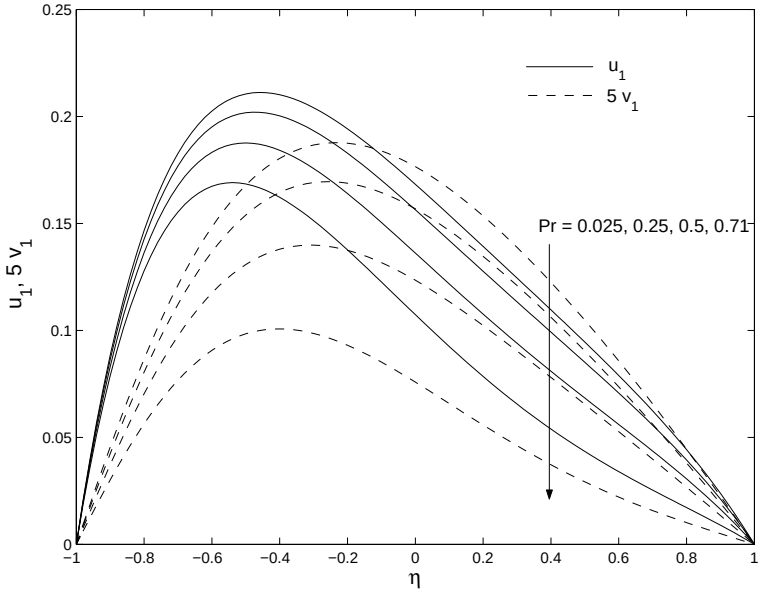

Figure 8.6: Primary and secondary velocities for Pr when $M^2 = 10$, $Gr = 5$, $\omega = 3$, $m = 0.5$, $R = 2$, $\tau = 1$ and $\phi = \frac{\pi}{4}$

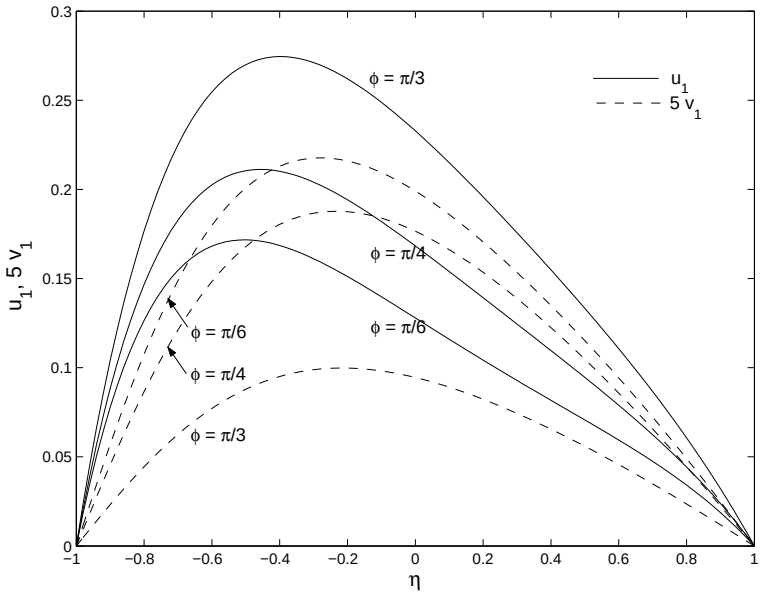

Figure 8.7: Primary and secondary velocities for ϕ when $M^2 = 10$, $Gr = 5$, $\omega = 3$, $m = 0.5$, $Pr = 0.025$, $\tau = 1$ and $R = 2$.

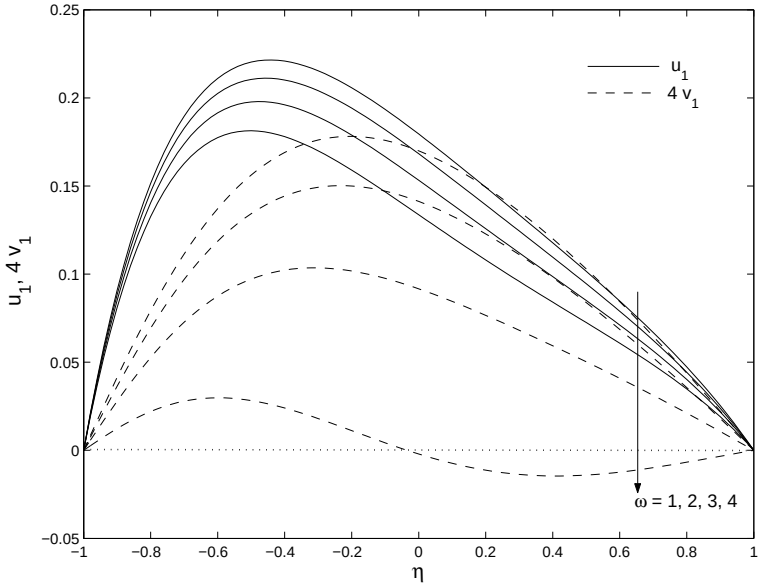

Figure 8.8: Primary and secondary velocities for ω when $M^2 = 10$, $Gr = 5$, $R = 2$, $m = 0.5$, $Pr = 0.025$, $\tau = 1$ and $\phi = \frac{\pi}{4}$

8.3.2 Effects of parameters on the temperature profiles

The effects of radiation parameter R, Prandtl number Pr, non-dimensional decay factor ω and time τ on the temperature distribution have been shown in **Figures 8.9-8.11**.

It is observed from **Figures 8.9-8.11** that the fluid temperature θ decreases with an increase in either radiation parameter R or Prandtl number Pr or non-dimensional decay factor ω.

This result qualitatively agrees with expectations, since the effects of radiation decrease the rate of energy transport to the fluid, thereby decreasing the temperature of the fluid.

The Prandtl number Pr is the ratio of the viscosity to the thermal diffusivity. An increase in thermal diffusivity leads to a decrease in Prandtl number. Therefore, thermal diffusion has a tendency to reduce the fluid temperature.

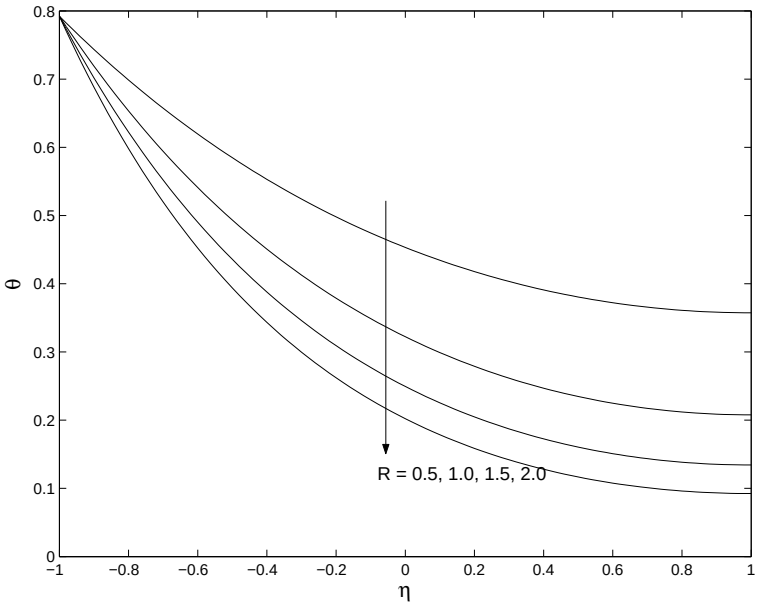

Figure 8.9: Temperature for R when $Pr = 0.025$, $\omega = 3$ and $\tau = 1$.

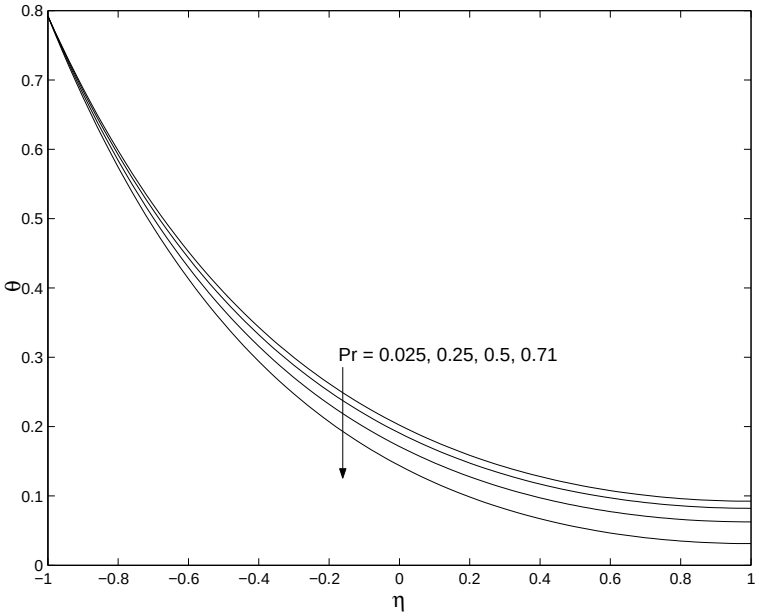

Figure 8.10: Temperature for Pr when $R = 2$, $\omega = 3$ and $\tau = 1$.

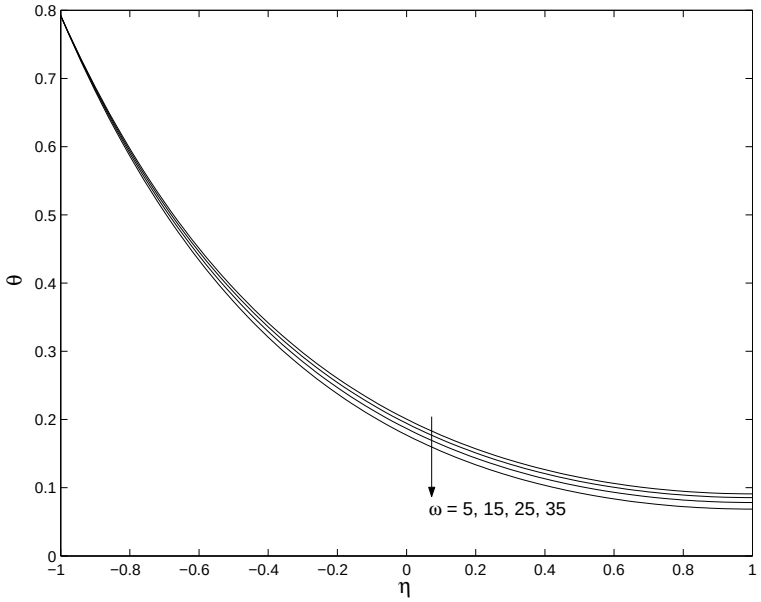

Figure 8.11: Temperature for ω when $Pr = 0.025$, $R = 2$ and $\tau = 1$.

8.3.3 Effects of parameters on the shear stresses at the plate

The non-dimensional shear stresses at the plate $\eta = 1$ are obtained as follows:

$$\tau_{x_1} + i\tau_{y_1} = \left(\frac{\partial F}{\partial \eta}\right)_{\eta=1}$$

$$= \begin{cases} \frac{Gr}{(1-Pr)}\Big[\frac{\sqrt{a}}{b}\,\text{cosech2}\sqrt{a}\left(1-\cosh 2\sqrt{a}\,\text{sech2}\sqrt{R}\right) \\ -\frac{e^{-\omega\tau}}{b-\omega}\sqrt{a-\omega}\,\text{cosech2}\sqrt{a-\omega} \\ \times\left(1-\cosh 2\sqrt{a-\omega}\,\text{sech2}\sqrt{R-\omega\,Pr}\right) \\ -\sum_{k=0}^{\infty}\frac{(2k+1)(-1)^k\,\pi\,e^{s_1\tau}}{4s_1(s_1+\omega)(s_1+b)\,Pr}\sqrt{s_1+a}\,\coth\sqrt{s_1+a} \\ -\sum_{k=0}^{\infty}\frac{\pi\,k\,(-1)^k\,e^{s_2\tau}}{2s_2(s_2+\omega)(s_2+b)}\left\{1-(-1)^k\,\text{sech2}\sqrt{s_2Pr+R}\right\}\Big] & \text{for } Pr \neq 1 \\ \\ \frac{Gr}{(a-R)}\Big[\frac{\sqrt{a}}{b}\,\text{cosech2}\sqrt{a}\left(1-\cosh 2\sqrt{a}\,\text{sech2}\sqrt{R}\right) \\ -\frac{e^{-\omega\tau}}{b-\omega}\sqrt{a-\omega}\,\text{cosech2}\sqrt{a-\omega} \\ \times\left(1-\cosh 2\sqrt{a-\omega}\,\text{sech2}\sqrt{R-\omega}\right) \\ -\sum_{k=0}^{\infty}\frac{(2k+1)(-1)^k\,\pi\,e^{s_3\tau}}{4s_3(s_3+\omega)}\sqrt{s_3+a}\,\coth\sqrt{s_3+a} \\ -\sum_{k=0}^{\infty}\frac{\pi\,k\,(-1)^k\,e^{s_2\tau}}{2s_2(s_2+\omega)}\left\{1-(-1)^k\,\text{sech2}\sqrt{s_2+R}\right\}\Big] & \text{for } Pr = 1, \end{cases} \tag{8.35}$$

where s_1, s_2, s_3 and a are given by equations (8.32) and (8.21) respectively.

Numerical results of the non-dimensional shear stresses at the plate $\eta = 1$ are presented in **Figures 8.12-8.16** for several values of Hall parameter m, radiation parameter R, Grashof number Gr, inclination of magnetic ϕ, non-dimensional decay factor ω and time τ when $Pr = 0.025$. **Figure 8.12** shows that the absolute values of the shear stress τ_{x_1} due to the primary flow and the shear stress τ_{y_1} due to the secondary flow at the plate $\eta = 1$ reduce with an increase in either radiation parameter R or magnetic parameter M^2. Since the intense amount of the magnetic field literally increases the Lorentz force that significantly opposes the flow in the reverse direction. Thus, the magnetic field acts as the retarding force that causes the shear stresses to decrease significantly. It is observed from **Figures 8.13-8.15** that the absolute values of the shear stresses increase with an increase in either m or Gr or inclination of magnetic field ϕ. This happens because the electrical conductivity of the fluid decreases with increasing m which ultimately reduces the magnetic damping force and hence the shear stresses are increased considerably. The absolute values of the shear stresses at the channel wall $\eta = 1$ enhance with increasing buoyancy force due to increase in flow velocity. An increase in non-dimensional decay factor ω also reduces the components of shear stress at the plate $\eta = 1$ shown in **Figure 8.16**.

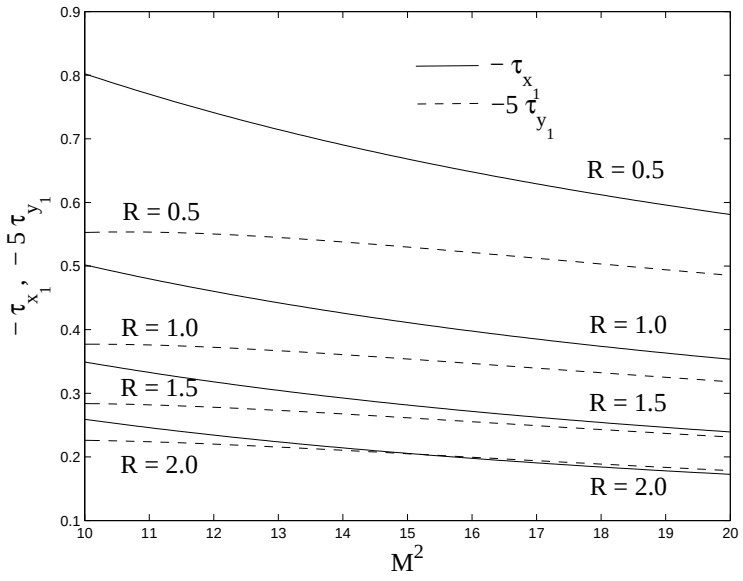

Figure 8.12: Shear stresses τ_{x_1} and τ_{y_1} for R when $m = 0.5$, $Gr = 5$, $\omega = 3$, $\tau = 1$ and $\phi = \frac{\pi}{4}$

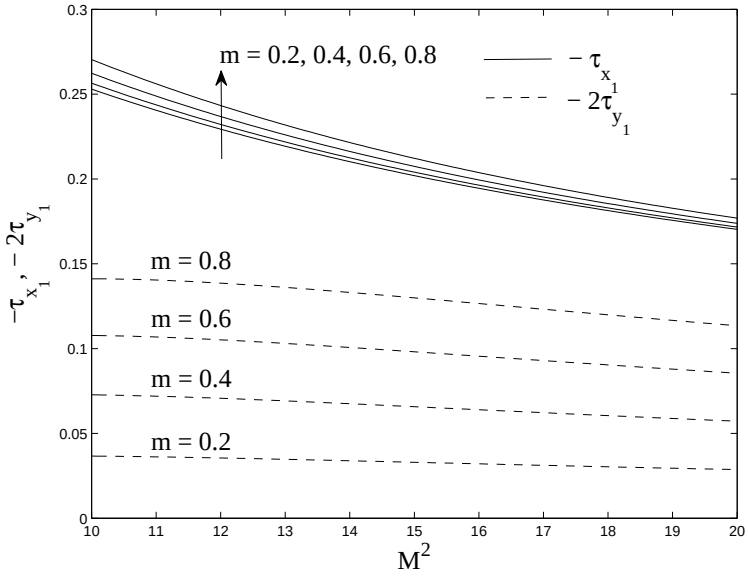

Figure 8.13: Shear stresses τ_{x_1} and τ_{y_1} for m when $R = 2$, $Gr = 5$, $\omega = 3$, $\tau = 1$ and $\phi = \frac{\pi}{4}$.

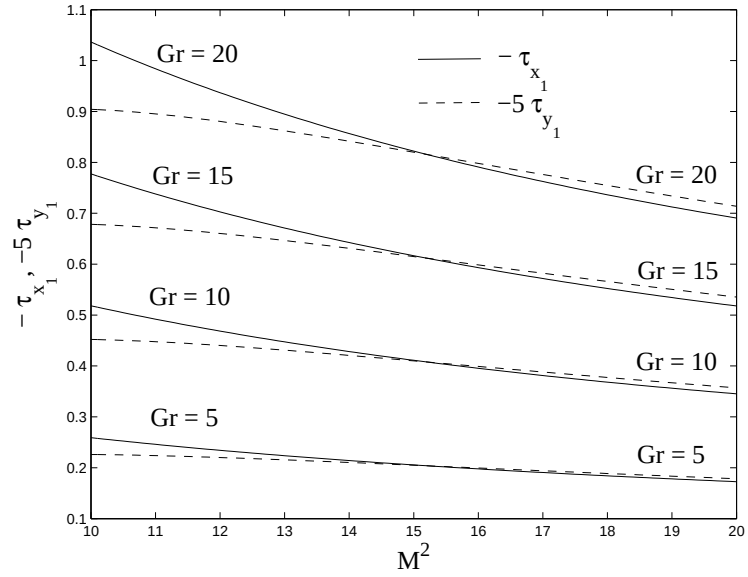

Figure 8.14: Shear stresses τ_{x_1} and τ_{y_1} for Gr when $R = 2$, $m = 0.5$, $\omega = 3$, $\tau = 1$ and $\phi = \frac{\pi}{4}$.

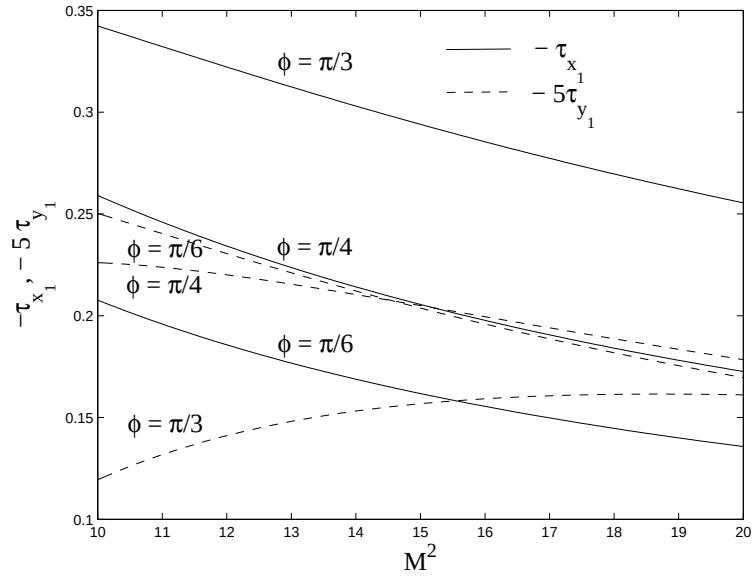

Figure 8.15: Shear stresses τ_{x_1} and τ_{y_1} for ϕ when $R = 2$, $Gr = 5$, $\omega = 3$ and $\tau = 1$.

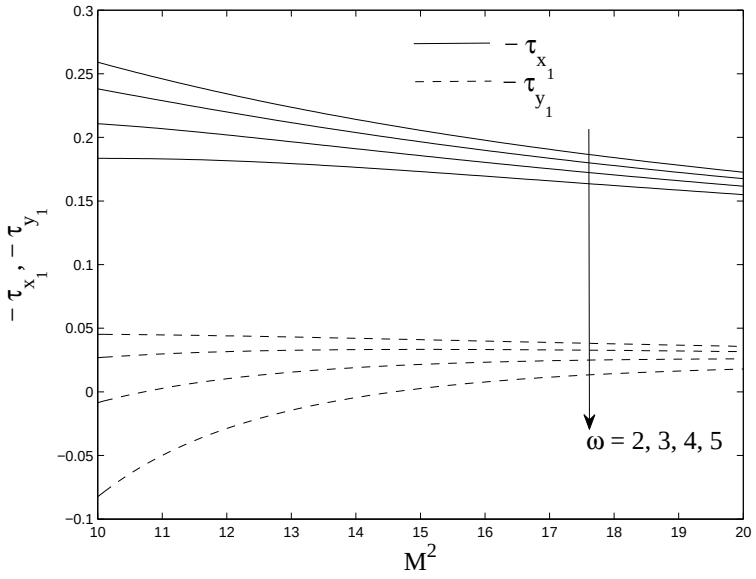

Figure 8.16: Shear stresses τ_{x_1} and τ_{y_1} for ω when $R = 2$, $Gr = 5$, $\tau = 1$ and $\phi = \frac{\pi}{4}$.

8.3.4 Effects of parameters on the rate of heat transfer at the plate

The rate of heat transfer is important in the heat transfer studies, since it is directly related to the heat transfer coefficient. The rate of heat transfer $\theta'(-1,\tau)$ $\left(= \frac{\partial\theta}{\partial\eta}\Big|_{\eta=-1}\right)$ and the temperature $\theta(1,\tau)$ at the plate $\eta = 1$ are respectively given by

$$\begin{aligned}\theta'(-1,\tau) &= -\sqrt{R}\tanh 2\sqrt{R} + \sqrt{R-\omega\,Pr}\tanh 2\sqrt{R-\omega\,Pr}\,e^{-\omega\,\tau} \\ &+ \sum_{k=0}^{\infty}\frac{(2k+1)^2\,\pi^2\,e^{s_1\tau}}{16\,s_1(s_1+\omega)\,Pr}, \qquad (8.36)\\ \theta(1,\tau) &= \mathrm{sech}2\sqrt{R} - e^{-\omega\,\tau}\,\mathrm{sech}2\sqrt{R-\omega\,Pr} \\ &+ \sum_{k=0}^{\infty}\frac{\pi(2k+1)\,(-1)^k\,e^{s_1\tau}}{4s_1(s_1+\omega)\,Pr}\,, \qquad (8.37)\end{aligned}$$

where s_1 is given by equation (8.32).

Numerical results of the rate of heat transfer $-\theta'(-1,\tau)$ at the plate $\eta = -1$ and the temperature $\theta(1,\tau)$ at the plate $\eta = 1$ for several values of radiation parameter R, Prandtl number Pr, non-dimensional decay factor ω and time τ are presented in the **Tables-I and II**.

Table-I shows that the rate of heat transfer $-\theta'(-1,\tau)$ increases with an increase in either radiation parameter R or Prandtl number Pr or non-dimensional decay factor ω or time τ. This can be attributed to the fact that as thermal radiation increases, the dominance effects of temperature gradient increases, leading to an increase in the rate of heat transfer. This may be also explained by the fact that frictional forces become dominant with increasing values of Prandtl number Pr and hence yield greater heat transfer rate. An increase in Prandtl number reduces the thermal boundary layer thickness. Prandtl number signifies the ratio of momentum diffusivity to thermal diffusivity. Fluids with lower Prandtl number will possess higher thermal conductivities so that heat can diffuse from the plate faster than for higher Pr fluids (thinner boundary layers). Hence, Prandtl number can be used to increase the rate of cooling in conducting flows. It is clear that the rate of heat transfer is more in the presence of thermal radiation. The negative value of $\theta'(-1,\tau)$ physically explains that there is heat flow from the hot plate $\eta = -1$ to the fluid.

It is observed from **Table-II** that the plate temperature $\theta(1,\tau)$ at $\eta = 1$ decreases with an increase in either radiation parameter R or Prandtl number Pr or non-dimensional decay factor ω. Further, it is seen from **Table-II** that the the plate temperature $\theta(1,\tau)$ at $\eta = 1$ increases with an increase in time τ.

Table-I
Rate of heat transfer $-\theta'(-1,\tau)$ at the plate $\eta = -1$.

	Pr			ω			τ		
R	*0.015*	*0.020*	*0.025*	*2*	*3*	*4*	1	1.5	2
0.5	*0.50292*	*0.50474*	*0.50657*	*0.50657*	*0.51127*	*0.51611*	*0.28164*	*0.36146*	*0.42290*
1.0	*0.76710*	*0.76828*	*0.76946*	*0.76946*	*0.77245*	*0.77549*	*0.40958*	*0.53729*	*0.63558*
1.5	*0.95850*	*0.95941*	*0.96032*	*0.96032*	*0.96262*	*0.96495*	*0.50475*	*0.66641*	*0.79084*
2.0	*1.11471*	*1.11548*	*1.11625*	*1.11625*	*1.11818*	*1.12013*	*0.58333*	*0.77244*	*0.91800*

Table-II
Temperature $\theta(1,\tau)$ at the plate $\eta = 1$.

	Pr			ω			τ		
R	*0.015*	*0.020*	*0.025*	*2*	*3*	*4*	1	1.5	2
0.5	*0.35996*	*0.35867*	*0.35736*	*0.35736*	*0.35397*	*0.35040*	*0.16919*	*0.23597*	*0.32692*
1.0	*0.20892*	*0.20836*	*0.20779*	*0.20779*	*0.20633*	*0.20482*	*0.10048*	*0.13856*	*0.19043*
1.5	*0.13489*	*0.13460*	*0.13429*	*0.13429*	*0.13352*	*0.13273*	*0.06566*	*0.09002*	*0.12319*
2.0	*0.09279*	*0.09261*	*0.09243*	*0.09243*	*0.09198*	*0.09151*	*0.04551*	*0.06216*	*0.08484*

8.4 Conclusion

Analytical solutions have been obtained for the transient MHD free convection flow in a heated vertical parallel plates channel in the presence of an inclined magnetic field taking Hall current into account. The effects of pertinent parameters on the velocity field, the temperature distribution, shear stresses and the rate of heat transfer have been discussed. It is found that both the primary velocity u_1 and the secondary velocity v_1 decrease with an increase in magnetic parameter M^2. This is because the presence of a magnetic field in an electrically conducting fluid introduces a Lorentz force (a resistive force similar to the drag force), which acts against the flow. This resistive force tends to slow down the fluid flow and hence the fluid velocity components decrease with an increase in magnetic parameter. This trend is consistent with many classical studies on magneto-convection flow. It is found that radiation has a retarding influence on both the primary and secondary velocity. An increase in angle of inclination of the magnetic field leads to accelerate the primary velocity while decelerate the secondary velocity. The primary velocity u_1 as well as the secondary velocity v_1 accelerate with an increase in Grashof number Gr. The fall of temperature θ will be shown with an increase in Prandtl number Pr. Prandtl number Pr is the ratio of the viscosity to the thermal diffusivity. An increase in thermal diffusivity leads to a decrease in Prandtl

number. Therefore, thermal diffusion has a tendency to reduce the fluid temperature. The absolute values of the shear stress τ_{x_1} due to the primary flow as well as the shear stress τ_{y_1} due to the secondary flow reduce with an increase in either radiation parameter R or magnetic parameter M^2. It is also found that the rate of heat transfer $-\theta'(-1,\tau)$ increases with an increase in radiation parameter R.

Bibliography

[1] Takenouchi K, J. Phys. Soc. Jpn.: **54**(1985), pp.1329.

[2] Hardianto T, Sakamoto N and Harada N, Int. J. Energy Technol. Policy: **6(12)**(2008), pp.96.

[3] Narasimhan MN, Technical Report, Wisconsin University-Madison, Math. Res. Center: (1963).

[4] Takhar HS and Ram PC, Astrophys. Space Sci.: **183**(1991), pp.193.

[5] Ryabinin AG and Khozhainov AI, Fluid Dynamics: **2(4)**(1967), pp.107.

[6] Barmin AA and Uspenskii VS, Fluid Dynamics: **21(4)**(1986), pp.18.

[7] Sutton G and Sherman A, Engg. Magnetohydrodynamics, McGraw-Hill, New York: (1965)

[8] Mazumder BS, Gupta AS and Datta N, Int. J. Heat Mass Trans.: **14**(1976), pp.285.

[9] Takhar HS and Ram PC, Astrophysics and Space Sci.: **183**(1991), pp.193.

[10] Gourla MG and Katoch S, Ganita: **42(2)**(1991), pp.143.

[11] Borkakati AK and Chakrabarty S, Indian J. Theoretical Phys.: **47(3)**(1999), pp.43.

[12] Jha BK, Heat and Mass Trans.: **37**(2001), pp.329.

[13] Singh KD and Pathak R, Int. J. Pure and Appl. Phys.: **50**(2012), pp.77.

[14] Das S, Sarkar BC and Jana RN, Open J. Fluid Dynamics: **2**(2012), pp.14.

[15] Mandal C, Das S and Jana RN, Int. J. Appl. Inf. Systems: **2(2)**(2012), pp.49.

[16] Sarkar BC, Das S and Jana RN, Int. J. Eng. Res. and Appl.: **2(4)**(2012), pp.2346.

[17] Seth GS and Ghosh SK, Int. J. Engg. Sci.: **27(4)**(1986), pp.1183.

[18] Pop I, Ghosh SK and Nandi DK, Magnetohydrodynamics: **37(4)**(2001), pp.348.

[19] Kalita B and Lahkar J, Adv. Studies Theor. Phys.: **6(16)**(2012), pp.765.

[20] Cowling TG, Magnetohydrodynamics, New York, Intersci.: (1957).

[21] Meyer RC, J. Aerospace Sci.: **25**(1958), pp.561.

[22] Cogley ACL, Vincentine WC and Gilles SE, Am. Inst. Aeronat. Astronaut., J.: **6**(1968), pp.551.

[23] Grief R, Habib IS and Lin JC, J. Fluid Mech.: **46**(1970), pp.513.

Chapter 9

Hall effects on an unsteady magneto-convection and radiative heat transfer past a vertical porous plate*

9.1 Introduction

A considerable interest has been shown in the study of thermal radiation on boundary layer flow and heat transfer in fluids due to its significant effects in the surface heat transfer. The radiation is another process of heat transfer through electromagnetic waves. Radiative convection flows are encountered in countless industrial and environment processes such as heating and cooling chambers, evaporation from large open water reservoirs, astrophysical flows and solar power technology, fossil fuel combustion energy processes and space vehicle re-entry. Radiative heat transfer in such processes plays very important role (see Hajmohammadi et al.[1]).

Thermal radiation transfer is also essential in Nuclear power plants, gas turbines and various propulsion devices for aircraft, missiles, satellites and space vehicles. The gravity-driven convection heat transfer is a vital phenomenon in the cooling mechanism of many engineering systems like electronic industries, solar collectors and cooling systems for nuclear reactors because of its minimum cost, low noise, smaller size and reliability.

* *Published in* **Alexandria Engg. J. (AEJ)(Elsevier)**, *ISSN: 1110-0168, 55(2)(2016), pp.1321-1331.*

Motsumi and Makinde[2] have studied the problem on MHD with convection boundary layer flow and heat transfer characteristics over a vertical plate.

The study of magneto hydrodynamic gravity-driven convection through an optically thick fluid past an infinite vertical plate is considered very essential in understanding the behaviour of the performance of fluid motion in several applications. The problem of gravity-driven convection in a regular fluid past a vertical plate is a classical problem solved by Ostrach[3]. Siegel[4] has studied the transient free-convective flow past a semi-infinite vertical plate by integral method. The convective flows with radiation are also encountered in many industrial processes such as heating and cooling of chambers, energy processes, evaporation from large reservoirs, solar power technology and space vehicle re-entry. Thermal radiation effects of an optically thin gray gas bounded by a stationary vertical plate have been investigated by England and Emery[5]. Soundalgekar and Takhar[6] have presented the free convective flow of an optically thin radiating gray gas past a semi-infinite vertical plate. Hossain and Takhar[7] have examined the radiation effects on mixed convection along an isothermal vertical plate.

The combined effects of Hall current and thermal radiation on the magnetohydrodynamic flows continue to draw the attention of researchers owing to extensive applications of such flows in the context of ionized aerodynamics, nuclear energy systems control, improved designs in aerospace MHD energy systems, manufacture of advanced aerospace materials etc. There is a vast amount of literature on the magnetohydrodynamic flows on taking Hall currents into account. Pop and Watanabe[8] have examined the Hall effects on a magnetohydrodynamic free convection past a semi-infinite vertical flat plate. The magnetohydrodynamic free convective heat and mass transfer of a heat generating fluid past an impulsively started infinite vertical porous plate with Hall currents and radiation absorption have been studied by Kinyanjui et al.[9].
Aboeldahab and Elbarbary[10] have analyzed the Hall effects on a magnetohydrodynamic free convective flow past a semi-infinite vertical plate with mass transfer. Takhar et al.[11] have considered the unsteady free convective flow past an infinite vertical porous plate on taking Hall currents into account. Aboeldahab and Aziz[12] have examined the effects of Hall and ion-slip currents on an MHD free convection from a vertical plate with power-law variation in surface temperature. Chaudhary and Jain[13] have addressed the Hall effects on an unsteady hydromagnetic flow of a visco-elastic fluid past a vertical porous plate. Abdul Hakeem and Sathiyanathan[14] have obtained an analytic solution of an oscillatory flow through a porous medium.
The effects of Hall current on MHD mixed convective flow over a vertical surface in porous medium have been described by Shateyi et al. [15]. Saha et al.[16] have pre-

sented the effects of Hall current on an MHD natural convective flow past a vertical permeable flat plate with uniform surface heat flux. Ali et al.[17] have examined the effects of Hall current on an MHD mixed convection boundary layer flow over a stretched vertical flat plate. Jain and Singh[18] have described the Hall and thermal radiative effects on an unsteady rotating free convective slip flow. Chaudhary et al.[19] have analysed the effects of Hall current and thermal radiation on an unsteady free convective slip flow along a vertical plate embedded in a porous medium with constant heat and mass flux.
The effects of Hall current and rotation on an MHD natural convective flow past an impulsively moving vertical plate with ramped plate temperature in the presence of thermal diffusion with heat absorption have been investigated by Seth et al.[20]. Das et al.[21] have examined the Hall effects on an MHD free convection boundary layer flow past a vertical flat plate. Sarkar et al.[22] have studied the Hall effects on an unsteady MHD free convective flow past an accelerated moving vertical plate with viscous and Joule dissipations. Seth et al.[23] have investigated the Hall effects on a natural convective flow past a moving vertical plate with heat and mass transfer.
Recently, Gireesha et al.[24] have reported the combined effects of the thermal radiation and Hall currents on boundary layer flow past a non-isothermal stretching surface embedded in porous medium with non-uniform heat source/sink and fluid-particle suspension. The conjugate natural convective flow over a vertical surface with radiation have been presented by Siddiqa et al.[25]. Kataria and Mittal[26] have developed a mathematical model for velocity and temperature of gravity-driven convective optically thick nanofluid flow past an oscillating vertical plate in the presence of magnetic field and radiation.

The main objective of this chapter study is to examine the effects of Hall current and thermal radiation on an MHD flow of a viscous incompressible electrically conducting fluid past a vertical porous plate in the presence of a uniform transverse magnetic field. It is assumed that the magnetic Reynolds number is small enough to neglect induced magnetic field. A strong magnetic field is assumed and thus the electromagnetic force becomes very large which results into the phenomenon of Hall currents.

The Hall currents give rise to a velocity in the cross flow direction. The governing equations are solved numerically using fourth-order Runge-Kutta scheme coupled with the shooting technique. The effects of the pertinent parameters on the velocity components, temperature distribution and rate of heat transfer and shear stresses are analyzed in detail.

9.2 Mathematical formulation

Consider the unsteady magnetohydrodynamic free convective flow of a viscous incompressible electrically conducting fluid past an infinite vertical porous plate in the presence of a uniform transverse magnetic field and thermal radiation. The motion of the fluid is induced by both pressure gradient and gravity. Choose a Cartesian co-ordinate system with x-axis along the plate in the direction of the flow vertically upward, y-axis is perpendicular to the plate and z-axis is normal to the xy-plane as shown in **Figure 9.1**. The plate at $y = 0$ is at rest and heated with the temperature T_w. A uniform magnetic field of strength B_0 is imposed perpendicular to the plate. It is assumed that the radiative heat flux in the x-direction is negligible as compared to that in the y- direction. As the plate is infinitely long along x and z-direction, the velocity field and temperature distribution are functions of y and t only. The equation of continuity $\nabla \cdot \vec{q} = 0$ gives $\frac{\partial v}{\partial y} = 0$ which on integration yields $v = -v_0$(constant), where $\vec{q} \equiv (u, -v_0, w)$. The constant v_0 denotes the normal velocity at the plate, is positive for suction and negative for blowing/injection.

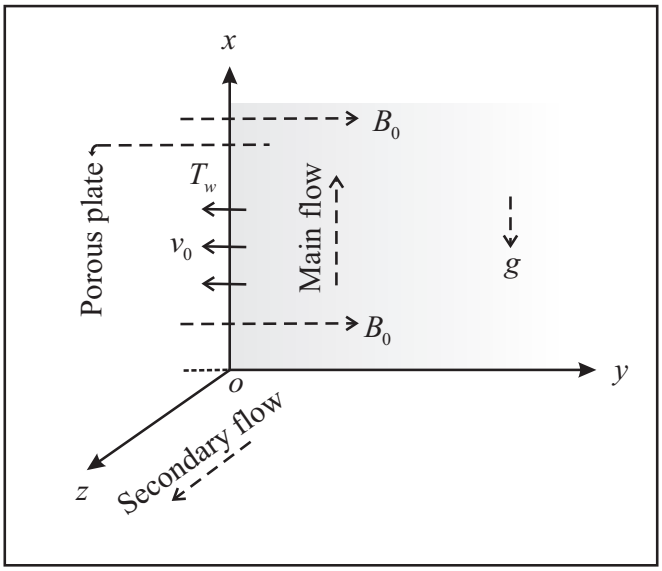

Figure 9.1: Geometry of the problem

It is assumed that the magnetic Reynolds number for the flow is small so that the induced magnetic field can be neglected such that $\vec{B} \equiv (0, 0, B_0)$. This assumption is justified since the magnetic Reynolds number is generally very small for metallic liquid or partially ionized gases (Shereliff[27]). Liquid metals can be used in a range of applica-

tions because they are nonflammable, nontoxic and environmentally safe. That is why, liquid metals have number of technical applications in source exchangers, electronic pumps, ambient heat exchangers and also used as a heat engine fluid. Moreover, in nuclear power plants sodium, alloys, lead-bismuth and bismuth are extensively utilized heat transfer fluids. Besides that, mercury play its role as a fluid in high-temperature Rankine cycles and also used in reactors in order to reduce the temperature of the system. For power plants which are exerted at extensively high temperature, sodium is treated as heat-engine fluid.

However, relative motion of the particles in the fluid can occur and the electron-atom collision frequency is assumed to be high enough for Hall currents to be significant. As such, an electric current density $\vec{j}$ is required to represent the relative motion of charges.

The generalized Ohm's law with Hall currents according to Cowling[28] is

$$\vec{j} + \frac{\omega_e \tau_e}{B_0}\left(\vec{j} \times \vec{B}\right) = \sigma\left(\vec{E} + \vec{q} \times \vec{B}\right), \tag{9.1}$$

where $\vec{q}$, $\vec{B}$, $\vec{E}$, $\vec{j}$, σ, ω_e and τ_e are respectively the velocity vector, the magnetic field vector, the electric field vector, the current density vector, the electric conductivity, the cyclotron frequency and electron collision time. In writing the equation (9.1), the ion-slip and the thermoelectric effects as well as the electron pressure gradient are neglected. An electromagnetic force is generated normal to both $\vec{E}$ and $\vec{B}$ in the z-direction. Such a force causes charged particles to migrate perpendicular to both $\vec{E}$ and $\vec{B}$, and this constitutes the Hall current.

We have assumed the fluid is isotropic and homogeneous and has the scalar constant viscosity and electric conductivity. We implement the Boussinesq approximation which implies that all thermodynamic quantities of the fluid are constant, except for the buoyancy term, which is retained in the x- direction momentum conservation equations. Hence, under these physical conditions, the momentum equations of motion along x and z-directions are

$$\frac{\partial u}{\partial t} - v_0 \frac{\partial u}{\partial y} = -\frac{1}{\rho}\frac{\partial p}{\partial x} + \nu \frac{\partial^2 u}{\partial y^2} + g\beta(T - T_\infty) + \frac{B_0}{\rho} j_z, \tag{9.2}$$

$$\frac{\partial w}{\partial t} - v_0 \frac{\partial w}{\partial y} = -\frac{1}{\rho}\frac{\partial p}{\partial z} + \nu \frac{\partial^2 w}{\partial y^2} - \frac{B_0}{\rho} j_x, \tag{9.3}$$

where u and w are the velocity components along x and z-directions respectively, ρ the fluid density, ν the kinematic viscosity, p the fluid pressure, β the coefficient of thermal expansion, g the acceleration due to gravity and j_x, j_z the components of current density along x, z-directions respectively.

It should be mention that $v_0 > 0$ corresponds to suction, $v_0 < 0$ corresponds to injection and $v_0 = 0$ corresponds to impermeable plate. Suction or blowing of a fluid through the bounding surface can significantly change the flow field. Injection or withdrawal of fluid through a porous bounding wall is of great interest in practical problems involving boundary layer control applications such as film cooling, and coating of wires. The process of suction/blowing has also its applications such as in the design of thrust bearing and radial diffusers, and thermal oil recovery. In general, suction is applied on chemical processes to remove reactants and blowing is used to add reactants, cool the surface, prevent corrosion or scaling and reduce the drag.
The energy equation is

$$\rho c_p \left(\frac{\partial T}{\partial t} - v_0 \frac{\partial T}{\partial y} \right) = k \frac{\partial^2 T}{\partial y^2} - \frac{\partial q_r}{\partial y}, \tag{9.4}$$

where T is the fluid temperature, k the thermal conductivity, c_p the specific heat at constant pressure and q_r the radiative heat flux. The Joule heating and viscous dissipation are neglected in this work.
The boundary conditions for the velocity field and temperature distribution are

$$\begin{aligned} &u = 0, \;\; w = 0, \;\; T = T_w \;\text{ at }\; y = 0 \;\text{ for }\; t > 0, \\ &u \to U, \;\; w \to 0, \;\; T \to T_\infty \;\text{ as }\; y \to \infty \;\text{ for }\; t > 0. \end{aligned} \tag{9.5}$$

Radiative magneto-convection fluid flow models find variety of applications at the industry level such as petroleum, chemical technology, food engineering, power engineering, underground spreading of chemical wastes, materials manufactured by extrusion processes and pharmaceutical manufacture.

The solenoidal relation $\nabla \cdot \vec{B} = 0$ for the magnetic field gives $B_y = B_0 =$ constant everywhere in the fluid where $\vec{B} \equiv (0, B_y, 0)$. The equation of the conservation of the charge $\nabla \cdot \vec{j} = 0$ gives $j_y =$constant. This constant is zero since $j_y = 0$ at the plate which is electrically non-conducting. Thus $j_y = 0$ everywhere in the flow field. Since the induced magnetic field is neglected, the Maxwell's equation $\nabla \times \vec{E} = -\frac{\partial \vec{B}}{\partial t}$ becomes $\nabla \times \vec{E} = 0$ which gives $\frac{\partial E_x}{\partial y} = 0$ and $\frac{\partial E_z}{\partial y} = 0$. This implies that $E_x =$ constant and $E_z =$ constant everywhere in the flow field.
Assuming $E_x = 0$ and $E_z = 0$, the equation (9.1) yields

$$j_x - m\, j_z = -\sigma w B_0, \tag{9.6}$$

$$j_z + m\, j_x = \sigma u B_0, \tag{9.7}$$

where $m = \omega_e \tau_e$ is the Hall parameter. For positive values of m, B_0 is along positive direction of y-axis and the electrons of the conducting fluid gyrate in anti-clockwise.

For negative values of m, B_0 is along negative direction of y-axis and the electrons gyrate in clockwise. In general, for an electrically conducting fluid, Hall currents affect the flow field in the presence of a strong magnetic field. The effects of Hall currents gives rise to a force in the z-direction.
Solving equations (9.6) and (9.7) for j_x and j_z, we get

$$j_x = \frac{\sigma B_0}{1+m^2}\left(mu - w\right), \tag{9.8}$$

$$j_z = \frac{\sigma B_0}{1+m^2}\left(mw + u\right). \tag{9.9}$$

On the use of equations (9.8) and (9.9) and infinity conditions, the equations of motion along x and z- directions are

$$\frac{\partial u}{\partial t} - v_0\frac{\partial u}{\partial y} = \nu\frac{\partial^2 u}{\partial y^2} - \frac{\sigma B_0^2}{\rho(1+m^2)}\left[mw + (u-U)\right] + g\beta\left(T - T_\infty\right), \tag{9.10}$$

$$\frac{\partial w}{\partial t} - v_0\frac{\partial w}{\partial y} = \nu\frac{\partial^2 w}{\partial y^2} - \frac{\sigma B_0^2}{\rho(1+m^2)}\left[w - m(u-U)\right], \tag{9.11}$$

It is also assumed that the fluid is an optically thick (photon mean free path is very small) gray gas (which emits and absorbs but does not scatter thermal radiation). In an optically thick medium, the radiation penetration length is small compare to the characteristic length. The photon mean path is the average distance travelled by a moving photon between successive collisions which modify its direction or energy or other particle properties.
According to the Rosseland diffusion approximation for radiation in an optically thick fluid the radiative heat flux is given by

$$q_r = -\frac{4\sigma^*}{3k^*}\frac{\partial T^4}{\partial y}, \tag{9.12}$$

where $\sigma^*(= 5.67 \times 10^{-8}\mathrm{W/m^2K^4})$ is the Stefan-Boltzman constant and $k^*(\mathrm{m}^{-1})$ the Rosseland mean absorption coefficient.
On the use of equation (9.12), the equation (9.4) becomes

$$\rho c_p\left(\frac{\partial T}{\partial t} - v_0\frac{\partial T}{\partial y}\right) = k\frac{\partial^2 T}{\partial y^2} + \frac{16\,\sigma^*}{3k^*}\left[T^3\frac{\partial^2 T}{\partial y^2} + 3T^2\left(\frac{\partial T}{\partial y}\right)^2\right]. \tag{9.13}$$

The last term in equation (9.13) is radiative heat flux which is expressed by using Rosseland diffusion approximation. Diffusion approximation can be used with certain limitations on the medium under consideration. It is valid in the interior of a medium but not employed near the boundaries and is good only for intensive absorption, that is,

for an optically thick boundary-layer. It cannot provide a complete description of the physical situation near the boundaries since it does not include any term for radiation from the boundary surface. However, the boundary surface effects are negligible in the interior of an optically thick region since radiation from the boundaries is attenuated before reaching the interior.

The following time-dependent similarity variables are introduced

$$\eta = \frac{y}{2\sqrt{\nu\, t}}, \;\; u = U\, f(\eta), \;\; w = U\, g(\eta), \;\; \theta(\eta) = \frac{T - T_\infty}{T_w - T_\infty}, \tag{9.14}$$

where η is the independent similarity variable, $f(\eta)$ the non-dimensional stream function and $\theta(\eta)$ the non-dimensional fluid temperature.

On the use of equation (9.14) in equations (9.10), (9.11) and (9.13), we obtain the following non-dimensional governing equations

$$f'' + 2(\eta + \mathrm{S})f' + \mathrm{Gr}\,\theta - \frac{M^2}{1+m^2}[(f-1) + mg] = 0, \tag{9.15}$$

$$g'' + 2(\eta + \mathrm{S})g' - \frac{M^2}{1+m^2}[g - m(f-1)] = 0, \tag{9.16}$$

$$\theta'' + 2(\eta + \mathrm{S})\theta' + \mathrm{Ra}[(\theta+\phi)^3\theta'' + 3(\theta+\phi)^2\theta'^2] = 0, \tag{9.17}$$

where $M^2 = \frac{4\sigma\, B_0^2\, t}{\rho}$ is the magnetic parameter, $\mathrm{Gr} = \frac{4g\beta_f(T_w - T_\infty)\, t}{U}$ the Grashof number, $\mathrm{Ra} = \frac{16\sigma^*(T_w - T_\infty)^3}{3k\, k^*}$ the radiation parameter, $\mathrm{S} = v_0(\frac{t}{\nu})^{\frac{1}{2}}$ the suction/injection parameter, $\phi = \frac{T_\infty}{T_w - T_\infty}$ the temperature difference parameter and $\mathrm{Pr} = \frac{\mu\, c_p}{k}$ the Prandtl number which measures the ratio of momentum diffusivity to the thermal diffusivity. The prime denotes the differentiation with respect to η.

The corresponding boundary conditions are

$$\begin{aligned} &f(0) = 0, \;\; g(0) = 0, \;\; \theta(0) = 1, \\ &f \to 1, \;\; g \to 0 \;\; \theta \to 0 \;\; \text{as} \;\; \eta \to \infty \end{aligned} \tag{9.18}$$

In the absence of magnetic field ($M^2 = 0$) as well as Hall currents ($m = 0$), the present problem reduces to the problem considered by Abdul Hakeem and Sathiyanathan[14]. It is observed that the trends of the velocity profiles are similar in the absence of magnetic field ($M^2 = 0$) as well as Hall currents ($m = 0$).

9.3 Numerical solution

The non-dimensional governing equations (9.15)-(9.17) with the boundary conditions (9.18) are solved numerically using fourth- order Rung-Kutta-Fehlberg method with

shooting technique. The resulting higher order ordinary differential equations are reduced to first order differential equations by introducing new variables

$$y_1 = f,\ \ y_2 = f',\ \ y_3 = g,\ \ y_4 = g',\ \ y_5 = \theta,\ \ y_6 = \theta'. \tag{9.19}$$

Thus, the corresponding higher order non-linear differential equations become

$$\begin{aligned}
y_1' &= y_2, \\
y_2' &= -2(\eta + \mathrm{S})y_2 - \mathrm{Gr}\, y_5 + \frac{M^2}{1+m^2}[(y_1 - 1) + m\, y_3], \\
y_3' &= y_4, \\
y_4' &= -2(\eta + \mathrm{S})y_4 + \frac{M^2}{1+m^2}[y_3 - m\,(y_1 - 1)], \\
y_4' &= y_6, \\
y_5' &= -\frac{1}{[1 + \mathrm{Ra}(y_5 + \phi)^3]}\left[2\mathrm{Pr}\,(\eta + \mathrm{S})\, y_6 + 3R(y_5 + \phi)^2 y_6^2\right],
\end{aligned} \tag{9.20}$$

with the boundary conditions

$$y_1(0) = 0,\ \ y_2(0) = a,\ \ y_3(0) = 0,\ \ y_4(0) = b,\ \ y_5(0) = 1,\ \ y_6(0) = c, \tag{9.21}$$

where a, b and c are unknown which are to be determined such that the boundary conditions $y_1(\infty) = 1$, $y_3(\infty) = 0$ and $y_5(\infty) = 0$ are satisfied. The shooting method is used to guess a, b and c by iterations until the boundary conditions are satisfied. The resulting differential equations can be integrated by Runge-Kutta-Fehlberg fourth order integration scheme. The accuracy of the assumed missing initial condition is checked by comparing the calculated value of the dependent variable at the terminal point with its given value there. If a difference exists, improved values of the missing initial conditions must be obtained and the process is repeated. The numerical computations are done by MATLAB sub-routine. The step-size is taken as $\eta = 0.01$. The above procedure is repeated until we get the converged results within a tolerance limit of 10^{-5}.

9.4 Results and discussion

In order to gain a clear physical insight of the problem, we examine the effects of the pertinent parameters, namely magnetic parameter M^2, Hall parameter m, Grashof number Gr, radiation parameter Ra, Prandtl number Pr and temperature difference parameter ϕ on the velocity, temperature, rate of heat transfer and shear stresses at the plate. Prandtl number (Pr) is chosen the values ranging from (metallic liquid or partially ionized fluid) $0.71 \leq \mathrm{Pr} \leq 2$ which are the most encountered fluids used in

plasma physics, engineering and industries. $M^2 = 0$ represents the case when there is no applied magnetic field. The case $m \to \infty$ gives the result of the hydrodynamic fluid case and $m = 0$ corresponds to an MHD fluid in the absence of Hall currents. The default values of the other parameters are mentioned in the description of the respective figures.

9.4.1 Effects of parameters on velocity components

The primary velocity $f(\eta)$ and the magnitude of the secondary velocity $g(\eta)$ enhance near the plate with an increase in magnetic parameter M^2 for both cases of suction and injection as shown in **Figures 9.2 and 9.3**. An increase in the strength of magnetic parameter M^2, the Lorentz force associated with the magnetic field makes the boundary layer thinner. The magnetic lines of forces move past the plate at the free stream velocity. The fluid which is decelerated by the viscous force, receives a push from the magnetic field which counteracts the viscous effects. Hence the velocity components increase as magnetic parameter M^2 increases. The secondary flow acceleration is beneficial in certain manipulation processes in MHD materials technology as it encourages a more homogenous constitution in materials. Therefore, in near-wall flows of MHD generators or indeed materials processing, the flow can very effectively controlled with a magnetic field. **Figure 9.4** reveals that the primary velocity $f(\eta)$ retards for suction (S = 0.5) and it decreases near the plate and increases for injection (S = −0.5) when Hall parameter m enlarges. **Figure 9.5** shows that the magnitude of the secondary velocity $g(\eta)$ enhances for suction (S = 0.5) and it increases near the plate and decreases away from the plate for injection (S = −0.5) with an increase in Hall parameter m.

The momentum boundary layer thickness increases for increasing values of m. The Hall parameter m has marked effects on the secondary velocity profiles. This is because the effective conductivity $\sigma/(1 + m^2)$ decreases as m increases. For small values of m, the term $1/(1 + m^2)$ decreases and thus the resistive magnetic force increases and the fluid velocity components are suppressed. This is a new phenomenon, which appears as a result of including the Hall currents.

The case $m = 0$ corresponds to the neglect of the Hall effects. Moreover, the primary and secondary profiles approach their classical hydrodynamic values when the Hall parameter tends to infinity. Since the magnetic force terms approach zero value for very large values of Hall parameter. This result is consistent with Gireesha et al.[24]
.

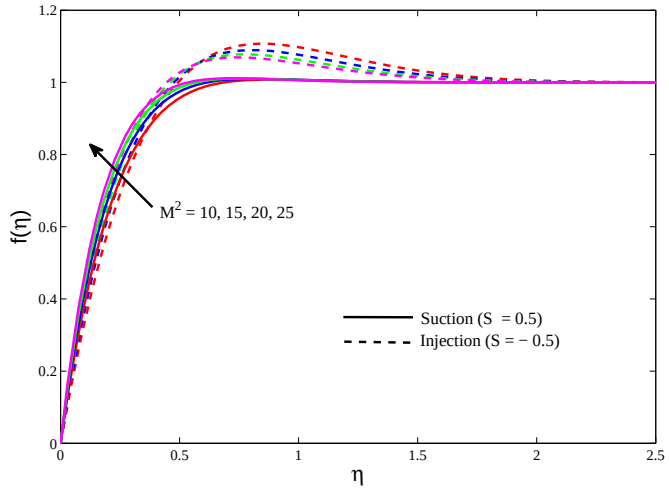

Figure 9.2: Primary velocity for different M^2 when $m = 0.5$, $\phi = 0.1$, Gr $= 5$, Ra $= 0.5$ and Pr $= 1.5$.

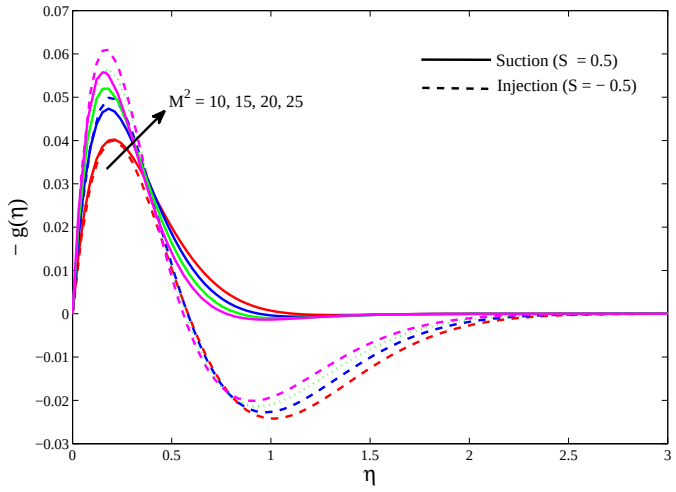

Figure 9.3: Secondary velocity for different M^2 when $m = 0.5$, $\phi = 0.1$, Gr $= 5$, Ra $= 0.5$ and Pr $= 1.5$.

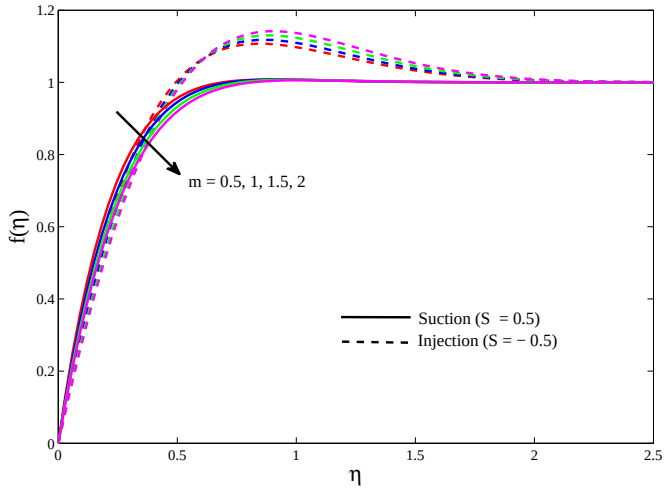

Figure 9.4: Primary velocity for different m when $M^2 = 10$, $\phi = 0.1$, Gr $= 5$, Ra $= 0.5$ and Pr $= 1.5$.

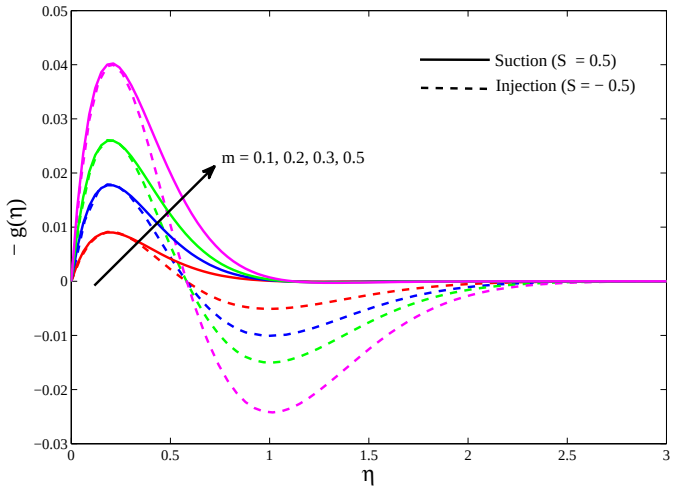

Figure 9.5: Secondary velocity for different m when $M^2 = 10$, $\phi = 0.1$, Gr $= 5$, Ra $= 0.5$ and Pr $= 1.5$.

The influence of thermal Grashof number Gr on the fluid velocity components is elucidated from **Figures 9.6 and 9.7**. It can be observed that the primary velocity $f(\eta)$ and the magnitude of the secondary velocity $g(\eta)$ decreases for the increasing values of Gr for both cases of $(\mathrm{S} = -0.5)$ and $(\mathrm{S} = 0.5)$.

Physically, because the thermal Grashof number Gr is the ratio of buoyancy to viscous forces in the boundary layer, the increase in its value suggests an increase in the buoyancy forces relative to the viscous forces and this is clearly reflected in the progressive increase in the velocity of the flow. The thermal Grashof number represents the effects of free convection currents.

Physically, $\mathrm{Gr} > 0$ means heating of the fluid of cooling of the boundary surface, $\mathrm{Gr} < 0$ means cooling of the fluid of heating of the boundary surface and $\mathrm{Gr} = 0$ corresponds the absence of free convection current.

The effects of radiation parameter R on the velocity components are presented in **Figures 9.8 and 9.9**. As the value of R increases, the primary velocity $f(\eta)$ increases and the magnitude of the secondary velocity $g(\eta)$ decreases for both cases of $(\mathrm{S} = -0.5)$ and $(\mathrm{S} = 0.5)$.

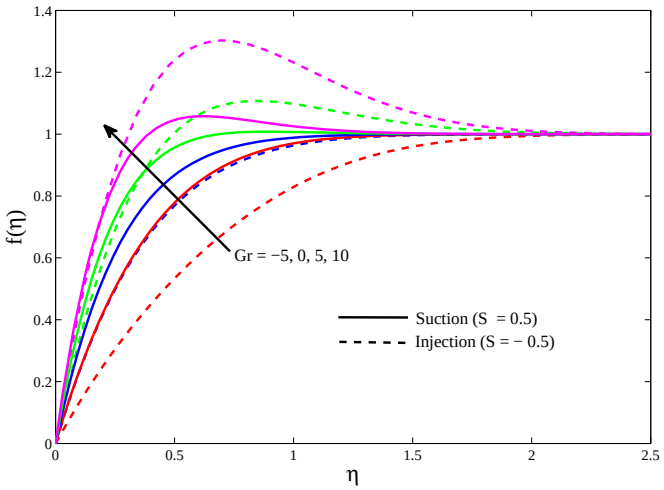

Figure 9.6: Primary velocity for different Gr when $m = 0.5$, $\phi = 0.1$, $M^2 = 10$, $\mathrm{Ra} = 0.5$ and $\mathrm{Pr} = 1.5$.

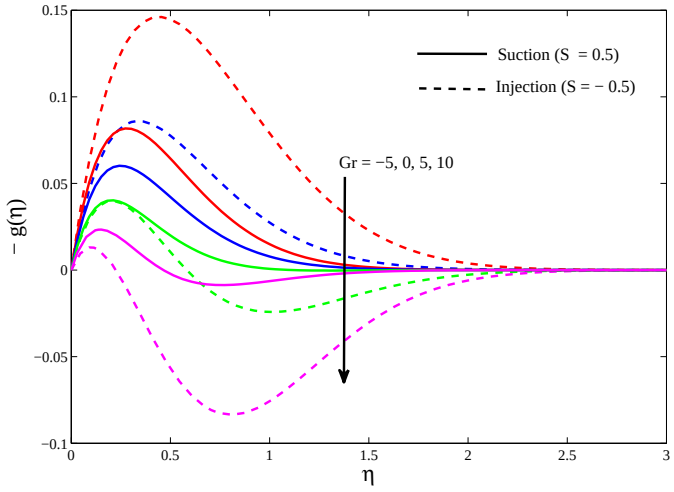

Figure 9.7: Secondary velocity for different Gr when $m = 0.5$, $\phi = 0.1$, $M^2 = 10$, Ra $= 0.5$ and Pr $= 1.5$.

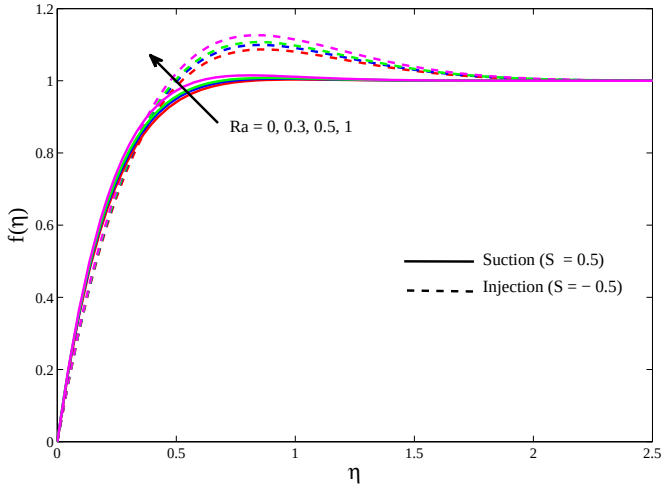

Figure 9.8: Primary velocity for different Ra when $m = 0.5$, $\phi = 0.1$, Gr $= 5$, $M^2 = 10$ and Pr $= 1.5$.

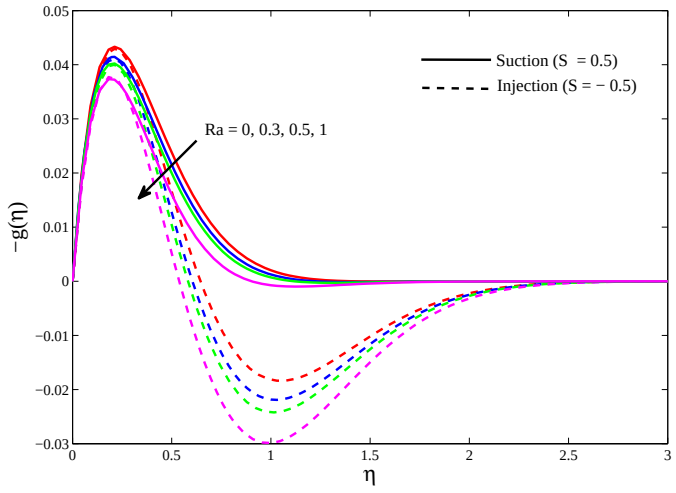

Figure 9.9: Secondary velocity for different Ra when $m = 0.5$, $\phi = 0.1$, Gr $= 5$, $M^2 = 10$ and Pr $= 1.5$.

Figures 9.10 and 9.11 present the variations of Prandtl number Pr on velocity components. It is seen that the primary velocity $f(\eta)$ retards and the magnitude of the secondary velocity $g(\eta)$ accelerates when Pr evolves for both cases of (S $= -0.5$) and (S $= 0.5$). The boundary layer thickness decrease as Prandtl number increases. Since Prandtl number represents ratio between kinematic viscosity and thermal diffusivity of the flow, an increase in the value of Pr gives higher resistance to the flow as visualized in **Figure 9.10**.

Figures 9.12 and 9.13 illustrate the effects of temperature difference parameter ϕ on velocity components. It is seen that the primary velocity $f(\eta)$ enhances whereas the magnitude of the secondary velocity $g(\eta)$ retards as ϕ increase for both cases of (S $= -0.5$) and (S $= 0.5$).

From **Figures 9.2-9.13**, it is revealed that injection causes increase in the primary as well as secondary velocity profiles. This is due to the fact that, while stronger injection is provided, the heated fluid is pushed farther away from the plate, the flow is accelerated. Suction tends to make the boundary layer thin causing increase in the velocity gradient which in turn increases the velocity of the flow. It is also noted that there occurs the backflow on the secondary velocity in the vicinity of the plate for blowing/injection.

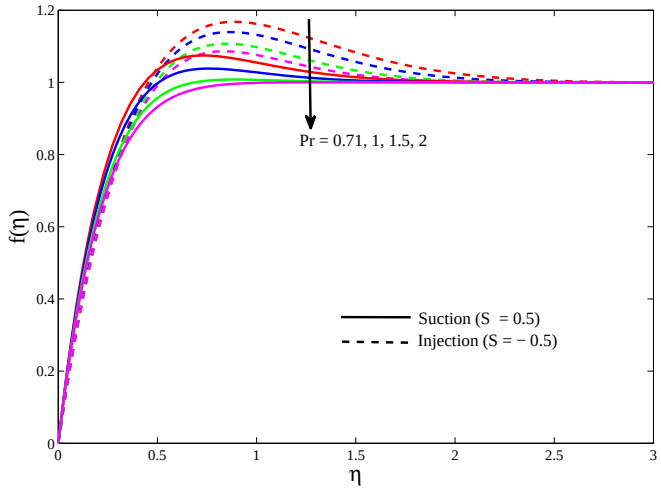

Figure 9.10: Primary velocity for different Pr when $m = 0.5$, $\phi = 0.1$, Gr $= 5$, Ra $= 0.5$ and $M^2 = 10$.

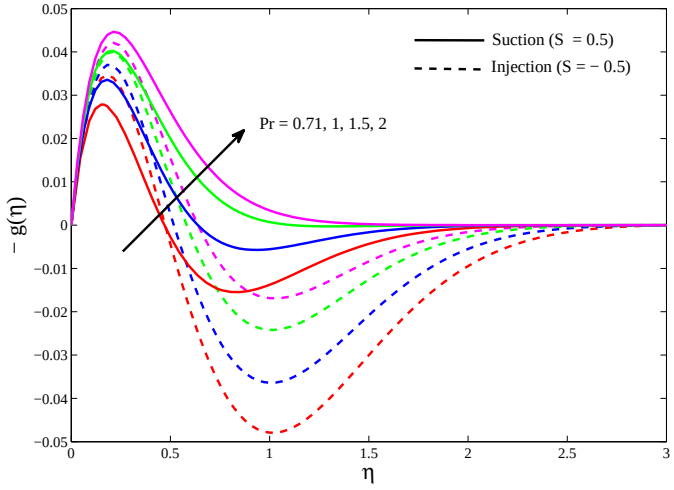

Figure 9.11: Secondary velocity for different Pr when $m = 0.5$, $\phi = 0.1$, Gr $= 5$, Ra $= 0.5$ and $M^2 = 10$.

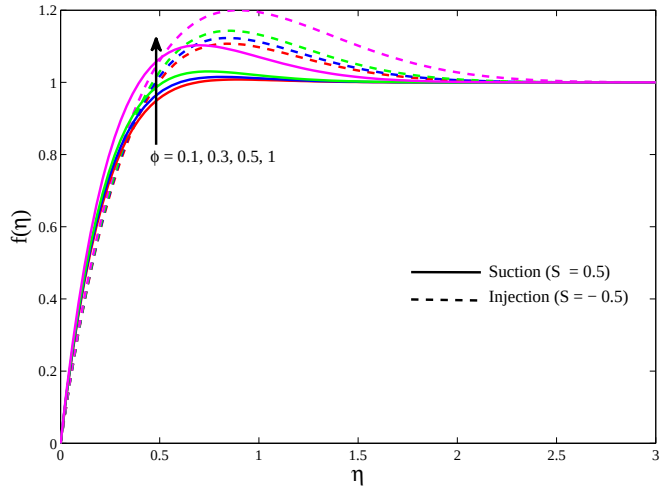

Figure 9.12: Primary velocity for different ϕ when $m = 0.5$, $M^2 = 10$, Gr $= 5$, Ra $= 0.5$ and Pr $= 1.5$.

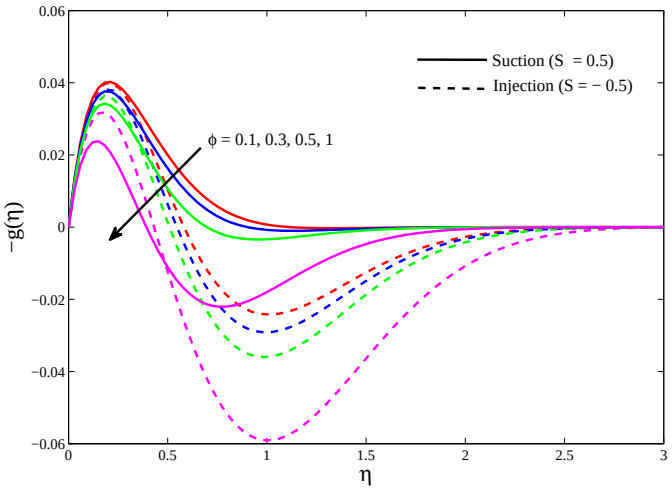

Figure 9.13: Secondary velocity for different ϕ when $m = 0.5$, $M^2 = 10$, Gr $= 5$, Ra $= 0.5$ and Pr $= 1.5$.

9.4.2 Effects of parameters on temperature profiles

It is observed from **Figure 9.14** that the fluid temperature $\theta(\eta)$ increases with an increase in radiation parameter Ra. Since divergence of the radiative heat flux $\frac{\partial q_r}{\partial y}$ increases, k^* decreases which in turn causes to increase the rate of radiative heat transfer to the fluid and hence the fluid temperature increases.

The radiation parameter Ra is responsible to thickening the thermal boundary layer. This enables the fluid to release the heat energy from the flow region and causes the system to cool.

Thus thermal radiation should be at its minimum in order to facilitate the cooling process. In view of this explanation, the effects of thermal radiation becomes more significant as Ra $\to \infty$ and can be neglected when Ra $\to 0$. These figures illustrate this agreement with the physical behavior.

Figure 9.15 illustrates the variations of fluid temperature $\theta(\eta)$ with respect to Prandtl number Pr. This figure depicts that the fluid temperature decreases when the values of Prandtl number Pr increase for suction/ injection.

This is due to the fact that a higher Prandtl number fluid has relatively low thermal conductivity, which reduces conduction and there by the thermal boundary layer thickness, as a result the fluid temperature decreases. Increasing Pr is to increase the heat transfer rate at the plate because the temperature gradient at the plate increases.

Figure 9.16 displays the effects of temperature difference parameter ϕ on the fluid temperature $\theta(\eta)$. The temperature $\theta(\eta)$ enhances as ϕ enlarges for both cases of (S $= -0.5$) and (S $= 0.5$). It is also observed that the thermal boundary layer is increased when ϕ increases. This agrees with the physical behavior that when ϕ increases the thermal state enhances and consequently the thermal boundary layer thickness increases. Thus, temperature difference parameter is responsible for the upraise in the temperature of the fluid. When injection (S < 0) takes place, the fluid temperature is higher compared with the suction (S > 0) as shown in **Figures 9.14-9.16**. These figures show that the suction (or injection) has a profound effects on the thermal boundary layer thickness in which the suction reduces the thermal boundary layer thickness whereas injection thickens it. So, we can conclude that the suction can be effectively used for the fast cooling of the plate.

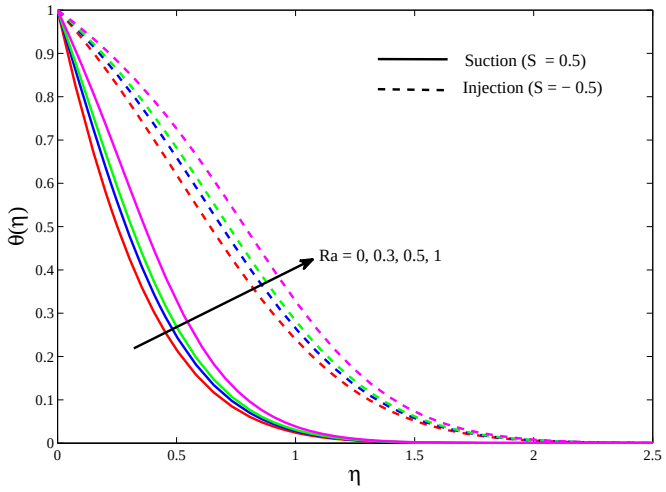

Figure 9.14: Temperature profile for different Ra when $\phi = 0.1$ and $\mathrm{Pr} = 1.5$.

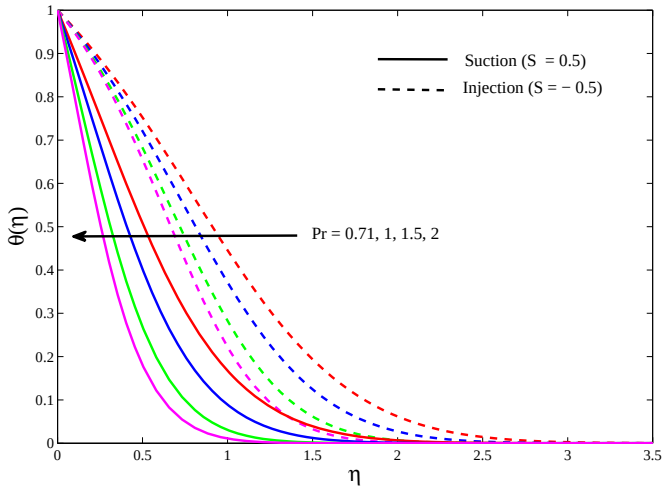

Figure 9.15: Temperature profile for different Pr when $\phi = 0.1$ and $\mathrm{Ra} = 0.5$.

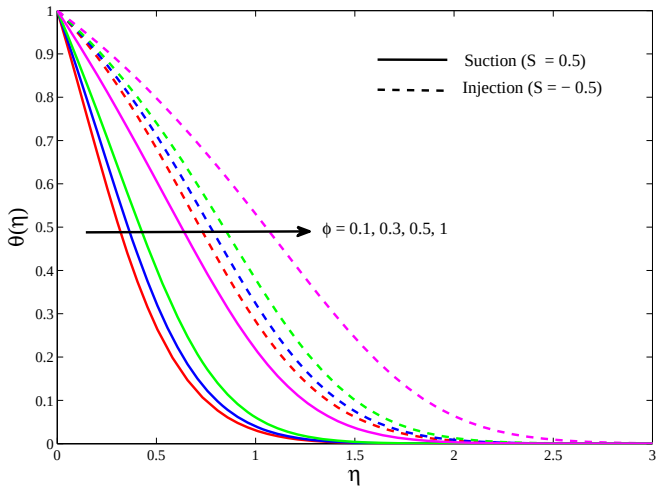

Figure 9.16: Temperature profile for different ϕ when Ra = 0.5 and Pr = 1.5.

9.4.3 Effects of parameters on shear stresses and rate of heat transfer

For engineering and practical purposes, one is usually more interested in the values of the skin friction or the rate of heat transfer than in the shape of the velocity or temperature profiles, so, our interest lies in the investigation of the important physical quantities of the flow behavior and heat transfer characteristics by analyzing the non-dimensional shear stresses and the rate of heat transfer at the plate. Numerical values of the rate of heat transfer $\theta'(0,\tau)$ and the shear stresses $f'(0,\tau)$ and $g'(0,\tau)$ at the plate $\eta = 0$ due to the primary and secondary flows respectively are presented in **Table-I** for several values of M^2, m, ϕ, S, Ra, Gr and Pr. The shear stress $f'(0,\tau)$ increase for increasing values of either M^2 or ϕ or S or Ra or Gr while it reduces with an increase in m.

Increasing strength of the magnetic field accelerates the primary velocity in the presence of free stream velocity. Thus, the magnetic field acts as the accelerating force that causes the shear stress $f'(0,\tau)$ to enhance significantly. Positive value of $f'(0,\tau)$ means the fluid exerts a drag force on the plate along x-direction, while a negative value of $f'(0,\tau)$ means the opposite. The shear stress $-g'(0,\tau)$ enhances for increasing values of either M^2 or m or S while it reduces with an increase in either ϕ or Ra or Gr. This happens because the electrical conductivity of the fluid decreases with increasing m which ultimately reduces the magnetic damping force and hence the shear stress $-g'(0,\tau)$ is increased considerably. Negative value of $g'(0,\tau)$ signifies that the plate

exerts a drag force on the fluid along z-direction.

It is also seen from **Table-I** that the rate of heat transfer $-\theta'(0,\tau)$ reduces for increasing values of either ϕ or Ra while it enhances with an increase in S or Pr. This means that, in order to facilitate the cooling process ϕ and Ra are should be at its minimum. The thermal boundary layer thickness decreases with the suction parameter S which causes an increase in the rate of heat transfer. The explanation for such behavior is that the fluid is brought closer to the surface and reduces the thermal boundary layer thickness. When fluid attains a higher Prandtl number, its thermal conductivity is lowered down and so its heat conduction capacity diminishes. Thereby the thermal boundary layer thickness gets reduced. As a consequence, the heat transfer rate at the plate is increased.

Table-I

The shear stresses $f'(0,\tau)$ and $g'(0,\tau)$ and the rate of heat transfer $\theta'(0,\tau)$ at the plate $\eta = 0$.

M^2	m	ϕ	S	Ra	Gr	Pr	$f'(0)$	$-g'(0)$	$-\theta'(0)$
10	*0.5*	*0.1*	*0.5*	*0.5*	*5*	*1.5*	*4.629913*	*0.519152*	
12	*0.5*	*0.1*	*0.5*	*0.5*	*5*	*1.5*	*4.841829*	*0.587537*	
15	*0.5*	*0.1*	*0.5*	*0.5*	*5*	*1.5*	*5.139197*	*0.680373*	
10	*0.1*						*4.834473*	*0.121467*	
10	*0.3*						*4.758508*	*0.344647*	
10	*0.5*						*4.629913*	*0.519152*	
		0.1					*4.629913*	*0.519152*	*1.608529*
		0.3					*4.692970*	*0.507348*	*1.344515*
		0.5					*4.762096*	*0.492941*	*1.131686*
			-0.5				*3.681728*	*0.507946*	*0.608789*
			0				*4.144986*	*0.514456*	*1.029743*
			0.5				*4.629913*	*0.519152*	*1.608529*
				0.1			*4.552746*	*0.531201*	*2.251850*
				0.5			*4.629913*	*0.519152*	*1.608529*
				1			*4.708789*	*0.505211*	*1.214757*
					-5		*2.654839*	*0.724096*	
					0		*3.642367*	*0.621620*	
					5		*4.629913*	*0.519152*	
						0.71			*1.608509*
						1			*1.608511*
						1.5			*1.608529*

9.5 Conclusion

The present investigation is a worthwhile attempt to study the effects of Hall current on an MHD free convective flow of a viscous incompressible electrically conducting optically thick radiating fluid past a vertical porous plate in the presence of an applied magnetic field and thermal radiation. Thermal radiation effects are noted on the basis of thick gas approximation or Rosseland diffusion approximation. The governing equations have been solved numerically using the fourth-order Runge-Kutta-Fehlberg method together with the shooting technique implemented on MatLab. Numerical results for the velocity field, temperature distribution, shear stresses and the rate of heat transfer at the plate are presented graphically for pertinent parameters. It is found that the velocity components $f(\eta, \tau)$ and $g(\eta, \tau)$ accelerate with an increase of the strength of magnetic field and buoyancy force. In the presence of thermal radiation, the temperature $\theta(\eta, \tau)$ of the fluid increases whereas it decreases when Prandtl number Pr enlarges. This is due to the fact that a higher Prandtl number fluid has relatively low thermal conductivity, which reduces conduction and there by the thermal boundary layer thickness, as a result the fluid temperature decreases. The presence of Hall current moderate the flow field significantly. Also, the fluid temperature enhances for increasing values of temperature difference parameter. Suction (or injection) has a profound effects on the boundary layer thickness in which the suction reduces the thermal boundary layer thickness whereas injection thickens it. It is found that the shear stress $f'(0, \tau)$ increases for increasing values of magnetic parameter M^2 while it reduces with an increase in Hall parameter m. Increasing strength of the magnetic field accelerates the primary velocity in the presence of free stream velocity. Thus, the magnetic field acts as the accelerating force that causes the shear stress $f'(0, \tau)$ to enhance significantly. Positive value of $f'(0, \tau)$ means the fluid exerts a drag force on the plate along x-direction, while a negative value of $f'(0, \tau)$ means the opposite. It is also found that the rate of heat transfer $-\theta'(0, \tau)$ reduces for increasing values of either ϕ or Ra while it enhances with an increase in either S or Pr.

Bibliography

[1] Hajmohammadi MR, Poozesh S and Hosseini R, J. Thermal Sci. Tech.: **7(4)**(2012), pp.677.

[2] Motsumi TG and Makinde OD, Phys. Scr.: **86**(2012), pp.8.

[3] Ostrach S, NACA Rep.: **1111**(1953), pp.63.

[4] Siegel R, Trans. Amer. Soc. Mech. Engg.: **80**(1958), pp.347.

[5] England WG and Emery AF, J. Heat Trans.: **91**(1969), pp.37.

[6] Soundalgekar VM and Takhar HS, Modelling Meas Control: **51**(1993), pp.31.

[7] Hossain MA and Takhar HS, J. Heat Mass Trans.: **31**(1996), pp.243.

[8] Pop I and Watanabe T, Int. J. Engg. Sci.: **32**(1994), pp.1903.

[9] Kinyanjui M, Kwanza JK and Uppal SM, Energy Conversion and Management: **42(8)**(2001), pp.917.

[10] Aboeldahab EM and Elbarbary EME, Int. J. Engg. Sci.: **39(14)**(2001), pp.1641.

[11] Takhar HS, Roy S and Nath G, Heat Mass Trans.: **39**(2003), pp.825.

[12] Aboeldahab EM and Aziz MAE, Appl. Math. Modelling: **29(6)**(2005), pp.579.

[13] Chaudhary RC and Jain P, UUR J. Phys.: **52(10)**(2007), pp.110.

[14] Hakeem AKA and Sathiyanathan K, Nonlinear Analysis, Hybrid Systems: **3**(2009), pp.288.

[15] Shateyi S, Mosta SS and Sibanda P, Mathematical Problems in Engg.: Article ID 627475(2010), pp.20.

[16] Saha LK, Siddiqa S and Hossain MA, Appl. Math. Mech. Engg. Ed.: **32(9)**(2011), pp.1127.

[17] Ali FM, Nazar R, Arifin NM and Pop I, Meccanica: **46**(2011), pp.1103.

[18] Jain NC and Singh H, Int. J. Appl. Mech. Engg.: **17(1)**(2012), pp.53.

[19] Chaudhary D, Singh H and Jain NC, Appl. Math. Phys.: **1(2)**(2013), pp.11.

[20] Seth GS, Mahato GK and Sarkar S, Int. J. Energy. Tech.: **5(16)**(2013), pp.1.

[21] Das S, Sarkar BC and Jana RN, Meccanica: **48(6)**(2013), pp.1387.

[22] Sarkar BC, Das S and Jana RN, Int. J. Computer Appl.: **70(24)**(2013), pp.19.

[23] Seth GS, Sarkar S and Hussain SM, Ain Shams Engg. J.: **5**(2014), pp.489.

[24] Gireesha BJ, Mahanthesh B, Gorla RSR and Manjunatha PT, Heat and Mass Trans.: **52(4)**(2016), pp.897.

[25] Siddiqa S, Hossain MA and Gorla RSR, Heat Mass Trans.: **52(6)**(2016), pp.1193.

[26] Kataria HR and Mittal AS, J. Nigerian Math. Society: **34**(2015), pp.303.

[27] Shereliff JA, London: Pergamon Press: (1965).

[28] Cowling TG, Magnetohydrodynamics, Intersci. Publisher, Inc, New York: (1957).

[29] Ko TH and Ting K, Energy: **31(12)**(2006), pp.2142.

Part III

Summary

Chapter 10

Conclusion and suggestion for future work

This chapter provides a summary of the thesis and presents conclusions from the research with suggestions for future work in the field. This chapter also summarizes the thesis, discusses its findings and contributions, points out limitations of the current work and outlines directions for future research. However, this chapter synthesizes the discussions and findings of Part-II (from chapter two to chapter nine) in the context based on several frame of geometry. Moreover, the strategic planning framework as well as background are presented in Part-I (chapter one). In this thesis, we studied some problems on magnetohydrodynamics with or without Hall currents. Some problems are studied in rotating environment. However, still many extensions of this research deserve further consideration.

The thesis consists of ten Chapters, **first chapter** presents the introductory part. A review of the field is presented here. Apart from giving a brief description of the basic MHD equations, a summary of various aspects of geometry is presented. In this section the various earlier works are given.

The unsteady MHD flow and heat transfer of an incompressible viscous fluid bounded by an infinite porous flat plate have been studied in **second chapter**. An exact solution of the governing equations have been obtained. The effects of pertinent parameters on the primary velocity, secondary velocity, shear stresses due to primary and secondary flow and temperature are studied. The primary velocity as well as the magnitude of the secondary velocity decrease with an increase in magnetic parameter. The variation of the magnetic parameter leads to the variation of the Lorentz force due to magnetic field and the Lorentz force produces more resistance to transport phenomena. The

mean wall temperature as well as the rate of heat transfer are also obtained. It is found that the mean temperature increases with an increase in either magnetic parameter or rotation parameter. The effects of transverse magnetic field on a viscous incompressible electrically conducting fluid is to suppress the velocity field which in turn causes the enhancement of the temperature field. The numerical values of amplitude of rate of heat transfer and tangent of the phase angle are given in tabular form. It is also found that both the amplitudes of shear stresses due to primary and secondary flow decrease with an increase in either magnetic parameter or frequency parameter.

In **third chapter**, the radiation effects on transient MHD convective Couette flow confined between two infinite vertical walls have been studied. The governing equations give an exact solution by using the Laplace transformation technique. The steady state solution for temperature distribution and velocity field are also studied. The shear stress and rate of heat transfer have been calculated. The vertical flow rate through the channel and critical Grashof number are also calculated and examined. The effects of pertinent parameters on the velocity field, temperature distribution, shear stress, rate of heat transfer, critical Grashof number and vertical flow rate are depicted either graphically or in tabular forms. Here we also consider the case for single vertical plate, which gives single deck boundary layer for the temperature distribution and double deck boundary layer for the velocity field. It is reveals that the velocity decreases with an increase in radiation parameter. This shows that there is a fall in velocity in the presence of high radiation. Moreover, the temperature decreases with an increase in radiation parameter. This is expected, since the effect of radiation is to decrease the rate of energy transport to the fluid, thereby decreasing the temperature of the fluid. It is found that for fixed values of magnetic parameter, the shear stress at the plate decreases with an increase in either radiation parameter or Prandtl number.

The effects of Hall currents and rotation on unsteady hydromagnetic flow of a viscous incompressible electrically conducting fluid past an accelerated porous plate in a rotating system have been carried out in **fourth chapter**. A uniform magnetic field is imposed perpendicular to the plate. The dimensionless governing partial differential equations are solved by the usual Laplace transform technique. We obtain an analytical solution for small as well as large times. It is seen that the small time solution converges more quickly than the general solution for small times. The effects of pertinent parameters on the velocity components and shear stresses are studied in details. The Hall currents tend to accelerate the primary as well as the secondary fluid velocity. The rotation has a tendency to retard the primary fluid velocity whereas accelerate the secondary fluid velocity. The primary and secondary fluid velocities are accelerated

with the progress of time. It is found that the absolute values of the shear stresses due to primary and secondary flow increase with an increase in rotation parameter. Therefore, rotation tends to enhance both the shear stresses at the plate.

The effects of Hall currents and radiation on MHD flow of a viscous incompressible electrically conducting fluid past a moving vertical plate with variable plate temperature in the presence of a uniform transverse magnetic field have been investigated in **fifth chapter**. The magnetic Reynolds number for the flow is small so that the induced magnetic field can be neglected. On the use of the Laplace transform technique, the governing equations give an exact solution. The numerical results for the velocity components, shear stresses and temperature are depicted graphically. The Hall parameter accelerates the primary velocity as well as the magnitude of the secondary velocity. The temperature reduces with an increase in radiation parameter. It is found that the absolute value of the shear stress due to the primary flow at the moving plate decreases whereas the absolute value of the shear stress due to the secondary flow at the moving plate increases with an increase in Hall parameter. It is also found that for fixed values of Prandtl number and time, the rate of heat transfer increases with an increase in radiation parameter.

In **sixth chapter**, the combined effects of Hall currents and rotation on MHD Couette flow between two infinitely long horizontal parallel porous plates in a rotating system in the presence of a uniform transverse magnetic field have been carried out. It is assumed that the fluid is incompressible and electrically conducting. The dimensionless governing differential equations are solved by the usual Laplace transform technique. In addition to that, we obtain the solution for small time. The effects of pertinent parameters are analyzed graphically on the velocity and shear stress. The solution for small time converges more rapidly than the general solution. The asymptotic behavior of the solution is analyzed for small as well as large values of magnetic parameter, rotation parameter and Reynolds number. It is observed that the primary velocity as well as the magnitude of the secondary velocity increase with an increase in Hall parameter. A thin boundary layer is formed near the stationary plate and the thicknesses of this layer increase with an increase in either Hall parameter or Reynolds number while it decreases with an increase in magnetic parameter. This is because the magnetic field has a retarding influence on the flow. Moreover, for large values of magnetic parameter, the boundary layer thickness is independent of the rotation parameter. It is found that the shear stress at the plate due to primary flow as well as the magnitude of the shear stress due to secondary flow decrease with an increase in magnetic parameter when the Hall parameter is fixed.

The combined effects of Hall currents and radiation on the unsteady MHD free convective flow in a vertical channel with an oscillatory wall temperature have been studied in **seventh chapter**. A uniform transverse magnetic field is applied perpendicular to the channel walls. We use the Cogley's approximation on an optically thin limit for a non-gray gas near equilibrium. The dimensionless governing equations are solved in exact form. The velocity field for impulsive motion as well as accelerated motion have been calculated and analyzed. The effects of radiation parameter and Prandtl number on the velocity field as well as on the temperature distribution are discussed. An increase in Grashof number leads to increase the primary velocity and the magnitude of the secondary velocity for both the impulsive as well as accelerated motions of one of the channel walls. It is found that the primary velocity and the magnitude of the secondary velocity increase with an increase in Hall parameter for both the impulsive as well as accelerated motions of one of the channel walls. The fluid temperature decreases with an increase in radiation parameter. The effects of pertinent parameter on shear stresses and rate of heat transfer are also studied in detail. It is also found that the shear stress due to primary flow and the magnitude of the shear stress due to secondary flow decrease for both impulsive as well as accelerated motions of one of the channel walls with an increase in radiation parameter.

The aim concerning in **eighth chapter**, is to study the transient MHD free convective flow in a heated vertical parallel plates channel in the presence of an inclined magnetic field on taking Hall currents into account. It is assumed that the magnetic Reynolds number for the flow is small so that the induced magnetic field can be neglected. An exact solution of the governing equations has been obtained. In addition to that, the problem gives an analytical steady state solution. The effects of pertinent parameters on the velocity field, temperature distribution, shear stresses and rate of heat transfer have been discussed. It is found that the primary velocity is accelerated whereas the secondary velocity is retarded with an increase in magnetic field inclination. As magnetic field inclination increases, the hydromagnetic drag force decreases. In consistency with this, it is observed that a rise in inclination clearly accelerates the primary flow and decelerates the secondary flow. An increase in thermal diffusivity leads to a decrease in Prandtl number. Therefore, thermal diffusion has a tendency to reduce the fluid temperature. Moreover, the non dimension shear stresses are presented graphically and a numerical result has been obtained for the rate of heat transfer. It is also found that the absolute values of the shear stress due to the primary flow as well as the shear stress due to the secondary flow at the plate reduce with an increase in either radiation parameter or magnetic parameter.

In **ninth chapter**, the effects of Hall currents on MHD free convective flow of a viscous incompressible electrically conducting optically thick radiating fluid past a vertical porous plate in the presence of an applied transverse magnetic field and thermal radiation have been studied. The governing equations have been solved numerically using the fourth-order Runge-Kutta-Fehlberg method together with the shooting technique implemented on MatLab. The numerical results for the velocity field, temperature distribution, shear stress and the rate of heat transfer at the plate are presented graphically for pertinent parameters. Increasing strength of the magnetic field accelerates the primary velocity in the presence of free stream velocity. The fluid temperature enhances for increasing values of temperature difference parameter. Suction/injection has a profound effect on the boundary layer thickness in which the suction reduces the thermal boundary layer thickness whereas injection thickens it. The shear stress enhances for increasing values of either magnetic parameter or Hall parameter while it reduces with an increase in either heat generation function or Grashof number. It is found that the rate of heat transfer at the plate reduces for increasing values of heat generation parameter while it enhances with an increase in either suction parameter or Prandtl number.

Future Research Scope

This section summarizes some scopes for future research works. To conclude this dissertation, we first like to remind the geometry of problems during this research work and in particular, the flow characteristics which have lead to novel ideas and some interesting results. Moreover, we can sketch the ideas that have arisen and given importance in the frame of future continuation of this work. Many new areas can yet be explored and some points from this work can be further clarified. Based on the current work done in this dissertation, to improve the effects of Hall currents, slip-condition, ion-slip condition, porous medium and nanofluid can be designed and developed. Extension of scopes exists in the second and third chapters on taking Hall currents into account. The effects of Hall and radiation on unsteady MHD flow past a heated moving vertical plate can be improved by considering porosity of the plate. The present research furnishes the analytical based solution of the effects of Hall currents on hydromagnetic free convection in a heated vertical channel in the presence of inclined magnetic field and thermal radiation. This study can be redesigned based on nanofluid. The present configuration of radiation effects on unsteady MHD free convective Couette flow of heat generation/absorbing fluid can be further improved by considering rotating frame

of reference. Combined effects of Hall currents and radiation on MHD free convective flow in a vertical channel with an oscillatory wall temperature can be improved by adding porous channel feature in a porous medium. There are several flow characteristics which may extend to improve the flow patterns for velocity field and temperature distributions.

List of publications

The thesis includes eight papers published in peer reviewed journals. List of publications during the thesis work as follows:

(i) Unsteady MHD flow and heat transfer past a porous flat plate in a rotating system, *published in International Journal of Computer Applications (IJCA), ISSN:0975-8887, 33(2)(2011), pp.17-26.*

(ii) Radiation effects on unsteady MHD free convective Couette flow of heat generation / absorbing fluid, *published in International Journal of Computer Applications (IJCA), ISSN:0975-8887, 39(3)(2012), pp.42-51.*

(iii) Hall effects on unsteady hydromagnetic flow past an accelerated porous plate in a rotating system, *published in Journal of Applied Fluid Mechanics (JAFM), ISSN:1735-3572, IF:0.89, 8(3)(2015), pp.409-417.*

(iv) Effects of Hall current and radiation on unsteady MHD flow past a heated moving vertical plate, *published in Journal of Applied Fluid Mechanics (JAFM), ISSN:1735-3572, IF:0.89, 7(4)(2014), pp.683-692.*

(v) Combined effects of Hall Currents and rotation on unsteady MHD Couette flow in a porous channel, *published in World Journal of Mechanics (WJM), ISSN:2160-049X, 1(3)(2011), pp.87-99.*

(vi) Combined effects of Hall current and radiation on MHD free convective flow in a vertical channel with an oscillatory wall temperature, *published in Open Journal of Fluid Dynamics (OJFD), ISSN:2165-3852, 3(1)(2013), pp.9-22.*

(vii) Hall effects on unsteady hydromagnetic free convective flow between two heated vertical plates in the presence of thermal radiation, *published in Turkish Journal of Engineering and Environmental Sciences (TJEES), ISSN:1300-0160, 38(3)(2014), pp.434-454.*

(viii) Hall effects on an unsteady magneto-convection and radiative heat transfer past a vertical porous plate, *published in Alexandria Engineering Journal (AEJ)(Elsevier), ISSN:1110-0168, 55(2)(2016), pp.1321-1331.*